Influence of neuroimplant materials, drugs and drug-material combinations on healthy cells of the brain

Dissertation

zur Erlangung des akademischen Grades
Doktor der Naturwissenschaften
(Dr. rer. nat.)
der Mathematisch-Naturwissenschaftlichen Fakultät

der Christian-Albrechts-Universität zu Kiel

vorgelegt von
Frau M. Sc. Christina Schmitt

Kiel
28.02.2020

Erste Gutachterin: PD Dr. Kirsten Hattermann-Koch

Zweite Gutachterin: Prof. Dr. Regina Scherließ

Tag der mündlichen Prüfung: 04.05.2020

Für meine Eltern

Ulla und Peter Schmitt

Preface

This dissertation was written cumulative. Parts of this dissertation have already been published or are submitted to a journal:

Schmitt C, Rasch F, Cossais F, Heldt-Feind J, Lucius R, Shaygan Nia A, Lohe MR, Feng X, Mishra YK, Adelung R, Schütt F, Hattermann K, Little, reversible glial scarring responses on tetrapod-shaped graphene oxide and reduced graphene oxide 3D scaffolds in brain in vitro and ex vivo models. 2020, submitted, Biomaterials Science

Schmitt C, Lechanteur A, Cossais F, Bellefroid C, Arnold P, Lucius R, Heldt-Feind J, Piel G, Hattermann K, Liposomal encapsulated curcumin effectively attenuates neuroinflammatory and reactive astrogliosis reactions in glia cells and organotypic brain slices. 2020, in revision, Int. J. Nanomed.

Rasch F*, **Schmitt C***, Saure LM*, Meyer R*, Adamski V, Dengiz D, Scherließ R, Lucius R, Synowitz M, Mishra YK, Hattermann K, Adelung R, Held-Feindt J[#], Schütt F[#]. Development of a 3 D porous PDMS-network for glioblastoma therapy. 2020, in revision, ACS Biomaterials Science & Engineering

Schmitt C*, Adamski V*, Rasch F, Adelung R, Lucius R, Synowitz M, Hattermann K, Held-Feindt J. Establishment of an *in vivo* adapted *in vitro* glioblastoma(in)complete resection co-culture model suitable for drug testing. Ann Anat., 228:151440, 2019 Nov 11. doi: 10.1016/j.aanat.2019.151440

Adamski V*, **Schmitt C***, Ceynowa F, Adelung R, Lucius R, Synowitz M, Hattermann K[#], Held-Feindt J[#]. Effects of sequentially applied single and combined temozolomide, hydroxychloroquine and AT101 treatment in a long-term stimulation glioblastoma *in vitro* model. J Cancer Res Clin Oncol,144:1475−1485, 2018. doi:10.1007/s00432-018-2680-y

*Authors share first authorship

[#]Authors share senior authorship

Abstract

Despite intensive research, many drugs or application forms are still not efficient enough for the adequate treatment of various brain disorders. The increasing knowledge of the respective diseases however can help to identify more suitable drugs or combinations to address the specific cellular disorder. The local drug-administration by drug delivery devices, such as implants, can improve treatment efficiency by increasing the bioavailability of a drug or overcoming systemic toxicity due to lower drug concentrations. Since implant materials or the infiltrated drugs themselves can elicit brain foreign body reactions of the healthy brain, implant materials or alternative drugs need to be investigated in suitable *in vitro* models. Therefore, selected alternative therapeutics, combination strategies as well as drug-loaded implant materials for the, as a model disease chosen highly malignant brain tumor *glioblastoma multiforme*, were investigated for their efficacy as well as biocompatibility in this thesis. A special focus was set on the investigation of brain foreign body reactions of the healthy brain towards possible brain implant materials and ways to elicit them.

Different treatment strategies have been tested by combining alternative therapeutic compounds with the standard chemotherapeutic temozolomide (TMZ) either simultaneously or sequentially in monocultures of human GBM cells as well as human astrocytes over several days. Especially the sequential treatment of the three days combination of TMZ and AT101, the R-(-)-enantiomer of the cottonseed-derived polyphenol gossypol, followed by the three days single AT101 stimulation, improved the therapy success in GBM cell lines significantly, whilst keeping healthy human astrocytes less affected than the standard treatment with TMZ. Interestingly, this approach was less successful in co-cultures of human primary GBM cells with human astrocytes and microglia mimicking the (in) complete resection of the tumor. Astrocytes and microglia seemed to have protective effects on the drug-induced cytotoxic and anti-proliferative effects on GBM cells. Likewise, GBM cells increased cytotoxic effects in astrocytes, in function of the GBM cell number present. To further improve the treatment efficiency by local drug administration, AT101 was infiltrated in biocompatible polydimethylsiloxane (PDMS) scaffolds with a hollow tetrapodal microtube network. We observed typical diffusion-based drug-release profiles with a therapeutic concentration range, which could be adjusted by scaffold size, porosity, open microchannels and infiltrated drug concentration. *In vitro* studies showed a sufficient treatment efficiency in GBM cells whilst not affecting astrocytes stronger than the free drug. Similar to this material scientific approach, graphene based three-dimensional scaffolds were produced for local drug-administration or electrical stimulation/recording applications in the brain. In suitable *in vitro* and *ex vivo* models of the healthy brain to study biocompatibility as well as brain foreign body reaction, we demonstrated that graphene oxide (GO) and reduced graphene oxide (rGO) scaffolds did hardly affect survival of human microglia, astrocytes and murine organotypic brain slices. Moreover, only moderate effects on material-specific inflammatory and glial scarring reactions occurred, however stronger for rGO scaffolds. These effects could be diminished in most cases to control levels by pre- and co-stimulations with the anti-inflammatory and fibrotic compound curcumin. Encapsulating curcumin into liposomes could significantly improve the long-term storage, bioavailability as well as *in vitro* efficacy to reduce inflammation and glial scarring reactions in *in vitro* models of reactive gliosis.

In conclusion, novel drug combinations can improve treatment efficacies in *glioblastoma multiforme* whilst also reducing adverse drug effects in the healthy brain. More realistic *in vitro* and *ex vivo* models help to analyze the efficacy of novel drugs and drug delivery systems as well as adverse drug effects and implant-mediated brain foreign body reactions in the healthy brain. Three-dimensional scaffolds from PDMS, GO and rGO seem to be promising materials for brain applications, as they offer unique and tailorable physico-chemical properties, drug loading capacity or conductivity with minimal effects on reactive gliosis *in vitro* and *ex vivo*. Anti-inflammatory drugs such as curcumin can be used as surface coatings to elicit brain foreign body reactions towards the materials. Hence, to improve a drugs bioavailability and stability, nanoformulations such as liposomes are easily accessible tools which can greatly improve a drugs *in vitro* efficacy.

Zusammenfassung

Trotz intensiver Forschung und Weiterentwicklung sind viele der momentan verfügbaren Medikamente oder ihre Verabreichungsformen nicht gut geeignet, um zahlreiche Erkrankungen des Gehirns adäquat zu behandeln. Ein wachsendes Verständnis über die jeweilige Erkrankung kann dazu beitragen, besser geeignete Wirkstoffe oder Wirkstoffkombinationen zu identifizieren, die die zelluläre Fehlfunktion möglichst passgenau adressieren. Lokale Freisetzungssysteme, beispielsweise Medikament beladene Implantate, können zudem die Wirksamkeit geeigneter Medikamente durch Erhöhung ihrer Bioverfügbarkeit verbessern oder ihre systemische Toxizität reduzieren. Da Implantate oder die damit beladenen Medikamente jedoch Fremdkörperreaktionen hervorrufen können, müssen vor allem Reaktionen des gesunden Gehirns auf alternative Wirkstoffe und Implantat-Materialien in geeigneten Testsystemen getestet werden. Daher wurden in dieser Arbeit ausgewählte alternative Wirkstoffe, Kombinationsstrategien und wirkstoffbeladene Modellimplantate zur Behandlung des als Modell-Erkrankung adressierten hochmalignen Hirntumors *Glioblastoma multiforme* in Hinblick auf ihre Wirksamkeit und Verträglichkeit untersucht. Ein besonderer Fokus lag hierbei auf der Untersuchung der Fremdkörperreaktion des Gehirns auf verschiedene potenzielle Gehirnimplantate und der Möglichkeit diese zu inhibieren.

Unterschiedliche Strategien zur Behandlung des *Glioblastoma Multiforme* wurden unter Einbezug alternativer Therapeutika in Kombination mit dem Standard-Therapeutikum Temozolomid (TMZ) verfolgt. Hierfür wurden Medikamente in simultanen oder sequenziellen Therapieschemata an Monokulturen von humanen GBM Zelllinien, sowie einer humanen Astrozyten-Zelllinie über mehrere Tage getestet. Vor allem eine sequenzielle Gabe versprach verbesserte Therapieerfolge in GBM Zellen, bei der über drei Tage eine Kombination aus TMZ und dem R-(-)-Enantiomer des Baumwoll-Polyphenols Gossypol (AT101), gefolgt der Gabe von AT101 über weitere drei Tage zur Behandlung eingesetzt wurde. Astrozyten waren bei dieser sequenziellen Kombinationstherapie weniger unerwünschten Nebenwirkungen ausgesetzt als durch die Standardtherapie mit TMZ. In Ko-Kulturen von primären GBM-Zellen mit gesunden Astrozyten und Mikrogliazellen, die eine vollständige und unvollständige Tumorresektion wiederspiegeln, war dieses Therapieschema interessanterweise weniger erfolgreich als in Monokulturen. Astrozyten schienen hier einen protektiven Effekt auf das Überleben der GBM Zellen auszuüben. Gleichermaßen erhöhten GBM-Zellen, in Abhängigkeit ihrer ausgesäten Zelldichte, die toxische Wirkung der Wirkstoff-Kombination auf Astrozyten. Um die so gewonnenen Erkenntnisse in Hinblick auf wirkstofffreisetzende Gehirnimplantate anzuwenden, wurden zunächst biokompatible Polydimethylsiloxan (PDMS) Gerüste mit hochporösen tetrapoden-förmigen hohlen Mikrokanälen hergestellt und nachfolgend mit AT101 infiltriert. Wir konnten eine klassische diffusions-basierte Medikamentenfreisetzung mit therapeutisch wirksamer Konzentration beobachten, die durch Variation der Templat-Größe, Porosität, Anzahl der offenen Mikrokanäle oder der infiltrierten AT101 Konzentration angepasst werden konnte. In *in vitro* Studien lieferten diese eine erfolgreiche Kontrolle des Tumorzellwachstums im Vergleich zu Stimulationen mit dem löslich applizierten AT101, ohne dabei negativ auf Astrozyten zu wirken. Ähnlich der mikrostrukturierten PDMS Matrizes wurden Graphen-basierte tetrapoden-förmige 3D-Gerüste produziert, die für eine Anwendung als *Drug Delivery System* oder aber zur elektrischen Stimulation/Messung geeignet sind. In geeigneten *in vitro* und *ex vivo* Modellen beeinflussten diese hochporösen Gerüste aus Graphenoxid (GO) und reduziertem Graphenoxid (rGO) die Viabilität humaner Mikrogliazellen und Astrozyten, sowie muriner organotypischer Gehirnschnitte nicht oder kaum. Sie lösten nur geringe Entzündungs- und Glianarbenreaktionen aus, hierbei waren die Effekte für rGO tendenziell etwas stärker. Beobachtete Effekte konnten durch Vor- oder Ko-Stimulationen mit dem anti-inflammatorischen und -fibrotischen Medikament Curcumin erfolgreich verringert werden. Durch das Einkapseln von Curcumin in liposomale Nanoformulierungen konnte im Weiteren die Bioverfügbarkeit und Stabilität des Medikamentes erhöht werden. Das liposomale Curcumin war nicht nur über eine Zeit von bis zu sechs Monaten stabil, sondern zeigte auch eine signifikant höhere *in*

vitro Effizienz, sodass es Entzündungsreaktionen und reaktive Gliose in *in vitro* Modellen effektiv reduzieren konnte.

Abschließend lässt sich zusammenfassen, dass neue Medikamente oder Kombinationen den Therapieerfolg bei der Behandlung des Glioblastoms signifikant erhöhen und darüber hinaus zusätzlich die negativen Medikamentenwirkungen im gesunden Gehirn reduzieren können. Realistischere *in vitro* Modelle wie Ko-Kulturen oder murine organotypische Gehirnschnitte können dabei helfen, neue Medikamente, Formulierungen oder *Drug Delivery Systeme* auf ihre Effizienz zu testen und die Fremdkörperreaktion im Gehirn besser zu verstehen. Drei-dimensionale hochporöse Gerüste aus PDMS, GO und rGO scheinen geeignete Materialien für Gehirnimplantate zu sein, da sie einzigartige physiko-chemische Eigenschaften wie die variable Porosität, Medikamenten Ladekapazität oder Leitfähigkeit besitzen, und zugleich nur geringe Glianarben-Prozesse im gesunden Gehirn auszulösen scheinen. Antiinflammatorische Medikamente wie Curcumin, beispielsweise in Beschichtungen auf das Implantat aufgebracht, können dabei helfen Materialreaktionen zu verhindern. Dabei können die Bioverfügbarkeit und Stabilität solcher Medikamente mit Hilfe von einfach herzustellenden Nanoformulierungen, wie Liposomen, im hohen Maße verbessert und damit die Wirkeffizienz erhöht werden.

Abbreviations

Abbreviation	Full name
^{131}I	Iodine-131
2D	Two-dimensional
3-BrPA	3-bromopyruvate
3D	Three-dimensional
α-SMA	Alpha smooth muscle actin
AP-1	Activator protein 1
ATP	Adenosine triphosphate
BBB	Blood-brain barrier
Bcl-2	B-cell lymphoma 2
BCRP	Breast cancer resistance protein
BH3	Bcl-2 homology domain 3
BM	Basement membrane
CED	Convection enhanced delivery
cm	Centimeter
CNS	Central nervous system
CNTF	Ciliary neurotrophic factor
CQ	Chloroquine
CRISPR	Clustered regularly interspaced short palindromic repeats
CSPG	Chondroitin sulfate proteoglycans
Cur	Curcumin
Da	Dalton
DEX	Dexamethasone
DCA	Dichloroacetic acid
DDS	Drug delivery systems
DNA	Deoxyribonucleic acid
dos	Days of stimulation
DPPC	1,2-dipalmitoyl-sn-glycero-3-phosphocholine
ECM	Extracellular matrix
EGF	Epidermial growth factor
EPC	Egg phosphatidylcholine
FDA	Food and drug administration
g	Gram
GBM	*Glioblastoma multiforme*
GFAP	Glial fibrillary protein
GO	Graphene oxide
GSLC	Glioma stem like cell-characteristics
h	Hours
HCQ	Hydroxychloroquine
IKVAV	Ile-Lys-Val-Ala-Val peptide
IL-1β	Interleukin 1 beta
IL-6	Interleukin 6
ISFI	*In situ* forming implants
i.v.	Intravenous
JAK/STAT3	Janus kinase/signal transducers and activators of transcription 3
JNK	C-Jun N-terminal kinases
LipoCur	Liposomal curcumin

Abbreviation	Full name
LPS	Lipopolysaccharide
M-CSF	Macrophage colony stimulating factor
Mdr1	Multi-drug-resistance-gene 1
mg	Milligram
min	Minute
MRI	Magnetic resonance imaging
mRNA	Messenger ribonucleic acid
MRP	Multidrug resistance proteine
NF-κB	Nuclear factor 'kappa-light-chain-enhancer' of activated B-cells
nm	Nanometer
nM	Nano molar
NO	Nitric oxide
NP	Nanoparticle
Nrf2	Nuclear factor E2-related factor
rGO	Reduced graphene oxide
p38MAPK	P38 mitogen-activated protein kinases
PARP	Poly(ADP-ribose)-polymerase
PC	Primary culture
PCPP-SA	Poly[bis(p-carboxy-phenoxy propane anhydride) sebacic acid]
PDMS	Polydimethylsiloxane
PGA	Poly(glycolic acid)
PLA	Poly(lactic acid)
PLGA	Poly(lactid-coglycolic acid)
PVA	Polyvinyl alcohol
RES	Reticuloendothelial system
RNA	Ribonucleic acid
SLN	Solid lipid nanoparticles
TEER	Transepithelial electrical resistance
Tf	Transferrin
T_g	Glass transition temperature
TGF-α	Transforming growth factor alpha
TGF-β	Transforming growth factor beta
TMZ	Temozolomide
TLR	Toll-like receptor
TNF-α	Tumor necrosis factor alpha
WHO	World health organization
WST-1	Water soluble tetrazolium 1
ZnO	Zinc oxide
µM	Micro molar
µm	Micrometer

List of figures

Table of content

1st CHAPTER

Fundamentals

"There comes a point in your life when you need to stop reading other people's books and write your own"

(Albert Einstein)

1.1 Introduction

For the pharmacological treatment of diseases, there are two main ways of drug administration, enteral (e.g. oral) or parenteral (e.g. intravenous (i.v.), nasal, inhalational, …), whereas the choice of application route influences greatly the bioavailability of a drug concomitant with the numbers of barriers to cross until reaching the blood system. While i.v. drug administration is very reliable to deliver a drug systemically by reaching a 100 % bioavailability, the most widely used application route remains oral, as it is well accepted with an improved patient compliance (Klueglich et al. 2005). However, orally administered drugs have a highly variable bioavailability, influenced by several factors such as food or metabolism (Martinez and Amidon 2002; Klueglich et al. 2005). Moreover, most application routes have in common, that only a small percentage of the total administered drug finally reaches the target site itself. This effect becomes stronger when talking about drug administration to the brain, since only a small amount of systemically administered drug reaches the blood-brain barrier (BBB) and can also pass it (Lingineni et al. 2017).

Besides these conventional ways to administer drugs, more modern forms such as local implants or depots have gained interest. These delivery systems offer the advantages of local drug administration with smaller therapeutically concentrations due to site-specific drug delivery as well as the option of a tailored drug release. Moreover, in applications such as cardiology or oncology, the effectiveness of treatment can be improved as well as negative side effects or toxicity and damage to healthy tissue minimized, as the systemically application route is bypassed (Kaurav and Kapoor 2017). Especially for brain tumors, whose standard treatment by chemotherapeutics causes a huge systemic toxicity, the local application of a drug by brain implants can be the favorable choice. Besides this, brain implants offer the possibility to use promising drugs with improved therapeutically efficacy for instance, which possibly failed clinical trials, due to low bioavailability when applied systemically, or bad transport through the BBB (Bikhezar et al. 2019; Gomez-Zepeda et al. 2019). To date, there are numerous of brain implants under investigation for either drug delivery applications or for deep-brain stimulation respectively microsensing devices (Aum and Tierney 2018; Patel et al. 2017). Amongst them, there are approaches for the treatment of Alzheimer's disease by Rivastigmine (Bastiat et al. 2010), the treatment of Schizophrenia by Haloperidol or Risperidone depots, microparticles and *in situ* forming implants (ISFI) (Lu et al. 2007; Rainer 2008) but also microelectrodes and microsensing devices for epilepsy seizure detection (Patel et al. 2017; Salam et al. 2011). More prominent however is the recent increase of drug delivery implants for the treatment of *glioblastoma multiforme* (GBM), a highly malignant brain tumor with a very low five years survival rate after surgery and conventional treatment (Ohgaki and Kleihues 2005). Most of them focus on the incorporation of alternative pharmaceutical compounds such as the FDA approved Carmustine Gliadel® Wafers that are already clinically used (Bota et al. 2007), polymeric microparticles incapsulating paclitaxel (Elkharraz et

al. 2006) or most recently electrospun PVA-Dacarbazine nanofibers (Steffens et al. 2019), instead of using the conventional therapeutic agent temozolomide (TMZ).

However, most studies about novel/alternative drug testing or implant drug delivery in the brain are limited on the target cells, such as GBM cells, but disregard the surrounding healthy brain tissues' response. Moreover, the healthy brain tissue is not only influenced by drugs, but also the surgery as well as the implant material and its shape, size and microstructure itself. As a matter of central nervous system (CNS) repair, glial cells such as microglia and astrocytes but also oligodendrocytes and their precursors respond to injury and disease and therefore trigger the so-called foreign body response (Burda and Sofroniew 2014; Cregg et al. 2014). In brief, microglial cells, the immune cells of the brain, become reactive, proliferate to the implant site and start to release cytokines and chemokines that force astrocytes in the surrounding tissue to become reactive as well. Reactive astrocytes migrate to the implant site and build a glial sheath around it, known as the glial scar. Used as a physiological protection mechanism of the brain against foreign bodies or damaged tissue, this glial scar can cause an alteration of the functionality of an implant, e.g. altered release-kinetics to the target tissue. Therefore, when building a brain implant, one must take these reactions of the non-target tissue into account as it influences strongly the implants' efficacy. Ways to avoid or alleviate these reactions can be either by tailoring the material-scientific implant properties, such as the shape, microstructure or surface functionalization to make the implant itself more biocompatible, but also pharmacologically by the use of anti-inflammatory and -fibrotic compounds that can directly diminish the brain foreign body response.

More information on the current drug delivery approaches for brain applications, in regard of the medical application of GBM treatment, as well as the detailed process of brain foreign body response can be found in the theoretical background chapters (Chapter 1.3 to 1.4) of this thesis.

1.2 Aim of the project

In this project, novel brain implant materials should be evaluated for their suitability in brain applications, however focusing especially on the reaction of healthy cells of the brain. As a medical problem/question, the highly malignant brain tumor *glioblastoma multiform*e was chosen as a model disease, which after more than 100 years of research only made little proceedings in chemo- and radiotherapy and consequently remains with poor patients' overall survival. The local application of drugs can improve current therapy approaches, since smaller concentrations are needed for therapeutically effects concomitant with bypassing systemic and off-target toxicity in other tissues and organs. However, as the conventional treatment of GBM is accompanied with chemoresistance and recurrences due to the heterogeneity and treatment-escape mechanisms of the tumor, novel treatment approaches are needed to improve the overall therapy success. Hence, focusing on the to be treated disease, most studies neglect the influence of drugs or implant materials on the healthy cells of the brain. Therefore, in this thesis, alternative drugs or drug combinations as well as implant-drug combinations for the treatment of GBM are being evaluated and characterized in suitable GBM *in vitro* tissue models, including the healthy brain tissue environment of the brain tumor. Moreover, as brain surgeries respective the implantation of materials into the brain cause a natural inflammatory reaction of immune cells of the brain and in most cases the encapsulation of implants by glial tissue as a foreign body response, the second focus of this thesis lies on the evaluation of foreign body responses of healthy brain tissue by the implementation of inflammation respective reactive gliosis *in vitro* models. In regard of these aspects, this project is divided into five major tracks, whereas corresponding publications, that are emerged in the framework of this thesis are shown in Chapter 2 **Publications**:

To develop safe drug delivery systems (DDS) for the treatment of GBM, not only implant materials, but also alternative drugs need to be evaluated on their effects on the healthy surrounding brain tissue. Therefore, in the first publication (Chapter 2.1 **Effects of sequentially applied single and combined temozolomide, hydroxychloroquine and AT101 treatment in a long-term stimulation glioblastoma *in***

***vitro* model.**) novel alternative drugs such as Hydroxychloroquine and AT101 as well as drug-combinations of those, for the treatment of GBM have been tested, in function of their improved influence on healthy brain cells' survival and toxicity.

Since there is the need for more realistic drug testing on *in vitro* systems, mimicking the *in vivo* situation after resection of a GBM tumor, the most promising drug combination from Chapter 2.1, to treat GBM cells whilst keeping healthy brain cells alive, has been tested on a dual co-culture system mimicking the complete and incomplete resection of a GBM tumor, which is depicted in Chapter 2.2 **Establishment of a glioblastoma *in vitro* (in)complete resection dual co-culture model suitable for drug testing**.

In a first attempt to incorporate the alternative compound AT101 into a size-tunable brain implant, highly porous polymeric templates have been produced in a collaborative work with material scientists and used as a scaffold for the loading with AT101. The effects of those in combination with the conservative therapeutic agent Temozolomide on proliferation as well as on cytotoxicity have been studied on healthy brain cells (see Chapter 2.3 **Macroscopic PDMS Microchannel Matrix for Tailored Drug Release and Localized Glioblastoma Therapy**).

However, not only polymeric drug delivery systems are of interest, but also graphene-based materials such as graphene oxide (GO) or reduced graphene oxide (rGO), whose biocompatibility especially for brain applications are not well known. Whereas rGO is highly conductive and can be therefore used for biosensing devices such as electrodes, GO that is lacking this property, can be used as an easily functionalize drug delivery system. Therefore, highly porous scaffolds of GO and rGO as brain implant materials were tested on healthy cells of the brain (human cell lines) as well as murine acute brain slices, to evaluate cytotoxicity as well as their influence on inflammation and reactive gliosis *in vitro*. In order to prevent foreign body reactions towards the materials, the anti-inflammatory compound curcumin was evaluated for its efficacy to alleviate these reactions (see Chapter 2.4 **Little, reversible glial scarring responses on tetrapod-shaped graphene oxide and reduced graphene oxide 3D scaffolds in brain *in vitro* and *ex vivo* models**).

Curcumin has shown to have promising anti-inflammatory and -glial scarring properties on the healthy brain (see Chapter 2.4). However, as the bioavailability due to the instability and light sensitivity of the drug remains poor, we encapsulated curcumin into liposomes and performed intensive studies on the long-term stability, cytotoxicity and proliferation, as well as on internalization studies or *in vitro* models of inflammation and glial scarring in human cell lines as well as murine acute brain slices, as depicted in Chapter 2.5 **Liposomal encapsulated curcumin effectively attenuates neuroinflammatory and reactive astrogliosis reactions in glia cells and organotypic brain slices**.

1.3 Theoretical background

1.3.1 *Glioblastoma multiforme* (GBM)

1.3.1.1 Characteristics of *glioblastoma multiforme*

Glioblastoma multiforme (GBM) are highly malignant brain tumors, derived from astrocytes and characterized by a fast and infiltrative progression (DeAngelis 2001). With an incidence rate of 2.98 cases per 100,000 individuals a year, GBM belongs to the most current brain tumors in adults (Ostrom et al. 2018; Leece et al. 2017). Although primary tumors of the CNS only represent around 1 % of all new cancer cases in western countries, they remain the ones with the highest death rate of around 70 % (American Cancer Society 2019). GBMs can be subcategorized into primary and secondary evolving tumors, as they can develop *de novo* in patients within three to six month or from low grade secondary astrocytomas grade II or III within two to five years (Ohgaki and Kleihues 2005; Pisapia et al. 2017; Louis et al. 2019). The world health organization (WHO) classifies them as grade IV astrocytomas since 2016, however the term *glioblastoma multiforme* was given over 90 years back by Bailey and Cushing due to the heterogeneity of the tumor (Bailey, P. and Cushing, H. 1926). Here, GBMs usually compose of more than one tumor cell population due to several molecular biological differences in their genetics, and therefore causing a varying response rate and resistance to chemotherapy due to versatile escape mechanisms. Those single resistant populations are presumably responsible for rapid relapses and therefore the reason for the still poor survival rate of only 5.6 % patients after five years (Ostrom et al. 2018; Stupp et al. 2005).

1.3.1.2 Therapeutically approaches

After the usual diagnosis via magnetic resonance imaging (MRI), most GBM patients undergo the conventional treatment by surgical removal, frequently followed combined radio-/chemotherapy with, as in most cases, the standard chemotherapeutic agent temozolomide (TMZ). To date, TMZ remains the most widely used first-line chemotherapeutic drug that is used with combined radiotherapy or solely administered for maintenance treatment (Yan et al. 2016). Yet, depending on the location of the tumor and the chances for a complete removal, either a complete or incomplete resection of the tumor can be performed (Chaichana et al. 2014; McGirt et al. 2009).

1.3.1.3 Alternative treatment approaches

As one major issue of GBM treatment is the already mentioned heterogeneity of the tumor causing chemotherapeutical resistances, there is an increasing need for more alternative drugs and smart drug combinations (Arévalo et al. 2017) to make the treatment more effective. One way to address this is by applying drugs with different mechanisms of action than the standard therapeutic agent TMZ, or for instance the simultaneous or consecutively combination of drugs to bypass chemoresistance. Regarding this, a broad variety of different alternative drugs have been already developed (Arévalo et al. 2017). As such, quinoline-based anti-malaria drugs like chloroquine (CQ) respective hydroxychloroquine (HCQ), as well as the R-(-)-enantiomer of the cottonseed-derived polyphenol gossypol, AT101, have been shown to be possible alternatives to TMZ (Golden et al. 2015) (see Figure 1, Alternative Therapeutics). Whereas the success of TMZ is based on its ability to alkylate/methylate deoxyribonucleic acid (DNA) of guanine residues (positions N-7 or O-6) yielding DNA string breaks, CQ and HCQ block autophagy and exert cytotoxic effects for instance (Golden et al. 2015; Yan et al. 2016). Contrary to that, the B-cell lymphoma 2 (Bcl-2) homology domain 3 (BH3) mimetic AT101 causes either autophagic cell death (Voss et al. 2010) or apoptosis caused by competitively binding to hydrophobic surface grooves of pro-survival Bcl-2 family members and therefore blocking their protective effects (Opydo-Chanek et al. 2017). Combining those quinoline- respective BH3-mimetic-based pharmaceutical compounds with TMZ, could be promising

approaches to evade chemoresistance and some of these approaches in fact have already been addressed. Golden and colleagues for example showed, that CQ and HCQ could improve TMZ cytotoxicity (Golden et al. 2015). Other groups could show an increase in chemosensitivity by blocking of autophagy, using CQ and HCQ (Yan et al. 2016; Golden et al. 2015). Moreover, a combined gossypol/TMZ treatment caused an inhibition of tumor associated angiogenesis as well as invasion and proliferation (Jarzabek et al. 2014). As a result of this success, both drug/drug families have been included into clinical trials (Li et al. 2008a; Briceño et al. 2007; Bushunow et al. 1999), however, the balance between low cytotoxic effects for healthy surrounding tissue and the positive therapeutic response in GBM tissue has not been evaluated yet for drug combinations, nor their sequentially application of them with TMZ for a longer period *in vitro*.

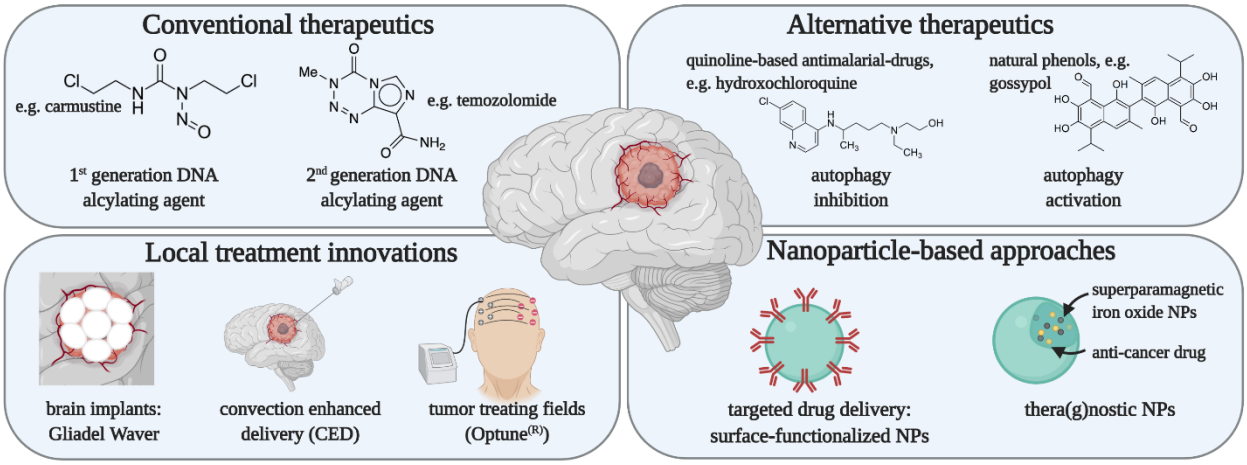

Figure 1: ***Current treatment approaches for glioblastoma multiforme (GBM) therapy.*** *Besides the conventional chemotherapeutics such as carmustine or temozolomide (upper left), alternative drugs that focus on different mechanisms of action can be employed (upper right). Besides surgery and systemic drug administration, GBM can be also therapized by local treatment approaches (lower left) or by modern nanoparticle-based platforms for drug delivery or thera(g)nostics (lower right). The figure was generated using Biorender software.*

Besides these strategies to increase treatment efficacies, other approaches focus on the development of novel DDS, such as nanocarriers or the direct administration of drugs via brain implants (Saad et al. 2017; Hicks et al. 2019; Cornelison and Munson 2018). Whereas several major clinical trials on new promising small molecules (e.g. gefitinib or erlotinib) failed, due to too low final concentrations in the brain, one approach to improve BBB permeability of drugs is the encapsulation into nano-formulations (Shergalis et al. 2018). By tailoring the particle size, surface charge, functionalization respectively the material itself, nano-formulated drugs can have improved BBB-permeability and bioavailability over the free drug (Fang et al. 2015; Mo et al. 2016). Therefore, it is no miracle that several clinical trials using liposomes or polymers, for brain-drug-delivery to treat GBM, are ongoing or already successfully completed (Clarke et al. 2017; Camp et al. 2013; Siefker-Radtke et al. 2016). Other groups however focus on the direct application of drugs into the brain, by implantable solid drug delivery devices but also nanocarriers (Bagó et al. 2016; La Rocca and Mehdorn 2009; Ranganath et al. 2010). For instance, the Gliadel® wafer, using carmustine as chemotherapeutic drug, is the only FDA approved implant for local treatment of GBM, next to the standard systemically TMZ therapy (Bota et al. 2007) and therefore yet the only local DDS for the treatment of GBM (Ashby et al. 2016) (see Figure 1, Treatment Innovations). However, although the implantation of the Gliadel® wafer into the resection cavity of GBM patients has shown great success in the survival, there are also negative sides including brain edema or intracranial infections for instance after implantation, which in some cases cause the revision of implantation (Ashby et al. 2016; Kuramitsu et al. 2015). Therefore, other groups try to approach this issue with different techniques. For instance, Steffens et al. showed, that the antitumor agent dacarbazine which effectively treats recurrent GBMs (Fazeny-Dörner et al. 2003) but lacks in high toxicity in healthy cells (Di Bei et al. 2009), was successfully incorporated into implantable

polymeric nanofibers with high drug loading capacities of around 84 %, a sustained drug release and efficient against GBM cells (Steffens et al. 2019). However, by only using monocultures of GBM cells, no information is given yet on the toxicity of this interesting approach on healthy cells of the brain. Other than solid implant matrixes, Bastiancich et al. respective Zhao et al. focus on the drug delivery via local injected hydrogels, however using different drugs such as gemcitabine or paclitaxel (Bastiancich et al. 2017; Bastiancich et al. 2016; Zhao et al. 2018). Moreover, Kim and others claim, that the tumors' non-cellular microenvironment plays a key role in tumor development and progression (Kim et al. 2005; Mikhailova et al. 2018). To address this issue, Belousov et al. suggest the embedding of brain DDS into brain specific matrix materials that include keyplayers of extracellular matrix molecules (ECM), since they not only play a structural role in tissues, but also in cell fate, maturation, migration and tumor cell invasion for example (Belousov et al. 2019). Taken these facts together, there are different ongoing approaches to develop suitable drug delivery devices including the huge variety of drugs that can be of interest when thinking about a non-systemically drug application, such as in the brain. However, there is a need to focus also on the test methods used for those DDS in parallel to the development and design of them, which will be addressed in chapter 1.3.1.4 **Alternative test methods**.

More detailed information about nano-formulations as well as implants as drug delivery devices are given in chapter 1.3.2 **Biomaterials for the central nervous system**.

1.3.1.4 Alternative test methods

As already mentioned, several promising drugs that are efficient against novel or recurrent GBM tumors, often fail when later being tested *in vitro* on healthy cells or even in clinical trials, due to the toxicity against the healthy brain tissue. Therefore, concomitant with different treatment approaches, new test methods and *in vitro* model systems that more closely mimic the *in vivo* situation of the heterogenous tumor and its microenvironment, are needed to evaluate more efficient suitable drugs and their efficacy, especially also on healthy tissue (Cornelison and Munson 2018). Current GBM *in vitro* models include for example tumor organoids, three-dimensional (3D) organotypic spheroids respective mini-brains and microfluidic systems (Balvers et al. 2017; Lenting et al. 2017; Caragher et al. 2019; Manini et al. 2018). For example, the influence of cell-cell connectivity is well reflected with tumor spheroids that are generated from human tumor biopsies and cultured stable in serum-free media with the addition of several growth factors and therefore promote the persistence of glioma stem like cell-characteristics (GSLC) (Caragher et al. 2019; Balvers et al. 2013; Brewer et al. 1993; Conti et al. 2005). However, Lenting et al. claim that the generation of those spherical cultures from patients seems to be challenging due to the highly heterogeneous tissue, as it is likely that the generated patient-derived glioma spheroid line only represents a small amount of the most aggressive cells from the original tumor (Lenting et al. 2017). In other approaches such as in microfluidic systems, GBM cells are cultured in hydrogel containing microfluidic channels, filled with circulating media, similar as in the brain (Li et al. 2018a). Nevertheless, while this approach is quite cost-intensive, it also represents only the mono-cultivation of the cells without the tumor microenvironment.

However, most of those *in vitro* models lack the influence of healthy cells on the tumor survival respectively the influence of drugs on the survival of healthy cells. Approaches including the tumor microenvironment and healthy brain tissue are for example the establishment of mini-brains respective organotypic brain slices, whereas patient-derived tumor cells can be implanted into human cerebral organoids (Ogawa et al. 2018) or into mouse brains (Eisemann et al. 2018; Sliwa et al. 2007; Marques-Torrejon et al. 2018), creating potential models for personalized medicine respective allowing interaction between tumor and non-tumor cells. Nonetheless, these models are time- and cost-intensive as well as foreign body reactions of the mouse host due to human cells can occur (Lenting et al. 2017). Moreover, single cell responses cannot be determined yet in those tissue models.

In summary, the research on alternative *in vitro* systems is growing enormous, to provide more efficient test methods for anti-glioma therapies, however more studies are needed that include the tumor microenvironment and therefore healthy cell responses.

1.3.2 Biomaterials for the central nervous system

For more contemporary approaches in the treatment of CNS diseases that do focus on the release of drugs from carrier materials or on the sensing and/or stimulation activities of electrodes, suitable biomaterials need to be identified. There is a wide variety of biomaterials used for central nervous system applications, including the treatment of malignant brain tumors such as GBM, epilepsies, or Alzheimer's disease for example (Aum and Tierney 2018). Amongst them, materials can be either used for neural electrodes to restore neurological functions respective micro sensing devices, as drug or gene delivery systems or for instance as scaffold materials for the promotion of tissue regeneration (Zhong and Bellamkonda 2008). Depending on the fate after injection or implantation, brain implant materials can either be biodegradable or non-biodegradable. Whereas in electrode design, the function of the implant needs to be restored and therefore non-biodegradable materials are used, drug delivery systems can require biodegradation of the scaffold or carrier material after drug-release (Zhong and Bellamkonda 2008). However, all applications have the need for materials with low off-target toxicity, high biocompatibility such as low inflammatory responses and without influencing neuronal fate for example in common (Donaruma 1988). In the following chapter, systemic and local drug delivery approaches such as nanoformulations or local implant materials, as well as neuronal electrodes as microsensing devices are discussed.

1.3.2.1 Drug delivery systems for brain applications

1.3.2.1.1 Systemic drug delivery systems

Nanoformulations

Whereas brain implants are directly placed into the brain, providing a direct drug delivery into the target site, nanoformulations can be used for both, the systemic or direct application. In general, nanoformulations are small particles with dimensions of 1-1000 nm in at least one dimension with tailorable properties such as surface charge, size and surface functionalization (Jeevanandam et al. 2018). As in most cases, nanoformulations are used for the delivery of drugs to the target site, however purposes can also be imaging as contrast agents, therapeutic applications or the combination of them as thera(g)nostics (Liong et al. 2008). Different systems such as polymeric nanoparticles (NPs), liposomes, micelles, ceramic NPs etc. are available for drug delivery applications to date (Lian and Ho 2001). Moreover, depending on the physical and chemical properties of a drug, the optimal delivery system and its material can be chosen. In fact, one major benefit of nanocarriers is the possibility to encapsulate hydrophilic or hydrophobic drugs respective the combination of them. Consequently, drugs that lack in efficiency due to low bioavailability, chemical instability or light sensitivity for instance, however with promising therapeutic effects can again be considered by exploiting nanotechnologies. Thereby, the stability of the drug can be improved as well as the drug-release kinetics adjusted. However, for brain delivery applications only lipid based nanocarriers including liposomes, solid lipid NPs (SLNs) respective micelles as well as polymeric NPs have been widely exploited (Garcia-Garcia et al. 2005; Khan et al. 2018). An overview of current drug delivery systems is given in figure 2. Polymer-based nanoparticles offer unique morphology, physicochemical and surface functionalization properties (Khan et al. 2018), such as their excellent carrier loading and tailorable release kinetics for instance (see figure 2, left). Therefore, they have gained great interest in brain delivery applications for example in cerebral disorders (Blasi et al. 2007), however polymer degradation and thereby caused toxic chemical production still limit their success in brain delivery applications (Blasi et al. 2007). Contrary to that liposomal formulations are biocompatible nanocarriers, with unique membrane permeability and long circulation half-life. Liposomes are small self-aggregating vesicles, formed by

unilamellar or multilamellar phospholipid bilayers of cholesterol and other non-toxic phospholipids (Akbarzadeh et al. 2013; Zhong and Bellamkonda 2008). In brief, lipid headgroups are exposed to the highly hydrophilic surrounding due to their polar character, whilst hydrophobic apolar chains promote interaction with one another. This amphiphilic character of the liposomal structure allows an encapsulation of drugs that are either hydrophilic, hydrophobic or even the combination of both, but also protein-based drugs or nucleic acid materials [see figure 2, left (Al-Jamal and Kostarelos 2007)]. Moreover, the change in toxicological profiles of a drug due to the encapsulation into liposomes has been highlighted in several clinical studies. For instance, by reducing chemotherapy-associated side effects such as nausea, vomiting and cardiotoxicity compared to unencapsulated drugs, the patient's outcome can be improved dramatically (Zamboni 2008; Lasic 1998; Silverman et al. 2013; Moen et al. 2009). Furthermore, the biocompatibility (Immordino et al. 2006) as well as the biological membrane-like structure with its lipophilic character facilitates drug transportation across membranes of brain endothelial cells and therefore excellent characteristics for brain uptake through the BBB but also for the distribution through the brain as in non-systemic applications (Khan et al. 2018; Agrawal et al. 2017).

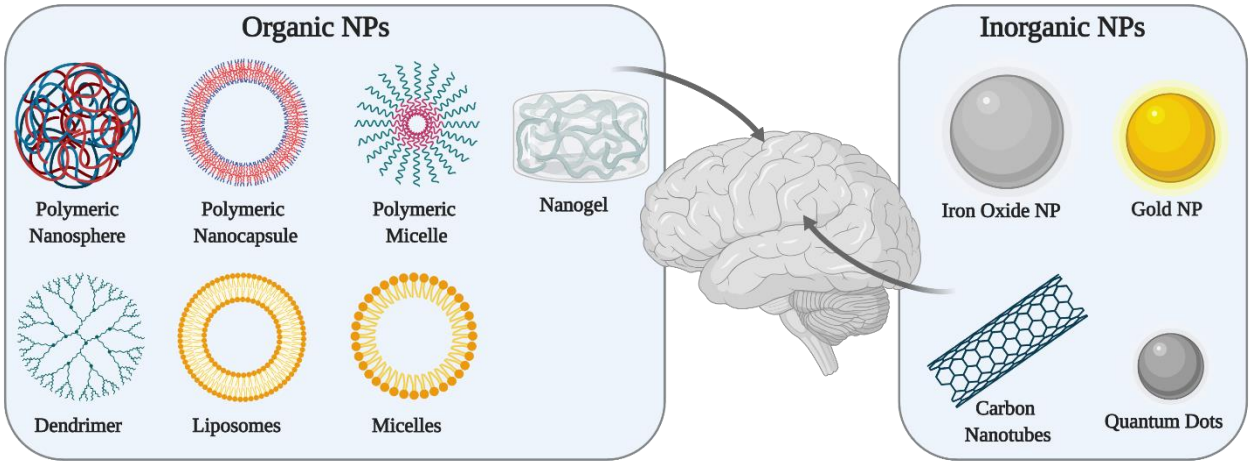

Figure 2: Nanosystems for brain applications. *For brain applications several different nanoformulations or -systems are available either for therapeutic purposes, diagnostic purposes or the combination as thera(g)nostics. Regarding the broad variety of materials possible, one can divide those materials into organic nanoparticles (NPs, left) or inorganic NPs (right). Organic NPs are mostly used for drug delivery purposes of hydrophilic, hydrophobic drugs or combinations of both, either inside of the particle core or in the particle membrane. Inorganic NPs are mostly used as contrast agents (iron oxide NPs) but also in therapy such as for gold NPs for instance. The figure was generated using the Biorender software.*

The systemic drug delivery is achieved by intraperiphal or intravenous injection of the carrier as a non-invasive treatment and can be repeated several times as needed. However, large concentrations are needed to reach therapeutic concentrations and therefore off-target cytotoxic effects can occur in organs and tissues. One approach to bypass this issue is the surface functionalization to selectively target or exploit biological molecules, carriers, surface receptors or mechanisms of the brain to enhance permeation through the blood-brain barrier (Schnyder and Huwyler 2005). For instance, cationized albumin, monoclonal antibodies to the insulin receptor or monoclonal antibodies to the transferrin (Tf) receptor are possible surface-functionalizations for a targeted receptor- or absorptive-mediated transcytosis through the BBB (Schnyder and Huwyler 2005; Pardridge et al. 1992). In GBM therapy, the surface decoration of resveratol encapsulating liposomes with Tf could extend the drug-release, increase the uptake and cytotoxicity in U-87 MG cells (Jhaveri et al. 2018). Other approaches in glioma therapy are doxorubicin encapsulating polymersomes, decorated with Des-octanoyl ghrelin and folate or SLNs decorated with Aprotinin and p97, which could inhibit tumor growth in a glioma mouse model (Yung-Chih und I-Hsuan 2016) respective enhanced BBB-passage and tumor growth inhibition efficacy (Yung-Chih and I-Hsuan 2016; Chen et al. 2014). Moreover, paclitaxel and curcumin encapsulating magnetic guided PLGA NPs decorated with the

T7 peptide could inhibit tumor progression and caused significantly higher cell uptake and brain accumulation (Cui et al. 2016). Furthermore, camptothecin carrying polymeric nanoparticles decorated with adenosine and TGN, a 12 amino acid peptide showed higher BBB transmigration efficiency, however with no benefits in survival at maximum tolerated doses (Saucier-Sawyer et al. 2015). Besides brain tumor targeting, drug delivery has been exploited also on neurodegenerative diseases for instance. As such, RVG29 modified liposomes carrying N-3,4-bis(pivaloyloxy)-dopamine have been evaluated for their efficacy to amplify therapeutic effects of dopamine derivate in a mouse model of Parkinson's disease (Qu et al. 2018). The group of Qu et al. could show the distribution of the nanocarriers to selective brain parts as well as accelerated the therapeutic effect of the drug (Qu et al. 2018). In Alzheimer's disease, multifunctional curcumin decorated liposomes targeting different ligands of the BBB such as amyloid, Tf receptor or LDLR have been evaluated in normal and transgenic mice, however curcumin did not significantly improve the ligand-targeting performance at the BBB (Papadia et al. 2017). In summary, due to these unique possibilities of targeted drug delivery, nanocarriers are therefore the most studied drug carriers for the delivery through the BBB into the brain, to date (Khan et al. 2018; Schnyder and Huwyler 2005). A detailed overview of the possible targeting-mechanisms for drug delivery through the BBB is described in chapter 1.3.3.1 **Blood-brain barrier** and is depicted in figure 3.

1.3.2.1.2 Local drug delivery systems

Brain implants for local drug delivery

The biggest challenge in conventional drug delivery to the brain still remains the passage through the BBB. Although many approaches focus on the target specific transport of nanoparticles through the BBB as seen in the previous chapter, one way to circumvent this issue is the local drug administration to the target site by brain implants. Brain implants offer huge advantages over the systemic application of a drug, as systemic side effects or cytotoxicity of systemic applied drugs or carriers can be decreased concomitant with smaller drug concentrations that are needed to reach therapeutic effects leading to an increase of treatment efficacies (Eccleston et al. 1996; Wang et al. 2002; Dong 2018). Especially in the case of recurrent GBM, the local administration of a drug can provide a promising strategy, as 80-90 % recur within the 2 cm tumor margin of the original resection (Zhong and Bellamkonda 2008; Wang et al. 2002). Most strategies for drug-loading brain implants are based on biocompatible polymeric scaffolds (Jain et al. 2006), which can be either biodegradable or non-biodegradable. Whilst with biodegradable polymers such as poly(lactic acid) (PLA), poly(lactic glycolic acid) (PLGA), poly(glycolic acid) (PGA), gelatin or collagen for instance (Fournier et al. 2003), the scaffold material will break down with the ongoing drug release into non-toxic products that can be further eliminated by the body, non-biodegradable scaffold materials will remain their size and shape even after full depletion of drug (Zhong and Bellamkonda 2008; Domb 1995). Amongst common non-biodegradable polymers, ethylene-vinyl acetate copolymers or various acrylate-based hydrogels are commonly used in experimental approaches for brain applications (Sawyer et al. 2006; Domb 1995). Although polymers such as PLGA have revealed some negative side effects in systemic applications, the tissue response in local injections/administration of PLGA into the brain was moderate, as only non-specific inflammatory reactions occurred possibly due to the mechanical trauma after implantation (Menei et al. 1993; Lillehei et al. 1996; Kou et al. 1997; Emerich et al. 1999; Fournier et al. 2003). Moreover, the drug-release properties of PLGA polymers can be tailored by the variation of lactic acid to glycolic acid monomer ratios (Lewis 1990). In 2007, different PLGA-based scaffolds such as microspheres, microparticles and discs for the local drug delivery of paclitaxel and etanidazole in C6 glioma mouse model have been evaluated for their *in vivo* performance (Kumar Naraharisetti et al. 2007). After 21 days, tumor volumes shrink upon treatment to up to 59 %, 65 % and 70 % for microspheres, microparticles respective discs (Kumar Naraharisetti et al. 2007). However, Wang and others claimed that the drug-release-driven bulk erosion of PLGA can cause sporadic dumping of drugs and therefore toxic effects (Wang et al. 2002; Brem

and Langer 1996). As a result, a biocompatible polymer whose degradation is based on surface-erosion, poly[bis(p-carboxy-phenoxy propane anhydride) sebacic acid] (PCPP-SA), was developed and successfully implemented as scaffold material for the release of carmustine, as the already mentioned Gliadel® wafer (Bota et al. 2007; Ashby et al. 2016). Since then, similar approaches based on PCPP-SA polymers have been followed. As such, cancer-cell specific aerobic glycolysis-inhibitors such as 3-bromopyruvate (3-BrPA) and dichloroacetic acid (DCA) have been loaded into PCPP-SA wafers and significantly increased survival in glioma animal models as well as the combination of 3-BrPA-polymer with TMZ could provide synergistic effects (Wicks et al. 2015). Moreover, the combination of carmustine and TMZ loaded in CPP-SA polymer scaffolds caused improved survival in rodent 9L gliosarcoma and F98 glioma *in vivo* models in combined X-ray treatment (Recinos et al. 2010).

Hence, Belousov et al. claim, that artificial implants for local drug administration in operation cavities should be incorporated into hydrogels that mimic biomechanical properties of the healthy brain tissue for vital function support for example (Belousov et al. 2019). In brief, the mechanical support of hydrogels can provide structural and functional restoration of damaged brain tissue and influence cell fate. The variety of hydrogel polymers, such as hyaluronic acid, collagen type I, alginate, chitosan, self-assembling proteins and peptides or poly(ethylene glycol) for instance, that are extensively studies in recent brain applications, offer broad tailorable physical, biological or chemical properties (Kornev et al. 2018).

However, disadvantages of local drug delivery by implants remain, that dosages can up to now be adjusted after implantation as well as that drug-release rates may start with an unwanted burst-release followed with a decrease over the time, requiring possibly repeated implantation and surgery (Zhong and Bellamkonda 2008; Meilander et al. 2003; Dang and Saltzman 1994). Therefore, the right delivery system with its properties such as drug loading, drug release kinetics, biocompatibility etc. must be chosen in advance for the respective disease.

Nanoformulations for local drug delivery

Moreover, also nanoformulations or combinations of nanoformulations in 3D scaffolds can be used for local drug administration in the brain. For example, nanocarriers can be incorporated into a scaffold material and placed into the resection cavity of the brain after surgery (similar as with brain implants) or used in flexible hydrogels that can be injected directly into the CNS via syringes. Several rodent *in vivo* studies based on the local injection of drug-carrying NPs to deliver anti-tumor agents such as mitoxantrone, platelet factor 4 fragment, carboplatin or hemopexin for instance (Chen et al. 1997; Menei et al. 1996; Benny et al. 2005), but also for the treatment of neurodegenerative diseases such as Parkinson's disease using the application of neurotransmitter encapsulated PLGA NPs (McRae and Dahlström 1994) have been performed. In more recent studies, drug-loaded PLGA NPs, such as camptothecin-loaded PLGA NPs, have been used for convection-enhanced delivery (CED), whereas syringe pumps generate an external pressure gradient for a continuous and well distributed drug delivery and have demonstrated to be effective in an intracranial tumor model [see figure 1, treatment innovations (Sawyer et al. 2011; Patel et al. 2017; Bobo et al. 1994)].

Besides the direct injection of the nanoparticles into the CNS, the incorporation into a hydrogel with similar properties as the brain tissue for a longer and more sustained release of the particles/drugs can be of interest (Belousov et al. 2019). For example De la Puente et al. could show improved survival and decreased tumor sizes of GBM mice, after treatment with Iodine-131 (^{131}I) and TMZ alginate-microparticles, when incorporated into hydrogels for chemo- as well as radiotherapy (La Puente et al. 2018). In a similar approach, however with different chemotherapeutic drugs such as Gemcitabine incorporated into a lipid nanocapsule-based hydrogel, Bastiancich et al. obtained over one month a sustained drug release concomitant with a significant increase of survival as well as decrease of recurrences in a tumor xenograft model (Bastiancich et al. 2017; Bastiancich et al. 2016). Tyler and others demonstrated in pre- and early clinical studies, that

paclitaxel loaded PLGA NPs incorporated into hydrogels (OngoGel™), could moderately increase survival in rat gliosarcoma model (Rahman 2014; Tyler et al. 2010). In other approaches, doxorubicin, paclitaxel, CRISPR/Cas-mediated DNA and proteins or camptothecin encapsulated in liposomes, micelles or polymeric NPs incorporated into hydrogels have successfully reduced tumor growth, increased cytotoxicity and elongated survival concomitant with sustained drug release profiles in different *in vitro* or rodent *in vivo* models (Arai et al. 2010; Tao et al. 2017; Chen et al. 2017; Ozeki et al. 2010; Ozeki et al. 2012; Basso et al. 2018). Other groups, that focus on the development of implantable scaffolds, that do not cause any inflammatory reactions and therefore brain foreign body responses, suggest the use of hydrogels as promising "buffer" materials for the incorporation of their scaffold (Maclean et al. 2018). Ashton et al. produced alginate hydrogels with adjustable degradation rates and encapsulating polymeric microspheres, that allowed neural progenitor cells to grow on and into that scaffold (Ashton et al. 2007) or in another approach, Maclean and others used a multifaced anti-inflammatory hydrogel system to reduce glial scarring after traumatic brain injury (Maclean et al. 2017). More information on the brain foreign body response and ways to alleviate them are discussed in chapter 1.3.3 **Challenges in brain drug delivery**.

1.3.2.2 Neural electrodes

Besides drug delivery approaches, there are many other biomaterial applications for the central nervous system. Amongst them are chronic electrode implants for the measurement or stimulation of neuronal activity in deep brain stimulation applications or brain-computer interfaces. Whereas recording-based devices are used for the control of a mechanical device such as the control of a motorized wheelchair by thoughts of a paralyzed person (Donoghue 2002; Pesaran et al. 2006), stimulation-based devices are mainly used for the symptom-reduction in Parkinson's disease or to restore hearing (Zhong and Bellamkonda 2008; Benabid et al. 2000; Colletti et al. 2001), to date. In other applications such as for patients with impaired movements caused by neurodegenerative diseases like multiple sclerosis respective amyotrophic lateral sclerosis or stroke or spine injuries, recording-based cortical neural prosthetics offer great promise, however remain still in research stage as of stability problems during long-term recording (Zhong and Bellamkonda 2008; Ludwig et al. 2006; Santhanam et al. 2006). One major contributing factor that influences the recording ability of implants is the formation of a glial scar around the electrodes, concomitant with an inflammatory reaction of the brain towards the foreign body and will be discussed in more detail in chapter 1.3.3.2 **Brain foreign body response**. Currently, many investigations are based on the development of multichannel microelectrode arrays for long-term cortical neuronal recordings, that include polymer substrate probes, silicon based micromachined microprobes but also microwires. Typical materials for microwire design are with Teflon or polyimide insulated conductive metals such as platinum, gold, iridium, tungsten or stainless steel. However, in the past decade, graphene-based materials have become a hot-spot so far, due to their remarkable electronic, mechanical, optical and thermal properties (Huang et al. 2012) and have been actively investigated to build new composite materials for instance (Wang et al. 2011; Li et al. 2008b). To mention some of them, graphene exhibits a large theoretic specific surface area (Stoller et al. 2008), a high Young's modulus (Lee et al. 2008) as well as excellent thermal stability and conductivity (Balandin et al. 2008; Huang et al. 2012). Especially its extraordinary conductive behavior makes graphene one of the most interesting materials in electrode design for solar cells or light emitting diodes, but also in brain applications. Whereas some biological studies on the effects of graphene-based materials, such as graphene oxide (GO) or reduced graphene oxide (rGO) are available, still little information is given about their *in vitro* and *in vivo* biocompatibility in brain applications, as well as their effects on glial scar formation and inflammation reactions. As such, Wang and others reported a dose-dependent systemic toxicity of GO nanoparticles when injected intravenous in mice (Wang et al. 2011) or on different cell lines (Liao et al. 2018; Pelin et al. 2018), Li et al. investigated the influence of GO/rGO surface chemistry among the lipid membrane and reported that hydrated GO micro sheets can cause membrane lysis and the destruction of cell integrity due to lipid oxidation (Li et al. 2018b), respective the investigation of macrophage immune

responses towards GO materials (Ma et al. 2015; Russier et al. 2013; Mendes et al. 2015), whereas macrophages induced several pro-inflammatory cytokines and chemokines upon contact with GO (Zhang et al. 2016), however rGO provoked higher levels of cytokine induction (Wu et al. 2018). In the few available reports on brain applications, Mendoza and colleagues investigated cytotoxic effects of rGO on cells of the blood-brain barrier (Mendonça et al. 2016a), however systemically applied rGO that passed the blood-brain barrier did not cause cytotoxic effects in mice, nor inflammation in rat hippocampus (Cherian et al. 2020; Mendonça et al. 2016b). Contrary to that, GO nanoparticles, when applied systemically, induced oxidative stress and therefore genomic instability and mutagenicity in mice liver and brain tissues (Mohamed et al. 2019), but showed promising results in neuron-encapsulation applications for the 3D tissue growth (Sakai et al. 2019), the differentiation and proliferation of neural stem cells (Fu et al. 2019) as well as nerve-tissue engineering (Ginestra 2019).

Exactly these contradictory findings enhance the necessity to investigate brain-graphene-based material interactions more deeply, to produce safe implants for brain applications.

1.3.3 Challenges in brain drug delivery

The drug delivery for the treatment of CNS diseases still remains a challenge due to the inability of therapeutic agents to cross the blood-brain barrier (BBB) (Patel et al. 2012; Yang 2010). In brief, there are two main criteria for lipid mediated free diffusion across the BBB, namely the size of the transport molecule which needs to be below 500 Da (molecular weight), as well as a high lipid solubility concomitant with low hydrogen bonding (Pardridge 2012). However, almost no drugs fulfill these criteria, increasing the need for alternative drug delivery approaches to the CNS. Whereas some approaches are based on the development of reengineered drugs or transport carriers such as the in chapter 1.3.2.1.1 **Systemic drug delivery systems** discussed nanoformulations, others focus on the local drug delivery via brain implants (chapter 1.3.2.1.2 **Local drug delivery systems**). However, also the local administration of drugs via implants requires careful consideration of the potentially damaged healthy brain tissue as well as surgery- and implant-mediated inflammatory reactions of the brain.

In this chapter, two biological challenges such as the BBB as well as the brain foreign body response for systemic respective local drug delivery are being highlighted.

1.3.3.1 Blood-brain barrier

The blood-brain barrier is a physiological barrier between the blood and the brain, whose function is to regulate CNS homeostasis as well as the protect the CNS from inflammation, toxins and pathogens but also injury and diseases (Daneman and Prat 2015). Therefore, BBB dysfunction which can be caused by neurological diseases or brain traumas, can lead to altered signaling homeostasis, the dysregulation of ions or the entry of immune cells into the brain and therefore lead to degenerative processes and neuronal dysfunction (Daneman and Prat 2015).

The BBB consists of two epithelial membranes, the abluminal and luminal membrane of the brain capillary endothelial cells, with an around 200nm thick gap of endothelial cytoplasm (Pardridge 2012). Moreover, the BBB is supported by immune cells, two basement membranes (BM; inner vascular and outer parenchymal BM, also called *vascular glia limitans perivascularis (Del Zoppo et al. 2006)*) of different extracellular matrix compositions as well as of astrocytes. Astrocytes are one major glial cell type of the brain with various functions such as metabolic and physical support of neurons, regulation of energy metabolism respective reaction to injury (Polikov et al. 2005). They play a role in BBB function and regulation by secreting several factors and provide a cellular link between the neuronal circuit and blood-distribution, due to the sheathing of blood vessels by astrocyte-endfeet (Daneman and Prat 2015). Consequently, astrocytes are enabled to regulate blood flow, such as the contraction/dilation via secretion

of signaling molecules as response to neuronal activity (Daneman and Prat 2015; Attwell et al. 2010; Gordon et al. 2011). However, although some studies highlight astrocytes function in BBB-formation, such as the induction of BBB properties in non-CNS vascular systems (Janzer and Raff 1987), others claim that the formation of BBB already happens before the generation of astrocytes (Daneman et al. 2010). Other important functions of astrocytes in the CNS are discussed in Chapter 1.3.3.2 **Brain foreign body response**.

Other than in the peripheral vascularization, the endothelial cells of the BBB are connected with each other by high resistance tight junctions with substantial transendothelial electrical resistance (TEER) and therefore creating a physical barrier for the paracellular transport of ions, molecules, cells and therapeutically substances to the brain (Patel et al. 2012; Zlokovic 2008; Daneman 2012). Besides this physical barrier, the BBB also contains metabolic barriers such as the minimal allowed pinocytosis of endothelial cells, for instance, which limits the highly nonspecific transcellular transport (Brightman and Reese 1969). Moreover, extracellular enzymes of BBB-endothelial cells can inactivate compounds in their try to pass the BBB and many efflux transporters are available on the capillary endothelium (Patel et al. 2012). Hence, efflux transporters such as multi-drug-resistance-gene 1 (Mdr1), breast cancer resistance protein (BCRP) or multidrug resistance proteines (MRPs) (Ha et al. 2007), which are polarized on the luminal surface of the epithelial cells, transport actively under hydrolysis of adenosine triphosphate (ATP), lipophilic molecules from the CNS towards the blood (Löscher and Potschka 2005; Cordon-Cardo et al. 1989; Thiebaut et al. 1989; Daneman and Prat 2015) and therefore strongly influence the success-rate of BBB-passaging substances (see figure 3, efflux transport).

As the para- and transcellular transport of substances is greatly inhibited physically by tight junctions respective metabolically by efflux transporters, only few other but also highly regulated pathways are available for the transportation of molecules or drugs to the CNS (figure 3). In brief, drugs can only enter the CNS via passive diffusion or by carrier/receptor mediated transport actively through the BBB. The passive diffusion of lipophilic or lipophobic drugs is controlled via concentration gradient, however paracellular pathways of lipophobic substances is negligible due to the tight junctions between epithelial cells (figure 3, right). Conversely, the receptor- respective carrier-mediated transport is controlled actively. As such, there are highly specific protein transporters available on epithelial cells such as glucose, lactate or pyruvate transporters (Daneman 2012; Zlokovic 2008), which allow the transport of nutrients across the BBB into the brain but also function in the clearance of waste products from the CNS into the blood (Mittapalli et al. 2010). Last, drugs can also pass the BBB via different endocytosis pathways, for instance the receptor-, adsorptive- or cell-mediated pathway (see figure 3, left). While proteins like insulin or transferrin can bind specifically to their membrane receptor and be transported through the epithelial cells by receptor-mediated endocytosis, albumin is transported via adsorptive-mediated transcytosis. Moreover, in case of inflammation due to neurological diseases for example, drugs or nanocarriers can be uptaken by immune cells and transported via cell-mediated transcytosis to the brain. A detailed overview of the different BBB-passage mechanisms is depicted in figure 3.

All these different transport mechanisms influence strongly the design of drugs or drug-carriers. Although many investigations to successfully transport drugs through the BBB are currently pursued, such as the targeted drug delivery via endothelial surface receptors and other examples highlighted in Chapter 1.3.2.1.1 **Systemic drug delivery**, *nanoformulations*, the BBB transport still remains a challenge. On the one hand, only 2 % of all small molecules which are supposed to cross freely the BBB also pass it in reality. On the other hand, substances that freely pass the BBB still have to be administered in systemically high concentrations to obtain blood concentrations high enough to allow a concentration gradient-dependent diffusion (figure 3, right). Likewise, high concentrations which may have therapeutically effects in the brain, can cause systemically toxicity in other organs. Moreover, with progressing age as well as neurodegenerative diseases such as Alzheimer's or Parkinson's disease but also brain tumors such as GBM,

the BBB structure and function changes, which complicates the universal fabrication of a drug delivery system (Pandit et al. 2019).

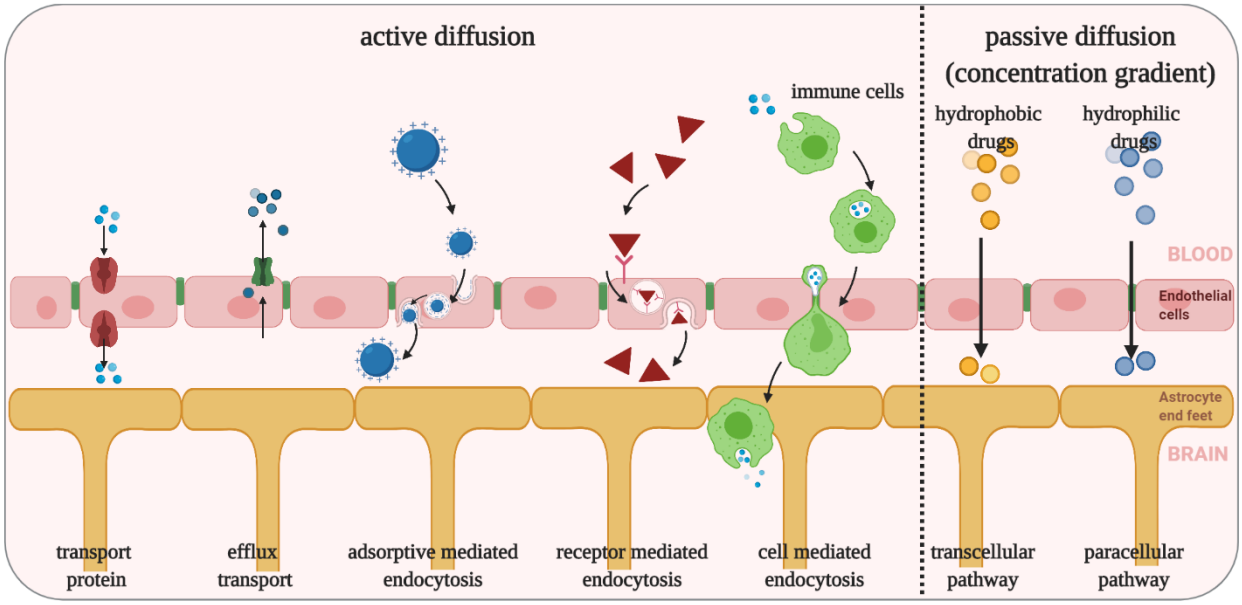

Figure 3: Possible transport mechanisms of drugs through the blood-brain barrier (BBB). *The blood-brain barrier consists of endothelial cells and their tight junctions (green), immune cells, two basement membranes as well as of astrocytes, which are sheathing the blood vessels with their end feet and therefore play an important role in BBB function and regulation. Transport mechanisms can be divided into active (left) and passive (right) transport mechanisms. Whereas in passive mechanisms, the transport is regulated by a concentration gradient that allows hydrophobic drugs to transcellular pass and hydrophilic drugs paracellular pass the blood-brain barrier, several different ways in active transport are possible. The active diffusion of drugs can be mediated by transport proteins or energy-consuming efflux transport, as well as by different types of endocytosis, depending on the molecular structure. Modified by Georgieva and van Rooy (Georgieva et al. 2014; van Rooy et al. 2011).*

1.3.3.2 Brain foreign body response

Especially in such medical cases, in which a patient anyway must undergo brain surgery (e.g. GBM tumor resection), the implantation of a local drug delivery device can be a promising tool to successfully circumvent the challenging drug-transport through the BBB and to locally treat remaining GBM-cells in lower concentrations post-surgery. Hence, an inflammatory reaction of the brain in response to surgery remains as well as the possibility of a brain foreign body response towards the implanted material.

In general, the brain foreign body response can be divided into three phases, as depicted in figure 4: the acute, the early and the chronic phase.

The insertion of a neuroimplant causes a brain injury which can impact nearby cell functions (Wellman and Kozai 2017). In fact, next to the disruption of the blood vessels concomitant with an influx of blood-derived immune cells and proteins (Spataro et al. 2005; Polikov et al. 2005), also nearby glial cells and neurons are damaged. In response to that, neurons and glial cells release several pro-inflammatory cytokines such as macrophage colony stimulating factor (M-CSF) respective ATP and therefore cause the activation of microglial cells in the direct surrounding of around 50 µm of the injury site (compare Figure 4 B) (Groothuis et al. 2014; Davalos et al. 2005).

The acute phase follows the early inflammatory phase of the brain tissue (see Figure 4 C) against the implant, which takes place in the first week after insertion. Due to the released cytokines and chemokines from activated microglial cells such as interleukin-6 (IL-6), interleukin-1β (IL-1β), transforming growth factor β (TGF-β), tumor necrosis factor α (TNF-α) or the monocyte chemotactic protein-1 (MCP-1), but

also reactive oxygen species (ROS) such as hydrogen peroxide, or reactive nitrogen intermediates such as nitric oxide (NO) (Woodroofe et al. 1991; Giulian et al. 1994a; Giulian et al. 1994b; Chabot et al. 1997; Babcock et al. 2003; Polikov et al. 2005; Zielasek et al. 1996), astrocytes become reactive and proliferate towards the implant site so that a loose sheath is built by activated glial cells. Further, these cytokines/chemokines also introduce additional stress on neurons and therefore causing neuronal apoptotic cell death (Wellman and Kozai 2017), but also negatively influence endothelial cells (Kozai et al. 2015).

Lastly, in a process over several weeks, the chronic phase takes place (Figure 4 D). A dense glial sheath is formed around the implant site, with special physical properties. The activated microglial cells still remain near the implant materials surface, which can be associated with microglial "frustrated phagocytosis" (Weldon et al. 1998) and are surrounded by a compact astrocyte layer. Since it has been shown that acute inflammation in investigations of stab wound studies can disappear after the healing of the tissue without the onset of chronic tissue responses, one can suppose that chronic inflammatory responses of the brain tissue are in line with the implantation of a foreign body and not due to the brain injury while implantation (Wellman and Kozai 2017).

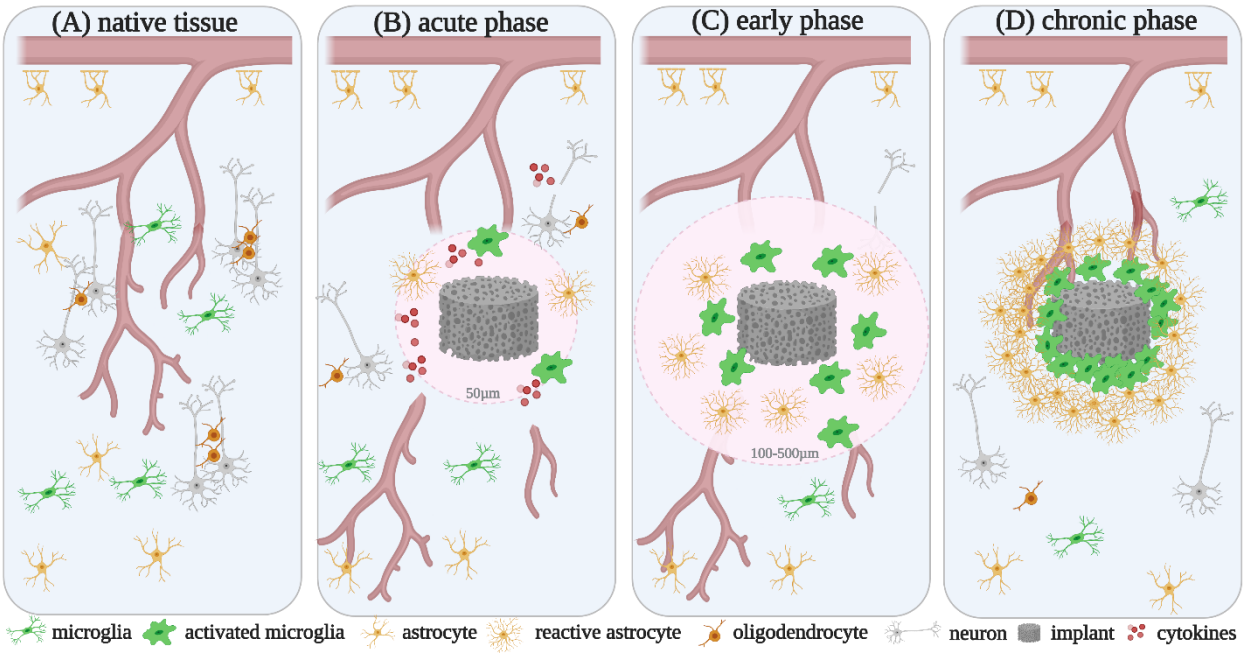

Figure 4: Simplified visualization of the brain foreign body response after the insertion of a brain implant. ***(A)*** *Cellular components in the native tissue.* ***(B)*** *In the acute phase of injury post implantation (several hours), vessel walls are disrupted, neurons and glial cells are damaged and therefore cause an influx of blood-born immune cells as well as release of pro-inflammatory cytokines from damaged cells. As inflammatory response, microglia and astrocytes of the direct implant surrounding (≈50 µm) become reactive.* ***(C)*** *In the early phase (first seven days), microglia and astrocytes in the larger surrounding (several hundred µm) become reactive due to the release of more pro-inflammatory cytokines by microglial cells. More astrocytes and microglia cells proliferate to the implant site and build a loose sheath around it.* ***(D)*** *The chronic phase (several weeks) is characterized by a dense glial sheath around the implant site. Although microglial cells are still associated to the implant-surrounding, the dense glial scar with its mechanical integration is caused by the reactive astrocytes. The figure was created with Biorender.com*

Consequences of these reactive tissue responses can be the encapsulation of the implant by glial cells and the thereby caused severe influence in implant function and performance of both drug delivery devices and electrodes. Since there is a long history in electrode design for brain applications more information is available on tissue reactions against those. In fact, electrodes are insulated from nearby neurons due to the glial sheath which is formed around it which in particular can cause an increase in impedance, hindering diffusion (Biran et al. 2005) as well as diminishes the ability to record and/or stimulate in long-term

applications (Marin and Fernández 2010; McConnell et al. 2009). Moreover, it has been shown that device implantation leads to an altered neurochemical signaling, which vice-versa also influences implant-performance (Kozai et al. 2015). In other studies on rigid silicon microelectrodes a multiphasic neuroinflammatory response after long-term insertion in rats has been observed (Potter et al. 2012), which in return could be prevented by antioxidant release with resveratol (Potter et al. 2013).

1.3.3.2.1 Neuroinflammation

A major key player of the brain foreign body response are microglial cells which constitute around 5-10 % of the glial cells in the CNS (Gaudet and Fonken 2018). They find their origin in the brain via prenatal infiltration by blood-borne hematopoetic cells (Polikov et al. 2005; Ling and Wong 1993) and remain as resident macrophages of the brain. In the healthy brain inactive microglia have a ramified morphology with many branches (Nimmerjahn et al. 2005) and minimal antigen-presenting machinery compared to peripheral macrophages (Ransohoff and Perry 2009). Moreover, microglia *in vivo* and *in vitro* differ morphologically, since cultured microglia can be rounder and less branchy than *in vivo* (Jeong et al. 2013). The function of microglia are quite divers: They are versatile orchestrators of nervous system development and homeostatic control [(Qingyun and Barres 2018), for review see (Gaudet and Fonken 2018) and figure 5, A] and as such use the complement system to influence synaptic activity (Zhang et al. 2014), they remove synapse or define circuits (Paolicelli et al. 2011; Schafer et al. 2012; Stevens et al. 2007), produce trophic factors for neuron survival (Ueno et al. 2013) and axon growth (Pont-Lezica et al. 2014) during development, but also play a role in CNS maintenance including the phagocytosis of cellular (Sierra et al. 2010; Brown and Neher 2014) or myelin components (Safaiyan et al. 2016) as well as in vascular complicity by regulation of endothelial cells (Fantin et al. 2010). Upon damage, toxic substances or material contact, microglia become reactive and are active key players in the wound-healing process and the immune response of the brain (Gaudet and Fonken 2018). As a result of activation (figure 5, C) , microglia change to an amoeboid morphology with less branches, however a highly motile and phagocytotic phenotype and release proinflammatory cytokines and chemokines (as mentioned above), which in response can active astrocytes.

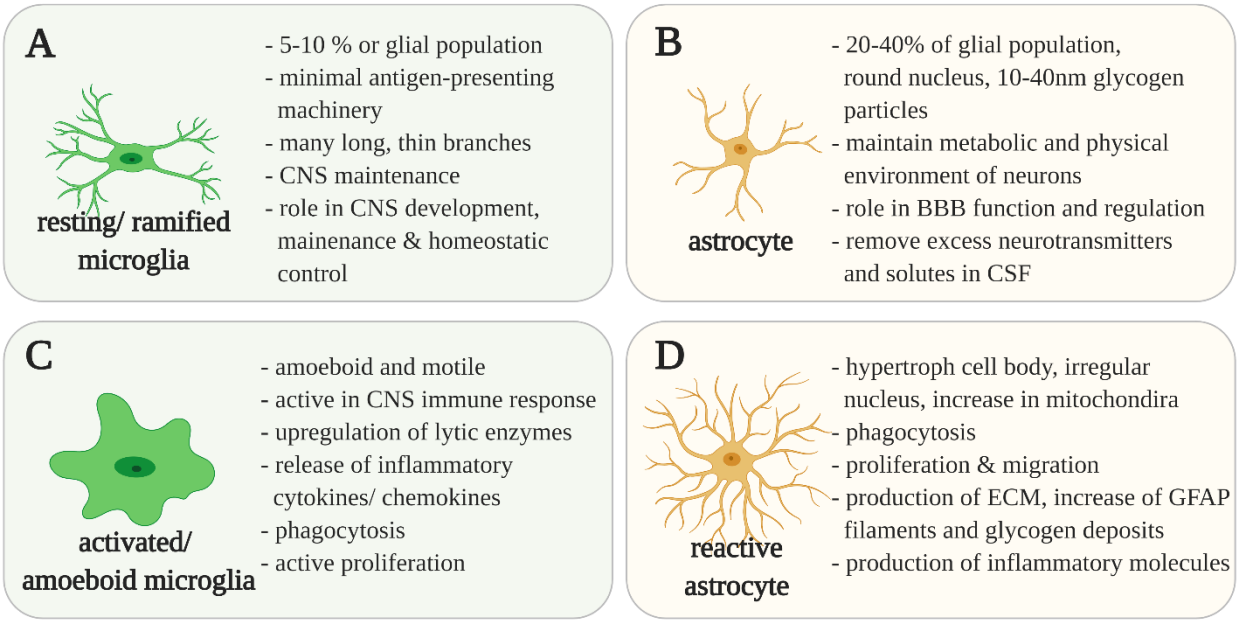

Figure 5: Schematic overview of physiology and functions of resting microglia (A) respective astrocytes (B) and their transformation after activation as response to disease, damage or brain implant materials (C, D). *Figure was generated using Biorender.io software*

1.3.3.2.2 Reactive astrogliosis

The reactive gliosis as a response to neuroinflammatory processes in the brain, is part of the brain foreign body response but also in brain injuries to protect healthy tissue from harmful/toxic outside influences and causes in chronic progression the formation of a glial scar respective glial sheath (Nathaniel and Nathaniel 1981; Landis 1994). The easy to visualize scar tissue is derived by changes in proliferation, morphology and gene and protein expression levels in astrocytes as response to pro-inflammatory cytokines and chemokines such as IL-1, IL-6, TNF-α or TGF-β. Astrocytes constitute around 20-40 % of all cells in the mammalian CNS, with a starshaped morphology in healthy brain and interact with nearly all other cell types in the brain (see figure 5, B). Besides their functions already mentioned in chapter 1.3.3.1 **Blood-brain barrier** and also depicted in figure 5 B, astrocytes control neuron health and activity (Nortley and Attwell 2017; Rose and Chatton 2016) and play a role in the removal of excess neurotransmitters from the extracellular space (Filosa et al. 2006; Petr et al. 2015) or solutes in the cerebrospinal fluid (Iliff et al. 2012) in the healthy brain. In response to inflammatory processes, damage or foreign bodies however, astrocytes become hypertrophic and produce different extracellular matrix molecules due to overexpression of certain genes (figure 5 D). The by far most described glial scarring marker is the glial fibrillary acidic protein (GFAP), whose overexpression is a hallmark of gliosis (Fawcett and Asher 1999; Fitch and Silver 2008; Gaudet and Fonken 2018). However, it has been shown, that the upregulation of certain genes in astrocytes is on the one hand dependent on the distance from the lesion/implant site, but also on the ontological identity of the cells. Hence, astrocytes are a heterogeneous cell population, which can be classified by their genetic variation, location in the brain or their origin and therefore do react differently in the process of glial scarring [for review see ley (Chaboub and Deneen 2012)]. In brief, whereas GFAP overexpression may extend around 1cm from the injury (Abnet et al. 1991; Eng et al. 1987), astrocytes that are more close to the lesion site upregulate nestin and vimentin for instance (Fawcett and Asher 1999). Vimentin, in particular, can be expressed in reactive astrocytes however not in mature astrocytes (Fitch and Silver 2008). Aside from that, neuronal stem cell derived astrocytes in fact express less GFAP in comparison to vimentin. Wang and Walz have described different areas of fibrotic tissue around a lesion core in adult rats, which could be classified with distinct expression of glial scarring markers such as S100β, GFAP and vimentin (Wang and Walz 2003). Moreover an increase of chondroitin sulfate proteoglycans (CSPGs) and extracellular proteins such as tenascin-c are part of the glial scar tissue (Gaudet and Fonken 2018; McKeon et al. 1991), however ependymal-derived astrocytes in the lesion penumbra do not synthesize CSPGs (Meletis et al. 2008). Besides the induced expression of extracellular matrix molecules, reactive astrocytes also upregulate the secretion of cytokines such as TGF-b, IL1-b or IL-6 for instance [(Karimi-Abdolrezaee and Billakanti 2012), for review see (Gaudet and Fonken 2018)].

Indeed, the glial scar tissue serves as a major barrier for the regeneration of axons as well as the function of an implant device such as the drug-release or electrode performance in drug delivery respective microsensing devices. Likewise, the heterogeneity of astrocyte population and their response upon reactivation increase the need for more realistic *in vitro* models to study the complex brain-implant material reactions.

1.3.3.3 Strategies to attenuate inflammatory and reactive gliosis reactions in the CNS

One way to address inflammatory and reactive gliosis reactions in the CNS is by the application of anti-fibrotic and -inflammatory drugs, such as the already mentioned drug resveratrol, which improved neuronal viability around implanted intracortical microelectrodes in rats (Potter et al. 2013),. Besides this, a strategy to attenuate those reactions can be by the adaption of implant design, material and microstructure for instance, which will be discussed in the following chapters.

1.3.3.3.1 Implant design and modification

Different strategies for the maintenance of implant as well as brain tissue integrity have been investigated. Amongst them, different size, shape and cross-sectional area (Polikov et al. 2005) as well as texture or electrode tip geometry (Szarowski et al. 2003) have been modified to minimize tissue reactions towards implants. In particular, Thelin et al. demonstrated that size and also fixation of implants strongly influences tissue reactions towards electrodes in rats *in vivo*. In brief, comparing implants of 50 to 200 µm in diameter with and without fixation to the scull, smaller and untethered implants could cause less tissue reactions (Thelin et al. 2011). Szarowski and others have shown that the reactivity of astrocytes is proportional with the increasing device diameter in rats over 12 weeks post implantation (Szarowski et al. 2003). Next to the physical parameters of the implant, other approaches are based on the surface modification of implants such as by biocompatible coatings or bioactive surfaces. Focusing on the survival and growth control of neurons, peptide modifications that are based on cell adhesion protein motifs such as RGD (Kam et al. 2002), or YIGSR (Cui et al. 2003) and IKVAV in extracellular matrix proteins such as in laminin (Kam et al. 2002) have been successfully exploited in *in vitro* and *in vivo* models. As such, the modification of polyimide microwires by the peptide KHIFSDDSSE which can be found on neural-cell adhesion molecules, caused astrocytes adhering within 24 hours and could effectively improve the tissue integration of active microglial cells on the device surface (Sridar et al. 2017). In a similar attempt, other groups focus on the attraction or repel of glial cells, rather than on neurons themselves (Polikov et al. 2005). In particular, Eles and others have shown, that the biomimetic surface coating of neural electrodes with the cell adhesion molecule L1 successfully attenuated microglial ensheathment towards the implanted probes in mice brain *in vivo* (Eles et al. 2017). Moreover, the embedding of brain implants into hydrogel systems, which was already discussed in chapter 1.3.2.1.2 **Local drug delivery systems** can be another strategy to diminish brain foreign body responses towards implants (Maclean et al. 2017).

1.3.3.3.2 Anti-inflammatory drugs in the CNS repair

Besides implant design and material, other approaches to reduce cellular reactions towards implant materials can be the use of anti-inflammatory respective -oxidative substances or the release of growth factors and chemoattractants (Polikov et al. 2005; Groothuis et al. 2014). In the past years, especially the corticosteroid anti-inflammatory drug dexamethasone (DEX) has shown great promises to reduce brain foreign body reaction *in vitro* and *in vivo*. Whereas DEX has a variety of negative side effects when applied systemically (Zhong and Bellamkonda 2007), many investigations focus on the incorporation of DEX into implant coatings (Zhong and Bellamkonda 2007) or by encapsulation of DEX into nanoparticles which can then be incorporated into polymer coats of implants (Mercanzini et al. 2010; Kim and Martin 2006) for local drug delivery. In 2007, Zhong and others could reduce astrocyte response as well as microglial reactivity and neuronal cell loss by surface coatings of implants with DEX-nitrocellulose after one to four weeks in rats *in vivo* (Zhong and Bellamkonda 2007). In retrodialysis application of DEX parallel with the implantation of implant probes in mice, DEX had profound effects on microglia morphology and activation (Kozai et al. 2016).

Curcumin

Amongst other possible anti-inflammatory compounds, the hydrophobic polyphenolic compound curcumin has gained significant interest in many studies as it is considered as an effective therapy for various diseases such as epilepsy, diabetic wound healing or even cancer (Babu et al. 2019; Djiokeng Paka et al. 2016). In particular, curcumin is a widely used food spicery and coloring agent, derived from the plant *curcuma longa*, which was found to be a very potent antioxidant and therefore its protective effects in different normal and cancer cells were evaluated previously [for review see (Lopresti 2018; Tejada et al. 2016; Di Meo et al. 2019)]. Systemically applied single doses of curcumin as food-supplement could halt lipopolysaccharide

(LPS)-induced neuroinflammation-associated neurodegeneration in rats via the JNK/NF-κB/Akt signaling pathway (Khan et al. 2019). In primary astrocyte *in vitro* models, 2 µM curcumin could effectively reduce LPS-induced apoptosis and glial scarring, by inhibition of GFAP, NF-κB and poly(ADP-ribose)polymerase (PARP) (Nedzvetsky et al. 2017). Others have shown, that curcumin alleviates oxidative stress and mitochondrial dysfunction in astrocyte cell lines *in vitro* (Daverey and Agrawal 2016) or curcumins anti-inflammatory and -oxidative properties on rat primary astrocytes by interference with toll-like receptor 4 (TLR4) and its downstream effectors such as NF-κB for instance (Yu et al. 2016). Moreover, in a clinical trial for the treatment of Alzheimer's disease, the systemically application of curcumin in oral doses up to 4 g/day over six months did not cause any chronic adverse effects nor effect patients' tolerability (Carroll et al. 2011).

However, curcumin is a highly hydrophobic and light sensitive drug, limiting its potential due to its low oral bioavailability and instability (Djiokeng Paka et al. 2016). Addressing this issue, the encapsulation of curcumin into nanoformulations as well as the local application of the drug can increase bioavailability and has been therefore shown in numerous publications (Djiokeng Paka et al. 2016; Basnet et al. 2012; Chen et al. 2012; Feng et al. 2017).

2nd CHAPTER

Publications

"It always seems impossible until it's done."

(Nelson Mandela)

Effects of sequentially applied single and combined temozolomide, hydroxychloroquine and AT101 treatment in a long-term stimulation glioblastoma *in vitro* model.

In this collaborative work, two potentially interesting drugs for the treatment of *glioblastoma multiforme* were employed for efficacy studies on two distinct TMZ-responding human glioblastoma cell lines (LN229, A172) as well as on human astrocytes (SVGA). Therefore, the BH3-mimetic AT101 as well as the quinoline based antimalarial drug HCQ were chosen, as their efficacy on GBM-treatment is based on different mechanisms of action than the standard therapeutic agent TMZ and therefore might positively influence GBM treatment considering tumor regression and treatment escape mechanisms. In brief, AT101 and HCQ were applied in drug concentrations of 2.5 µM respective 6 µM and used for constant stimulations of the single drug or in combination with 50 µM TMZ over six days. In comparison to that, sequential applied drug combinations of these alternative therapeutics and TMZ were employed by switching on day three either from a single drug (AT101,HCQ) to TMZ until day six and vice versa, or by switching from single drugs (AT101, HCQ or TMZ) to the combination of TMZ and the respective alternative drug and vice versa. The treatment efficacy and advantage over standard TMZ treatment was evaluated by comparing the cytotoxicity as well as effects on proliferation after three and six days of each drug combo in comparison to six days simultaneous stimulation with TMZ. To quantify the efficacy of sequentially applied drug combinations over the single drugs, combination indices were determined.

We could show, that sequentially applied single drugs, with the exception of HCQ/TMZ, are not favorable over the standard therapy using TMZ, as cytotoxic effects were less prominent as with TMZ solely. However, starting with HCQ and switching after three days to TMZ (HCQ/TMZ) gained slightly higher cytotoxicity levels and an improved growth control in GBM cell lines whilst not affecting healthy astrocytes, compared to TMZ standard treatment. Moreover, drug combinations starting with TMZ either continuously or when sequentially applied, did significantly increase cytotoxicity and reduce proliferation in in GBM cells and caused mostly similar effects in SVGA astrocytes compared to TMZ treatment, especially for the continuous simultaneous stimulation of TMZ+AT101 over six days or the sequential stimulation with TMZ and TMZ+AT101. However, while most stimulations with HCQ and its combinations also affected relative growth rates in healthy astrocytes, combinations with AT101 seemed to be the most promising ones as they did not or even positively affected growth rates in astrocytes, whilst having a better

tumor growth control in GBM cells comparted to TMZ treatment alone. Therefore, sequential treatment-combinations of drugs with different mechanisms of action seem to be promising strategies to reduce negative side effects for healthy astrocytes while maintaining efficient tumor cell toxicity in the long-term treatment of GBM patients.

The article is published in the "*journal of cancer research and clinical anatomy*".

Own contribution, presented in this article:

- Conceptualization and design of study
- Performing of *in vitro* experiments on human astrocyte cell line (SVGA)
- Analysis of data
- Discussion and interpretation of results on healthy and glioblastoma cells
- Editing of manuscript

The following content in this chapter is reproduced with permission.

Journal of Cancer Research and Clinical Oncology (2018) 144:1475–1485
https://doi.org/10.1007/s00432-018-2680-y

ORIGINAL ARTICLE – CANCER RESEARCH

Effects of sequentially applied single and combined temozolomide, hydroxychloroquine and AT101 treatment in a long-term stimulation glioblastoma in vitro model

Vivian Adamski[1] · Christina Schmitt[2] · Florian Ceynowa[3] · Rainer Adelung[3] · Ralph Lucius[2] · Michael Synowitz[1] · Kirsten Hattermann[2] · Janka Held-Feindt[1]

Received: 11 April 2018 / Accepted: 27 May 2018 / Published online: 1 June 2018

Abstract

Purpose *Glioblastoma multiforme* (GBM) is a poorly curable disease due to its heterogeneity that enables single cells to survive treatment regimen and initiate tumor regrowth. Although some progress in therapy has been achieved in the last years, the efficient treatment of GBMs is still a clinical challenge. Besides the standard therapeutic drug temozolomide (TMZ), quinoline-based antimalarial drugs such as hydroxychloroquine (HCQ) and BH3 mimetics such as AT101 were considered as possible drugs for GBM therapy.

Methods We investigated the effects of sequentially applied single and combined TMZ, HCQ and AT101 treatments in a long-term stimulation GBM in vitro model. We performed all investigations in parallel in human astrocytes and two differentially TMZ-responsive human GBM cell lines and adjusted used drug concentrations to known liquor/plasma concentrations in patients. We determined amounts of dead cells and still remaining growth rates and depicted our results in a heatmap-like summary to visualize which sequential long-term treatment schedule seemed to be most promising.

Results We showed that sequential stimulations yielded higher cytotoxicity and better tumor growth control in comparison to single TMZ treatment. This was especially the case for the sequences TMZ/HCQ and TMZ + AT101/AT101 which was as effective as the non-sequential combination TMZ + AT101. Importantly, those affected both less and more TMZ-responsive glioma cell lines, whilst being less harmful for astrocytes in comparison to single TMZ treatment.

Conclusions Sequential treatment with mechanistically different acting drugs might be an option to reduce side effects in long-term treatment, for example in local administration approaches.

Keywords R-(−)-gossypol · Alternative drugs · Sequential treatment · Quinoline-based drugs · BH3 mimetics · Autophagocytosis

Abbreviations

CHOP	CCAAT-enhancer-binding protein homologous protein
CI	Combination index
CQ	Chloroquine
DMEM	Dulbecco's modified Eagle's medium
DMSO	Dimethyl sulfoxide
ER	Endoplasmatic reticulum
FBS	Fetal bovine serum

Vivian Adamski and Christina Schmitt share first authorship.

Kirsten Hattermann and Janka Held-Feindt share senior authorship.

Electronic supplementary material The online version of this article (https://doi.org/10.1007/s00432-018-2680-y) contains supplementary material, which is available to authorized users.

✉ Janka Held-Feindt
Janka.Held-Feindt@uksh.de

[1] Department of Neurosurgery, University Medical Center Schleswig-Holstein UKSH, Campus Kiel, Arnold-Heller-Str.3, Building 41, 24105 Kiel, Germany

[2] Department of Anatomy, University of Kiel, 24118 Kiel, Germany

[3] Institute for Materials Science, University of Kiel, 24143 Kiel, Germany

GAAD-153	Growth arrest and DNA-damage-inducible protein
GBM	Glioblastoma multiforme
HCQ	Hydroxychloroquine
PARP	Poly-ADP ribose polymerase
TMZ	Temozolomide
QNX	Quinacrine

Introduction

Glioblastomas (GBMs) are highly malignant primary intracranial tumors that are characterized by prompt and infiltrative progression. Despite great improvements in (micro-) surgery and aggressive upfront treatment, patients' prognosis remains poor due to rapid relapses and a pronounced resistance to chemo- and radiotherapy (Ohgaki and Kleihues 2005). One major reason for this resistance is the complex intra- and intertumoral heterogeneity of GBMs. Here, GBMs are almost never composed of a single tumor cell population, but rather of a heterogeneous ensemble of cells that differ in many biological features, such as proliferation rate and drug resistance (Bonovia et al. 2011). As a result, under selective pressure (e.g. chemotherapy) individual GBM cell populations, that have acquired resistant properties, survive and are responsible for a tumor relapse after treatment (Bonovia et al. 2011).

To date, temozolomide (TMZ) is the most widely used first-line chemotherapeutic drug, concomitantly utilized with radiotherapy, for the treatment of adults with GBMs, as well as using solely TMZ as a maintenance treatment (Yan et al. 2016). However, to overcome the pronounced chemoresistance of GBMs and in perspective to promote local drug administration with minor side effects, several alternative drugs have been developed (Arevalo et al. 2017).

Besides others, quinoline-based antimalarial drugs such as quinacrine (QNX), chloroquine (CQ) or hydroxychloroquine (HCQ) (Golden et al. 2015), as well as BH3 mimetics such as AT101, the R-(−)-enantiomer of the natural occurring cottonseed-derived polyphenol gossypol (Lu et al. 2017; Opydo-Chanek et al. 2017) were considered as possible drugs for GBM therapy. Importantly, in contrast to TMZ whose therapeutic benefit depends on its ability to alkylate/methylate DNA most frequently at the N-7 or O-6 positions of guanine residues, quinoline-based drugs and BH3 mimetics own different mechanisms of action. CQ and HCQ are able to block autophagy and exert cytotoxic effects not only by promoting endoplasmatic reticulum (ER) stress, but also by induction of CCAAT-enhancer-binding protein homologous protein (CHOP)/growth arrest and DNA-damage-inducible protein (GADD-153) and poly(ADP-ribose) polymerase (PARP) expression (Golden et al. 2015; Yan et al. 2016). AT101 competitively binds to hydrophobic surface grooves of pro-survival Bcl-2 family members, counteracting their protective effects and facilitating apoptosis in tumor cells (Opydo-Chanek et al. 2017) and is also able to trigger autophagic cell death (Voss et al. 2010; Warnsmann et al. 2018). Consequently, when complementing the different kinds of action of TMZ/quinoline-based drugs or TMZ/BH3 mimetics, this could be a promising approach to overcome GBM chemoresistance.

Indeed, some of such combined drug treatment strategies were investigated. For instance, Jarzabek and colleagues (2014) showed that a combined gossypol/TMZ treatment of GBM was associated with inhibition of tumor-associated angiogenesis, invasion and proliferation, and Keshmiri-Neghab et al. (2014) demonstrated that gossypol significantly inhibited clonogenic growth of radiation-affected GBM cells. Further, CQ, HCQ and QNX were able to enhance TMZ cytotoxicity (Golden et al. 2015) and could potentiate chemosensitivity of glioma cells to TMZ via blocking autophagy (Lee et al. 2015; for review; Yan et al. 2016). Consequently, both gossypol and quinoline-based drugs were included in clinical trials. In detail, gossypol had a low but measurable response rate in patients with recurrent or progressive GBMs (Bushunow et al. 1999), and was implemented in a non-randomized phase I trial in combination with TMZ with or without radiation therapy for patients having newly diagnosed GBMs (NCT00390403). In combination with conventional GBM therapy, CQ revealed the ability to prolong survival from 11.4 to 25 months in patients with GBM (Bricenõ et al. 2007), and the combination of quinoline-based drugs and TMZ significantly increased the number of therapy-associated autophagic vacuoles in the peripheral blood mononuclear cells of GBM patients (Li et al. 2008). Since studies demonstrated that CQ and HCQ were equipotent autophagy inhibitors, but HCQ was characterized by a safer toxicity profile (Gunja et al. 2009), HCQ was tested also in phase I/II trials in conjunction with radiation therapy and concurrent and adjuvant temozolomide treatment in patients with newly diagnosed GBMs (NCT00486603, Rosenfeld et al. 2014) as well as in patients with advanced solid tumors and melanoma (Rangwala et al. 2014).

Although some of these approaches seem to be promising, the balance of a useful dose-limiting toxicity versus a consistent positive therapeutic response is still a clinical challenge. Recent approaches usually focus on effects of combined TMZ/quinoline-based drugs or TMZ/BH3 mimetics (accompanied or not by radiotherapy). The therapeutic response to sequentially long-term applied conventional GBM drugs (TMZ) and quinoline-based drugs or BH3 mimetics has not been consistently analyzed, yet. Such a sequential approach could be preferable due to (possibly) smaller side effects, the application of (possibly) lower drug concentrations based on a long-term treatment, and,

finally since it could be transferred to a local drug administration system with long-term sequential drug release, in perspective.

Thus, we consistently investigated the effects of sequentially applied single and combined TMZ, HCQ and AT101 treatments in a long-term stimulation GBM in vitro model. Regarding not only the known toxicity of different drugs on healthy cells (Bae et al. 2014; Lu et al. 2017; Rangwala et al. 2014; Rosenfeld et al. 2014), but also the differerential chemosensitivity of individual GBM cells (Bonovia et al. 2011), we performed all investigations in parallel under exactly the same conditions in human astrocytes (SVGA) and two different human GBM cell lines (LN229 and A172). Referring to published results of our own and other groups (Adamski et al. 2017; Lee 2016; Parazzoli et al. 2015), both GBM cell lines are principally TMZ-sensitive but respond to different extents to TMZ treatment, and have the possibility to escape from TMZ treatment by switching into a dormant state (Adamski et al. 2017). Based on our own investigations and published results, we adjusted used drug concentrations (as low as possible) to measured liquor/plasma concentrations in treated patients (Ostermann et al. 2004; Rosenfeld et al. 2014; Zerp et al. 2015). We consistently determined amounts of dead cells and still remaining growth rates of all cell types under all treatment schedules in parallel, and depicted our results in a heatmap-like summary to comprehensively visualize the most promising sequential long-term treatment schedules in our GBM in vitro model.

Materials and methods

Cultivation of cell lines

The human glioblastoma cell lines A172 (ECACC 880624218) and LN229 (ATCC-CRL-2611) were purchased from the European Collection of Cell Cultures (ECACC, Salisbury, UK) or the American Type Culture Collection (ATCC, Manassas, VA, USA). The human fetal astrocyte cell line SVGA was kindly provided by the group of Christine Hanssen Rinaldo, University Hospital of North Norway (Henriksen et al. 2014) with the permission of W. J. Altwood (Schweighardt et al. 2001). All cell lines were cultured in Dulbecco's modified Eagle's medium (DMEM; Life Technologies, Carlsbad, CA, USA) supplemented with 10% fetal bovine serum (FBS; Invitrogen, Carlsbad, CA, USA or PAN-Biotech GmbH, Aidenbach, Germany), 1% Penicillin–Streptomycin (10,000 U/ml; Thermo Fisher Scientific, Waltham, MA, USA), and either 2 mM (A172, LN229) or 6 mM (SVGA) additional L-glutamine (Thermo Fisher Scientific). Cells were routinely checked for mycoplasma contamination by bisbenzimide staining, and for identity by Short Tandem Repeat profiling at the Department of Forensic Medicine (Kiel, Germany) employing the Powerplex HS Genotyping Kit (Promega, Madison, WC) and a 3500 Genetic Analyser (Thermo Fisher Scientific, Waltham, MA, USA).

Stimulation of cell lines

For stimulation, the cell lines were seeded with 10% confluency in 6-well culture dishes measured by the determined size of the cell body compared to the culture-free area (25,000 cells for SVGA, 20,000 cells for A172 and 45,000 for LN229, respectively). Subsequently, the cells were stimulated with either 50 µM TMZ [stock dissolved at 100 mM in dimethyl sulfoxide (DMSO; Sigma-Aldrich, St. Louis, MO, USA); Sigma-Aldrich], 2.5 µM AT101 (stock dissolved at 100 mM in DMSO; Tocris, Bristol, UK) or 6 µM HCQ (stock dissolved at 100 mM in ultra-pure H_2O; Sigma-Aldrich) as well as a combination of 50 µM TMZ plus 2.5 µM AT101 or 50 µM TMZ plus 6 µM HCQ, respectively, in DMEM without phenol-red (Life Technologies) supplemented with 10% FBS for 6 days. In case of sequential stimulations with different drugs or drug combinations the treatment was changed after 3 days for another stimulation period of further 3 days. Controls were stimulated with the equal volume of either DMSO [0.05% (v/v)] or H_2O, respectively. A detailed overview of analyzed treatment schedules is depicted in Fig. 1 Supplement.

Cytotoxicity assay

To determine the cytotoxic effects the CytoTox-Fluor™ Cytotoxicity Assay (Promega, Madison, WI, USA) was performed according to the manufacturer's instruction. Briefly, supernatants of stimulated cells were collected at day 3 and 6 of stimulation and mixed with the fluorogenic bis-AAF-R110 substrate. The emerging fluorescence was measured in a microplate reader (GENios, Tecan Group, Maennedorf, Switzerland) at 485/535 nm. The exact numbers of dead cells were determined according to different numbers of digitonin-lysed (82.5 µg/ml; Merck Millipore, Burlington, MA, USA) cell-dilutions of each cell line. Moreover, the cell survival was determined by counting of viable cells with a hemocytometer at day 0, 3 and 6 of the stimulation. Growth rates were calculated as n-fold amount of alive cells compared to day 0 of the stimulation ($n = 3–5$ independent experiments).

Combination index

To analyze the influence of different drug combinations and their synergy quantification over the influence of their single effect, the Chou–Talalay method was used, using the CompusSyn software (http://www.combosyn.com; Chou and Talalay 1984; Chou 2010). This analysis determines if the

effect of a combined treatment with drugs is antagonistic [combination index (CI) > 1], additive (CI ~ 1), or synergistic (CI < 1).

Statistical analysis

All data have been analyzed with the GraphPad Prism 5 Software (GraphPad Software, La Jolla, CA, USA). To check for statistical significance, a two-way-ANOVA followed by a Bonferroni's multiple comparison test, comparing all pairs of columns with the control column (=DMSO or unstimulated control) was employed for data sets (growth rates/percentage of dead cells) that were constantly treated with the same drug or drug combination for 6 days, whereas a repeated one-way-ANOVA followed by Dunnett's multiple comparison test, comparing all pairs of columns with the control column (=TMZ), was employed for all sequential stimulation schedules at day 6 (growth rates/percentage of dead cells). Asterisks as well as hashtags indicate statistical significance: $^{*}p < 0.05$, $^{**}p < 0.01$, $^{***}p < 0.001$ respective $^{\#}p < 0.05$, $^{\#\#}p < 0.01$ and $^{\#\#\#}p < 0.001$.

Results

Long-term model for single drug and combined treatment with temozolomide and alternative drugs

To assess in a first step the effects in our long-term GBM in vitro model, we performed single (TMZ; HCQ; AT101) and combined (TMZ + HCQ; TMZ + AT101) drug stimulations for the whole stimulation period, and analyzed cytotoxic effects after day 3 and 6. Here, we used drug concentrations adjusted to those measured in liquor/plasma in treated patients of temozolomide (TMZ, 50 µM) and the alternative drugs hydroxychloroquine (HCQ, 6 µM) and AT101 (2.5 µM) to treat human astrocytes (SVGA) and two different glioblastoma cell lines (LN229 and A172) for 3 and 6 days. In general, after 3 days of treatment, amounts of dead cells were only slightly increased in comparison to control samples that were left untreated (unstimulated) or obtained the solvent DMSO in equal volumes as used to solve TMZ and AT101 (Fig. 1). After 6 days, treatment with TMZ, the gold standard therapeutic in glioblastoma therapy, yielded significantly increased amounts of dead cells for the glioblastoma cell cultures A172 [9.95-fold ± 4.29; less TMZ-responsive (Adamski et al. 2017)] and especially LN229 [12.54-fold ± 3.12, more TMZ-responsive (Adamski et al. 2017)], and also for the astrocytes SVGA (8.12-fold ± 4.29), but to lesser extent. In comparison to these cytotoxic effects, single treatment with HCQ (Fig. 1a) and AT101 (Fig. 1b) were (in some cases significantly) less effective, yielding at maximum a 4.98-fold ± 3.28 increase of dead cells in LN229 cells for AT101. However, in combined treatment of TMZ with HCQ or AT101, cytotoxic effects were drastically elevated, yielding a 24.84-fold ± 7.86 (A172) and 38.77-fold ± 16.98 (LN229) increase of dead cells in glioma cultures after TMZ + HCQ treatment for 6 days, and 26.11-fold ± 5.13 (A172) and 33.18-fold ± 17.92 (LN229) increase of dead cells after TMZ + AT101 treatment. In comparison to glioma cell cultures, the SVGA astrocytes were less affected, however drug/combinations partly significantly increased amounts of death cells [8.12-fold ± 4.29 (TMZ), 3.52-fold ± 2.09 (HCQ), 9.88-fold ± 3.39 (TMZ + HCQ), 2.55-fold ± 1.05 (AT101) and 5.49-fold ± 0.82 (TMZ + AT101) increase of dead cells]. To assess the value of combined drug administration in our treatment schedules, we calculated combination indices based on the determinations of cytotoxicity for HCQ and TMZ (Fig. 1c) and AT101 and TMZ (Fig. 1d) employing schedules, respectively. Concerning the non-sequential treatments with TMZ and HCQ (TMZ/TMZ, HCQ/HCQ and TMZ + HCQ/TMZ + HCQ), cytotoxic effects act antagonistic in SVGA cells, meaning the cytotoxicity observed upon TMZ + HCQ treatment was lower compared to the sum of single TMZ and single HCQ toxicity. In glioma cells, however, the combined treatment had additive or even synergistic effects, showing that the combination of TMZ + HCQ was more effective than the (expected) effect of the single drugs. Regarding the treatment schedules with AT101, the non-sequential treatments with the combination TMZ + AT101/TMZ + AT101 yielded additive effects in SVGA astrocytes and synergistic effects in A172 and LN229 glioma cells in comparison to the single drugs (TMZ/TMZ and AT101/AT101, compare also Fig. 1b). Thus, we could confirm that our long-term GBM in vitro model is useful to investigate the effects of different drug/combinations at concentrations comparable to those observed in vivo.

Sequential treatment schedules reveal most effective drug combinations

In a next step, we investigated the cytotoxic effects of TMZ and the alternative drugs HCQ and AT101 alone or in combination with TMZ in defined sequential treatment schedules for 6 days, in which the treatment was switched after 3 days (compare Fig. 1 Supplement). Amounts of dead cells are shown in Fig. 2a (schemes with HCQ) and Fig. 2b (schemes with AT101) normalized to single treatment with the gold standard TMZ for 6 days, so *n*-fold values in the graphs and in the following refer to increased amounts of dead cells in comparison to TMZ. Additionally, we investigated the proliferation of the remaining cells that were not hit by the cytotoxic treatment and may therefore model the tumor cell fraction initializing recurrences (selected growth rates in Fig. 3a–c, further data in Fig. 2 Supplement). Please refer

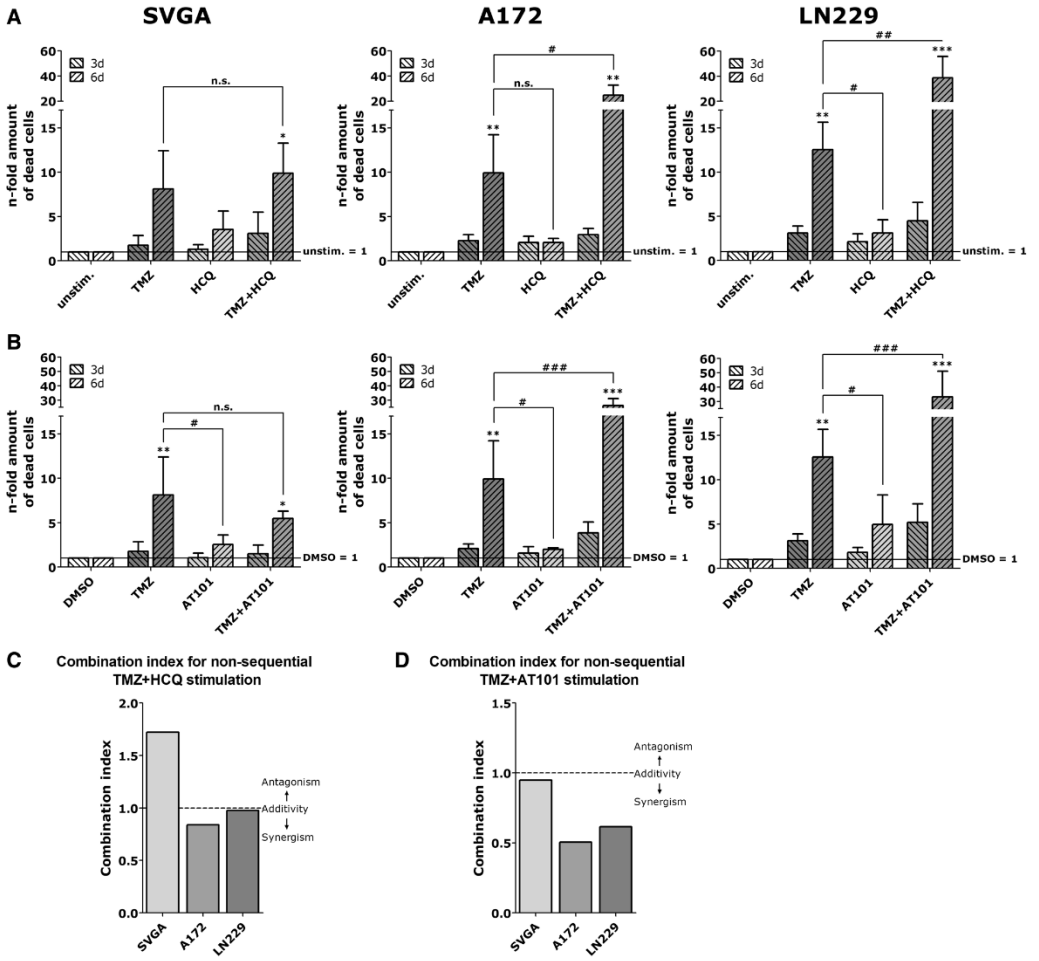

Fig. 1 Effect of non-sequential treatments on n-fold amounts of dead cells compared to control stimulations of astrocytes and two different GBM cell lines treated with either TMZ, an alternative drug or the combination of TMZ plus an alternative drug. Cells were treated with either 50 µM TMZ, 6 µM HCQ (**a**) respective 2.5 µM AT101 (**b**) or the combination of TMZ plus HCQ (**a**) respective AT101 (**b**) for 6 days. Cytotoxicity assays were performed at day 3 and 6 of the stimulation ($n = 3$–5). Number of dead cells are depicted as *n*-fold amount compared to the respective control [dimethylsulfoxide (DMSO) or unstimulated]. Obtained data were further analyzed in terms of the combined effect of the different drugs by the Chou–Talalay method (combination index, **c** for TMZ + HCQ, **d** for TMZ + AT101 stimulation). Means of raw data are significantly different for * or $^{\#}p < 0.05$, ** or $^{\#\#}p < 0.01$ respective *** or $^{\#\#\#}p < 0.001$

also to the heatmap in Fig. 4 comprehensively showing beneficial and detrimental effects (*n*-fold amounts of dead cells and growth rates of remaining cells) of different treatment schedules in comparison to TMZ for astrocytes and glioma cell lines.

Regarding treatment schedules with HCQ, schedules starting with 3 days TMZ and then switching to HCQ or TMZ + HCQ were not significantly more cytotoxic (Fig. 2a) for SVGA astrocytes, but the switch to TMZ + HCQ yielded slightly reduced proliferation of SVGA in comparison to the switch to HCQ (Fig. 3a, left). In A172 cells, the subsequent treatment with HCQ or TMZ + HCQ after an initial TMZ phase yielded only slightly higher cytotoxicity (Fig. 2a) and reduced proliferation (Fig. 3b, left) in comparison to

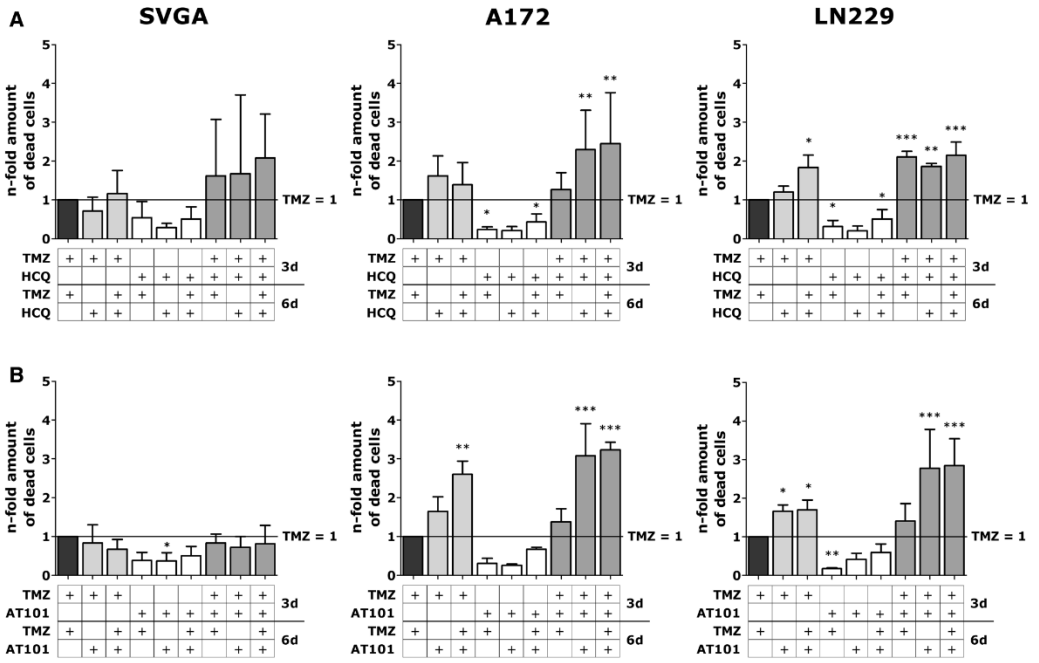

Fig. 2 Effect of sequential treatments on *n*-fold amounts of dead cells compared to the gold standard TMZ of astrocytes and two different GBM cell lines treated with TMZ in combination with the alternative therapeutics HCQ and AT101. Cells were treated with either 50 µM TMZ, 6 µM HCQ (**a**) or 2.5 µM AT101 (**b**) or their combinations depending on the corresponding treatment schedule used (see Fig. 1 Supplement) over 6 days. Cytotoxicity assays were performed at day 3 and 6 of the stimulation ($n = 3$–5). Numbers of dead cells are depicted as *n*-fold amounts compared to the single TMZ stimulation. Means of raw data are significantly different for $^{*}p < 0.05$, $^{**}p < 0.01$ respective $^{***}p < 0.001$

single TMZ treatment. In LN229 cells, the switching from TMZ to HCQ yielded slightly higher amounts of dead cells, being significantly increased after switching to the combination TMZ + HCQ, and in both schedules, the growth rate was also lower than for single TMZ treatment (Fig. 3c, left). Thus, when summarizing these results for all cell types, starting with TMZ treatment and switching to HCQ was slightly beneficial, but switching to TMZ + HCQ was more harmful in comparison to the single TMZ treatment. Sequential stimulations starting with 3 days treatment with HCQ did not yield any increased cytotoxicity and showed higher growth rates in comparison to single TMZ treatment in glioma cells. Thus, sequential stimulations were in some cases even significantly less effective, but also less harmful for SVGA astrocytes (Fig. 3a and Supplement Fig. 2). The combined treatment of TMZ + HCQ had already been shown to be significantly more cytotoxic to glioblastoma cells in the 6-day treatment period (Fig. 1a), but is also quite harmful for astrocytes. In the sequential treatment starting with TMZ + HCQ and switching to the single drugs TMZ or HCQ, the cytotoxic effects and growth rates were only slightly affected for glioma cells as well as for astrocytes compared to the non-sequential treatment with TMZ + HCQ (Fig. 2a).

Focusing on the treatment schedules with AT101, schedules starting with 3 days TMZ and then switching to AT101 or TMZ + AT101 were both a little less harmful for SVGA astrocytes showing slightly less dead cells (Fig. 2b) and higher proliferation rates in case of TMZ/AT101 (Fig. 3a) in comparison to TMZ. In glioma cells however, they were more effective (significant increases for the switch to TMZ + AT101 especially in A172 cells, and to lower extents to AT101 and TMZ + AT101 in LN229 cells) while the growth rates were comparable to those observed in single TMZ treatment. Thus, a sequential stimulation switching from TMZ to AT101 or TMZ + AT101 was beneficial in comparison to non-sequential single TMZ treatment. Treatment schedules starting with AT101 were less cytotoxic than the gold standard TMZ in glioma cells, no matter which drug/combination was applied after the

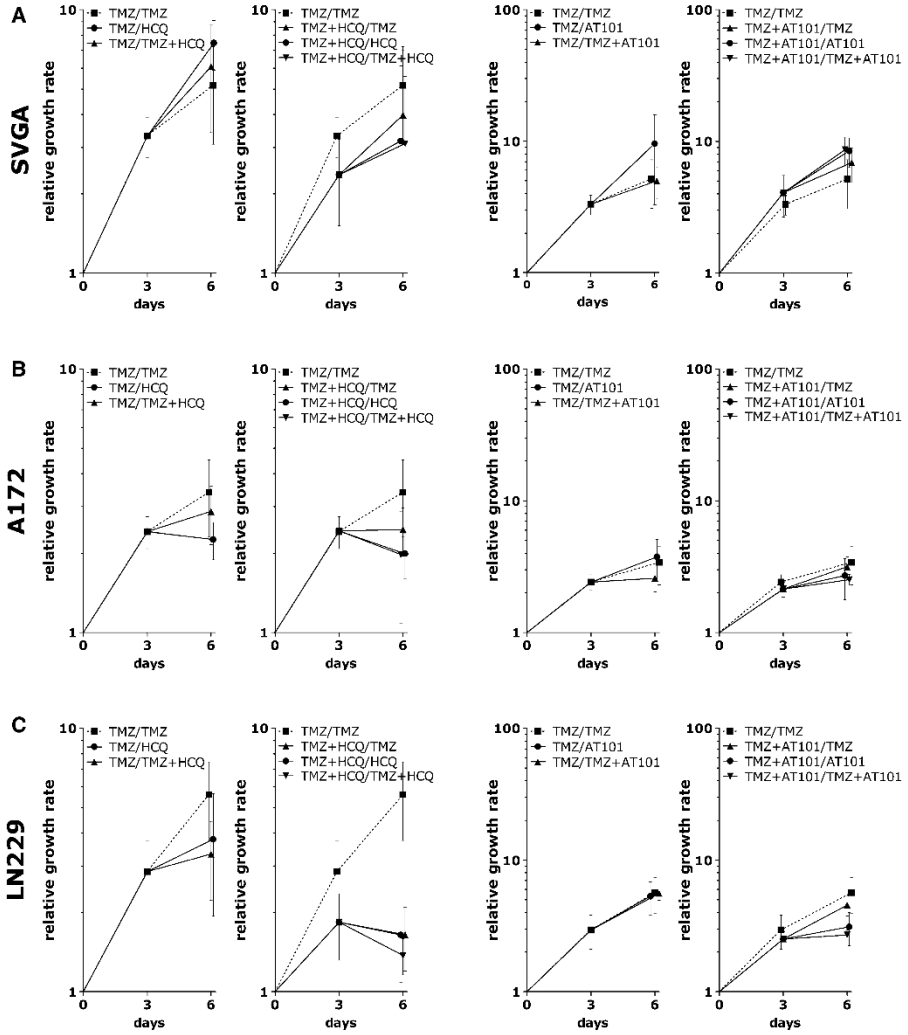

Fig. 3 Effect of selected sequential stimulations on growth rates of astrocytes and two different GBM cell lines treated according to the treatment schedules (ref. Fig. 1 Supplement). The relative growth rates for day 3 and day 6 of SVGA (**a**), A172 (**b**) and LN229 (**c**) were determined compared to the number of cells at day 0 of the treatment. Growth rates of cells treated with the gold standard TMZ are highlighted with dashed lines

initial 3 days of AT101 treatment. However, these schedules were also less harmful for astrocytes (Fig. 2b, Supplement Fig. 2). Moreover, treatment schedules starting with a combined TMZ + AT101 stimulation were also promising. Surprisingly, amounts of dead cells were only slightly increased in glioma cells in comparison to single TMZ treatment when TMZ + AT101 was switched to TMZ, but the switch from TMZ + AT101 to AT101 alone yielded almost as high cytotoxic effects (Fig. 2b) and lowered proliferation rates (Fig. 3b, c) as the non-sequential combination treatment TMZ + AT101. These effects were significantly higher than the cytotoxic effect of single TMZ treatment. Sequential treatments starting with TMZ + AT101 for 3 days were not more or even slightly less harmful for SVGA astrocytes (Figs. 2b, 3a).

		n-fold amount of dead cells (TMZ = 1)			*growth rate*		
stimulus I	*stimulus II*	SVGA	A172	LN229	SVGA	A172	LN229
TMZ	TMZ	1.00	1.00	1.00	2.35	1.41	2.01
	HCQ	0.71	1.62	1.20	3.32	0.92	1.35
	TMZ+HCQ	1.16	1.39	1.83	1.79	1.17	1.25
HCQ	TMZ	0.54	0.23	0.31	2.65	3.25	2.40
	HCQ	0.29	0.21	0.20	3.20	5.57	2.88
	TMZ+HCQ	0.50	0.43	0.50	2.08	3.56	2.07
TMZ+HCQ	TMZ	1.62	1.26	2.11	1.60	1.01	0.90
	HCQ	1.68	2.30	1.86	1.20	0.84	0.89
	TMZ+HCQ	2.07	2.44	2.14	1.14	0.82	0.77
TMZ	TMZ	1.00	1.00	1.00	2.35	1.41	2.01
	AT101	0.84	1.64	1.67	4.14	1.57	1.84
	TMZ+AT101	0.67	2.59	1.70	3.92	1.10	1.93
AT101	TMZ	0.37	0.30	0.18	2.42	2.30	2.79
	AT101	0.38	0.25	0.42	4.04	3.71	2.19
	TMZ+AT101	0.50	0.67	0.60	2.89	1.98	1.93
TMZ+AT101	TMZ	0.84	1.38	1.41	3.57	1.51	1.80
	AT101	0.72	3.08	2.78	2.98	1.28	1.22
	TMZ+AT101	0.81	3.24	2.85	2.18	1.19	1.08

Fig. 4 Summarized overview over the effect of (non)-sequential treatment on the *n*-fold amount of dead cells respective growth rates of astrocytes and two different GBM cell lines depicted as heatmap. Data were evaluated based on the comparison to the TMZ treatment, therefore a yellow color (value ~ 1) indicates an equal effect in comparison to the gold standard therapy. For astrocytes (SVGA) red colors indicate more cytotoxic effects or lower growth rates compared to TMZ, whereas a green color indicates a less cytotoxic effect respective higher growth rates compared to TMZ. For GBM cells (A172 and LN229) colors indicate the opposite: green colors illustrate a higher cytotoxic effect respective lower growth rate, whereas red illustrates a lower cytotoxic effect respective higher growth rate. Therefore, most promising stimulations for all cells are predominantly the ones with greenish color

Taking together the summarized data in the heatmap (Fig. 4), we could show in our long-term GBM in vitro model that sequential stimulations with TMZ and alternative drugs like HCQ or AT101 may yield higher cytotoxicity and better tumor growth control in comparison to single TMZ treatment. This was especially the case for the sequences TMZ/HCQ and TMZ + AT101/AT101 which was as effective as the non-sequential combination TMZ + AT101. Additionally, these treatment schedules affected both less and more TMZ-responsive glioma cell lines, whilst being less harmful for astrocytes. Therefore, the sequential treatment with mechanistically differently acting drugs might be an option to reduce side effects in long-term treatment, for example in local administration approaches.

Discussion

The efficient treatment of highly malignant, heterogeneously composed GBMs is still a clinical challenge. Although the quality of life for GBM patients has been improved after establishment of concomitant radiation therapy with TMZ followed by maintenance TMZ (Stupp et al. 2005) and also by further other advances in therapy, only limited effects have been achieved in extending survival times of patients after diagnosis of the disease. The fundamental problem in the successful treatment of these tumors is their highly infiltrative behavior and their pronounced resistance towards conventional radio- and/or chemotherapy (Ohgaki and Kleihues 2005).

Since autophagy has been demonstrated to be an adaptive response to both radiation and TMZ (Kanzawa et al. 2004; Katayama et al. 2007) and, besides others, Bcl-2 proteins enhance resistance to chemotherapeutic agents, such as TMZ (Krakstad and Chekenya 2010), targeting both autophagy and Bcl-2 proteins could have therapeutic benefits. Thus, quinoline-based antimalarial drugs (e.g. HCQ, CQ, QNX) and BH3 mimetics like AT101 which are well known to induce autophagic cell death and/or facilitate apoptosis by competitive inhibition of Bcl-2 proteins (Golden et al. 2015; Opydo-Chanek et al. 2017; Voss et al. 2010; Warnsmann et al. 2018; Yan et al. 2016) were considered as additional

GBM therapeutics (Bricenõ et al. 2007; Golden et al. 2015; Jarzabek et al. 2014; Keshmiri-Neghab et al. 2014; Lee et al. 2015; Li et al. 2008; Rangwala et al. 2014; Rosenfeld et al. 2014; Yan et al. 2016). However, recent approaches mainly focus on effects of combined TMZ/quinoline-based drugs or TMZ/BH3 mimetics (accompanied or not by radiotherapy), such as the approach of Hsu et al., who investigated the combined effect of temozolomide, sirolimus and CQ (Hsu et al. 2018). Anyhow, HCQ was shown to have a safer toxicological profile than CQ (Gunja et al. 2009).

Therefore, we consistently investigated the effects of sequentially applied single and combined TMZ, HCQ and AT101 treatments in a long-term stimulation GBM in vitro model and showed that sequential stimulations yielded higher cytotoxicity and better tumor growth control in comparison to single TMZ treatment. This was especially the case for the sequences TMZ/HCQ and TMZ + AT101/AT101 which was as effective as the non-sequential combination TMZ + AT101. Importantly, these treatment schedules affected both the less and the more TMZ-responsive glioma cell line (A172 respective LN229) and were less harmful for astrocytes, which were comprehensively analyzed in parallel.

Concerning the efficiency of HCQ for GBM treatment different results have been presented in the current literature. Golden et al. (2015) nicely demonstrated that quinoline-based drugs blocked autophagy and exerted cytotoxic effects on drug-sensitive and drug-resistant glioma cells with varying potency (e.g. QNX < HCQ > CQ) and also killed glioma cells that were highly resistant to TMZ. Rosenfeld et al. (2014) noted in a phase I/II clinical trial of HCQ in combination with radiotherapy and concurrent and adjuvant TMZ treatment (NCT00486603) that, indeed, a therapy-associated increase in autophagic vacuoles and LC3-II as an autophagocytic marker could be observed in peripheral blood mononuclear cells. This effect correlated with higher HCQ exposure, but, unfortunately, dose-limiting toxicity prevented escalation to higher doses of HCQ. When looking at the results of our GBM in vitro model, we could indeed reconstruct these in vivo results: the combination of HCQ and TMZ was clearly more effective in inducing glioma cell death and preventing glioma growth, but also quite harmful for astrocytes. Since we used drug concentrations which were maximal effective on glioma cells but minimal toxic on astrocytes, and also adjusted them to known measured liquor/plasma concentrations (Rosenfeld et al. 2014), our in vitro conditions were approximately comparable to concentrations used in vivo (~600–800 mg/day to ~4.5–6 µM). Interestingly and in contrast, Rangwala et al. (2014) presented in a phase I trial of HCQ with dose-intense TMZ in patients with advanced solid tumors (e.g. brain metastases) and melanoma that the combination of high-dose HCQ and dose-intense TMZ was safe and tolerable, and was associated with autophagy modulation in patients. Here, a 2 weeks run-in of single agent HCQ (200–1200 mg/day) was followed by a combined therapy with dose-intense TMZ (150 mg/m^2/day). This schedule corresponds roughly to our sequential stimulations starting with 3 days treatment with HCQ and e.g. switching to HCQ + TMZ. Though, in this sequential schedule we did not observe any increased cytotoxicity in comparison to single TMZ treatment in glioma cells, so that this schedule was even significantly less effective, but also less harmful for SVGA astrocytes. However, Rangwala et al. (2014) themselves stated that their dose escalation trail was not designed to look at efficiency, so that randomized studies would be necessary to determine if HCQ followed by TMZ treatment is an advanced treatment schedule. Therefore, taking into account that sequential stimulations of HCQ and TMZ seem to be preferable in contrast to combined strategies, we were able to show now that starting with TMZ treatment and switching to HCQ was (slightly) beneficial compared to single TMZ treatment. Thus, further investigations focusing on the effects of TMZ and HCQ should also include an alternating treatment schedule of TMZ and HCQ.

Concerning the efficiency of AT101 for GBM treatment it has been nicely demonstrated that a combined gossypol/TMZ treatment was associated with inhibition of tumor-associated angiogenesis, invasion and clonogenic growth (Jarzabek et al. 2014; Keshmiri-Neghab et al. 2014), and that AT101 potentiated cell death induced by TMZ (Voss et al. 2010). Here, lentiviral knockdown of Beclin1 and Atg5 in glioma cell lines strongly diminished the extent of cell death induced by AT101 and combined treatment with TMZ indicating that autophagy contributed to this type of cell death (Voss et al. 2010). Further, Antonietti et al. (2017) showed that the HSF1/HSP70/BAG3 pathway played a pivotal role for overexpression of pro-survival Bcl-2 proteins and cell death resistance in glioma. Furthermore, BAG3 silencing could significantly enhance AT101-induced glioma cell death. Beyond, a treatment with gossypol selectively increased the hydrogen peroxidase levels and impaired mitochondrial respiration in GBM cells providing new insights into functional anti-tumorigenic effects of gossypol (Warnsmann et al. 2018). Thus, gossypol and especially its R-(−)-enantiomer AT101 seem to affect tumor growth in several different ways making them promising candidates for future GBM therapy. Contrary to that, although being well tolerated, gossypol had only a low (but nevertheless measurable) response rate in a group of heavily pretreated, poor-prognosis patients with recurrent gliomas (Bushunow et al. 1999). Indeed, results from Bushunow et al. (1999) are in accordance with those found in our GBM in vitro model. Here, treatment schedules starting with AT101 were not as effective in killing glioma cells as single TMZ treatment, no matter which drug/combination was applied after the initial 3 days of AT101 treatment. Anyhow, these schedules were

also less harmful for astrocytes. However, results from a phase II study of AT101 in recurrent GBMs to determine the acute and late toxicity of AT101 and the tumor response rate (NCT00540722) have not yet been published (Krakstad and Chekenya 2010).

In our hands, more promising treatment schedules were the sequential stimulation switching from TMZ to AT101 or TMZ + AT101 and from TMZ + AT101 to AT101 alone which yielded almost as high cytotoxic effects and lowered proliferation rates as the non-sequential combination treatment with TMZ + AT101. These schedules were clearly beneficial in comparison to non-sequential single TMZ treatment. Although results from a phase I trial investigating the side effects and dosage of AT101 in combination with TMZ with or without radiation in patients newly diagnosed with GBM (NCT00390403) have not yet been published (Krakstad and Chekenya 2010), phase IIb clinical trials of gossypol tested in combination with chemotherapeutic drugs for treating prostate cancer and other cancers such as lymphocytic leukemia, non-small-cell and small-cell lung cancer were completed. Here, different results were obtained. Whereas AT101 was well tolerated in combination with cisplatin and etoposide with growth factor support and had antitumor activity in a variety of cancers including extensive-stage small-cell lung cancer (Schelman et al. 2014), AT101 was tolerable but did not extend overall survival when combined with docetaxel plus prednisone in castration-resistant prostate cancer (Sonpavde et al. 2012). Moreover, AT101 could not reach beneficial response rates when combined with topotecan in refractory small-cell lung cancer (Heist et al. 2010). Thus, and in accordance with the results from our GBM in vitro model, combined AT101 treatment schedules need not to fit for all types of cancer pointing to the imperative to comprehensively evaluate sequential treatment schedules which possibly can overcome tumor resistance being associated with lower side effects.

Summarized, we showed that especially sequentially applied single and combined TMZ, HCQ and AT101 treatment yielded higher cytotoxicity and better tumor growth control in comparison to single TMZ treatment in a GBM in vitro model and were also less harmful for human astrocytes. Additionally, these schedules could be useful for long-term treatment by e.g. advanced local approaches which can realize a constant drug release with lower side effects. Indeed, some initial steps towards this way were performed by producing either molecularly imprinted polymer structures for selective recognition and adsorption of gossypol (Zhi et al. 2018) or versatile hyaluronic acid modified AQ4N-Cu(II)-gossypol infinite coordination polymer nanoparticles (Shen et al. 2018), as wells as by loading HCQ into liposomes decorated with a pH-sensitive TH-RGD targeting peptide (Wang et al. 2016). In perspective, managing GBM chemoresistance in connection with a suitable quality of life for treated patients will require both improved treatment strategies and alternative drug delivery systems.

Acknowledgements We thank Fereshteh Ebrahim, Brigitte Rehmke, Judith Becker and Sonja Dahle for expert technical assistance.

Author contributions JHF, KH conceived and designed the study; VA, CS, JHF and KH performed the experiments and analyzed the data; FC, RA, RL and MS contributed materials and assisted in data analysis; JHF and KH wrote the paper, and all authors revised the manuscript.

Funding This study was funded by the German Research Foundation (DFG) as part as of the Research Training Group "Materials4Brain" (GRK2154; P3, P7 and P8).

Compliance with ethical standards

Conflict of interest Author Vivian Adamski declares that she has no conflict of interest. Author Christina Schmitt declares that she has no conflict of interest. Author Florian Ceynowa declares that he has no conflict of interest. Author Rainer Adelung declares that he has no conflict of interest. Author Ralph Lucius declares that he has no conflict of interest. Author Michael Synowitz declares that he has no conflict of interest. Author Kirsten Hattermann declares that she has no conflict of interest. Author Janka Held-Feindt declares that she has no conflict of interest.

Ethical approval This article does not contain any studies with human participants or animals performed by any of the authors.

References

Adamski V, Hempelmann A, Flüh C, Lucius R, Synowitz M, Hattermann K, Held-Feindt J (2017) Dormant human glioblastoma cells acquire stem cell characteristics and are differentially affected by temozolomide and AT101 treatment strategies. Oncotarget 8:108064–108078

Antonietti P, Linder B, Hehlgans S, Mildenberger IC, Burger MC, Fulda S, Steinbach JP, Gessler F, Rödel F, Mittelbronn M, Kögel D (2017) Interference with the HSF1/HSP70/BAG3 pathway primes glioma cells to matrix detachment and BH3 mimetic-induced apoptosis. Mol Cancer Ther 16:156–168

Arevalo Á, Erices J, Uribe D, Howden J, Niechi I, Muñoz S, Martín R, Monrás C (2017) Current therapeutic alternatives and new perspectives in glioblastoma multiforme. Curr Med Chem 24:2781–2795

Bae SH, Park M-J, Lee MM, Kim M, Lee S-H, Cho SY, Kim Y-H, Kim YJ, Park C-K, Kim C-Y (2014) Toxicity profile of temozolomide in the treatment of 300 malignant glioma patients in Korea. J Korean Med Sci 29:980–984

Bonovia R, Inda M, Cavenee W, Furnari F (2011) Heterogeneity maintenance in glioblastoma: a social network. Cancer Res 71:4055–4060

Bricenõ E, Calderon A, Sotelo J (2007) Institutional experience with chloroquine as an adjuvant to the therapy for glioblastoma multiforme. Surg Neurol 67:388–391

Bushunow P, Reidenberg MM, Wasenko J, Winfiled J, Lorenzo B, Lemke S, Himpler B, Corona R, Coyle T (1999) Gossypol treatment of recurrent adult malignant gliomas. J Neurooncol 43:79–86

Chou TC (2010) Drug combination studies and their synergy quantification using the Chou–Talalay method. Cancer Res 70:440–446

Chou TC, Talalay P (1984) Quantitative analysis of dose-effect relationships: the combined effects of multiple drugs or enzyme inhibitors. Adv Enzyme Regul 22:27–55

Golden EB, Cho H-Y, Hofman FM, Louie S, Schönthal AH, Chen TC (2015) Quinoline-based antimalarial drugs: a novel class of autophagy inhibitors. Neurosurg Focus 38:E12

Gunja N, Roberts D, McCoubrie D, Lamberth P, Jan A, Simes DC, Hackett P, Buckley NA (2009) Survival after massive hydroxychloroquine overdose. Anaesth Intensive Care 37:130–133

Heist RS, Fain J, Chinnasami B, Khan W, Molina JR, Sequist LV, Temel JS, Fidias P, Brainerd V, Leopold L, Lynch TJ (2010) Phase I/II study of AT-101 with topotecan in relapsed and refractory small cell lung cancer. J Thorac Oncol 5:1637–1643

Henriksen S, Tylden GD, Dumoulin A, Sharma BN, Hirsch HH, Hanssen Rinaldo C (2014) The human fetal glial cell line SVG p12 contains infectious BK polyomavirus. J Virol 88:7556–7768

Hsu SPC, Kuo JS, Chiang HC, Wang HE, Wang YS, Huang CC, Huang YC, Chi MS, Mehta MP, Chi KH (2018) Temozolomide, sirolimus and chloroquine is a new therapeutic combination that synergizes to disrupt lysosomal function and cholesterol homeostasis in GBM cells. Oncotarget 9:6883–6896

Jarzabek MA, Amberger-Murphy V, Callanan JJ, Gao C, Zagozdzon AM, Shiels L, Wang J, Ligon KL, Rich BE, Dicker P, Gallagher WM, Prehn JH, Byrne AT (2014) Interrogation of gossypol therapy in glioblastoma implementing cell line and patient-derived tumor models. Br J Cancer 11:2275–2286

Kanzawa T, Germano IM, Komata T, Ito H, Kondo Y, Kondo S (2004) Role of autophagy in temozolomide induced cytotoxicity for malignant glioma cells. Cell Death Differ 11:448–457

Katayama M, Kawaguchi T, Berger MS, Pieper RO (2007) DNA damaging agent-induced autophagy produces a cytoprotective adenosine triphosphate surge in malignant glioma cells. Cell Death Differ 14:548–558

Keshmiri-Neghab H, Goliaei B, Nikoofar A (2014) Gossypol enhances radiation-induced autophagy in glioblastoma multiforme. Gen Physiol Biophys 33:433–442

Krakstad C, Chekenya M (2010) Survival signaling and apoptosis resistance in glioblastomas: opportunities for targeted therapeutics. Mol Cancer 9:135

Lee SY (2016) Temozolomide resistance in glioblastoma multiforme. Genes Dis 3:198e210

Lee SW, Kim HK, Lee NH, Yi HY, Kim HS, Hong SH, Hong YK, Joe YA (2015) The synergistic effect of combination temozolomide and chloroquine treatment is dependent on autophagy formation and p53 status in glioma cells. Cancer Lett 360:195–204

Li S, Jiang T, Li G, Wang Z (2008) Impact of p53 status to response of temozolomide in low MGMT expression glioblastomas: preliminary results. Neurol Res 30:567–570

Lu Y, Li J, Dong C-E, Hunag J, Zhou H-B, Wang W (2017) Recent advances in gossypol derivatives and analogs: a chemistry and biology view. Future Med Chem 9:1243–1275

Ohgaki H, Kleihues P (2005) Epidemiology and etiology of gliomas. Acta Neuropathol 109:93–108

Opydo-Chanek M, Gonzola O, Marzo I (2017) Multifaceted anticancer activity of BH3 mimetics: current evidence and future prospects. Biochem Pharmacol 136:12–23

Ostermann S, Csajka C, Buclin T, Leyvraz S, Lejeune F, Decosterd LA, Stupp R (2004) Plasma and cerebrospinal fluid population pharmacokinetics of temozolomide in malignant glioma patients. Clin Cancer Res 10:3728–3736

Parazzoli G, Prados J, Ortiz R, Caba O, Cabeza L, Berdasco M, Gónzalez B, Melguizo C (2015) Temozolomide resistance in glioblastoma cell lines: implication of MGMT, MMR, P-glycoprotein and CD133 expression. PLoS One 10:e0140131

Rangwala R, Leone R, Chang YC, Fecher LA, Schuchter LM, Kramer A, Tan KS, Heitjan DF, Rodgers G, Gallagher M, Piao S, Troxel AB, Evans TL, DeMichele AM, Nathanson KL, O'Dwyer PJ, Kaiser J, Pontiggia L, Davis LE, Amaravadi RK (2014) Phase I trial of hydroxychloroquine with dose-intense temozolomide in patients with advanced solid tumors and melanoma. Autophagy 10:1369–1379

Rosenfeld MR, Ye X, Supko JG, Desideri S, Grossman SA, Brem S, Mikkelson T, Wang D, Chang YC, Hu J, McAfee Q, Fisher J, Troxel AB, Piao S, Heitjan DF, Tan KS, Pontiggia L, O'Dwyer PJ, Davis LE, Amaravadi RK (2014) A phase I/II trial of hydroxychloroquine in conjunction with radiation therapy and concurrent and adjuvant temozolomide in patients with newly diagnosed glioblastoma multiforme. Autophagy 10:1359–1368

Schelman WR, Mohammed TA, Traynor AM, Kolesar JM, Marnocha RM, Eickhoff J, Keppen M, Alberti DB, Wilding G, Takebe N, Liu G (2014) A phase I study of AT-101 with cisplatin and etoposide in patients with advanced solid tumors with an expanded cohort in extensive-stage small cell lung cancer. Investig New Drugs 32:295–302

Schweighardt B, Shieh JT, Atwood WJ (2001) CD4/CXCR4-independent infection of human astrocytes by a T-tropic strain of HIV-1. J Neurovirol 7:155–162

Shen S, Wu Y, Li K, Wang Y, Wu J, Zeng Y, Wu D (2018) Versatile hyaluronic acid modified AQ4N-Cu(II)-gossypol infinite coordination polymer nanoparticles: multiple tumor targeting, highly efficient synergistic chemotherapy, and real-time self-monitoring. Biomaterials 154:197–212

Sonpavde G, Matveev V, Burke JM, Caton JR, Fleming MT, Hutson TE, Galsky MD, Berry WR, Karlov P, Holmlund JT, Wood BA, Brookes M, Leopold L (2012) Randomized phase II trial of docetaxel plus prednisone in combination with placebo or AT-101, an oral small molecule Bcl-2 family antagonist, as first-line therapy for metastatic castration-resistant prostate cancer. Ann Oncol 23:1803–1808

Stupp R, Mason WP, van den Bent MJ, Weller M, Fisher B, Taphoorn MJ, Belanger K, Brandes AA, Marosi C, Bogdahn U, Curschmann J, Janzer RC, Ludwin SK, Gorlia T, Allgeier A, Lacombe D, Cairncross JG, Eisenhauer E, Mirimanoff RO, European Organisation for Research and Treatment of Cancer Brain Tumor and Radiotherapy Groups, National Cancer Institute of Canada Clinical Trials Group (2005) Radiotherapy plus concomitant and adjuvant temozolomide for glioblastoma. N Engl J Med 352:987–996

Voss V, Senft C, lang V, Ronellenfitsch MW, Steinbach JP, Seifert V, Kögel D (2010) The pan-Bcl-2 inhibitor (−)gossypol triggers autophagic cell death in malignant gliomas. Mol Cancer Res 8:1002–1016

Wang Y, Shi K, Zhang L, Hu G, Wan J, Tang J, Yin S, Duan J, Qin M, Wang N, Xie D, Gao X, Gao H, Zhang Z, He Q (2016) Significantly enhanced tumor cellular and lysosomal hydroxychloroquine delivery by smart liposomes for optimal autophagy inhibition and improved antitumor efficiency with liposomal doxorubicin. Autophagy 12:949–962

Warnsmann V, Meyer N, Hamann A, Kögel D, Osiewacz (2018) A novel role of the mitochondrial permeability transition pore in (−) gossypol-induced mitochondrial dysfunction. Mech Ageing Dev 170:45–58

Yan Y, Xu Z, Dai S, Qian L, Sun L, Gong Z (2016) Targeting autophagy to sensitive glioma to temozolomide treatment. J Exp Clin Cancer Res 35:23

Zerp SF, Stoter TR, Hoebers FJP, van den Brekel MWM, Dubbelman R, Kuipers GK, Lafleur MVM, Slotman BJ, Verheij M (2015) Targeting anti-apoptotic Bcl-2 by AT-101 to increase radiation efficacy: data from in vitro and clinical pharmacokinetic studies in head and neck cancer. Radiat Oncol 10:158

Zhi K, Wang L, Zhang Y, Zhang X, Zhang L, Liu L, Yao J, Xiang W (2018) Preparation and evaluation of molecularly imprinted polymer for selective recognition and adsorption of gossypol. J Mol Recognit. https://doi.org/10.1002/jmr.2627

Establishment of a glioblastoma *in vitro* (in)complete resection dual co-culture model suitable for drug testing.

In this work, we addressed the challenge of *in vitro* drug testing for GBM therapeutics regarding the *in vivo* situation after complete or incomplete resection of a tumor as well as its microenvironment. Besides endothelial cells, especially astrocytes and microglial cells are part of the tumor microenvironment and have been shown to influence therapy approaches (Manini et al. 2018; Gieryng et al. 2017a; Matias et al. 2018). To realize an effective long-term drug treatment of GBM patients with small side effects which focusses on the local application of drugs in the tumor cavity after resection, we evaluated the numeric tumor and healthy cell ratios after complete and incomplete resection on available *in vivo* data. Therefore, two human primary GBM cultures (primary culture 1 and 2, PC1 and 2) with different respond-rates on TMZ treatment were chosen and co-cultivated with healthy human astrocyte (SVGA) as well as human microglia (HMC3) cell lines. We applied a generic drug treatment of three days combined TMZ and AT101 stimulation, followed by three days single AT101 stimulation, which was evaluated in our previous study as effective for the treatment of GBM cells whilst not affecting healthy human astrocytes [(Adamski et al. 2018) see previous publication in chapter 2.1].To be able to analyze effects of co-cultivation as well as drug-treatment on the respective single cell population, cells were kept in a dual co-culture, allowing the exchange of signaling molecules however without direct contact with each other. Our investigations show that in both models, GBM primary cultures are highly affected by the sequentially applied treatment of TMZ and AT101 on survival as well as their relative growth rate, however in smaller extend than in monocultures, indicating a protection mechanism of GBM cells from treatment. Moreover, whereas human microglial cells are not affected by the treatment in both co-culture models, cytotoxic effects on astrocytes are significantly increased upon co-cultivation with GBM cells and microglia cells in the incomplete resection model. To analyze more detailed the correlation between tumor size respective growth and astrocyte survival, different amounts of primary GBM cells (PC1) were seeded in the dual co-culture model of incomplete resection whilst keeping astrocytes and microglial cell numbers fixed. Moreover, the influence of signaling molecules on astrocytes in the incomplete resection model has been evaluated at the timepoint of biggest distinction between mono- and co-culture results, namely after three days stimulation. Our results suggest high correlations between PC1 cell number and overall astrocyte growth rate and survival, as the influence of GBM cells on astrocytes increases with the increase of GBM cell number. Concomitant with this, different cytokines and chemokines which are induced upon chemotherapeutic stimulation in PC1 cells, and of which astrocytes have proven to have surface receptors, are reduced upon co-cultivation in the dual co-culture of the incomplete resection model, enhancing the importance to include the tumor microenvironment in approaches to develop efficient treatment strategies for GBM therapy.

The results have been published in the journal "*Annals of Anatomy: Anatomischer Anzeiger*".

Own contribution, presented in this article:

- Conceptualization and design of study
- Assay development of the *in vitro* dual co-culture resection models
- Experimental investigations based on the complete dual co-culture resection model
- Analysis of data & visualization
- Discussion and interpretation of results
- Writing of the original draft for submission

The following content in this chapter is reproduced with permission.

Annals of Anatomy 228 (2020) 151440

Contents lists available at ScienceDirect

Annals of Anatomy

journal homepage: www.elsevier.com/locate/aanat

Research article

Establishment of a glioblastoma *in vitro* (in)complete resection dual co-culture model suitable for drug testing

Christina Schmitt[a,1], Vivian Adamski[b,1], Florian Rasch[c], Rainer Adelung[c], Ralph Lucius[a], Michael Synowitz[b], Kirsten Hattermann[a], Janka Held-Feindt[b,*]

[a] Institute of Anatomy, Kiel University, D-24118 Kiel, Germany
[b] Department of Neurosurgery, University Medical Center Schleswig-Holstein UKSH, Campus Kiel, D-24105 Kiel, Germany
[c] Institute for Materials Science, Kiel University, D-24143 Kiel, Germany

ARTICLE INFO

Article history:
Received 8 July 2019
Received in revised form 25 October 2019
Accepted 1 November 2019

Keywords:
Glioma co-culture *in vitro* model
R-(−)-gossypol
AT101
Temozolomide
Sequential treatment
Resection grade
Tumor microenvironment

ABSTRACT

Background: The treatment of glioblastomas (GBM) is still a clinical challenge. Current GBM therapeutic plans focus on the development of new strategies for local drug administration in the tumor cavity to realize an efficient long-term treatment with small side-effects. Here, different amounts of residual GBM cells and healthy brain cells define the microenvironment of the tumor cavity after individual surgical GBM resection (complete or incomplete).
Methods: We evaluated available *in vivo* data and determined the required amounts and numerical ratios of GBM and healthy brain cells for our *in vitro* (in)complete resection dual co-culture model. We applied a generic two-drug treatment [Temozolomide (TMZ) in combination with AT101, followed by single AT101 treatment] strategy and analyzed the results in comparison with appropriate mono-culture systems to prove the applicability of our model.
Results: We established a suitable GBM dual co-culture model, mimicking the complete and incomplete resection *in vitro*, giving stable and reliable results on drug testing. Both dual co-culture conditions protectively influenced on cell death and growth rates of primary GBMs when treated with TMZ + AT101/AT101, although the treatment strategy *per se* was still efficient. Cell death of astrocytes correlated with amounts of increasing GBM cell numbers in the incomplete resection model upon drug treatment, and probably GBM-released chemokine and cytokines were involved in this interplay.
Conclusions: Our results suggest that this dual co-culture model provides a biologically relevant platform for the discovery and compound screening of local GBM treatment strategies.

1. Introduction

Glioblastomas (GBMs) are highly malignant primary brain tumors characterized by a pronounced resistance to chemo- and radiotherapy and an infiltrative progression resulting in the development of rapid relapses (Ohgaki and Kleihues, 2005). Despite great improvements in microsurgery and aggressive upfront treatment, patients' prognosis still remains poor (Ohgaki and Kleihues, 2005). Current guidelines for the treatment of GBMs include tumor resection followed by a combined radiochemotherapy. Complete resection of the contrast-enhancing tumor bulk is still a mainstay of GBM therapy offering the best chance for prolonged patients' survival (Bette et al., 2018; Grabowski et al., 2014; Kreth et al., 2013; Trifiletti et al., 2017). However, due to the typical diffuse tumor extension affecting often eloquent regions and several other patient-related risk factors (*e.g.* advanced age, low Karnofsky Performance Scale scores, co-morbidity), the majority of GBM patients still undergo incomplete resection (Grabowski et al., 2014; Kreth et al., 2013). As a result, post-surgery chemotherapeutic treatment has to deal with a complex patient-personalized situation – different sizes and amounts of still existing tumor volumes/cells have to be ideally eradicated without affecting healthy brain cells. Indeed, it was shown that the resection grade clearly influences the chemotherapeutic treatment efficiency. When analyzing cohorts of GBM patients with low/high residual tumor volume treated

Abbreviations: DMEM, Dulbecco's modified Eagle's medium; DMSO, dimethyl sulfoxide; FBS, fetal bovine serum; GBM, glioblastoma multiforme; PC, primary culture; TAM, tumor associated macrophages; TMZ, Temozolomide.

* Corresponding author at: Department of Neurosurgery, University Medical Center Schleswig-HolsteinUKSH, Campus Kiel, Arnold-Heller-Str.3, Building 41, 24105 Kiel, Germany.
E-mail address: Janka.Held-Feindt@uksh.de (J. Held-Feindt).
[1] Shared first authorship.

https://doi.org/10.1016/j.aanat.2019.151440

Table 1
Calculations on cells for the establishment of the (in)complete resection model.

	Mean size [cm^2]	Human astrocytes $3.15*10^{-5}$	Human microglia 2.7^{-5}	Human primary GBM (PC1/PC2) $3.3*10^{-5}$
Incomplete resection	% cells	1%	29%	70%
	Number of cells in 28.3 cm^2	$8.9*10^3$	$2.9*10^5$	$6*10^5$
	Actual seeded number of cells	$2.7*10^3$	$8.7*10^4$	$1.8*10^5$
Complete resection	% cells	80%	10%	10%
	Number of cells	$7.1*10^5$	$1*10^5$	$8.6*10^4$
	Actual seeded number of cells	$1.2*10^5$	$1.7*10^4$	$1.5*10^4$

with/without combined radiochemotherapy, those with low residual volumes ("complete resection") and Stupp scheme treatment showed the best prognosis, whereas patients with high residual volumes ("incomplete resection") without Stupp scheme exhibited the worst prognosis (Bette et al., 2018). Thus, besides its importance for the analysis of patients' overall survival, this data clearly implicates that GBM resection grade has to be taken into account when proving the efficiency of current and new drug treatment strategies.

Contrary to this, current GBM *in vitro* models used for preclinical testing of promising new drugs or treatment strategies mostly neglect the importance of the complete or incomplete GBM resection situation. Although a variety of different GBM *in vitro* models and novel culture sytems were developed – *e.g.* 3D organotypic spheroids, tumor organoids, brain slices, microfluidic systems or "mini-brains" (Balvers et al., 2017; Caragher et al., 2019; Lenting et al., 2017; Manini et al., 2018; William et al., 2017) – different proportions of tumor and healthy cells representing the complete and incomplete resection are still not common in these models. This point becomes even more relevant when the applicability of systems for local drug treatment strategies of GBMs should be evaluated. After placement in the resection cavity and according to the individual resection situation, these systems and the released drugs influence different proportions of healthy and tumor cells. Whilst after a complete resection of the tumor the relation of single remaining GBM cells is very low compared to healthy cells in the wall of the resection cavity, the proportion of GBM cells after an incomplete resection is much higher.

To deal especially with this point, we now established and tested the applicability of a GBM dual co-culture model, mimicking *in vitro* the complete and incomplete resection, by using different proportions of healthy and tumor cells and applying an exemplary two-drug treatment strategy. Since in our hands GBM cells influenced on the death of astrocytes in the incomplete resection dual co-culture model, we analyzed in a first attempt, which GBM-released soluble factors may be involved in this interplay, and whether a minimal amount of GBM cells was essential to trigger this effect.

2. Materials and methods

2.1. Cultivation of primary cells and cell lines

Human primary GBM samples were surgically dissected at the Department of Neurosurgery (Kiel, Germany) in accordance with the Helsinki Declaration of 1975 and with approval of the ethics committee of the University of Kiel, Germany, after written informed consent of donors (file references: D471/15 and D524/17). Tumors were diagnosed and classified according to WHO criteria by a pathologist. Cultured human primary GBM cells were generated by dissociation of tumor material and cultured under non-stem cell conditions as previously described (Hattermann et al., 2010). The human fetal astrocyte cell line SVGA was kindly provided by the group of Christine Hanssen Rinaldo, University Hospital of North Norway (Henriksen et al., 2014) with the permission of W. J. Altwood (Schweighardt et al., 2001). The human microglial cell line HMC3 was purchased by the American Type Culture Collection (ATCC, Manassas, Virginia, USA). All primary cells or cell lines were cultured in Dulbecco's modified Eagle's medium (DMEM; Life Technologies, Carlsbad, CA, USA) supplemented with 10% fetal bovine serum (FBS; PAN-Biotech GmbH, Aidenbach, Germany), 1% Penicillin-Streptomycin (10,000 U/ml; Thermo Fisher Scientific, Waltham, MA, USA), and 2 mM additional L-glutamine (Thermo Fisher Scientific). Cells were routinely checked for *Mycoplasma* contamination by bisbenzimide staining.

2.2. Stimulation of cell lines

For stimulation, primary tumor cells as well as SVGA and HMC3 were seeded in numbers as depicted in Table 1 or as given in the result part in DMEM without phenol-red (Life Technologies) supplemented with 10% FBS, 1% Penicillin-Streptomycin and 2 mM L-glutamine (from now on named as stimulation medium) to adhere overnight at 37 °C/5% CO_2. Cells which were seeded on coverslips (Ø 18 mm) were allowed to adhere in 30 µL medium for three hours, prior to the flooding of the cell culture inserts (Millicell®-CM 0.4 µm, Merck Millipore, Burlington, MA, USA) with 2 mL medium. On the following day, cells where washed with PBS, medium was exchanged to stimulation medium containing 50 µM TMZ [stock dissolved at 100 mM in dimethyl sulfoxide (DMSO; Sigma-Aldrich, St. Louis, MO, USA)] and 2.5 µM AT101 (stock dissolved at 100 mM in DMSO; Tocris, Bristol, UK), and cells were cultured up to three days. On day three medium was exchanged to DMEM without phenol-red including supplements plus 2.5 µM AT101, and cells were cultivated for another three days. This therapeutic plan was shown to be highly efficient in a long-term glioblastoma *in vitro* model published by our group before (Adamski et al., 2018). Controls were stimulated with the equal volume of DMSO. Cytotoxicity assay (see below) was performed after three and six days of stimulation, respectively.

2.3. Cytotoxicity assay

To determine the cytotoxic effects, the quantitative CytoTox-Fluor™ Cytotoxicity Assay (Promega, Madison, WI, USA) was performed according to the manufacturer's instruction. Briefly, supernatants of stimulated cells were collected at day three and six of stimulation, respectively, and mixed with the fluorogenic bis-AAF-R110 substrate, at which supernatants were taken from each compartment in order to measure cytotoxicity for each cell type separately. The emerging fluorescence was measured in a microplate reader (GENios, Tecan Group, Maennedorf, Switzerland) at 485/535 nm. The exact numbers of dead cells were determined according to different numbers of digitonin-lysed (82.5 µg/ml; Merck Millipore, Burlington, MA, USA) cell-dilutions of each cell line. The percentage of dead cells on day three and six, respectively, was determined as described in equation 1 and 2. Moreover, the cell survival was determined by counting of viable cells with a hemocytometer at day 0, 3 and 6 of the stimulation. Growth rates were

calculated as n-fold amount of alive cells compared to day 0 of the stimulation ($n = 3–5$ independent experiments).

$$\text{dead cells (day 3)}[\%] = \frac{\text{amount of dead cells (day 3)}}{\text{amount of dead cells(day 3)} + \text{amount of viable cells(day 3)}} \times 100 \quad (1)$$

$$\text{dead cells (day 6)}[\%] = \frac{\text{amount of dead cells (day3 + day6)}}{\text{amount of dead cells(day3 + day 6)} + \text{amount of viable cells (day 6)}} \times 100 \quad (2)$$

2.4. Quantitative reverse transcription-polymerase chain recation (qRT-PCR)

RNAs of different mono- and co-culturted cell types were isolated with the TRIzol® Reagent (Thermo Fisher Scientific) or with the ARCTURUS® PicoPure® RNA Isolation Kit (Applied Biosystems, Waltham, MA, USA) according to the manufacturer's instructions at day three of stimulation. DNase digestion, cDNA synthesis, and qRT-PCR were performed as described before (Hattermann et al., 2010) using TaqMan primer probes (Applied Biosystems): CCL3 (Hs00234142_m1), CCR1 (Hs00174298_m1), CCR4 (Hs00747615_s1), CCR5 (Hs00152917_m1), interleukin-1β (IL-1β) (Hs01555410_m1), interleukin-1β receptor (IL-1βR) (Hs00991010_m1), interleukin-6 (IL-6) (Hs00985639_m1), interleukin-6 receptor (IL-6R) (Hs01075664_m1), tumor necrosis factor-α (TNF-α) (Hs00174128_m1), tumor necrosis factor-α receptor 1 (TNF-αR1) (Hs01042313_m1), glycerinaldehyde 3-phosphate dehydrogenase (GAPDH) (Hs99999905_m1). Cycles of threshold (C_T) were determined, and ΔC_T values of each sample were calculated as $CT_{\text{gene of interest}} - CT_{\text{GAPDH}}$. The induction of gene expression upon stimulation is displayed as n-fold expression changes $= 2^{\Delta CTcontrol - \Delta CTstimulus}$.

2.5. Statistical analysis

All data has been analyzed with the GraphPad Prism 5 Software (GraphPad Software, La Jolla, CA, USA) and is dispicted as mean ± standard deviation, if not described different. To check for statistical significance on percentage of dead cells between treatment and control, a paired student *t*-test (for mono-culture controls) and a repeated-measures Two-Way ANOVA followed by Bonferroni's multiple comparison test (co-cultures) was employed. To study the effect between culture conditions (mono- *vs.* co-culture) on the percentage of dead cells, a repeated measures Two-Way ANOVA followed by Bonferroni's multiple comparison test was applied, comparing all cells on different days of culture. To compare growth rates of mono- and co-cultures upon different treatment over the time (three *vs.* six days), a Two-Way-ANOVA followed by Bonferroni's multiple comparison test was used. To study the differences in gene expression upon treatment as well as the cultivation technique after three days in PC1 cells, a repeated-measures Two-Way ANOVA followed by Bonferroni's multiple comparison test of the ΔΔCT values was used. The native expression of the respective receptors on SVGA and HMC3 cells was analyzed for statistical significance by a repeated measures Two-Way ANOVA followed by Bonferroni's multiple comparison test, comparing the ΔCT values of each cell line in mono- *vs.* co-culture. To determine the influence of PC1 cell density on the growth rate as well as cytotoxicity on SVGA cells in the incomplete resection model, a one-tailed correlation analysis by Pearson was employed. R values are dispicted in the graphs, whereas values close to 1 respectively −1 indicate correlation respectively inverse correlation between analyzed parameters. Asterisks indicate statistical significance: $^{*}p < 0.05$, $^{**}p < 0.01$, $^{***}p < 0.001$ respective $^{****}p < 0.0001$.

3. Results

3.1. Establishment of the GBM (in)complete resection dual co-culture model

Glioblastoma tumor tissue does not only consist of tumor cells, but also of normal brain cells, which are part of the tumor microenvironment. To mimic *in vitro* the *in vivo* influence of the tumor microenvironment on GBM-treatment strategies, we developed two *in vitro* models which either mimic the total resection (complete) or the subtotal resection (incomplete) of the tumor mass. To estimate the cell numbers needed for the (in)complete resection models *in vitro*, different assumptions were made:

(1) Cell amounts and ratios of healthy and GBM cells after the (in)complete resection of the tumor were determined according to published results. The majority of non-tumorus cells in the tumor microenvironment are glial cells (30% of the bulk tumor mass), which can be divided into 29% tumor-associated microglia/macrophages and 1% reactive astrocytes (Roggendorf et al., 1996; Matias et al., 2018; Guan et al., 2018). Therefore, cell ratios were chosen as 70%, 29% respective 1% for primary GBM cells, HMC3 microglia and SVGA astrocytes respectively, for an incomplete resection of the tumor. In contrast to that, the complete resection mimics the ratios of normal brain tissue with little amount of remaining GBM cells. However, the knowledge of cell ratios in the healthy brain is quite diverse, with an average of around 40% oligodendrocytes, 40% astrocytes and 20% microglia (Bartheld et al., 2016). Moreover, precise cell ratios after a complete resection of a GBM tumor are not yet described in literature, to our knowledge, whereas it is known that GBM cells strongly interact with the surrounding tissue by *e.g.* attracting astrocytes toward the tumor side and therefore influencing their proliferation (Matias et al., 2018; Oliveira et al., 2017; Quail and Joyce, 2017). Therefore, expecting an increased number of astrocytes and a decreased number of microglia (due to the removal of the direct tumor microenvironment during the full resection), cell ratios of 80%, 10% and 10% were chosen for SVGA astrocytes, HMC3 microglia respective GBM primary cells for the complete resection model of a GBM tumor.

(2) Cell numbers on the surface area of the resection cavity were determined after calculation of the surface of the resection hole and the 2D-sizes of the different cell types. The surface area of the resection hole was calculated as 28.3 cm^2, assuming a typical tumor diameter of 3 cm (Murray, 2012; Bette et al., 2018). Therefore, the volume of the tumor cavity to be filled with cerebrospinal fluid was calculated to be 14.1 mL for a 3 cm tumor in diameter. The mean 2D-sizes of primary GBM cells, HMC3 microglia and SVGA astrocytes were determined by scaling of cells with the Fiji software (Fiji contributors), after taking phase-contrast images with an Axiovert 200 microscope (Carl Zeiss AG) and the AxioVision 40 software (Carl Zeiss AG). After this, the cell numbers to be found on the surface area of the resection cavity were calculated based on the cell-ratios present in the different resection models (see Table 1).

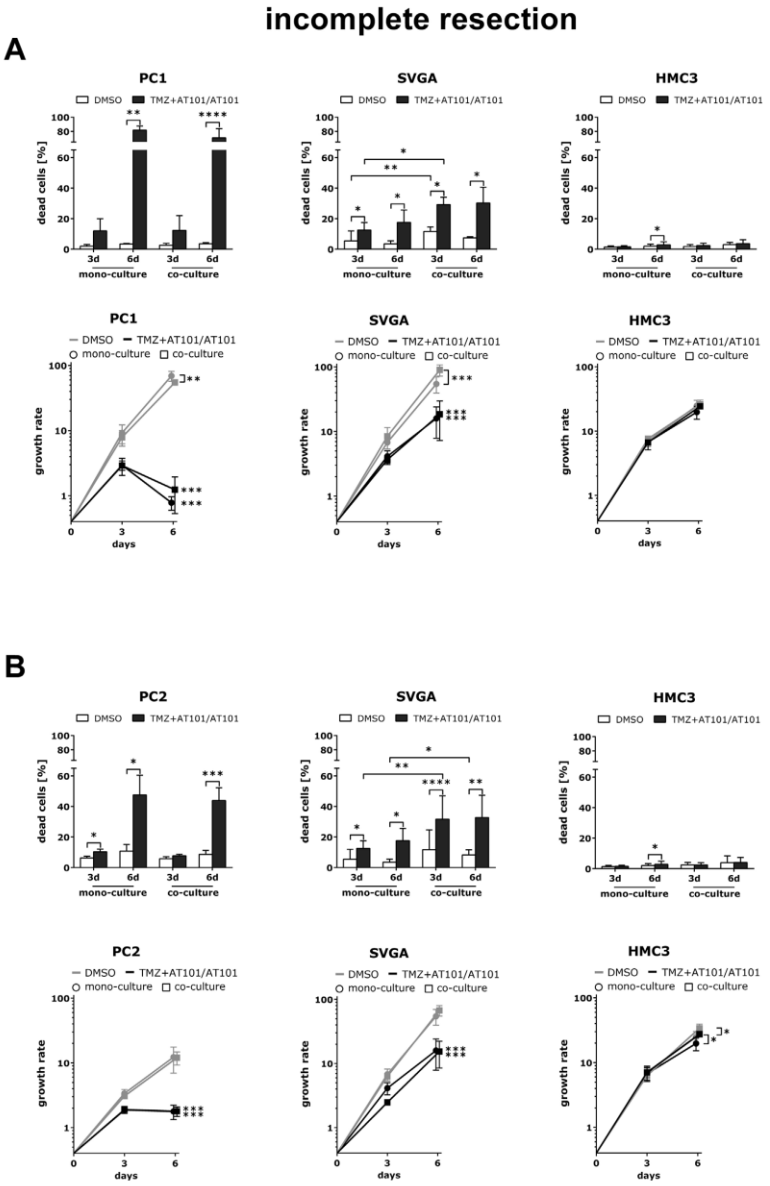

Fig. 1. Effects of the Temozolomide (TMZ) + AT101/AT101 treatment in the **incomplete resection model** on the percental amounts of dead cells and individual growth rates of two different mono- *vs.* co-cultured primary human glioblastoma cultures (PC1 and PC2), associated human astrocytes (SVGA) and microglial cells (HMC3) compared to appropriate dimethyl sulfoxide (DMSO)-treated control samples (**A and B**, respectively). Cells were treated with 50 μM TMZ and 2.5 μM AT101 for three days, followed by 2.5 μM AT101 without additional TMZ for another three days. Cytotoxicity assays and cell counting were performed at day three and six of the stimulation ($n = 3–5$). Means of raw data are significantly different for $^{*}p < 0.05$, $^{**}p < 0.01$, $^{***}p < 0.001$ respective $^{****}p < 0.0001$.

(3) Cells must survive in our dual co-culture model for up to six days without any trypsinization (cell de-attachment) process.

According to these three topics, we scaled down numbers and ratios of different cell types proportionately to be practicable for *in vitro* handling. As a result, cell numbers and ratios of the complete and incomplete resection dual co-culture model differed in the two models at the beginning of experiments (Table 1), but, this was necessary to approximately represent the *in vivo* situation. However, of course they did not differ between control and stimulated samples of the individual complete or incomplete model, respectively.

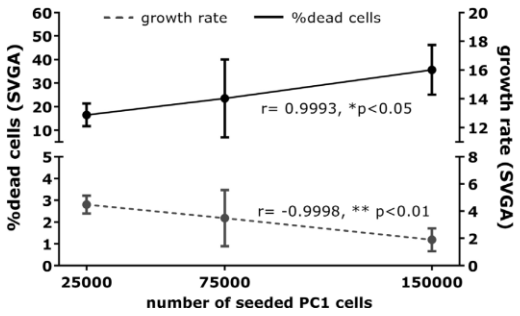

Fig. 2. Correlation analysis between seeded glioblastoma cell amounts and percentages of dead astrocytes and growth rates in the **incomplete resection model** determined after three days of treatment with TMZ + AT101/AT101. Variable amounts (25,000 up to 150,000 cells) of co-cultured primary human glioblastoma cells (PC1) were chosen, whilst cell amounts of co-cultured human astrocytes (SVGA) and microglial cells (HMC3) remained constant in the incomplete resection model. Cells were treated with 50 μM TMZ and 2.5 μM AT101 for three days, and cytotoxicity assays and cell counting were performed ($n = 3$). *R* values close to 1 respectively −1 indicate correlation respectively inverse correlation between analyzed parameters. Correlation coefficients r after Pearson are significant for $^{*}p < 0.05$ respective $^{**}p < 0.01$.

To finally create the two *in vitro* co-culture models, cells were co-cultivated guaranteeing the exchange of molecules (crosstalk), but without a direct contact between the cell types. Hence, cells were either seeded in 10 cm culture dishes (greater cell population) or grown on cover slips (smaller cell populations) in cell culture inserts (0.4 μm pore size) placed into the culture dish on top of the greater cell population. To mimic the free cavity volume to be filled with cerebrospinal fluid after the removal of the tumor, 10 mL culture medium was added to the 10 cm culture dish, whilst 2 mL medium was added to each insert, yielding total of 14 mL in the system.

3.2. Applicability and biological relevance of the GBM (in)complete resection dual co-culture model

To prove the applicability and biological relevance of our *in vitro* GBM (in)complete resection dual co-culture model, we chose a therapeutic plan recently published by our group shown to be useful for the treatment of human mono-cultured commercial GBM cell lines and similarly protective for human mono-cultured astrocytes *in vitro* (Adamski et al., 2018). Here, a sequential treatment with Temozolomide (TMZ) and AT101, the R-(−)-enantiomer of the naturally occurring cottonseed-derived polyphenol gossypol, firstly applied as a combination for three days followed by single AT101 treatment for another three days (TMZ + AT101/AT101), yielded higher cytotoxicity and better tumor growth control in comparison to *e.g.* single TMZ treatment.

We applied this therapeutic plan to our GBM (in)complete resection dual co-culture model using human primary GBM cells and different portions of normal brain and tumor cells according to the resection grade, compared our findings to appropriate monocultures of the different cells types and summarized our results in Figs. 1–4.

When looking at the GBM incomplete resection model (Fig. 1), TMZ + AT101/AT101 was clearly efficient to kill and inhibit the growth of two different primary GBMs (PC1 and PC2, Fig. 1, left column) grown in mono- and co-cultures after six days of treatment. However, the amounts of dead cells (PC1 and PC2) and the inhibition of proliferation (PC1) were less in co-cultures compared to mono-cultures even though these effects were not statistically significant (Fig. 1, A/B, PC1 and PC2). Interestingly, dimethyl sulfoxide (DMSO)-treated PC1 controls grown in co-cultures were characterized by a slightly slower growth rate *vs.* mono-cultured ones, and this effect was significant between the different culture conditions ($p < 0.01$).

The survival of human astrocytes grown in mono- and co-cultures in the incomplete resection model was also slightly affected by the treatment, however, this effect was clearly more pronounced in co-cultures pointing to an additional influence of GBM cells on the treatment-dependent survival of human astrocytes (Fig. 1, A/B middle column, different amounts of dead cells statistically significant between varying culture conditions after three days of treatment, $p < 0.05$ and $p < 0.01$ for PC1 and PC2 mono-/co-cultured SVGA cells). An influence of GBM cells on SGVA cells was also detectable after three days (PC1 mono- *vs.* co-cultured SVGA cells) and six days (PC2 mono- *vs.* co-cultured SVGA cells) of cultivation time in DMSO-treated control samples ($p < 0.01$ and $p < 0.05$). Further, PC1 co-cultured DMSO-treated astrocytes showed in comparison to mono-cultured ones an increased growth rate ($p < 0.001$). However, this increased proliferation rate was not observable in PC2 co-cultured astrocytes, although the TMZ + AT101/AT101 treatment slightly influenced the growth rate of both PC1 and PC2 co-cultured SVGA cells (Fig. 1, A/B middle column). Interstingly, when applying different amounts of PC1 GBM cells (25,000; 75,000; 150,000) whilst cell amounts of SVGA and HMC3 remained constant in the incomplete resection model upon drug treatment, a significant positive correlation between numbers of GBM cells and percentages of dead astrocytes was detectable (Fig. 2). Here, increasing amounts of GBM cells caused a decrease on the survival of co-cultured astrocytes. Concomitant with these observations, a significant negative correlation was detectable for the growth rate of astrocytes upon rising PC1 GBM cell concentrations (Fig. 2).

Human HMC3 microglia cells were not notably affected by the TMZ + AT101/AT101 treatment and the different culture conditions (Fig. 1, A/B right column). No clear effects were detectable for both controls and drug-treated samples with exception of a slightly increased growth rate of PC2 co-cultured HMC3 cells compared to mono-cultured ones (Fig. 1, B right column, bottom, $p < 0.05$).

To determine in a first attempt, which GBM-released soluble factors maybe responsible for the influence of GBM cells on co-cultured healthy brain cells in the incomplete resection situation, we exemplarily analyzed the mRNA expression of GBM-releasable factors in PC1 cells after three days of treatment, and *vice versa* the expression of possible receptors in astrocytes and microglia cells as well. Since it is well known that chemokines as well as cytokines are important mediators in the brain and GBM biology (Matias et al., 2018), we restricted our investigations first of all on these factors choosing exemplarily interleukin (IL)-1 and IL-6 with their corresponding receptors IL-1R and IL-6R, tumor necrosis factor-α (TNF-α) and its receptor TNF-RSF1, and the chemokine ligand 3 (CCL3) with its receptors CCR1, CCR4 and CCR5. Results are depicted in Fig. 3, A–D. Interstingly, IL-1, IL-6, TNF-α and CCL3 mRNA expression was induced in both mono- and co-cultured TMZ plus AT101-treated GBM cells compared to appropriate controls samples, but to clearly lower amounts in co-cultured GBM cells compared to mono-cultured ones. These effects (induction under drug-treatment irrespective of culture conditions and lower induction in co-cultured GBM cells) were most pronounced and statistically significant for CCL3 (Fig. 3, D). Further, the corresponding receptors of investigated cyto- and chemokines were found to be expressed on both astrocytes and microglia cells with exception of the CCL3 receptor CCR5 (data not shown). However, basic expression of different receptors did not differ between different culture conditions (Fig. 3, A–D).

When looking at the GBM complete resection model (Fig. 4), TMZ + AT101/AT101 was also efficient to kill and inhibit the growth

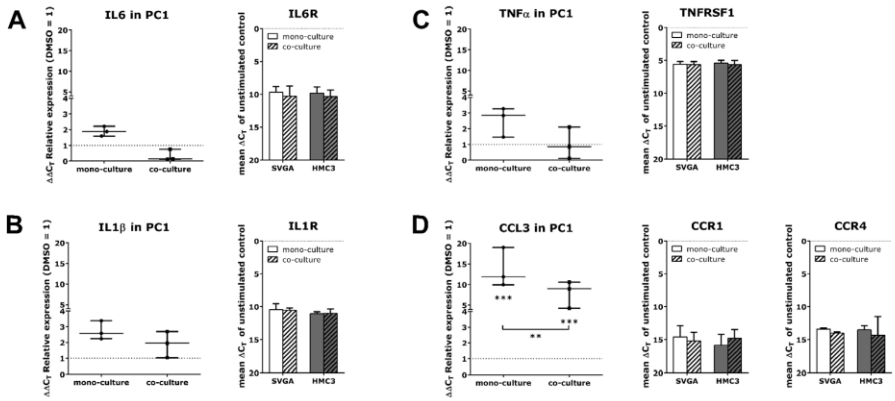

Fig. 3. mRNA expression of different chemokines and cytokines in PC1 cells, SVGA and HMC3 in the **incomplete resection model.** Co- and mono-cultured cells were treated with 50 μM TMZ and 2.5 μM AT101 for three days, respectively, RNA was isolated and qRT-PCR was performed ($n = 3$). Cycles of threshold (CT) were determined, and ΔCT values of each sample were calculated as CT_{gene} of interest − CT_{GAPDH}. The induction of gene expression upon stimulation is displayed as n-fold expression changes = $2^{\Delta CTcontrol - \Delta CTstimulus}$. Data is significantly different for $^{**}p < 0.01$ respective $^{***}p < 0.001$.

of PC1 and PC2 primary GBMs (Fig. 4, A/B, left column) grown in mono- and co-cultures – especially after six days of treatment. However, for PC1 the treatment was less effective in both mono- and co-cultured cells when comparing the results to the data of the incomplete resection model (Figs. 1 and 4, A, right column). Additionally, the treatment was less effective in co-cultured PC1 and PC2 *vs.* mono-cultured ones in the complete resection model reflected by less amounts of dead cells (different amounts of PC1 dead cells statistically significant between varying culture conditions after six days of treatment, $p < 0.01$). Moreover, the growth rates of DMSO-treated control samples were slightly increased in co-cultured *vs.* mono-cultured PC1 and PC2 cells, whereas the growth rates of drug-treated co-cultured samples varied between in- or decreased effects in comparison to investigated GBM mono-cultures. However, all these effects were not statistically significant between different culture conditions.

The survival of human astrocytes grown in mono- and co-cultures in the complete resection model was only very slightly affected by the treatment and also less pronounced in comparison to the results of the incomplete resection model (Figs. 1 and 4 A/B, middle column). Remarkably, in the complete resection model, co-culture conditions did not increase the cytotoxic effects of treatment in SVGA cells as it was observed in the incomplete model. The growth rate of human astrocytes was also slightly influenced by the treatment, but no differences were detectable between different culture conditions with exception of a minimally decreased growth rate of PC2 co- *vs.* mono-cultured SVGA cells in the control samples (Fig. 4, B, middle column, bottom, $p < 0.05$).

Human HMC3 microglia cells were not notably affected by the TMZ + AT101/AT101 treatment and the different culture conditions (Fig. 4, A/B right column). However, slightly increased amounts of dead HMC3 cells were detectable in DMSO-treated control samples grown for three days in co-cultures compared to mono-cultures (Fig. 4, A, right column, top, $p < 0.001$). Additionally, no clear effects were detectable for the growth rates of the microglia cells with exception of a slightly decreased growth rate of PC1 co-cultured control-treated HMC3 cells *vs.* mono-cultured ones (Fig. 4, B right column, top, $p < 0.05$).

Summarized, our *in vitro* GBM (in)complete resection dual co-culture model was suitable for drug testing giving stable and reliable results. Here, co-culture conditions clearly influenced the amounts of dead cells and the growth rates of especially primary GBMs and – to clearly less extents – normal astrocytes when treated with TMZ + AT101/AT101, although the treatment strategy *per se* was still efficient to kill primary GBM cells. Further, it seems that GBM cells influenced on the survival of normal astrocytes dependently on their cell amounts in the incomplete resection model, probably by the involment of different GBM-released chemokines and cytokines. Both the incomplete and especially the complete resection co-culture protected GBM cells from the drug treatment.

4. Discussion

The treatment of GBMs, which are known as heterogeneously composed, chemoresistant and highly malignant brain tumors, is still a clinical challenge. Although a broad range of different therapeutic strategies were developed in the past years, most drugs failed to predict clinical efficiency (Caragher et al., 2019). To overcome this problem, various improved pre-clinical *in vitro* test systems were designed. The use of patient-derived GBM cells, the addition of different growth factors and tumor-secreted mediators, the imitation of the brain's unique extracellular matrix and circulatuing structures as well as the establishment of complex co-culture and 3D-culturing systems including normal brain cells and various nutrient sources for the tumor metabolism (*e.g.* organotypic spheroids, 3D scaffolds, brain slices, cerebral or tumor organoids) are only some examples for these constant efforts (Caragher et al., 2019). However, more and more current GBM therapeutic plans focus on the development of new strategies for placement of promising drugs directly in the tumor cavity to realize an efficient long-term treatment with small side-effects. In this special case, different amounts of residual GBM cells and healthy brain cells define the microenvironment of the tumor cavity according to the individual surgical GBM resection grade (complete or incomplete). Consequently, to prove the treatment efficiency of promising drugs for their local administration, the development of specialized *in vitro* systems are mandatory.

Thus, we established a GBM dual co-culture model, mimicking the complete and incomplete resection *in vitro*. To this, we obtained available *in vivo* data according to known average GBM sizes, resection grades, volumes and compositions (Bette et al., 2018; Gieryng et al., 2017; Grabowski et al., 2014; Graeber et al., 2002; Trifiletti et al., 2017; Quail and Joyce, 2017; Bartheld et al., 2016), calculated the tumor surface area and measured the mean size of our used

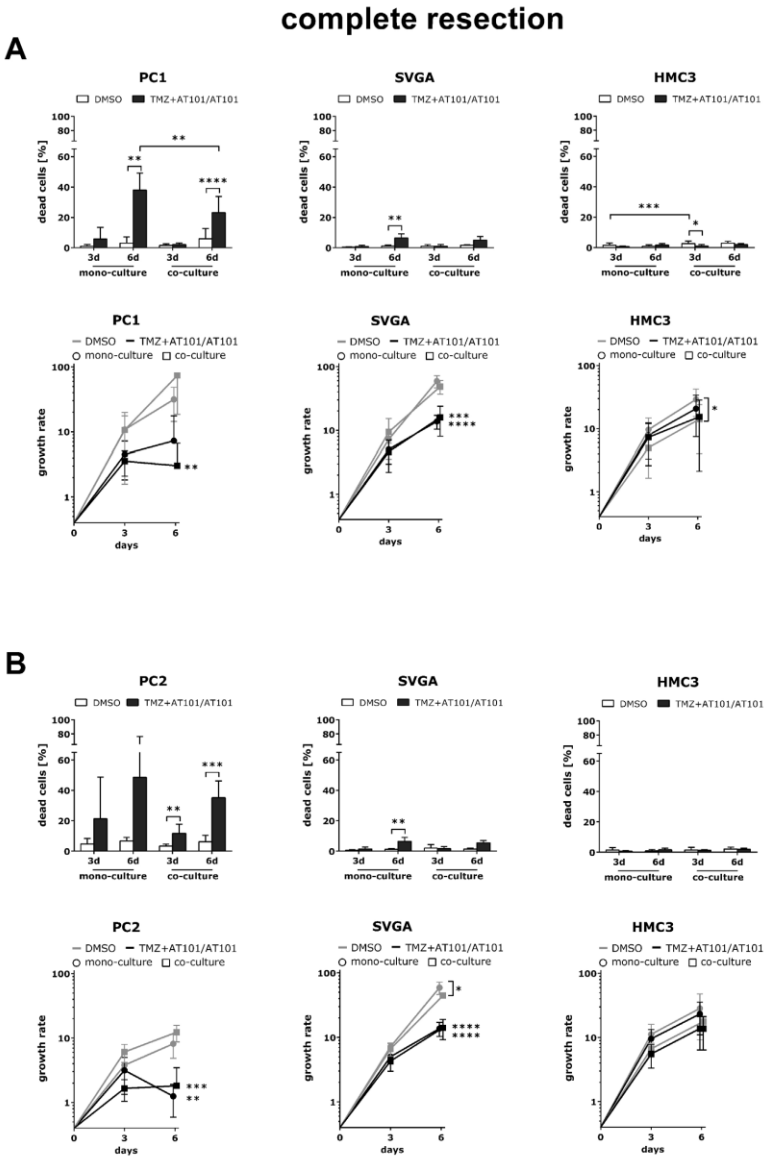

Fig. 4. Effects of the Temozolomide (TMZ) + AT101/AT101 treatment in the **complete resection model** on the percental amounts of dead cells and individual growth rates of two different mono- vs. co-cultured primary human glioblastoma cultures (PC1 and PC2), associated human astrocytes (SVGA) and microglial cells (HMC3) compared to appropriate dimethyl sulfoxide (DMSO)-treated control samples (**A and B**, respectively). Cells were treated with 50 μM TMZ and 2.5 μM AT101 for three days, followed by 2.5 μM AT101 without additional TMZ for another three days. Cytotoxicity assays and cell counting were performed at day three and six of the stimulation ($n = 3–5$). Means of raw data are significantly different for $^{*}p < 0.05$, $^{**}p < 0.01$, $^{***}p < 0.001$ respective $^{****}p < 0.0001$.

primary GBM and healthy brain cells, and determined in this manner the required amounts and numercial ratios of GBM and healthy brain cells for our *in vitro* (in)complete resection model.

To date a multitude of different GBM *in vitro* models were developed (reviewed in Balvers et al., 2017; Caragher et al., 2019; Lenting et al., 2017; Manini et al., 2018). Ideally, they have to deal with several topics to approximatively reflect the *in vivo* situation: *e.g.* tumor heterogeneity, cellular plasticity, microenvironmental factors including the brain extracellular matrix, regional differences in the tumor microenvironment, nutrient availability and metabolism, and the existence of non-tumor cells, which produced and are influenced by secreted factors as well as contact-mediated

interactions (Caragher et al., 2019; Lenting et al., 2017; Manini et al., 2018). When comparing the dual co-culture model used in this study to mono-culture systems including *e.g.* GBM neurospheres, or solely GBM-cells containing three-dimensional (3D) scaffolds, probably, our model will better predict *in vivo* responses since it includes the paracrine communication of different cell types in a surgical-relevant manner. Further, cell retrieval from polystyrene scaffolds is never 100% effective probably selecting cell subpopulations that are more loosely attached to the matrix (Caragher et al., 2019). Since we used culture dishes as well as cover slips in cell culture inserts as basis for cell attachment, we have the possibility to efficiently retrieve different cell types in our model. Therefore, although only a parcrine communication between the different cell types is allowed in our model, we are able to analyze the response to *e.g.* drug treatment on the different cell types separatively. However, the missing of the cell-cell interconnectivity in our dual co-culture model is a clear limitation of our *in vitro* system. The influence of cell-cell-interconnectivity is better reflected by *e.g.* organotypic spheroids derived from biopsies or brain tumor slices comprising directly interconnected multiple cell types (Caragher et al., 2019; Lenting et al., 2017; Manini et al., 2018). However, using these systems it is not possible to mimick the complete and incomplete resection situation *in vitro* since defined cell amounts and ratios of different cell types could not be easily obtained. Nevertheless, these systems could be more stable to drug treatment strategies also under cultivation conditions without or with only low serum addition. In our system, healthy brain cells (especially HMC3 microglia cells) were strongly affected already in control samples without drug treatment when cultured up to six days only with addition of 0.5% FCS (data not shown). As a result, cultivation must be realized with 10% FCS supplementation in our dual co-culture model. Nevertheless, it is kown that high serum addition does not represent the physiological *in vivo* situation favoring *e.g.* epigentic changes as well as alterations in copy numbers of growth receptors (William et al., 2017), therefore this limitation of our model should be clearly stated. Further improvements in the co-culture methodology yielded into the development of the so-called lab-on-a-chip technology that allowed the creation of *in vitro* models mimicking the complexity of the *in vivo* environment (Menon et al., 2014). However, it is still rather challenging to create co-culture systems allowing cell-cell interactions combined with an easy control of different colonies of cells. Yet, Menon et al. (2014) published a possibility for discriminative cell seeding and to induce cellular interaction in a co-culture region. Further, Lin et al. (2018) developed a biomimetric microsystem that reconstitutes glioma perivascular niches on a chip to precisely control stem cell co-culture, Liu et al. (2017) simulated a three-dimensional tumor-microvascular structure on a microfluidic chip to study antioxidants effects on glioma cells *in vitro*, and Marino et al. (2018) fabricated a 3D real-scale, biomimetic and biohybrid model of the blood-brain barrier through two-photon lithography to co-culture endothelial and glioma cells.

To prove the applicability of our model, we applied a generic two-drug treatment strategy and analyzed the results in comparison to appropriate mono-culture systems. In our hands, GBM cells co-cultured in both model variants, complete or incomplete resection, responded less (but still efficient) to the TMZ + AT101/AT101 treatment compared to the corresponding mono-cultured cells. Consistently, recent studies showed distinct differences between drug effects on tumor cells cultured in a monolayer *vs.* a 3D heterogeneous cell culture environment (Chadwick et al., 2015; Kenny et al., 2015). Interestingly, both the complete and the incomplete culture conditions were protective for the tumor cells irrespective of the microenvironmental compositions with many tumor cells and less normal brain cells (incomplete resection) or *vice versa* less tumor cells and many normal brain cells (complete resection) in our model.

Indeed, Osswald et al. (2015) stated that glioma cells are able to communicate and cooperate with each other in a complex but ordered manner like a functional organ. It was shown that microtube-connected glioma cells were protected from cell death induced by radiotherapy and increased both their microtube number and their calcium communication as a reaction to the therapy (Osswald et al., 2015). Besides, it is well known that microglial cells and astrocytes play a critical role in promoting GBM growth (Matias et al., 2018). Microglial cells activated several pro-invasive signaling pathways (Gieryng et al., 2017; Manini et al., 2018), and tumor associated macrophages/microglia (TAMs) tended to be pro-tumorigenic, accumulated with higher tumor grade and produced different levels of pro- and anti-inflammatory cytokines (Hattermann et al., 2014). Further, glioma-secreted CX3CL1 enhanced the expression of different matrix metalloproteases in TAMs favoring the migratory and invasive potential of GBM cells (Held-Feindt et al., 2010). However, the effects of targeting TAMs in brain tumors were more context-regulated depending on different preclinical models tested (Pyonteck et al., 2013; Quail et al., 2016; Quail and Joyce, 2017). For astrocytes, several mechanisms are known in which way they favored GBM growth, chemoresistance, invasion and proliferation (for review: Brandao et al., 2019; Guan et al., 2018). For example, it was shown that glioma cells co-cultured with astrocytes were protected against apoptosis in response to TMZ and vincristine by establishing functional gap junctions for bidirectional communication (Brandao et al., 2019; Chen et al., 2016). Interestingly, in our hands, increasing amounts of GBM cells caused a decrease on the survival of co-cultured astrocytes upon drug treatment. Contrary, the complete resection microenvironment had no or only a minimal protective effect on the survival of astrocytes. Anyhow, a bi-directional communication between astrocytes and GBM cells is well known to be caused by several mediators (for review: Brandao et al., 2019; Guan et al., 2018). Thus, this effect could be possible mediated by different chemokines and cytokines, which are released by the GBM cells and due to expression of potential corresponding receptors are probably able to activate co-cultured astrocytes and microglial cells. Here, beside others, chemokines and cytokines are well known to be involved in the interplay of glioma cells, astrocytes and microglia cells (Matias et al., 2018). Indeed, in our hands, IL-1, IL-6, TNF-α and CCL3 were upregulated in GBM cells during dug-treatment, however, to smaller exents in co-cultured GBM cells. Interestingly, the pre-exposure of glial cells to conditioned medium from GBM cells led to the upregulation of several proteins related to inflammatory response, cell adhesion and extracellular structure organization within the secretome of the glial cells. *Vice versa*, conditioned medium of these primed glial cells promoted viability of GBM cells pointing to the modulation of GBM cells particularly by a paracrine activity (Oliveira et al., 2017). Additionally, microRNAs from astrocyte-derived exosomes were capable to favor outgrowth of brain metastatic cells (Zhang et al., 2015), and melanoma-derived cells within the brain became surrounded by astrocytes resulting in the suppression of apoptosis in response to several types of chemotherapy (Lin et al., 2010). However, Valiente et al. (2014) demonstrated that astrocytes reduced the survival of metastatic cells within the brain pointing to the assumption that astrocytes may play distinct roles in tumor-stroma interactions (Quail and Joyce, 2017). Summarizing all these different aspects, glioma biology includes a sophisticated interplay of different cell types with various functions, activation grades, paracrine and autocrine as well as direct communication skills yielding to a complex tumor ecosystem, which complicates the development of efficient teatment strategies.

5. Conclusion

In summary, we were able to etablish an (in)complete GBM resection dual co-culture model. Furthermore, our results suggest that drug discovery using this dual co-culture model for the human GBM disease is practical. Thus, our complex *in vitro* model may help to reduce the need for animal testing, since it provides a biologically relevant platform especially for screening compounds which are estimated for local treatment strategies.

Authors' contributions

Christina Schmitt: Data curation; Formal analysis; Investigation; Visualization; Validation; Software; Methodology; Writing – Original draft preparation. **Vivian Adamski**: Data curation; Formal analysis; Investigation; Visualization; Validation; Software; Methodology; Writing – Original draft preparation. **Florian Rasch**: Project administration; Resources Data curation; Investigation; Writing – review and editing. **Rainer Adelung**: Funding acquisition; Resources; Writing – review and editing. **Ralph Lucius**: Resources; Writing – review and editing; **Michael Synowitz**: Resources; Writing – review and editing. **Kirsten Hattermann**: Conceptualization; Funding acquisition; Project administration; Writing – review and editing. **Janka Held-Feindt**: Conceptualization; Funding acquisition; Project administration; Supervision; Methodology; Writing – Original draft preparation.

Funding

This work was funded by the German Research Foundation (DFG) as part of the Research Training Group "Materials4Brain" (RTG2154; P3, P7 and P8). The funding source is not involved in study design, in the collection, analysis and interpretation of data, in the writing of the report or in the decision to submit the article for publication.

Ethical statement

Human primary GBM samples were surgically dissected at the Department of Neurosurgery (Kiel, Germany) in accordance with the Helsinki Declaration of 1975 and with approval of the ethics committee of the University of Kiel, Germany, after written informed consent of donors (file references: D536/15, D471/15 and D524/17).

Acknowledgments

We thank Fereshteh Ebrahim, Brigitte Rehmke and Judith Becker for expert technical assistance.

References

Adamski, V., Schmitt, C., Ceynowa, F., Adelung, R., Lucius, R., Synowitz, M., Hattermann, K., Held-Feindt, J., 2018. Effects of sequentially applied single and combined temozolomide, hydroxychloroquine and AT101 treatment in a long-term stimulation glioblastoma in vitro model. Cancer Res. Clin. Oncol. 144, 1475–1485.

Balvers, R.K., Dirven, C.M., Leenstra, S., Lamfers, M.L., 2017. Malignant glioma in vitro models: on the utilization of stem-like cells. Curr. Cancer Drug Targets 17, 255–266.

Bartheld, C.S., Bahney, J., Herculano-Houzel, S., 2016. The search for true numbers of neurons and glial cells in the human brain: a review of 150 years of cell counting. J. Comp. Neurol. 524, 3865–3895.

Bette, S., Barz, M., Wiestler, B., Huber, T., Gerhardt, J., Buchmann, N., Combs, S.E., Schmidt-Graf, F., Delbridge, C., Zimmer, C., Kirschke, J.S., Meyer, B., Ryang, Y.M., Ringel, F., Gempt, J., 2018. Prognostic value of tumor volume in glioblastoma patients: size also matters for patients with incomplete resection. Ann. Surg. Oncol. 25, 558–564.

Brandao, M., Simon, T., Critchley, G., Giamas, G., 2019. Astrocytes, the rising stars of the glioblastoma microenvironment. Glia 67, 779–790.

Caragher, S., Chalmers, A.J., Gomez-Roman, N., 2019. Glioblastoma's next top model: novel culture systems for brain cancer radiotherapy research. Cancers (Basel) 11, E44.

Chadwick, E.J., Yang, D.P., Filbin, M.G., Mazzola, E., Sun, Y., Behar, O., Pazyra-Murphy, M.F., Goumnerova, L., Ligon, K.L., Stiles, C.D., Segal, R.A., 2015. A brain tumor/organotypic slice co-culture system for studying tumor microenvironment and targeted drug therapies. J. Vis. Exp. 105, e53304.

Chen, Q., Boire, A., Jin, X., Valiente, M., Er, E.E., Lopez-Soto, A., Jacob, L.S., Patwa, R., Shah, H., Xu, K., Cross, J.R., Massagué, J., 2016. Carcinoma-astrocyte gap junctions promote brain metastasis by cGAMP transfer. Nature 533, 493–498.

Gieryng, A., Pszczolkowska, D., Walentynowicz, K.A., Rajan, W.D., Kaminska, B., 2017. Immune microenvironment of gliomas. Lab. Invest. 5, 498–518.

Grabowski, M.M., Recinos, P.F., Nowacki, A.S., Schroeder, J.L., Angelov, L., Barnett, G.H., Vogelbaum, M.A., 2014. Residual tumor volume versus extent of resection: predictors of survival after surgery for glioblastoma. J. Neurosurg. 121, 1115–1123.

Graeber, M.B., Scheithauer, B.W., Kreutzberg, G.W., 2002. Microglia in brain tumors. Glia 40, 252–259.

Guan, X., Hasan, M.N., Maniar, S., Jia, W., Sun, D., 2018. Reactive astrocytes in glioblastoma multiforme. Mol. Neurobiol. 8, 6927–6938.

Hattermann, K., Held-Feindt, J., Lucius, R., Sebens Müerköster, S., Penfold, M.E., Schall, T.J., Mentlein, R., 2010. The chemokine receptor CXCR7 is highly expressed in human glioma cells and mediates anti-apoptotic effects. Cancer Res. 70, 3299–3308.

Hattermann, K., Sebens, S., Helm, O., Schmitt, A.D., Mentlein, R., Mehdorn, H.M., Held-Feindt, J., 2014. Chemokine expression profile of freshly isolated human glioblastoma-associated macrophages/microglia. Oncol. Rep. 32, 270–276.

Held-Feindt, J., Hattermann, K., Müerköster, S.S., Wedderkopp, H., Knerlich-Lukoschus, F., Ungefroren, H., Mehdorn, H.M., Mentlein, R., 2010. CX3CR1 promotes recruitment of human glioma-infiltrating microglia/macrophages (GIMs). Exp. Cell Res. 316, 1553–1566.

Henriksen, S., Tylden, G.D., Dumoulin, A., Sharma, B.N., Hirsch, H.H., Hanssen Rinaldo, C., 2014. The human fetal glial cell line SVG p12 contains infectious BK polyomavirus. J. Virol. 88, 7556–7768.

Kenny, H.A., Lal-Nag, M., White, E.A., Shen, M., Chiang, C.Y., Mitra, A.K., Zhang, Y., Curtis, M., Schryver, E.M., Bettis, S., Jadhav, A., Boxer, M.B., Li, Z., Ferrer, M., Lengyel, E., 2015. Quantitative high throughput screening using a primary human three-dimensional organotypic culture predicts in vivo efficacy. Nat. Commun., E6220.

German Glioma NetworkKreth, F.W., Thon, N., Simon, M., Westphal, M., Schackert, G., Nikkhah, G., Hentschel, B., Reifenberger, G., Pietsch, T., Weller, M., Tonn, J.C., 2013. Gross total but not incomplete resection of glioblastoma prolongs survival in the era of radiochemotherapy. Ann. Oncol. 24, 3117–3123.

Lenting, K., Verhaak, R., Ter Laan, M., Wesseling, P., Leenders, W., 2017. Glioma: experimental models and reality. Acta Neuropathol. 133, 263–282.

Lin, Q., Balasubramanian, K., Fan, D., Kim, S.J., Guo, L., Wang, H., Bar-Eli, M., Aldape, K.D., Fidler, I.J., 2010. Reactive astrocytes protect melanoma cells from chemotherapy by sequestering intracellular calcium through gap junction communication channels. Neoplasia 12, 748–754.

Lin, C., Lin, L., Mao, S., Yang, L., Yi, L., Lin, X., Wang, J., Lin, Z.X., Lin, J.M., 2018. Reconstituting glioma perivascular niches on a chip for insights into chemoresistance of glioma. Anal. Chem. 90, 10326–10333.

Liu, H., Jie, M., He, Z., Li, H.F., Lin, J.M., 2017. Study of antioxidant effects on malignant glioma cells by constructing a tumor-microvascular structure on microchip. Anal. Chim. Acta 978, 1–9.

Manini, I., Caponnetto, F., Bartolini, A., Ius, T., Mariuzzi, L., Di Loreto, C., Beltrami, A.P., Cesselli, D., 2018. Role of microenvironment in glioma invasion: what we learned from in vitro models. Int. J. Mol. Sci. 19, E147.

Marino, A., Tricinci, O., Battaglini, M., Filippeschi, C., Mattoli, V., Sinibaldi, E., Ciofani, G., 2018. A 3D real-scale, biomimetic, and biohybrid model of the blood–brain barrier fabricated through two-photon lithography. Small 14, 6.

Matias, D., Balça-Silva, J., da Graça, G.C., Wanjiru, C.M., Macharia, L.W., Nascimento, C.P., Roque, N.R., Coelho-Aguiar, J.M., Pereira, C.M., Dos Santos, M.F., Pessoa, L.S., Lima, F.R.S., Schanaider, A., Ferrer, V.P., Spohr, T.C.L.S., Moura-Neto, V., 2018. Microglia/astrocytes-glioblastoma crosstalk: crucial molecular mechanisms and microenvironmental factors. Front. Cell Neurosci. 12, 235.

Menon, N.V., Chuah, Y.J., Ca, B., Lim, M., Kang, Y., 2014. A microfluidic co-culture system to monitor tumor-stromal interactions on a chip. Biomicrofluidics 8, 064118.

Murray, J.D., 2012. Glioblastoma brain tumours: estimating the time from brain tumour initiation and resolution of a patient survival anomaly after similar treatment protocols. J. Biol. Dyn. 6, 118–127.

Ohgaki, H., Kleihues, P., 2005. Epidemiology and ethiology of gliomas. Acta Neuropathol. 109, 193–198.

Oliveira, A.I., Anio, S.I., Vieira de Castro, J., Serra, S.C., Salgado, A.J., Manadas, B., Costa, B.M., 2017. Crosstalk between glial and glioblastoma cells triggers the "go-or-grow" phenotype of tumor cells. Cell Commun. Signal. 2, e37.

Osswald, M., Jung, E., Sahm, F., Solecki, G., Venkataramani, V., Blaes, J., Weil, S., Horstmann, H., Wiestler, B., Syed M, Huang, L., Ratliff, M., Karimian Jazi, K., Kurz, F.T., Schmenger, T., Lemke, D., Gömmel, M., Pauli, M., Liao, Y., Häring, P., Pusch, S., Herl, V., Steinhäuser, C., Krunic, D., Jarahian, M., Miletic, H., Berghoff, A.S., Griesbeck, O., Kalamakis, G., Garaschuk, O., Preusser, M., Weiss, S., Liu, H., Heiland, S., Platten, M., Huber, P.E., Kuner, T., von Deimling, A., Wick, W., Winkler, F., 2015. Brain tumour cells interconnect to a functional and resistant network. Nature 528, 93–98.

Pyonteck, S.M., Akkari, L., Schuhmacher, A.J., Bowman, R.L., Sevenich, L., Quail, D.F., Olson, O.C., Quick, M.L., Huse, J.T., Teijeiro, V., Setty, M., Leslie, C.S., Oei, Y.,

Pedraza, A., Zhang, J., Brennan, C.W., Sutton, J.C., Holland, E.C., Daniel, D., Joyce, J.A., 2013. CSF-1R inhibition alters macrophage polarization and blocks glioma progression. Nat. Med. 19, 1264–1272.
Quail, D.F., Bowman, R.L., Akkari, L., Quick, M.L., Schuhmacher, A.J., Huse, J.T., Holland, E.C., Sutton, J.C., Joyce, J.A., 2016. The tumor microenvironment underlies acquired resistance to CSF-1R inhibition in gliomas. Science 352, aad3018.
Quail, D.F., Joyce, J.A., 2017. The microenvironmental landscape of brain tumors. Cancer Cell 33, 326–341.
Roggendorf, W., Strupp, S., Paulus, W., 1996. Distribution and characterization of microglia/macrophages in human brain tumors. Acta Neuropathol. 92, 288–293.
Schweighardt, B., Shieh, J.T., Atwood, W.J., 2001. CD4/CXCR4-independent infection of human astrocytes by a T-tropic strain of HIV-1. J. Neurovirol. 7, 155–162.
Trifiletti, D.M., Alonso, C., Grover, S., Fadul, C.E., Sheehan, J.P., Showalter, T.N., 2017. Prognostic implications of extent of resection in glioblastoma: analysis from a large database. World Neurosurg. 103, 330–340.
Valiente, M., Obenauf, A.C., Jin, X., Chen, Q., Zhang, X.H., Lee, D.J., Chaft, J.E., Kris, M.G., Huse, J.T., Brogi, E., Massague, J., 2014. Serpins promote cancer cell survival and vascular co-option in brain metastasis. Cell 156, 1002–1016.
William, D., Mokri, P., Lamp, N., Linnebacher, M., Classen, C.F., Erbersdobler, A., Schneider, B., 2017. Amplification of the EGFR gene can be maintained and modulated by variation of EGF concentrations in in vitro models of glioblastoma multiforme. PLOS ONE 12, e0185208.
Zhang, L., Zhang, S., Yao, J., Lowery, F.J., Zhang, Q., Huang, W.C., Li, P., Li, M., Wang, X., Zhang, C., Wang, H., Ellis, K., Cheerathodi, M., McCarty, J.H., Palmieri, D., Saunus, J., Lakhani, S., Huang, S., Sahin, A.A., Aldape, K.D., Steeg, P.S., Yu, D., 2015. Microenvironment-induced PTEN loss by exosomal microRNA primes brain metastasis outgrowth. Nature 527, 100–104.

Macroscopic PDMS Microchannel Matrix for Tailored Drug Release and Localized Glioblastoma Therapy

In a collaborative work between the technical faculty, the university hospital (UKSH) as well as the institute of anatomy in Kiel, macroscopic PDMS microchannel matrixes were produced for the drug loading with the previously used alternative drug AT101 (see chapters 2.1-2.2) and the perspective of local drug delivery with tailorable release kinetics in GBM therapy. Micro- and nanochannel based systems for drug delivery applications have gained interest in recent investigations, as they offer improved control over drug release and in fact provide the possibility of a zero-order drug release (Celia et al. 2014; Yang et al. 2018). However, scaling problems of most systems remain, since their top-down microfabrication limits their applicability with only two dimensions. Respecting this, our approach to produce macroscopic PDMS matrixes composed of interconnected microchannels is based on a bottom-up approach using a highly sacrificial ZnO template as reported previously (Mishra et al. 2013; Gedamu et al. 2014; Mishra et al. 2015). We could demonstrate a tailorable release-kinetic of methylene blue (as model molecule) over 10 days by adjustment of template size, microchannel density and surface fraction of open microchannels as well as the drug concentration. Moreover, for long-term efficacy studies over six days on human GBM cell lines as well as healthy human astrocytes *in vitro*, a sustained drug release profile which will reach therapeutically concentrations in the respective time frame was mandatory. For this approach, different concentrations of AT101 were incorporated into our templates of various microchannel densities (porosities) and release-kinetics were measured photometrically over six days.

Hence, we were able to produce a diffusion-controlled polymer matrix with unique tailorable physical properties by bottom-up fabrication, which when loaded with AT101 and adapted to our previously developed GBM-treatment plan by sequential stimulation of AT101 and TMZ, could effectively reduce proliferation and provoke cytotoxic effects in tumor cells as by free drug stimulations. Moreover, healthy astrocytes were equally affected by stimulation of AT101-relasing polymer matrixes in combination with free TMZ, indicating no additional material-induced negative side effects. Therefore, our investigations proof an efficient biological activity of PDMS-released AT101 vs. free drug, and in perspective these PDMS microchannel matrixes can be interesting and useful drug delivery systems in brain drug delivery, especially for GBM treatment.

Own contribution, presented in this article:

- Conceptualization and design of study
- Experimental part about *in vitro* analysis on human astrocytes
- Data analysis and visualization
- Editing of original draft

Macroscopic PDMS Microchannel Matrix for Tailored Drug Release and Localized Glioblastoma Therapy

Florian Rasch[1], Christina Schmitt[2*], Lena M. Saure[1*], Rieke Meyer[3*], Vivian Adamski[3], Duygu Dengiz[1], Regina Scherließ[4], Ralph Lucius[2], Michael Synowitz[3], Yogendra K. Mishra[5], Kirsten Hattermann[2], Rainer Adelung[1], Janka Held-Feindt[3#], Fabian Schütt[1#]*

[1]*Chair for Functional Nanomaterials, Institute for Materials Science, Kiel University, Kaiser Str. 2, 24143 Kiel, Germany*

[2]*Department of Anatomy, Kiel University, Otto-Hahn-Platz 8, 24118 Kiel, Germany*

[3]*Department of Neurosurgery, University Medical Center Schleswig-Holstein UKSH, Campus Kiel, Arnold-Heller-Str. 3, House D, 24105 Kiel, Germany*

[4]*Department of Pharmaceutics and Biopharmaceutics, Kiel University, Grasweg 9a, 24118 Kiel, Germany*

[5]*Mads Clausen Institute, NanoSYD, University of Southern Denmark, Alsion 2, 6400 Sønderborg, Dennmark*

[*]*shared first authorship*
[#]*shared senior authorship*

E-mail: flce@tf.uni-kiel.de;
fas@tf.uni-kiel.de

Keywords: PDMS, microchannels, local drug delivery, glioblastoma, localized therapy

Abstract

Localized therapy of the highly malignant brain tumor *Glioblastoma multiforme* (GBM) could help to drastically improve the treatment efficiency and increase the patient's median survival. Here, a macroscopic PDMS matrix composed of interconnected microchannels for tailored drug release and localized GBM therapy is introduced. Based on a simple bottom-up fabrication method using a highly versatile sacrificial template, the presented strategy solves the scaling problem associated with the previously developed microchannel-based drug delivery systems, which were limited to two dimensions due to the commonly employed top-down microfabrication methods. Additionally, tailoring of the microchannel density, the fraction of drug-releasing microchannels and the macroscopic size of the drug delivery systems enabled precise adjustment of the drug release kineticsfor more than 10 days. As demonstrated in a long-term GBM *in vitro* model, the release kinetics of the exemplarily chosen GBM drug AT101 could be tailored by variation of the microchannel density and the initial drug concentration, leading to diffusion-controlled AT101 release. Adapting a previously developed GBM treatment plan based on a sequential stimulation with AT101, measured anti-tumorigenic effects of free *versus* PDMS-released AT101 were comparable in human GBM cells and demonstrated efficient biological activity of PDMS-released AT101.

1. Introduction

The clinical need for localized cancer therapy has led to extensive research in the field of local drug delivery systems (DDS) during the last decades[1–4]. Various material strategies have already emerged which rely on different release mechanisms, *e.g.* drug release based on solvent-activated hydrogels or osmotic pumps[5,6], chemically controlled biodegradable materials[7–9], and diffusion-governed matrices and reservoirs[10,11]. Among these approaches, which all offer different pros and cons, micro- and nanofluidics based DDS have attracted increasing attention in recent years owing to the rapid development in nano- and microfabrication technology.[11,12] Particularly, micro- and nanochannel based systems have been developed which show improved control of the drug release kinetics, including zero-order and pulsatile release.[13–17] However, the fabrication of these DDS is cost- and time-effective as several steps are typically involved in the commonly applied lithography process. In addition, the existing fabrication approaches do not allow for the formation of macroscopic 3D microchannel systems, since the maximum height (few 100 µm) of the structures is restricted by the utilized techniques like spin coating, reactive ion etching, or sputtering.[11,12,18] Consequently, the amount of loadable drug is also limited and represents a considerable constraint in view of the intended use as a local DDS for cancer treatment over long time periods.

Glioblastoma multiforme (GBM) is the most common primary brain tumor in adults and characterized by its highly invasive potential and heterogeneity, leading to chemoresistance and rapid tumor relapse.[19,20] Despite a typically quite aggressive clinical treatment consisting of surgical tumor resection and successive combined radio- and chemotherapy, the median patient´s survival is only 12-15 months.[21] Hence, there is an urgent need for alternative, more advanced treatment strategies in order to improve the patient´s long-term survival. Compared to the conventional systemic therapy, localized treatment with DDS could entail major advantages, including increased drug efficacy, reduced side effects, and higher patient

compliance. Several DDS for GBM treatment have already been proposed – most of them based on biodegradable polymeric systems – and showed promising results.[22–24] The most well-studied system is probably the Gliadel® wafer, a biodegradable polyanhydride implant containing the chemotherapeutic carmustine, which has already been investigated in multiple clinical trials and has been approved by the U.S. Food and Drug Administration (FDA).[25,26] However, the anti-tumorigenic effects of the wafer are still insufficient to significantly improve current GBM treatment strategies and alternative drug delivery strategies for the local treatment are required.

For the first time, we introduce a macroscopic 3D microchannel matrix for local drug delivery and GBM treatment. In contrast to the existing top-down methods, the presented fabrication method is based on a bottom-up approach and enables the preparation of macroscopic PDMS matrices with high control over the release properties (**Scheme 1**).

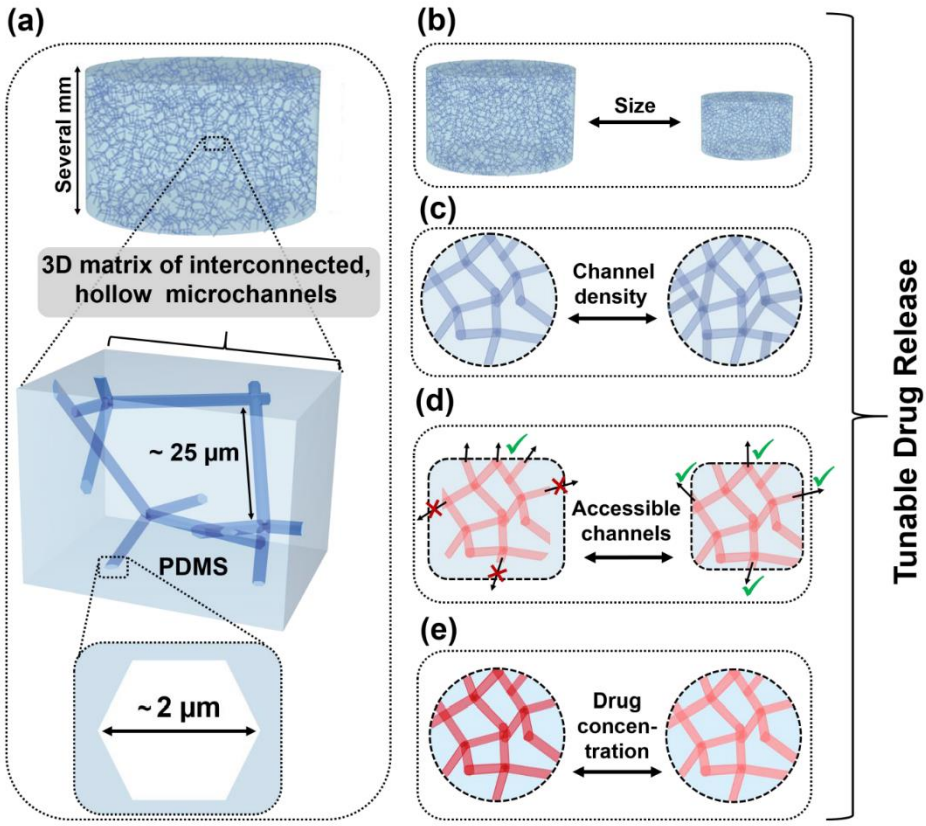

Scheme 1. 3D PDMS matrix of interconnected microchannels for drug release: Illustration of the concept of this work, introducing **(a)** a macroscopic PDMS matrix which constitutes a 3D network of interconnected, hollow microchannels for diffusion-driven drug release. The release kinetics can be tailored by varying **(b)** the size of the macroscopic PDMS matrix, **(c)** the number of microchannels for a given volume, **(d)** the fraction of open (accessible) channels which release the drug, and **(e)** the concentration of the dissolved drug.

As illustrated in Scheme 1a, the DDS constitutes a network (diameter and height few mm) of interconnected, hollow microchannels (length ~ 25 µm, diameter ~ 2 µm) which, after drug loading, act as diffusion pathways for the drug molecules and lead to prolonged release. Since the fabrication is based on a highly versatile sacrificial template[27], the drug release kinetics can be tailored by varying various material parameters, including the macroscopic size of the DDS (Scheme 1b), and the number of microchannels for a given matrix volume (Scheme 1c). Additionally, variation of the fraction of accessible (open) microchannels utilizing laser surface structuring further enhances the control of the release kinetics (Scheme 1d). Combined with the

variation of drug concentration within the microchannels (Scheme 1e), this toolbox allows for controlled tailoring of the release kinetics.

2. Results and Discussion

The individual fabrication steps for the DDS are schematically shown in **Figure 1a**. The process is based on a highly versatile sacrificial template which consists of interconnected tetrapod-shaped ZnO (t-ZnO) microparticles (length ~ 25 µm, diameter ~ 2 µm). The fabrication of the t-ZnO template follows a bottom-up approach and has already been described more detailed in previous works.[27–29] In brief, t-ZnO microparticles are synthesized with high yield using the flame transport synthesis, and the resulting loose powder is pressed into macroscopic tablets of any desired shape (cylinders, cubes, rings, *etc.*) and size (up to several cm^3 volume), as shown in **Figure S1** (Supporting Information). Importantly, high-temperature annealing of the templates at 1150 °C leads to interconnections between the individual tetrapods (**Figure S2**, Supporting Information) and, therefore, ensures interconnectivity of the entire network.

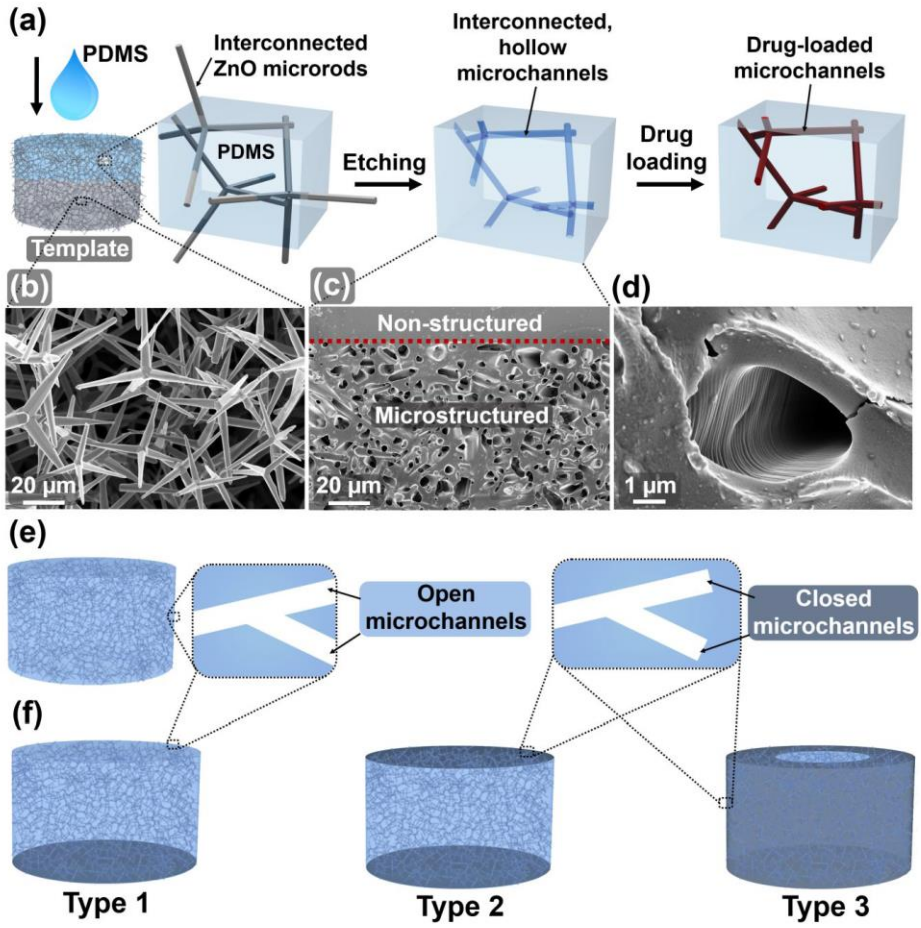

Figure 1. Fabrication of drug delivery system: (a) Schematic drawing of the preparation steps for fabrication of the PDMS-based drug delivery system. **(b)-(d)** Scanning electron microscopy (SEM) images with increasing magnification showing **(b)** the t-ZnO template and **(c)-(d)** the cross-section of a PDMS matrix with 48% porosity. **(e)-(f)** Schematic representation of **(e)** PDMS matrix with open microchannels (used for *in vitro* experiments due to the required relatively fast initial drug release) and **(f)** 3 types of PDMS matrices with increasing surface fraction of closed microchannels (detailed fabrication steps in **Figure S2**, Supporting Information).

The template exhibits an open porous framework-like structure constituting interpenetrating ZnO microrods, resulting in a highly accessible free volume (Figure 1b). This is crucial for the subsequent infiltration of the t-ZnO template with a PDMS solution, in order to fill the entire free volume of the network. After curing of PDMS and wet-chemical etching of the t-ZnO

template, the final PDMS-based matrix represents the inverse structure of the sacrificial template and features a 3D network of interpenetrating microchannels. Figure 1c shows a scanning electron microscopy (SEM) image of the cross-section of a prepared sample, revealing a clear difference between the non-structured and the microstructured PDMS. As demonstrated by the high-magnification SEM image in Figure 1d, the microchannels adopt the characteristic rippled surface morphology of the t-ZnO template, which proves highly uniform filling of the entire free volume with PDMS. In the final step, the porous PDMS matrix is loaded with the drug by vacuum-assisted infiltration of the microchannels with the drug solution.

The template-based fabrication method directly allows to tailor the release kinetics of the DDS. For instance, the porosity of the t-ZnO template can be adjusted between ~ 50% and ~ 98% by changing the initial amount of t-ZnO powder for a given volume of the tablet. In particular, a decreasing porosity of the template corresponds to an increasing porosity of the resulting PDMS microchannel matrix due to an increased microchannel density (**Figure S3**, Supporting Information).

In addition to the microchannel density, the fraction of open (*i.e.* drug-releasing) microchannels of the macroscopic DDS can be tailored to adjust the release kinetics. In general, a PDMS matrix with entirely open microchannels (Figure 1e) exhibits a faster drug release compared to PDMS matrices with increased surface fractions of closed (*i.e.* not drug-releasing) microchannels (Figure 1f). To control the fraction of open microchannels, a simple laser structuring process was utilized, which is illustrated in **Figure S4** (Supporting Information) and described in more detail in the experimental section. Briefly outlined, the approach allows for the fabrication of a multitude of cylindrical samples from a larger PDMS/t-ZnO composite by employing a CO_2 laser. While the ZnO microrods at the top and bottom side of the cylindrical sample remain covered with PDMS, they become exposed at the laser cut sides. Consequently, after wet-chemical etching of the ZnO template a DDS with open and drug releasing

microchannels at the sides is formed. Additionally, the laser can be used to precisely ablate a thin layer of the PDMS (~ 50 µm) from the top or bottom side of the sample to expose additional ZnO microrods. Employing this method, three different types of PDMS matrices were fabricated for this study, which possess a decreasing surface fraction of open microchannels (type 1-3, Figure 1f). Type 1 with sealed bottom (37.5% sealed surface fraction), type 2 with sealed top and bottom (75%), and type 3 with almost entirely sealed surface except a circular pattern (3 mm diameter) on the top side (90.6%). SEM images of the cross-section of a partially sealed microchannel matrix are shown in **Figure S5** (Supporting Information).

To study the release kinetics of the laser structured DDS, the microchannel matrices were loaded with the hydrophilic model drug methylene blue (MB). The MB release profiles of the different types are presented in **Figure 2a**. Strikingly, all types revealed characteristic release profiles for diffusion-controlled release[56], exhibiting a relatively fast initial release which slowed down with progressing time and finally saturated. The initial release rate, however, differed considerably and decreased with increasing surface fraction of closed microchannels (type 1-3). Consequently, most of MB was already released within relatively short time (~ 5 hours) from type 1 whereas the MB release was prolonged for the types 2 and 3 and saturates after more than 2 days. Hence, tailoring the amount of open microchannels affects the drug release kinetics. Particularly, the observed decreased release rate with reduced fraction of open microchannels can be associated with partly longer diffusion pathways for the MB molecules close to the sealed channels. Besides temporal control of the drug release, the surface structuring approach also enables spatially controlled release by adjusting the regions with open (drug-releasing) microchannels. This might be especially relevant for the desired *in vivo* applications which require temporally and spatially controlled release kinetics at the tumor site to ensure maximum efficacy.

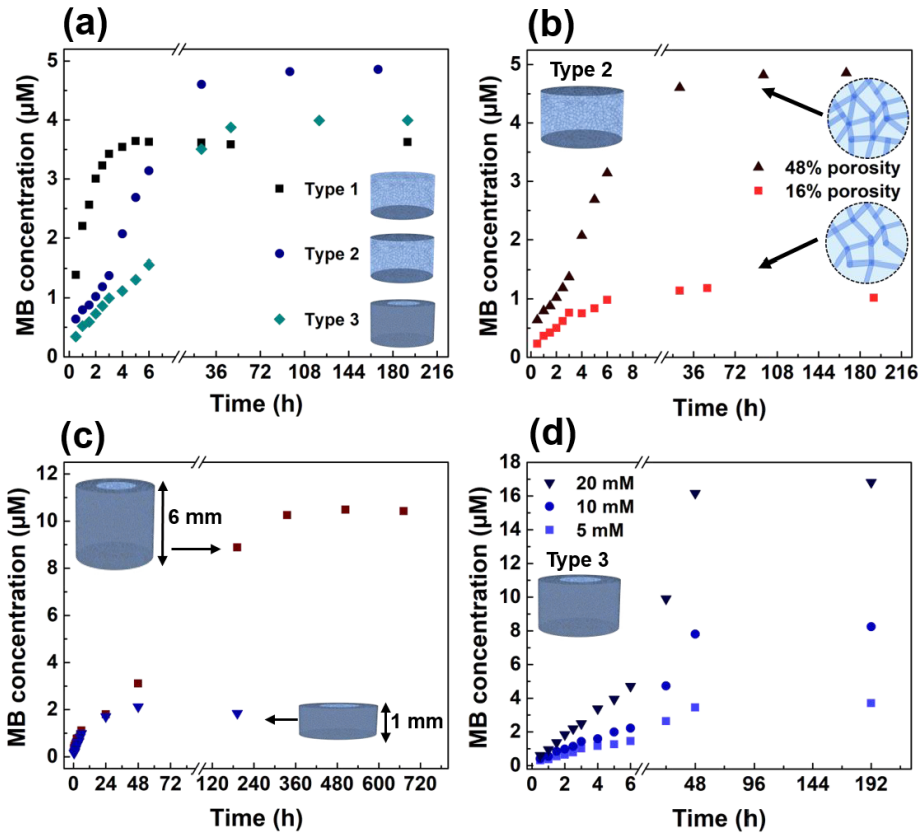

Figure 2. Tunable release kinetics: MB release profiles of microstructured PDMS matrices with **(a)** 3 different surface fractions of open (accessible) microchannels (type 1-3, all samples with 48% porosity), **(b)** different porosities (*i.e.* microchannel densities), **(c)** different sample heights (32% porosity), and **(d)** different concentrations of infiltrated MB solutions (48% porosity). Except for the height variation in (c), cylindrical samples with diameter = 6 mm and height = 1 mm were used.

As stated above, in addition to tailoring of the accessible surface fraction of the DDS, the porosity (microchannel density) of the PDMS matrices can also be tuned in order to adjust the release kinetics. Figure 2b shows the MB release profiles from microchannel matrices with two different porosities (16% and 48%), revealing both a considerably higher release rate and amount of released drug for the DDS with 48% porosity. This is directly linked to the higher microchannel density which enables more drug loading and offers more diffusion pathways combined with increased surface fraction of drug-releasing microchannels.

Owing to the high versatility of the employed sacrificial template for the DDS fabrication, macroscopic PDMS matrices with any desired shape and size can be prepared. This represents a big advantage compared to other DDS for local therapy[57,58], as it allows to adapt to the specific requirements or limitations especially in *in vivo* experiments. For instance, the size of the remaining cavity after tumor resection can vary strongly depending on the tumor progression and, thus, requires DDS with varying size in order to fill the particular cavity and maximize the efficacy of the treatment. Figure 2c depicts the MB release profiles from two microstructured PDMS matrices with two different macroscopic volumes (0.03 cm^3 and 0.17 cm^3). While both DDS revealed a similar initial release rate, the MB release was prolonged for the larger sample and lasts for more than 10 days (> 2 days for small DDS) until it saturated. Naturally, increasing the macroscopic volume of the DDS enables loading of more drug and, thus, drug release over a longer time period.

Besides tailoring of the material properties, the initial concentration of the loaded drug solution affects the release kinetics as well. As depicted in Figure 2d, the MB release from PDMS matrices with ~ 10% open microchannels (type 3) was measured for three different MB concentrations. The initial release rate increased with the concentration of the loaded drug. This observed correlation can be qualitatively explained with Fick's first law of diffusion, which states that the flux of particles is proportional to the concentration gradient of the diffusing species.[59] Analogously, an increased initial MB concentration implicates a larger concentration gradient at the boundaries between the DDS and the surrounding medium, giving rise to a higher release rate. With progressing time, the concentration gradient declines due to decreasing MB concentration within the microchannel matrix and increasing MB concentration in the surrounding medium, slowing down the drug release which finally stops when the concentration gradient approaches zero.

To evaluate the release kinetics and the biological activity toward human GBM cell lines and human astrocytes *in vitro,* microstructured PDMS matrices (diameter = 6 mm, height = 1 mm) were loaded with the exemplarily chosen GBM drug AT101, visual by a color change from white to yellow characteristic for dissolved AT101 (**Figure 3a**). This drug, which is the R-(-)-enantiomer of the naturally occurring cottonseed-derived polyphenol gossypol, has recently emerged as a promising alternative drug for GBM therapy[30–32]. The release of AT101 was performed in artificial cerebrospinal fluid (aCSF) at 37 °C/5% CO_2 under continuous planar rotation at 25 rpm and analyzed spectrophotometrically at 290 nm as one of the specific absorption peaks of AT101[33,34] after different time periods ranging from 30 min to six days.

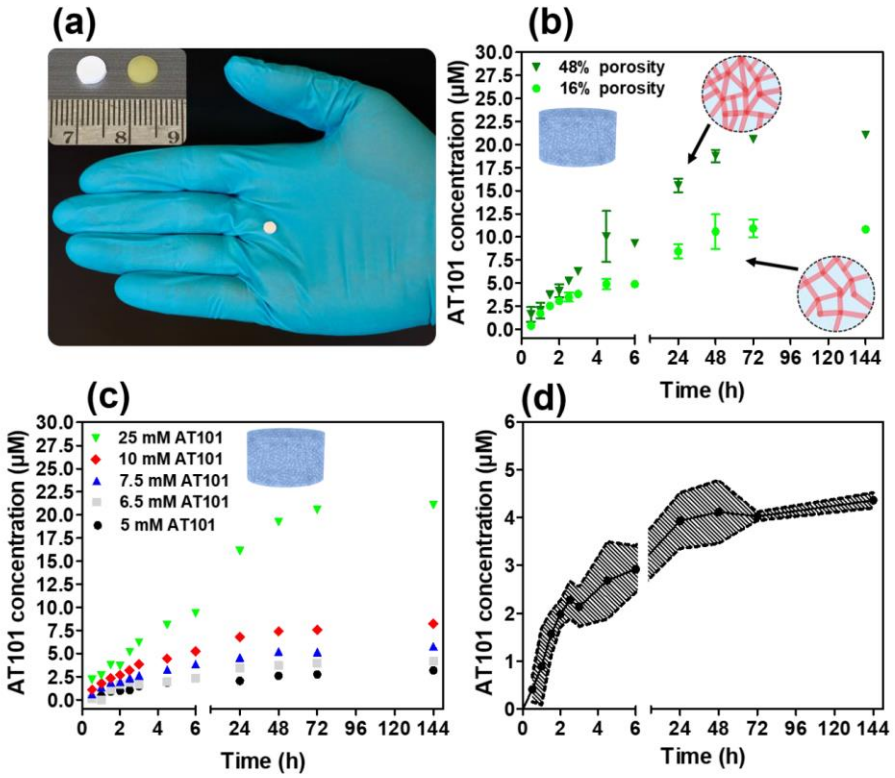

Figure 3. AT101 release kinetics: (a) Photograph of cylindrical microstructured PDMS matrix (6 mm diameter, 1 mm height). The inset photograph shows the sample before (left) and after infiltration with a 5 mM AT101 solution. **(b)** AT101 release profile from PDMS matrices with different microchannel densities (porosities). For both samples, the concentration of the infiltrated drug solution was 25 mM AT101. **(c)** AT101 release from PDMS matrices (48% porosity) using different concentrations of infiltrated drug. **(d)** AT101 release profile for PDMS matrix with 48% porosity and drug loading concentration of 6.5 mM AT101. The same sample type was also used for *in vitro* experiments. The shaded area marks the range which is given by the standard deviation.

Figure 3b shows the AT101 release from PDMS microchannel matrices with different porosities (16% and 48%) and same concentration of infiltrated AT101 solution (25 mM). For both DDS, nearly half of the infiltrated drug was released within the first 6 hours, and almost the entire amount was released after six days (compare to estimated maximum AT101 release in **Table 1**).

Table 1: Calculated maximum AT101 release based on porosity of microchannel matrix and concentration of infiltrated AT101 solution.

Porosity (%)	Loaded AT101 (mM)	Calculated maximum released AT101 (µM)
16	25	7.8
48	25	23.4
48	10	9.3
48	7.5	7
48	6.5	6.1
48	5	4.6

The release rate and the maximum released drug amount, however, were both considerably higher for the microchannel matrix with 48% porosity. This is directly linked to the higher microchannel density (*i.e.* more free volume) which allows for more drug loading and provides more diffusion pathways for the drug molecules, resulting in a faster AT101 release and higher final AT101 concentration. Besides the porosity of the DDS, the concentration of the infiltrated AT101 was also varied to tailor the release kinetics. Increasing the AT101 concentration from 5 mM to 25 mM AT101 resulted in a higher initial release rate and a higher final AT101 concentration (Figure 3c). This is expected, since the release mechanism is dominated by diffusion and, therefore, concentration-dependent. It is worth noting that the drug release from the microchannel matrices was feasible for both hydrophilic (MB) and hydrophobic (AT101) drugs. The solubility of the respective drug, however, has to be considered as is strongly affects the release kinetics. Generally, hydrophilic drugs are expected to show faster release rates in water based media compared to hydrophobic drugs.

Summarized, the AT101 release could be measured at early time points (30 min), was continuous over several days, and could be tailored by adjusting the porosity of the microchannel matrix and the concentration of the infiltrated drug solution in a controlled manner. This data is in line with previously published studies demonstrating that other techniques, such as 3D printing of PDMS layers cross-linked by UV light, were suitable to

achieve a long-term drug release, *e.g.* 20% release of prednisolone within 28 days[35]. Furthermore, solvent casting and leaching methods yielded 85% porosities and prolonged release of dexamethasone for 30 days[36,37]. However, burst effects were not prevented[38]. For gossypol, the sustained release from a chitosan-coated nanofibrous poly(L-lactide-co-D,L-lactide) implant after 7 hours was adjusted by introducing PEG into the matrix promoting a maximum release of 15% or respective 55% after approx. 2-4 hours accompanied by a plateau[39,40]. This fits well to the presented results showing an initial release of the half amount of infiltrated AT101 after 6 hours. Another possibility to establish a sustained release is the usage of degradable polymers including implants as the Gliadel® wafer[41–44]. Here, the sustained release of the drug carmustine was guaranteed by the degradation of the polymer. Indeed, manifold formulations of polymers and liposomes were investigated aiming at a controlled and sustained drug release superior to the approved Gliadel® wafers[45,46]. However, despite innovative ideas, for example to grow hydrogel within the tumor cavity by photopolymerization[41], and even though some promising attempts showed an improved tumor growth control[24,41,44,45,47], a comparative clinical study to standard therapy is still missing.

Next, to proof the anti-tumorigenic effects of drug-loaded microchannel matrices we used a long-term GBM *in vitro* model. Since the *in vitro* model required drug treatment over six days with relatively fast release of ~ 4.5 µM AT101 within the first 24 hours, a microchannel matrix with 48% porosity loaded with 6.5 mM AT101 was selected due to the suitable release kinetics (Figure 3d, shaded area marks the range which is given by the standard deviation, n = 3 independent experiments). It should be noted that the relatively high release rate favorable for *in vitro* conditions does not resemble the optimal *in vivo* conditions which require a prolonged and sustained release. The latter could be achieved by reducing the number of open (drug-releasing) microchannels using the aforementioned laser structuring approach.

For the investigation of the anti-tumorigenic effects of drug-loaded microchannel matrices (48% porosity, 6.5 mM infiltrated AT101, ~ 4.5 µM released AT101 after 24 h), two different GBM cell lines (LN229 and A172) and normal human astrocytes (SVGA) were stimulated with a combined temozolomide (TMZ; always manually added and AT101 (manually added *versus* PDMS-released) treatment plan. In detail, different cell lines were stimulated for the first three days with a combination of TMZ and AT101, followed by stimulation with AT101 alone. This sequential treatment plan was previously shown to be highly sufficient yielding high cytotoxicity and good tumor growth control, whilst being less harmful for astrocytes [48]. To compare whether AT101 released from the microchannel matrix (AT101 concentration ~ 4.5 µM) is as efficient as free AT101 added manually to cell culture medium (AT101 concentration 4.5 µM), two parallel approaches (manually added/free *versus* released AT101) were performed for all investigated cell lines together with appropriate control samples [manually added/free *versus* released AT101 solvent (DMSO:aCSF; 2:1)]. The results are depicted in Figure 4.

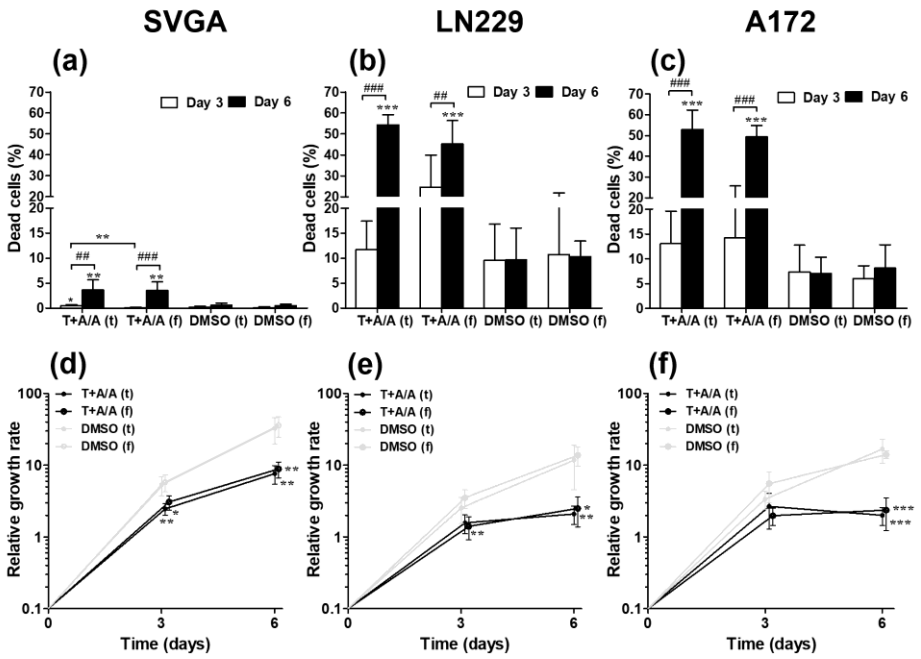

Figure 4. Cytotoxicity and proliferation of astrocytes and GBM cell lines: Effect of sequential treatment consisting of TMZ+AT101 stimulation followed by single AT101 stimulation on cytotoxicity of **(a)** SVGA (astrocytes), **(b)** LN229 (GBM), and **(c)** A172 (GBM) cell lines, and relative growth rates of **(d)** SVGA, **(e)** LN229, and **(f)** A172 cell lines. AT101 is either added manually (f) or released from the microchannel matrix (t). Means of raw data are significantly different for * or $^{\#}p<0.05$, ** or $^{\#\#}p<0.01$ and *** or $^{\#\#\#}p<0.001$.

Both GBM cell lines were affected to similar statistically significant extents by the sequential TMZ+AT101 treatment plan irrespective whether AT101 was added manually to the cell culture medium or released by the microchannel matrix. In particular, for both LN229 and A172 cell lines, 50-60% dead cells were detectable after six days of treatment, and this effect was statistically significant compared to both individual DMSO control samples and percentages of dead cells after three days of treatment (Figure 4 b-c). In contrast, human SVGA astrocytes were affected to only small and equal amounts by both treatment approaches (Figure 4a). In accordance with this, the relative growth rate of both LN229 and A172 GBM cells was clearly reduced by the sequential TMZ+AT101 plan (AT101 free/manually added or released) compared to appropriate control samples with both approaches reaching similar efficiency, whereas the growth rate of SVGA cells was influenced only moderately (Figure 4d-f).

These results are in good accordance with previous published ones showing that a sequentially applied or combined TMZ+AT101/single AT101 treatment was highly efficient and showed an inhibition of GBM proliferation[30,48]. Here, TMZ and AT101 are mechanistically different, synergistically acting drugs[48]. While the therapeutic benefit of TMZ depends on its ability to alkylate/methylate DNA most frequently at the N-7 or O-6 positions of guanine residues, AT101 competitively binds to hydrophobic surface grooves of pro-survival Bcl-2 family members, counteracting their protective effects and facilitating apoptosis in tumor cells[32], and is also able to trigger autophagic cell death[49,50]. Recently, to further improve the anti-cancer potential of AT101, liposome-based delivery of gossypol has been used[51–53]. Interestingly, these nanoparticle approaches with AT101-loaded liposomes, micelles or polymeric capsules were not able to show increased cytotoxicity of encapsulated compared to free drug in prostate, ovarian and breast cancer cell lines[51,52,54,55]. Complementing these results, we demonstrated tunable AT101 release from the 3D microchannel matrices, inducing significant anti-tumorigenic effects in human GBM cell lines whilst leaving the human astrocytes largely unaffected.

3. Conclusion

In summary, a simple and versatile bottom-up fabrication of a macroscopic PDMS-based 3D microchannel matrix for diffusion-controlled drug release has been introduced. In contrast to the existing microchannel based DDS relying on microfabrication techniques in the clean room, the presented approach eliminates the associated scaling problem and allows for simple fabrication of macroscopic samples without any spatial limitations. Due to the high control over the macroscopic and microscopic properties of the employed sacrificial template, the drug release kinetics of the final microchannel matrix could be precisely tailored by changing the macroscopic size of the DDS, the microchannel density, the fraction of open (drug-releasing) microchannels, and the concentration of the loaded drug. The direct impact of these parameters

on the release kinetics was demonstrated in release measurements with the model drug MB, revealing tunable release rates and MB release up to 10 days. The potential use for localized GBM therapy was proven in *in vitro* experiments which showed adjustable AT101 release over several days and significant anti-tumorigenic effects in human GBM cells. Combined with the facile fabrication allowing high drug-loading capacity, the developed 3D microchannel matrix represents a promising strategy for local drug delivery and localized GBM therapy.

4. Experimental Section

Fabrication of sacrificial t-ZnO template

For fabrication of the sacrificial templates, the tetrapodal ZnO (t-ZnO) microparticles were first synthesized using the flame transport synthesis which is described detailed in previous works[27,60,61]. Briefly, a mixture of polyvinyl butyral (PVB) and zinc powder (grain size 1-5 µm) was prepared with mass ratio 2:1 and subsequently heated in a muffle furnace for 30 minutes at 900 °C (heating rate of 60 °C min^{-1}). Using a cylindrical mould, the obtained fluffy t-ZnO powder was pressed into cylindrical pellets (6 mm diameter, 1 mm height) with desired porosity of the formed network. After sintering of the template at 1150 °C for 5 hours, interconnections between the tetrapods were formed, resulting in a macroscopic framework.

Fabrication of PDMS microchannel matrix

For preparation of the silicone solution, a two-part PDMS solution (Sylgard 184) was mixed with mass ratio 10:1 of base and curing agent. Subsequently, the prepared mixture was stored in the desiccator for 30 minutes to remove remaining gas bubbles. Afterwards, the template was immersed in the PDMS solution under low vacuum (in the desiccator) for 10 minutes to facilitate filling of the entire free volume of the t-ZnO template with the PDMS solution. After that, the infiltrated template was rinsed in hexane to remove excess PDMS solution and stored in the furnace for 2 hours at 80 °C for polymer curing. Then, the sacrificial template (t-ZnO) was removed by wet-chemical etching in 4 M HCl for 7 days. After etching of the template, the resulting PDMS microchannel matrix was thoroughly washed in water (1x) and absolute ethanol (5x) to remove any remaining acid.

Laser structuring of PDMS microchannel matrices

For preparation of microchannel matrices with tailored surface fraction of open microchannels, a CO_2 laser cutter (GS 6090 PU, GS Laser Systems) was used. The individual processing steps are illustrated in Figure S4 (Supporting Information). In detail, a large t-ZnO template (several

cm^2 surface area, 1 mm height) was infiltrated with PDMS (followed by curing of polymer), and cylindrical samples (6 mm diameter, 1 mm height) were cut out using the laser cutter. These samples were then etched in 4 M HCl for 7 days and thoroughly washed in absolute ethanol (5x). After drying, the samples represent type 2 with open microchannels at the side and closed microchannels on top and bottom side. Starting from type 2, the other two types were fabricated. For type 1 (bottom side sealed), the top side of the microchannel matrix was ablated with the laser cutter, resulting in opening of the microchannels. For type 3 (small surface area on top side with open microchannels), the sides of then microchannel matrix (type 2) were first sealed manually with PDMS. Afterwards, the laser cutter was used to create a surface pattern on the top side (circular shape, 3 mm diameter), resulting in open microchannels. After treatment with the laser cutter, the PDMS samples were sonicated in isopropanol for 15 minutes in order to remove residuals.

Determination of AT101 release

In order to determine the release kinetics of AT101 from different cylindrical microstructured PDMS matrices, AT101 concentrations were quantitatively determined by ultraviolet/visible (UV/Vis) spectroscopy with the Libra UV/Vis spectrophotometer S60 (Biochrom GmbH, Berlin, Germany) using QS High Precision Cell cuvettes (Hellma GmbH, Müllheim, Germany). In detail, different concentrations of AT101 (5 mM, 6.5 mM, 7.5 mM, 10 mM, 25 mM), diluted in a 2:1-mixture of dimethylsulfoxide (DMSO; Sigma-Aldrich, St. Louis, MO, USA) and artificial cerebrospinal fluid (aCSF) containing 124 mM NaCl, 5 mM KCl, 26 mM $NaHCO_3$, 1.3 mM $MgCl_2$, 2 mM $CaCl_2$, 10 mM D-Glucose in aqua bidest, pH 7.3, were loaded by wet-chemical infiltration under low vacuum on cylindrical shaped PDMS matrices (1 mm in height and 6 mm in diameter) of different porosities (16% and 48%). AT101-loaded PDMS matrices were placed into Millicell® cell culture inserts (0.4 µm, Merck Millipore, Burlington, MA, USA) containing 1.5 ml aCSF plus 0.05% (w/v) bovine serum albumin (BSA) and placed into a 10 cm cell culture dish with 13 ml aCSF plus 0.05% (w/v) BSA solution. The release of

AT101 was monitored under sterile conditions at 37 °C/5% CO_2 under continuous planar rotation at 25 rpm with the KM CO_2-FL small shaker (Edmund Bühler GmbH, Tübingen, Germany). Released amounts of AT101 were analyzed spectrophotometrically at 290 nm after different time points ranging from 30 min to ultimately six days, and determined according to defined standard AT101 dilutions. AT101 standards were prepared freshly on each day of quantification, whereas the drug was diluted in aCSF solution that was incubated at 37 °C/5% CO_2 for the exact time periods just as the samples.

Cultivation of cell lines

Human glioblastoma cell lines A172 (ECACC 880624218) and LN229 (ATCC-CRL-2611) were acquired from the American Type Culture Collection (ATCC, Manassas, Virginia, USA) or the European Collection of Cell Cultures (ECACC, Salisbury, UK). The human fetal astrocyte cell line SVGA was kindly provided by the group of Christine Hanssen Rinaldo, University Hospital of North Norway[62] with the permission of W. J. Altwood[63]. Cell lines were cultured in Dulbecco's modified Eagle's medium (DMEM; Life Technologies, Carlsbad, CA, USA) with 10% fetal bovine serum (FBS; Invitrogen, Carlsbad, CA, USA or PAN-Biotech GmbH, Aidenbach, Germany), 1% Penicillin-Streptomycin (10,000 U/ml; Thermo Fisher Scientific, Waltham, MA, USA), and 2 mM additional L-Glutamine (Thermo Fisher Scientific). Cells were routinely checked for *Mycoplasma* contamination using the Venor®GeM Classic *Mycoplasma* detection kit for conventional PCR (Minerva Biolabs, Berlin, Germany), and for identity by Short Tandem Repeat profiling at the Department of Forensic Medicine (Kiel, Germany) employing the Powerplex HS Genotyping Kit (Promega, Madison, WC) and a 3500 Genetic Analyser (Thermo Fisher Scientific).

Stimulation of cell lines and cytotoxicity assay

For stimulation, 150,000 LN229, A172 or SVGA cells were seeded in 10 cm culture dishes in DMEM supplemented with 10% FBS. On the next day, after washing with phosphate-buffered saline (PBS), medium was changed to DMEM without phenol-red (Life Technologies)

supplemented with 10% FBS. Cells were either stimulated for the first three days with 50 µM temozolomide (TMZ; stock dissolved at 100 mM in DMSO; Sigma-Aldrich) combined with manually added free 4.5 µM AT101 (stock dissolved at 100 mM in DMSO; Tocris, Bristol, UK) or with 50 µM TMZ combined with a cylindrical microstructured PDMS matrix infiltrated with 6.5 mM AT101 (appropriate to ~4.5 µM released AT101). After three days, media were exchanged and cells were stimulated for another three days with solely free AT101 or with a PDMS matrix infiltrated with 6.5 mM AT101 (corresponding to ~4.5 µM released AT101). Here, cylindrical microstructured PDMS matrices were placed in Millicell® cell culture inserts (0.4 µm, Merck Millipore), controls were stimulated with the equal volume of either free DMSO (0.05% (v/v)) or DMSO-loaded microstructured PDMS matrices, and experiments were performed under continuous planar rotation at 25 rpm with the KM CO_2-FL small shaker (Edmund Bühler GmbH). To determine cytotoxic effects, the CytoTox-Fluor™ Cytotoxicity Assay (Promega) was performed according to the manufacturer's instruction and as described before[48]. The emerging fluorescence was measured in a microplate reader (GENios, Tecan Group, Maennedorf, Switzerland) at 485/ 535 nm. The exact numbers of dead cells were determined according to different numbers of digitonin-lysed (82.5 µg/ ml; Merck Millipore) cell-dilutions of each cell line (n = 3-4 independent experiments). Percentages [%] of dead cells in relation to the total amount of measured cells were calculated as described in equations 1 and 2 after 3 respective 6 days of stimulation.

[1] $$[\%]\ dead\ cells\ (day\ 3) = \frac{number\ of\ dead\ cells\ (day\ 3)}{number\ of\ dead\ cells\ (day\ 3) + vital\ cells\ (day\ 3)} \times 100$$

[2] $$[\%]\ dead\ cells\ (day\ 6) = \frac{number\ of\ dead\ cells\ (day\ 3 + day\ 6)}{number\ of\ dead\ cells\ (day\ 3 + day\ 6) + vital\ cells\ (day\ 6)} \times 100$$

The cell survival was determined by counting viable cells at day 0, 3 and 6 of stimulation. Cell viabilities were calculated as *n*-fold numbers of alive cells compared to the initial cell number counted at day 0, respectively.

Statistical analysis

All data was analyzed with the GraphPad Prism 5 Software (GraphPad Software, La Jolla, CA, USA). To check for statistical significance, a One-Way-ANOVA followed by a Bonferroni's multiple comparison test was performed to study the effects on day 3 or day 6 between different stimulations, whereas a Two-Way-ANOVA followed by a Bonferroni's multiple comparison test was employed to study the effects of the different stimulations over the time (3 days vs. 6 days treatment). Asterisks as well as hashtags indicate statistical significance: * $p < 0.05$, ** $p < 0.01$, *** $p < 0.001$ respective $^{\#\#}$ $p < 0.01$ and $^{\#\#\#}$ $p < 0.001$.

Determination of MB release

After fabrication of the laser-structured microchannel matrices, the samples were infiltrated with a 5 mM MB (Sigma-Aldrich) solution (in water) under low vacuum in a desiccator, leading to filling of the microchannel network. After carefully rinsing the samples with water to remove excess MB solution, the MB release was measured in 14.5 ml deionized water after 0.5 h, 1 h, 1.5 h, 2 h, 2.5 h, 3 , 4 h, 5 h, 6, 24 h, 48 h and 8 days with a UV-VIS spectrometer (Lambda 900, Perkin Elmer). After each measurement, the measured solution was poured back into the container to maintain a constant release volume. The containers were stored in a dark environment to prevent degradation of MB.

Acknowledgements

This work was funded by the German Research Foundation (DFG) as part of the Research Training Group "Materials4Brain" (RTG2154).

Author Contributions

FR, CS, VA, KH, JHF and FS came up with the concept. FR, CS, VA, FS, RS, RL, MS, KH, YKM, RA, JHF, and FS designed the study. FR, LMS and DD fabricated the samples. FR, CS, LMS, RM, VA and FS analyzed the data. RM, VA and JHF carried out the AT101 release measurements and corresponding analysis. CS, RM, and VA carried out the cell culture experiments and corresponding analysis. FR carried out SEM measurements. LMS carried out the MB release measurements and analyzed the data. FR, JHF and FS finalized the study and wrote the paper. All the authors have contributed to the discussion of the results and reviewed the manuscript.

Supporting Information Available

Additional supplementary figures.

References

[1] O. S. Fenton, K. N. Olafson, P. S. Pillai, M. J. Mitchell, R. Langer, *Adv. Mater.* **2018**, *30*, 1705328.

[2] J. B. Wolinsky, Y. L. Colson, M. W. Grinstaff, *J. Control. Release* **2012**, *159*, 14.

[3] J. R. Weiser, W. M. Saltzman, *J. Control. Release* **2014**, *190*, 664.

[4] M. W. Tibbitt, J. E. Dahlman, R. Langer, *J. Am. Chem. Soc.* **2016**, *138*, 704.

[5] C. Bastiancich, P. Danhier, V. Préat, F. Danhier, *J. Control. Release* **2016**, *243*, 29.

[6] R. K. Verma, S. Arora, S. Garg, *Crit. Rev. Ther. Drug Carrier Syst.* **2004**, *21*, 477.

[7] H. K. Makadia, S. J. Siegel, *Polymers (Basel).* **2011**, *3*, 1377.

[8] A. Kumari, S. K. Yadav, S. C. Yadav, *Colloids Surfaces B Biointerfaces* **2010**, *75*, 1.

[9] J. Zeng, X. Xu, X. Chen, Q. Liang, X. Bian, L. Yang, X. Jing, *J. Control. Release* **2003**, *92*, 227.

[10] R. LANGER, J. FOLKMAN, *Nature* **1976**, *263*, 797.

[11] C. L. Stevenson, J. T. Santini, R. Langer, *Adv. Drug Deliv. Rev.* **2012**, *64*, 1590.

[12] N. Gao, X. J. Li, *Microfluid. Devices Biomed. Appl.* **2013**, 167.

[13] C. Celia, S. Ferrati, S. Bansal, A. L. van de Ven, B. Ruozi, E. Zabre, S. Hosali, D. Paolino, M. G. Sarpietro, D. Fine, et al., *Adv. Healthc. Mater.* **2014**, *3*, 230.

[14] R. Duan, F. Xia, L. Jiang, *ACS Nano* **2013**, *7*, 8344.

[15] S. Y. Yang, J.-A. Yang, E.-S. Kim, G. Jeon, E. J. Oh, K. Y. Choi, S. K. Hahn, J. K. Kim, *ACS Nano* **2010**, *4*, 3817.

[16] G. B. Lesinski, S. Sharma, K. A. Varker, P. Sinha, M. Ferrari, W. E. Carson, *Biomed.*

Microdevices **2005**, *7*, 71.

[17] D. Yang, J. S. Lee, C.-K. Choi, H.-P. Lee, S.-W. Cho, W. Ryu, *Acta Biomater.* **2018**, *68*, 249.

[18] F. Martin, R. Walczak, A. Boiarski, M. Cohen, T. West, C. Cosentino, M. Ferrari, *J. Control. Release* **2005**, *102*, 123.

[19] A. M. Stark, J. Hedderich, J. Held-Feindt, H. M. Mehdorn, *Neurosurg. Rev.* **2006**, *30*, 56.

[20] A. Omuro, L. M. DeAngelis, *JAMA* **2013**, *310*, 1842.

[21] R. Stupp, W. P. Mason, M. J. van den Bent, M. Weller, B. Fisher, M. J. B. Taphoorn, K. Belanger, A. A. Brandes, C. Marosi, U. Bogdahn, et al., *N. Engl. J. Med.* **2005**, *352*, 987.

[22] S. H. Ranganath, Y. Fu, D. Y. Arifin, I. Kee, L. Zheng, H.-S. Lee, P. K.-H. Chow, C.-H. Wang, *Biomaterials* **2010**, *31*, 5199.

[23] M. S. Lesniak, U. Upadhyay, R. Goodwin, B. Tyler, H. Brem, *Anticancer Res.* **2005**, *25*, 3825.

[24] R. Ramachandran, V. R. Junnuthula, G. S. Gowd, A. Ashokan, J. Thomas, R. Peethambaran, A. Thomas, A. K. K. Unni, D. Panikar, S. V. Nair, et al., *Sci. Rep.* **2017**, *7*, 43271.

[25] S. Kunwar, S. Chang, M. Westphal, M. Vogelbaum, J. Sampson, G. Barnett, M. Shaffrey, Z. Ram, J. Piepmeier, M. Prados, et al., *Neuro. Oncol.* **2010**, *12*, 871.

[26] M. J. McGirt, K. D. Than, J. D. Weingart, K. L. Chaichana, F. J. Attenello, A. Olivi, J. Laterra, L. R. Kleinberg, S. A. Grossman, H. Brem, et al., *J. Neurosurg.* **2009**, *110*, 583.

[27] Y. K. Mishra, S. Kaps, A. Schuchardt, I. Paulowicz, X. Jin, D. Gedamu, S. Freitag, M. Claus, S. Wille, A. Kovalev, et al., *Part. Part. Syst. Charact.* **2013**, *30*, 775.

[28] Y. K. Mishra, S. Kaps, A. Schuchardt, I. Paulowicz, X. Jin, D. Gedamu, S. Wille, O. Lupan, R. Adelung, *KONA Powder Part. J.* **2014**, *31*, 92.

[29] Y. K. Mishra, R. Adelung, *Mater. Today* **2018**, *21*, 631.

[30] M. A. Jarzabek, V. Amberger-Murphy, J. J. Callanan, C. Gao, A. M. Zagozdzon, L. Shiels, J. Wang, K. L. Ligon, B. E. Rich, P. Dicker, et al., *Br. J. Cancer* **2014**, *111*, 2275.

[31] Y. Lu, J. Li, C.-E. Dong, J. Huang, H.-B. Zhou, W. Wang, *Future Med. Chem.* **2017**, *9*, 1243.

[32] M. Opydo-Chanek, O. Gonzalo, I. Marzo, *Biochem. Pharmacol.* **2017**, *136*, 12.

[33] B. Marciniak, H. Kozubek, J. Koput, S. Paszyc, *Zeitschrift für Naturforsch. A* **1990**, *45*, 179.

[34] R. Adams, E. C. Kirkpatrick, *J. Am. Chem. Soc.* **1938**, *60*, 2180.

[35] J. Holländer, R. Hakala, J. Suominen, N. Moritz, J. Yliruusi, N. Sandler, *Int. J. Pharm.* **2018**, *544*, 433.

[36] E. Pedraza, A.-C. Brady, C. A. Fraker, C. L. Stabler, *J. Biomater. Sci. Polym. Ed.* **2013**, *24*, 1041.

[37] K. Jiang, J. D. Weaver, Y. Li, X. Chen, J. Liang, C. L. Stabler, *Biomaterials* **2017**, *114*, 71.

[38] A. W. Frei, Y. Li, K. Jiang, P. Buchwald, C. L. Stabler, *J. Tissue Eng. Regen. Med.* **2018**, *12*, 393.

[39] M. Ignatova, K. Kalinov, N. Manolova, R. Toshkova, I. Rashkov, M. Alexandrov, *J. Biomater. Sci. Polym. Ed.* **2014**, *25*, 287.

[40] M. Ignatova, N. Manolova, R. Toshkova, I. Rashkov, E. Gardeva, L. Yossifova, M. Alexandrov, *Int. J. Pharm.* **2012**, *436*, 10.

[41] M. Zhao, F. Danhier, C. Bastiancich, N. Joudiou, L. P. Ganipineni, N. Tsakiris, B. Gallez, A. des Rieux, A. Jankovski, J. Bianco, et al., *Int. J. Pharm.* **2018**, *548*, 522.

[42] P. Menei, L. Capelle, J. Guyotat, S. Fuentes, R. Assaker, B. Bataille, P. François, D. Dorwling-Carter, P. Paquis, L. Bauchet, et al., *Neurosurgery* **2005**, *56*, 242.

[43] L. K. Fung, M. G. Ewend, A. Sills, E. P. Sipos, R. Thompson, M. Watts, O. M. Colvin, H. Brem, W. M. Saltzman, *Cancer Res.* **1998**, *58*, 672.

[44] S. H. Ranganath, C.-H. Wang, *Biomaterials* **2008**, *29*, 2996.

[45] T. Arai, O. Benny, T. Joki, L. G. Menon, M. Machluf, T. Abe, R. S. Carroll, P. M. Black, *Anticancer Res.* **2010**, *30*, 1057.

[46] N. L. Elstad, K. D. Fowers, *Adv. Drug Deliv. Rev.* **2009**, *61*, 785.

[47] C. Bastiancich, L. Lemaire, J. Bianco, F. Franconi, F. Danhier, V. Préat, G. Bastiat, F. Lagarce, *Nanomedicine* **2018**, *13*, 1999.

[48] V. Adamski, C. Schmitt, F. Ceynowa, R. Adelung, R. Lucius, M. Synowitz, K. Hattermann, J. Held-Feindt, *J. Cancer Res. Clin. Oncol.* **2018**, *144*, 1475.

[49] V. Voss, C. Senft, V. Lang, M. W. Ronellenfitsch, J. P. Steinbach, V. Seifert, D. Kogel, *Mol. Cancer Res.* **2010**, *8*, 1002.

[50] V. Warnsmann, N. Meyer, A. Hamann, D. Kögel, H. D. Osiewacz, *Mech. Ageing Dev.* **2018**, *170*, 45.

[51] G. Zhai, J. Wu, X. Zhao, B. Yu, H. Li, Y. Lu, W. Ye, Y. C. Lin, R. J. Lee, *Anticancer Res.* **2008**, *28*, 2801.

[52] C.-L. JIN, M.-L. CHEN, Y. WANG, X.-C. KANG, G.-Y. HAN, S.-L. XU, *Exp. Ther. Med.* **2015**, *9*, 675.

[53] V. Heleg-Shabtai, R. Aizen, E. Sharon, Y. S. Sohn, A. Trifonov, N. Enkin, L. Freage, R. Nechushtai, I. Willner, *ACS Appl. Mater. Interfaces* **2016**, *8*, 14414.

[54] H. Cho, T. C. Lai, G. S. Kwon, *J. Control. Release* **2013**, *166*, 1.

[55] H. Liu, K. Li, L. Lan, J. Ma, Y. Zeng, L. Xu, D. Wu, *J. Mater. Chem. B* **2014**, *2*, 5238.

[56] J. Siepmann, F. Siepmann, *J. Control. Release* **2012**, *161*, 351.

[57] R. . Malcolm, S. . McCullagh, A. . Woolfson, S. . Gorman, D. . Jones, J. Cuddy, *J. Control. Release* **2004**, *97*, 313.

[58] P. P. Wang, J. Frazier, H. Brem, *Adv. Drug Deliv. Rev.* **2002**, *54*, 987.

[59] A. Paul, T. Laurila, V. Vuorinen, S. V. Divinski, in *Thermodyn. Diffus. Kirkendall Eff. Solids*, Springer International Publishing, Cham, **2014**, pp. 115–139.

[60] Y. K. Mishra, G. Modi, V. Cretu, V. Postica, O. Lupan, T. Reimer, I. Paulowicz, V. Hrkac, W. Benecke, L. Kienle, et al., **2015**, *7*, 14303.

[61] D. Gedamu, I. Paulowicz, S. Kaps, O. Lupan, S. Wille, G. Haidarschin, Y. K. Mishra, R. Adelung, *Adv. Mater.* **2014**, *26*, 1541.

[62] S. Henriksen, G. D. Tylden, A. Dumoulin, B. N. Sharma, H. H. Hirsch, C. H. Rinaldo, *J. Virol.* **2014**, *88*, 7556.

[63] B. Schweighardt, W. J. Atwood, *AIDS Res. Hum. Retroviruses* **2001**, *17*, 1133.

For Table of Content only

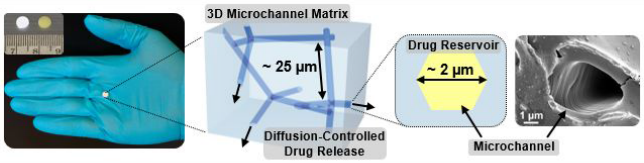

Little, reversible glial scarring responses on tetrapod-shaped graphene oxide and reduced graphene oxide 3D scaffolds in brain *in vitro* and *ex vivo* models

In this collaborative work with Florian Rasch (technical faculty Kiel), two macroscopic graphene-based matrixes of interconnected microchannels out of graphene oxide (GO) respective reduced graphene oxide (rGO) were produced in a similar approach as previously described in chapter 2.3 and tested for their brain-biocompatibility on human astrocytes and microglia *in vitro* models as well as on a murine organotypic brain slice model. With their unique physical properties, the two highly porous material-scaffolds can be either used for biofunctionalization in drug delivery applications (for GO) or for electrode design and sensing/recording (for rGO), respective. Since the biocompatibility as well as brain foreign body reaction is highly dependent on the material but also its size, shape and microstructure, no information on brain-reactions is available yet regarding highly porous GO/rGO material scaffolds with tetrapodal microstructure. Therefore, cell dependent reactions of astrocytes (SVGA) as well as microglia (HMC3) on both materials were evaluated after indirect incubation with the material for 24h. In addition, the possible protective effect of conditioned media from material challenged microglial cells on astrocytes was analyzed after 24h. We investigated effects on proliferation, cytotoxicity as well as on gene expression level to determine neuroinflammatory or glial scarring reactions *in vitro* and prospectively evaluated the effects of the anti-inflammatory compound curcumin in pre-/co-stimulations with both materials in its efficacy to alleviate material-specific reactions on cells. In HMC3 and SVGA only slight effects of the percentage of dead cells as well as growth rates were detectable after GO and rGO incubation, however more pronounced in astrocytes and stronger upon GO incubation. Moreover, the gene expression of typical inflammation or glial scarring related genes were slightly to moderately upregulated upon material-incubation, however in most cases more pronounced for rGO scaffolds than for GO. Hence, effects were diminished for SVGA cells when incubated with material challenged microglia media as well as when pre-/co-stimulated with curcumin. Since the conditioned HMC3 material-media affected positively material-induced reactions of single cell populations in astrocytes, we investigated also effects of both materials in a highly preserved cell-microenvironment in murine acute brain slices over six days *in vitro*, whereas also here the protective effect of curcumin on the tissue reactions was evaluated. GO and rGO challenged brain slices only slightly showed cytotoxic effects over three and five days, however inflammation and glial scarring related genes such as IL-6, tenascin or nestin were upregulated upon rGO incubation whilst not upon GO. Moreover, in immunohistochemical stainings of brain slices GO and rGO did not seem to negatively affect neurons and oligodendrocytes however showed similar effects on the induction of glial scarring as on messenger ribonucleic acid (mRNA) level, in this setting to almost equal extends for GO and rGO. In conclusion, we were able to produce highly porous microstructured GO/rGO-templates with unique physical and mechanical properties and various promising possibilities in brain-applications, such as the loading or coating with foreign body reaction attenuating drugs like curcumin.

Own contribution, presented in this article:

- Design of the study
- Performance of *in vitro* experiments
- Data analysis and visualization
- Discussion and interpretation of results
- Writing of original draft

Little, reversible glial scarring responses on tetrapod-shaped graphene oxide and reduced graphene oxide 3D scaffolds in brain *in vitro* and *ex vivo* models

Christina Schmitt[1], Florian Rasch[2], François Cossais[1], Janka Held-Feindt[3], Ralph Lucius[1], Ali Shaygan Nia[4], Martin R. Lohe[4], Xinliang Feng[4], Yogendra K. Mishra[5], Rainer Adelung[2], Fabian Schütt[2], Kirsten Hattermann[1*]

[1] Institute of Anatomy, Kiel University, Olshausenstr. 40, D-24098 Kiel, Germany

[2] Institute for Materials Science, Kiel University, D-24143 Kiel, Germany

[3] Department of Neurosurgery, University Medical Center Schleswig-Holstein UKSH, Campus Kiel, Arnold-Heller-Str.3, building 41, D-24105 Kiel, Germany

[4] Department of Chemistry and Food Chemistry, Center for Advancing Electronics Dresden (cfaed), Technische Universität Dresden, 01062 Dresden, Germany

[5] Mads Clausen Institute, NanoSYD, University of Southern Denmark, Alsion 2, 6400 Sønderborg, Denmark

*Author to whom correspondence should be addressed:

Kirsten Hattermann, PhD

Email: k.hattermann@anat.uni-kiel.de

phone: +49 431 880 2460

Institute of Anatomy, University Kiel, Olshausenstr. 40, D-24105 Kiel

Abstract

Brain implants are promising instruments for a broad variety of nervous tissue diseases with a wide range of applications, e.g. for stimulation, signal recording or local drug delivery. Recently, graphene-based scaffold materials have emerged as attractive candidates as neural interfaces, 3D scaffolds, or drug delivery systems due to their excellent properties like flexibility, high surface area, conductivity, and lightweight. To date, however, there is a lack of appropriate studies of the foreign body response, especially glial scar formation, towards graphene-based materials. In this work, we investigated the effects of macroscopic, highly porous (>99.9%) graphene oxide (GO) and reduced graphene oxide (rGO) (conductivity ~ 1 S m^{-1}) scaffolds on human astrocyte and microglial cell viability and proliferation as well as expression of neuroinflammation and astrogliosis associated genes. In this *in vitro* model, as well as *ex vivo* in organotypic murine brain slices, we could demonstrate that both GO and rGO based 3D scaffolds exert only slight effects on the glial cell populations which cause glial scarring. Additionally, these effects were in most cases completely abolished by curcumin, a known anti-inflammatory and anti-fibrotic drug that could in perspective be applied to brain implants as a protectant.

Key words

Brain implant materials, glial scar, graphene oxide, reduced graphene oxide, curcumin, neuroinflammation

Abbreviations

BBB, blood brain barrier; CT, cycle of threshold; Cur, curcumin; DBS, deep brain stimulation; div, days *in vitro*; dos, days of stimulation; FDA, U.S. Food and Drug Administration; GAPDH, glyceraldehyde 3-phosphate; GFAP, glial fibrillary acidic protein; GO, graphene oxide; ICC, immunocytochemistry; IL, interleukin; MBP, myelin basic protein; NF, neurofilament; qRT-PCR, quantitative reverse transcription PCR; rGO, reduced graphene oxide; SEM, scanning electron microscopy; TGFβ, tumor growth factor-β; TNFα, tumor necrosis factor-α

Introduction

Therapy of brain disorders remains a great challenge, as successful treatment with systemically applied drugs often fails. This can in parts be attributed to the blood brain barrier (BBB) that effectively protects the central nervous system (CNS) from the periphery, affording high systemic drug concentrations to reach therapeutic concentrations in the brain or even shielding almost completely a majority of drugs from the central nervous system [1]. On the other hand, neuronal networks cooperate in a highly complex manner, and local dysfunctions can hardly be restored specifically by pharmacological approaches.

Facing the problems of systemic treatment, the idea of local therapeutic concepts – apart from surgery - has been pursued for decades for a variety of different brain disorders. These approaches include for instance the chronical implantation of electrodes to apply electrical currents to distinct cortical or deep brain areas [2, 3] and novel strategies for local administration of chemotherapeutics into the resection cavities of brain tumor, e.g. by micropumps or drug-loaded polymers (for review: [4]). As an initial but limited success in local drug administration, a biodegradable polymer (Polifeprosan 20) wafer impregnated with carmustine (Gliadel®) has been shown to be safe and effective in the treatment of newly diagnosed and recurrent high grade gliomas [5-7], and approved by the FDA as an adjunct to surgery or surgery and radiation in 2003. However, there are also severe concerns about the local toxicity and the complication rate when using carmustine impregnated polymers [8, 9]. In contrast, the non-pharmacological approach of chronic electrode implantation to stimulate (and within irritate) distinct brain regions by cortical or deep brain stimulation has been very successfully established for several neurological disorders, for example in the treatment of advanced Parkinson's disease by subthalamic nucleus stimulation [10], and specific modes of tremor and epilepsy by stimulation of distinct thalamic nuclei [11, 12].

Post-mortem analyses of the electrode-tissue interface after long-term deep brain stimulation in human patients revealed, however, extensive histological changes including fibrous sheaths around the electrodes, fibrillary gliosis and reactive astrocytes, infiltration of immune cells and

neuronal loss, which seem to be independent from the duration of the deep brain stimulation [13, 14]. These acute and chronic reactions on the implantation of foreign materials to the brain have also been described as a major problem for intracortical recording electrodes, where the glial scar formation considerably impairs sensitivity and function of the recording devices [15, 16]. Being thus one of the major obstacles for the clinical application of recording electrodes, the tissue foreign body response is also a limiting factor for the applicability of novel drug-releasing devices. While the fibrous sheath may influence the diffusion capability and thereby drug release, the infiltrating immune cells may additionally change the microenvironment and the metabolism of applied drugs. Hence, it is crucial to develop implants which meet the complex material-based requirements such as mechanical flexibility, easy bio-functionalization, or high physicochemical stability, and do not induce significant inflammatory response in the surrounding tissue. In recent years, the 2D carbon nanomaterial graphene and its derivatives have emerged as promising materials for biomedical applications in the brain due to their outstanding properties [17, 18]. For instance, the high electrical conductivity, flexibility and biocompatibility of graphene makes it a suitable material for neural brain electrodes and substrates for neural cell growth [19, 20]. Additionally, the extremely high specific surface area (~2600 $m^2 g^{-1}$) [17] allows for high drug loading capacity, which is desired for drug delivery applications. In particular, the derivative graphene oxide (GO) – chemically modified graphene with several oxygen-containing functional groups like hydroxyl, epoxy, and carboxyl – has already been explored for several drug delivery applications, as it enables efficient drug loading via non-covalent bonding like π-π stacking [21], electrostatic interaction [22], or hydrogen bonding [23]. Despite the reported *in vitro* biocompatibility of graphene-based substrates in neuronal tissue [19, 24, 25], only few studies have investigated the glial scar formation induced by graphene scaffolds [26, 27]. Particularly, the reports lack investigation of macroscopic graphene-based structures, which are required in the final application as e.g. 3D scaffolds, electrodes, or long-term drug delivery systems.

Apart from the choice of brain implant materials, also modifications and designs have been adjusted to alleviate foreign body responses [28]. As a further possibility to reduce e.g. glial scar

formation, brain implants could release specific compounds as already proposed [29]. Curcumin is such a compound, that has recently been described to prevent glial scar formation in spinal cord and brain injuries [30-33]. In experimental studies on spinal cord injuries, curcumin could *in vitro* and *in vivo* reduce the production of pro-inflammatory mediators (e.g. NO, TNFα, IL1β) and reduce the reactive expression of gliosis/fibrosis markers (e.g. glial fibrillary acidic protein, GFAP) and deposition of chondroitin sulfate proteoglycans, presumably by modulating different signaling pathways [31-34]. However, the compound curcumin, which is also prominently discussed as an anti-cancer agent [35], is hydrophobic, quite instable in aqueous solutions, sensitive to light and hardly bioavailable in experimental studies [36, 37].

In this study, we investigate glial scarring responses of human astrocyte and microglia cell lines towards highly porous (>99%) macroscopic 3D scaffolds based on interconnected, hollow GO and reduced GO (rGO) microtubes [38], and analyzed the rescuing effect of curcumin. In addition, we incubated the scaffolds with and without curcumin on murine acute brain slices to investigate their biocompatibility and the glial scar preventing effects of curcumin in the complex tissue composition *in vitro*. A graphical summary is depicted in Figure 1.

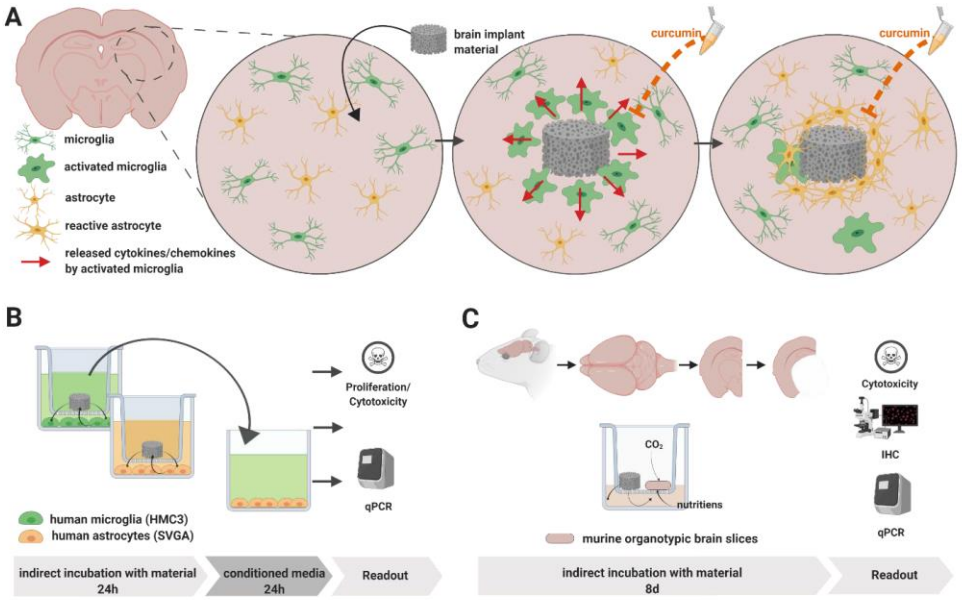

Figure 1: Graphical summary of study design (A) and experimental procedures using human glial cell lines (B) and organotypic mouse brain cultures (C) to investigate foreign body response to graphene oxide and reduced graphene oxide brain implant 3D scaffolds. The figure was generated using the Biorender.com software.

Experimental

Fabrication of *graphene oxide dispersion*

Graphene oxide (GO) was prepared according to previously reported procedures [39, 40]. Subsequently, the as produced GO powder was dispersed in deionized water assisted by tip sonication to achieve a homogeneous and stable dispersion.

Fabrication of GO/rGO scaffolds

To fabricate the GO/r-GO scaffolds, as a starting material we used highly porous ZnO templates consisting of interconnected, tetrapod-shaped zinc oxide (t-ZnO) microparticles that were prepared by flame transport synthesis as explained in detail in previous works [41, 42]. Briefly summarized, a mixture of zinc powder (grain size 1-5 µm) and polyvinyl butyral powder with mass ratio 1:2 was prepared in a crucible and heated in a muffle furnace for 30 minutes at 900°C (heating rate 60°C). Afterwards, the obtained fluffy t-ZnO powder was harvested and pressed into cylindrical tablets (diameter = 6 mm, height = 2 mm) and sintered for 5 h at 1150°C, resulting in highly porous (94%) networks of interconnected t-ZnO microparticles.

In the next step, the t-ZnO templates were coated with a thin (~ 25 nm) GO film using the recently introduced wet-chemical infiltration technique [38]. In short, an aqueous GO dispersion (2 mg/mL) was dripped on the hydrophilic and highly porous t-ZnO template, until the entire free volume was filled. Afterwards, the infiltrated template was dried at 50°C for 5 h to allow evaporation of the solvent (water) which resulted in simultaneous assembly of the individual GO flakes on the surface of the t-ZnO network. To prepare a reduced graphene oxide (rGO) coating, the infiltrated and dried templates were reduced chemically in diluted L-ascorbic acid (Merck KGaA, Darmstadt, Germany; 0.1 mg/mL) for 24 h (at 50°C). After that, the sample was washed thoroughly in deionized water. To remove the sacrificial t-ZnO templates, the coated samples were etched in 1 M HCl for 24 h, and subsequently washed in deionized water (1 time) and absolute ethanol (5 times). Thereafter, the GO and rGO scaffolds (99.9% porosity) were dried by critical point drying using an EMS 3000 (Tousimis, Rockville, MD).

Scanning electron microscopy (SEM) analysis of t-ZnO templates and scaffolds

Prior to the characterization, the samples were mounted on sample holders using conductive carbon tape (Agar scientific, Stensted, UK). The SEM analysis was carried out using a Zeiss Supra 55VP (Zeiss, Oberkochem, Germany) with an acceleration voltage of 8 kV.

Cell lines and cell culture

The human fetal astrocyte cell line SVGA was kindly provided by the group of Christine Hanssen Rinaldo, University Hospital of North Norway [43] with the permission of W.J. Altwood [44]. The human microglia cell line HMC3 was obtained from the American Type Culture Collection (ATCC, Manassas, Virginia, USA). Cells were grown in Dulbecco's modified Eagle's medium (DMEM; Life Technologies, Carlsbad, CA, USA) supplemented with 10% fetal bovine serum (FBS; PAN-Biotech GmbH, Aidenbach, Germany), 1% Penicillin-Streptomycin (10,000 U/ml; Thermo Fisher Scientific, Waltham, MA, USA) and 2 mM additional L-Glutamine (Thermo Fisher Scientific). To exclude *Mycoplasma* contamination, cells were routinely checked by nuclei staining and mycoplasma-specific PCR.

Cell incubation with materials and cell stimulations

For the analysis of acute brain-foreign body reactions of human microglia (HMC3) and astrocytes (SVGA) on GO and rGO scaffolds *in vitro*, 150.000 cells/well were seeded in 6-wells one day prior the stimulation to adhere over night at 37°C/5% CO_2. On the same day, GO and rGO scaffolds were sterilized in 70% ethanol (abs.) for 15 min, air-dried for 30 min and stored for 24 h at 4°C in DMEM without phenol red (Life Technologies, Paisley, UK) supplemented with 10% fetal bovine serum, 1% Penicillin-Streptomycin and 2 mM additional L-Glutamine (from now on named stimulation medium). On day of experiment, cells were washed once with phosphate buffered saline (PBS) and medium was exchanged to 1.5 mL stimulation medium

supplemented or not with 1 µM curcumin (Sigma-Aldrich/Merck). Cell culture inserts (PICM03050, Millicell®-CM 0.4 µm, Merck Millipore, Burlington, MA, USA) were placed into 6-wells, materials were added in the center of the inserts and inserts were filled with 1.5 mL stimulation medium (with or without curcumin), to obtain a total of 3 mL stimulation medium in both compartments. To study the influence of microglial cells on the acute foreign body reaction of astrocytes, the supernatants of HMC3 cells (lower compartment of transwell) were centrifuged after 24 h for 5 min, 300xg at 4°C, to separate microglia cells from conditioned HMC3-material medium, and put for another 24 h on one day prior seeded SVGA astrocytes. Cytotoxicity assay and cell counting were performed for indirectly incubated cells (HMC3 and SVGA) as well as conditioned HMC3-material medium incubated SVGA cells after 24 h. In brief, the cell survival was determined by counting of viable cells with a hemocytometer after 24 h of incubation. Growth rates were calculated as n-fold amount of the unstimulated control. Cell pellets of all stimulations were kept for qPCR analysis.

Generation and stimulation of organotypic brain slices

For the preparation of organotypic brain slices, female Sox10flox hGFAP:creeRT2 mice (16-24 weeks old; the genetic modification was not relevant for the experimental procedure) were sacrificed by cervical dislocation. All experiments were performed in compliance with the author's institute's policy on animal use and ethics, and with the agreement of the local Ethics Committee: V 242-70056/2015(91-7/15). Brains were carefully removed from the scull and rinsed in artificial cerebrospinal fluid (aCSF, 2 mM $CaCl_2$, 10 mM D-Glucose, 1.3 mM $MgCl_2$, 5 mM KCl, 124 mM NaCl, 26 mM $NaHCO_3$) and dissected to obtain the cerebral cortex regions from both hemispheres. These tissues were placed on wet filter papers, which were fixed below the blade of a digital tissue slicer (Stölting, Wood Dale, IL), and tissue slices of 400 µm were cut. The blade was wetted with aCSF before every cut to lower the surface tension [45]. Slices were prepared, separated, controlled under a binocular microscope and placed on membrane inserts (PICM03050, Millicell®-CM 0.4 µm) in 6-well plates. To allow the brain slices to be

provided with nutrients from the bottom and CO_2 from the top, wells below the insert were supplemented with 1.2 mL of MEM/HEPES (Thermo Fisher Scientific) containing 24% horse serum (Sigma Aldrich/ Merck), 1% glutamine, 1% penicillin and streptomycin, 6 mg/mL glucose and 168 µg/mL sodium hydrogen phosphate (modified protocol based on [45-47]). To study curcumin effects, cultivation media were supplemented with 1 µM curcumin (or not for controls) starting from the day 0 *in vitro* (0 div), this procedure will be termed "pre-stimulation" in the following, although the curcumin concentration was maintained during the whole incubation period. For indirect incubation of brain slices with materials (GO and rGO), implant materials were placed next to the brain slices on cell culture inserts on day 2 *in vitro* (2 div), without allowing a direct contact between brain tissue and materials themselves. Cytotoxicity assays were performed on day 5 and 8 *in vitro* (3 and 6 days of stimulation, dos) and brain slices were harvested on 8 div (6 dos) for qPCR analysis and immunohistochemical staining.

Cytotoxicity assay

To analyze cytotoxic effects of materials and the protective effects of curcumin, cells and brain slices were incubated indirectly for either 24 h (cell lines) or 3 respective 6 days (brain slices) with GO and rGO scaffolds, with or without pre-incubation with 1 µM curcumin. As positive controls, different amounts of digitonin-lysed cell-dilutions as well as digitonin-treated brain slices (83.2 ng/mL, Merck Millipore) were used to determine the exact number of dead cells, respective the n-fold percentage of dead brain slices compared to the unstimulated control. In brief, supernatants of cell cultures and brain slices were collected after 24 h respective 5 and 8 div (3 or 6 dos) and cytotoxicity was analyzed using the the CytoTox-Fluor™ Cytotoxicity Assay (Promega, Madison, WI) as described previously [48]. Moreover, the cell survival was determined by counting of viable cells after 24 h indirect incubation with materials or after 24 h incubation with conditioned HMC3-material medium, respectively.

Quantitative Reverse Transcription PCR (qPCR)

Cells were harvested and tissues homogenized using the QIAzol lysis reagent (Qiagen, Hilden, Germany) and total RNA was isolated following the manufacturer's protocol. Using RNase-free Dnase (1 U/µL, Promega), genomic DNA was digested, and cDNA was synthesized with the RevertAid™ H Minus M-MuLV Reverse Transcriptase (200 U/µL, Thermo Fisher Scientific). TaqMan primer probes and TaqMan™ Gene expression Master Mix (Thermo Fisher Scientific) were employed to analyze samples with the ABI PRISM 7500 Sequence detection system. Analyzed genes were *gapdh* (human: Hs99999905_m1, mouse: Mm99999915_g1), *il6* (human: Hs00985639_m1, mouse: Mm00446190_m1), *tnfα* (human: Hs00174128_m1, mouse: Mm00443258_m1), *tgfβ* (human: Hs00171257_m1, mouse: Mm01178820_m1), *tenascin* (human: Hs01115665_m1), *nestin* (human: Hs0070120_s1), and *fibronectin* (human: Hs00277509_m1). Cycle of Threshold values (CT) were determined, and ΔCT values = CT [gene of interest] – CT [GAPDH] were calculated. Due to the logarithmic reaction mode, a ΔC_T value of 3.33 corresponds to one magnitude lower gene expression compared to GAPDH. For material-induced mRNA regulation ΔΔCT values were calculated: $\Delta\Delta CT = 2^{-(\Delta CT[stimulus] - \Delta CT[control])}$.

Immunohistochemistry

After cultivation of brain slices for 8 days (6 dos), slices were briefly rinsed with PBS, fixed in 4% paraformaldehyde (in Tris-buffered saline, TBS) over night, equilibrated in 30% sucrose (in TBS, until sinking to the bottom), embedded and frozen in Shandon Cryomatrix (Thermo Fisher Scientific) and cut in 10 µm cryosections. Sections on glass slides were washed with 0.1% Tween in TBS (TBS-T), blocked for autofluorescence with 1% sudan black (Merck, in 70% ethanol) and for unspecific antibody binding with 0.5% glycine/0.5% bovine serum albumin (BSA, in TBS-T). The incubation with primary antibodies was performed at 4°C (overnight), afterwards, slices were washed 3x, incubated with Alexa Fluor 488 or 555 labelled secondary antibodies against respective host species (donkey IgG, 1:800, Thermo Fisher Scientific) at 37°C for 1 h, washed (2x, TBS-T, 1x TBS), and nuclei were counterstained with

DAPI (Sigma-Aldrich). Slides were embedded with Shandon Immu-Mount™ (Thermo Fisher Scientific) after washing in TBS-T and water. For secondary antibody controls, primary antibodies were omitted (Figure S2, Supporting Information). Commercially available primary antibodies were anti-GFAP (glial fibrillary acidic protein; rabbit, 1:100; DAKO, Glostrup, Denmark, Z0334), anti-fibronectin (rabbit, 1:400; Novus biologicals, Wiesbaden, Germany; NBP1-91258), anti-MBP (myelin basic protein; mouse, 1:400; Novus, NBP2-22121), anti-nestin (mouse, 4D11, 1:200; Novus, NBP1-92717) and anti-vimentin (chicken, 1:200; Novus, NB300-223). The monoclonal antibody against neurofilament-M (clone 2H3) developed by T.M Jessell and J. Dodd, HHMI/Columbia University was obtained from the Developmental Studies Hybridoma Bank, created by the NICHD of the NIH and maintained at The University of Iowa, Department of Biology, Iowa City, IA 52242. Sections were inspected and documented using an Axiovert 200M Fluorescence Microscope (Zeiss).

Statistical analysis

All values are shown as mean values ± standard deviation (SD). Statistical analysis was performed using GraphPad Prism® 5, (GraphPad Software, Inc.Version, CA). Asterisks or rhombs indicate statistical significance, whereas p values < 0.05 were considered as significant. Different statistical analyses were applied in function of experiments and are stated in the figure legends.

Results

Preparation and analysis of templates

The fabrication of the 3D scaffolds follows a simple bottom-up approach which allows for precise control over both microstructure (porosity, pore size) and macrostructure (shape, size) of the resulting graphene-based scaffolds [38]. The process is based on a highly porous (up to 94%) sacrificial template, which consists of interconnected, tetrapod-shaped zinc oxide (t-ZnO) microparticles (SEM images in Figure S1, Supporting Information). As schematically shown in Figure 2A, the template was infiltrated with an aqueous dispersion of graphene oxide (GO) sheets, resulting in filling of the entire free volume of the porous and hydrophilic t-ZnO network.

After drying of the infiltrated template, the individual GO sheets assembled uniformly on the surface of the ZnO tetrapods and formed a nanoscopic thin (~ 25 nm) coating. In the final step, the sacrificial template was removed wet-chemically by HCl and, to prepare reduced graphene oxide (rGO)-based scaffolds, reduced in ascorbic acid. Figure 2B shows a photograph of the employed template and the prepared GO and rGO scaffolds which exhibit an extremely high porosity (>99.9%) and a low density similar to air (~ 2 mg/cm^3). As revealed by the SEM images in Figure 2C-D, the tetrapodal morphology of the template was perfectly adopted by the final scaffolds which constitute networks of interconnected, hollow GO or rGO microtubes.

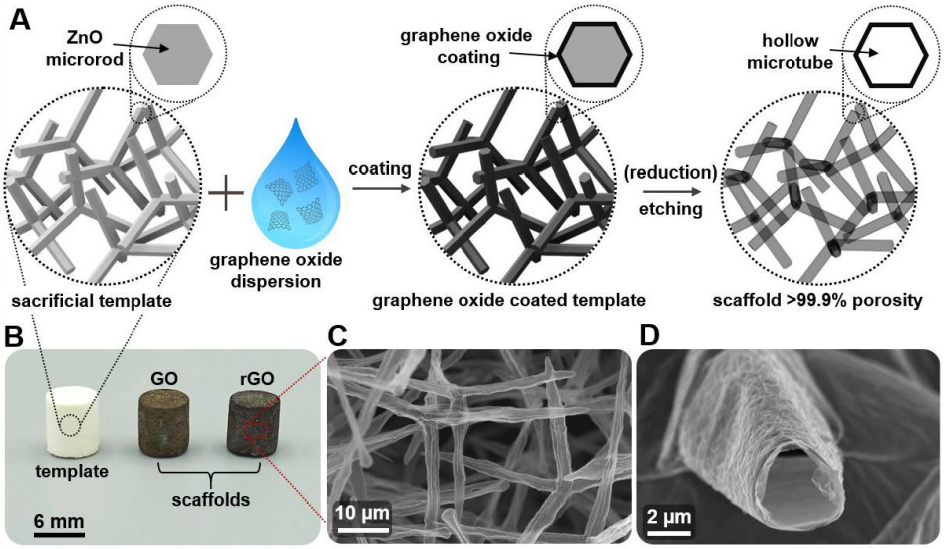

Figure 2. Highly porous graphene based 3D scaffolds: A) Schematic presentation of the bottom-up fabrication of the GO and rGO based 3D scaffolds. As illustrated, a sacrificial template composed of interconnected ZnO microrods was infiltrated with an aqueous GO dispersion, resulting in wet-chemical assembly of the GO sheets on the surface of the ZnO microrods. After chemical reduction and/or wet-chemical etching of the coated template, highly porous (>99.9% porosity) scaffolds are formed, consisting of interconnected, hollow GO or rGO microtubes. B) Photograph of employed t-ZnO template and the fabricated GO and rGO scaffolds. C)-D) SEM images of rGO scaffold, revealing perfect adoption of the tetrapodal template morphology and the nanoscopic wall thickness of the hollow microtubes.

Human microglia and astrocyte response on 3D scaffolds and reversibility by curcumin

In a next step, we investigated the effects of the GO and rGO scaffolds on brain cells that contribute to tissue foreign body responses. We also performed co-stimulations with curcumin, to show that material effects can putatively be reversed by gliaprotective drugs. Curcumin is a a well-known anti-inflammatory and neuro- and gliaprotective drug serving here as a model drug to attenuate implant caused foreign body reactions.

In this experimental setting, we analyzed the material induced cytotoxicity in microglia and astrocyte cultures after 24 h challenge with the materials (Figure 3A, left and middle). In

addition, we analyzed cytotoxicity in astrocytes incubated for 24 h with conditioned medium from material challenged microglia (Figure 3A, right). Materials only slightly increased the percentage of dead cells (from ~ 2% to ~5% depending on cell type), and these effects were completely abolished by co-stimulation with curcumin. Moreover, we determined the growth rates of differentially stimulated cells by cell counting at the beginning and after 24 h of stimulation (Figure 3B). Growth rates of microglia were only slightly reduced by GO and rGO, however these effects could be restored by co-stimulation with curcumin. In fact, astrocytes were more sensitive, they showed significantly reduced growth rates after GO and rGO challenge, and these effects could not be restored significantly by co-stimulation with curcumin. However, astrocyte cultures did not show any differences between growth rates when exposed to conditioned media from microglia that were exposed or not to material for 24 h (experimental procedure described in Figure 1B). In this experimental setting, material effects seemed to be ameliorated by microglia influence, and co-stimulation with curcumin did not yield any further reduction.

Further, we analyzed the expression of inflammatory related genes by microglia cells as well as reactive gliosis related genes by astrocytes after incubation with GO and rGO (Figure 3C respective D) or on astrocytes after incubation with conditioned medium, generated from microglia incubation with GO and rGO (Figure 3E). Interestingly, although GO and rGO scaffolds did not cause cytotoxic effects in HMC3 microglial cells, inflammation related genes such as interleukin6 (IL6) or tumor necrosis factor-α (TNFα) were clearly induced after 24 h, depending on material and gene to up to ~ 30 fold, and with high variations between independent experiments. However, whilst IL6 and TNFα overexpression was more pronounced for rGO scaffold materials, transforming growth factor-β (TGFβ) expression was stronger for cells challenged with GO. SVGA astrocytes challenged with materials for 24h showed slightly induced expression of glial scarring related genes tenascin C and nestin after challenging with rGO and GO, however to a lesser extent (up to ~ 3-fold) than inflammation related markers, and high variations did hardly allow for any detection of significance. Fibronectin, however, was not at all regulated. Moreover, when SVGA astrocytes were

stimulated with conditioned-material medium from HMC3 microglia, glial scarring related genes were not significantly induced upon stimulation. Overall, the pre-incubation with curcumin could significantly restore these effects completely to the control level.

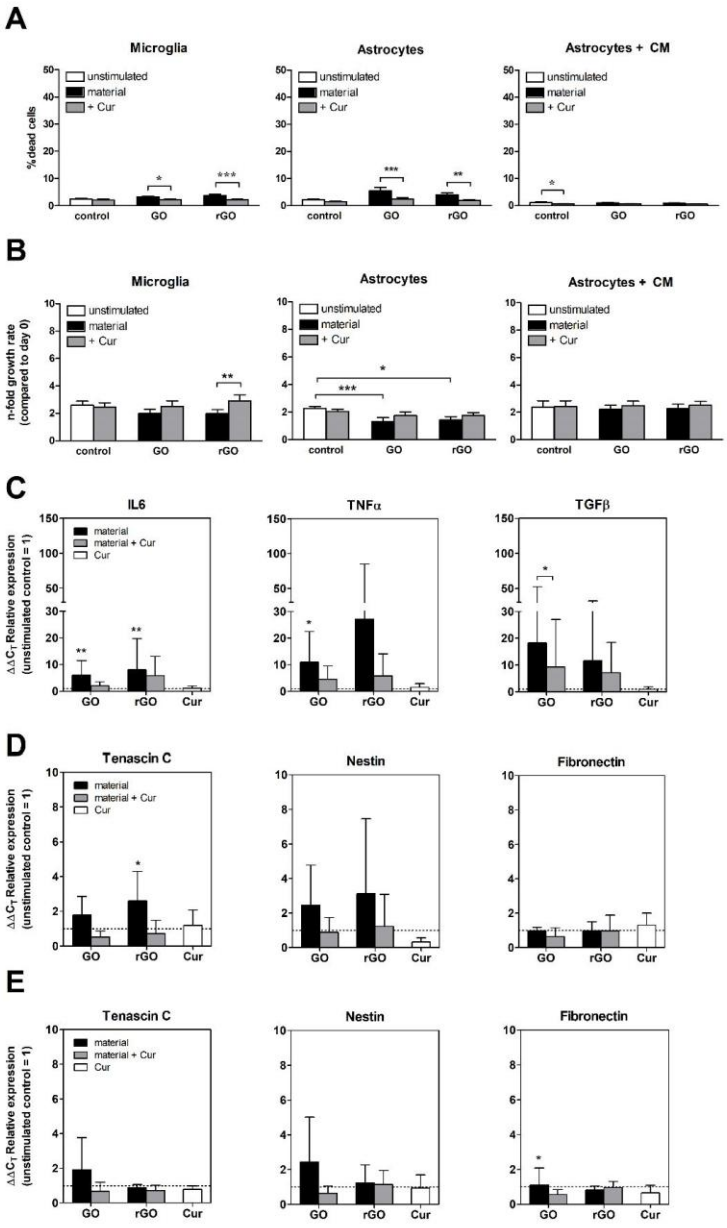

Figure 3: Responses of human HMC3 microglial cells and SVGA astrocytes towards graphene oxide (GO) and reduced graphene oxide (rGO) with or without co-stimulation with curcumin regarding cytotoxicity (A), proliferation (B) as well as mRNA regulation of pro-inflammatory cytokines (C) and astrogliosis associated genes (D, E). Materials were either incubated with HMC3 microglia (A,B left, C) and SVGA astrocytes (A,B middle, D) directly for 24 h, or SVGA were incubated with conditioned medium (CM) of material challenged HMC3 for 24 h (A,B right, E) with or without co-stimulation with 1 µm curcumin (cur). (A) The percentage of dead cells in cultures of material challenged microglia (left), astrocytes (middle) and astrocytes incubated with CM from material challenged microglia was measured by cytotoxicity assay of supernatants from n = 7 independent experiments after 24 h. (B) The growth rate of differentially stimulated cells was determined by cell counting at the beginning and after 24 h of stimulation from n = 6 independent experiments. (C) Relative gene expression HMC3 microglia (up) and SVGA astrocytes (middle) on GO and rGO materials, as well as of SVGA astrocytes, challenged with conditioned HMC3-material medium (right) for a choice of typical inflammation related (n = 5-8) as well as reactive gliosis genes (n = 4-8). Data is depicted as mean ± standard deviation. Significant differences between material stimulations and the co-stimulation with curcumin were determined by (if applicable repeated measures) Two-Way-ANOVA followed by Bonferroni's multiple comparison test. Differences between unstimulated controls and material stimulations were determined by (if applicable repeated measures) One-Way-ANOVA followed Dunn's multiple comparison test. Data is significant for *p<0.05, **p<0.01 and ***p<0.001

In summary, GO and rGO did hardly influence viability of human microglia and astrocytes or of astrocytes via conditioned microglia-material media. Moreover, material-induced slight effects on cell viability, proliferation and expression could largely be reduced by curcumin or in case of astrocytes by the conditioned media from microglial cells.

Cellular responses on 3D scaffolds in organotypic brain slices and reversibility by curcumin

Due to the fact, that monocultures lack the information of the complex microenvironment of a tissue, we decided to use organotypic brain slices as a 3D approach, which more closely resembles the *in vivo* situation. Organotypic brain slices preserve the different neuronal and glial cell types in their tissue environment, enabling us to investigate the effects of GO and rGO scaffolds, pre-incubated or not with curcumin, on this comprehensive brain tissue model for a period of 6 days (Figures 4 and 5).

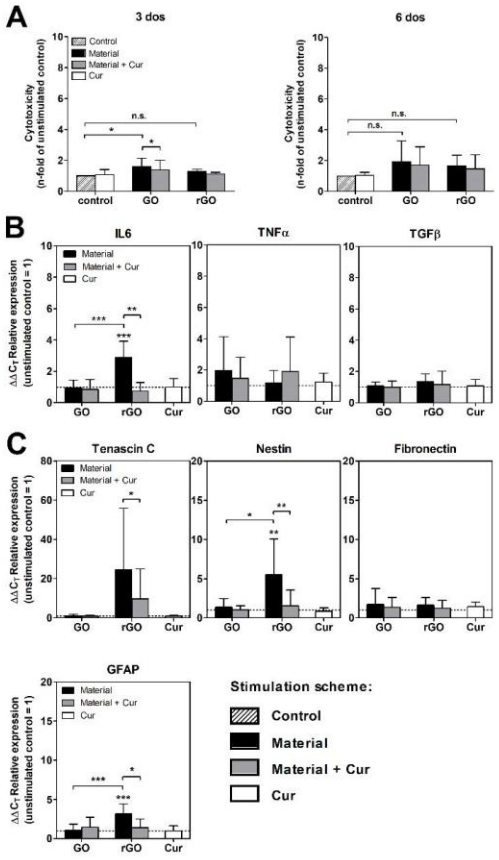

Figure 4: Responses of murine organotypic brain slice cultures towards graphene oxide (GO) and reduced graphene oxide (rGO) with or without curcumin pre-incubation regarding cytotoxicity (A) and mRNA regulation of pro-inflammatory cytokines (B) and astrogliosis associated genes (C). Brain slices were pre-incubated with 1 µM curcumin for 2 div, and co-incubated with materials for 3 (A left) or 6 further days (A right, B,C). (A) The cytotoxic effects were measured from supernatants and normalized to unstimulated controls (=1) in n = 3-4 independent experiments. (B,C) Relative gene expression of organotypic brain slices for a choice of typical inflammation related (B) as well as reactive gliosis genes (C) from n = 3-9 independent experiments. Data is depicted as mean ± standard deviation. Significant differences between material stimulations and pre-incubation with curcumin were determined by Two-Way-ANOVA followed by Bonferroni's multiple comparison test. Differences between unstimulated controls and material stimulations were determined by (if applicable repeated measures) One-Way-ANOVA followed Tukey's multiple comparison test. Data is significant for *p<0.05, **p<0.01 and ***p<0.001

First, we could show that both materials, GO as well as rGO, had only very small effects in cytotoxicity analyses of organotypic brain slices compared to the control levels at early (3 dos) and late (6 dos) time points of incubation (Figure 4A). At most, GO did slightly increase cytotoxicity after 3 dos (Figure 4A, left), and the addition of 1 μM curcumin could reduce this effect, but in general, measured cytotoxicity was very low.

Furthermore, we analyzed the expression of IL6, TNFα and TGFβ as examples for pro-inflammatory cytokines (Figure 4B), and tenascin C, nestin, fibronectin and glial fibrillary acidic protein (GFAP) as examples for reactive gliosis related markers (Figure 4C) on mRNA level at 6 dos. Whereas GO had no or only little effects on the expression of IL6, TNFα or TGFβ (Figure 4B), and these effects could be alleviated by curcumin pre-incubation, rGO yielded significant induction of IL6 to ~ 3 fold (Figure 4B, left).

However, the pre-incubation with curcumin could significantly restore this effect completely to the control level. TNFα and TGFβ where not induced by rGO and therefore curcumin did not show any alleviating effects. Comparable results were obtained for the regulation of reactive gliosis markers. Whereas rGO induced tenascin C, nestin and GFAP expression significantly (up to ~25, ~6 and ~3 fold, respectively), GO did not influence reactive gliosis associated gene expression. Fibronectin was again neither induced by GO nor by rGO. Curcumin could successfully restore the expression of (almost) all regulated genes to the control level. At this point, one has to keep in mind that the microglial as well as astrocyte cell populations in a brain slice only represent respective parts of the total cell population, leading to possibly smaller effects and higher standard deviations than in monocultures. On the other hand, less or more pronounced effects might be caused by regulatory effects of the cellular neighbors and microenvironment, which are well preserved in this brain slice model.

Finally, GO and rGO-mediated cellular changes in organotypic brain slices and the restoration by curcumin pre-incubation, was visualized using fluorescence immunohistochemistry (Figure 5). Stainings of neurons (NF, neurofilament) and oligodendrocytes (MBP, myelin basic protein) revealed, that the neuronal network and oligodendrocytes were clearly unaffected by GO or

rGO incubation after 6 dos. Curcumin did either not affect or positively influence the neuronal network as well as oligodendrocytes (Figure 5). The glial fibrillary acidic protein (GFAP), specific for astrocytes and elevated in reactive astrocytes, showed strong immunoreactivity upon GO and rGO incubation compared to unstimulated and curcumin pre-incubated control slices, whereas the pre-incubation with 1 µM curcumin could mostly alleviate this response. Moreover, the number of cells positively stained for nestin, a marker of glial precursors and reactive glial cells, did not visually differ from control slices upon GO and rGO stimulation. However, the cell size of nestin positive cells did increase upon material incubation, and this effects was again reduced by curcumin for rGO incubated slices to the control level (Figure 5). Staining of fibronectin revealed slightly more positive cells upon GO and rGO incubation, whereas curcumin pre-incubation could alleviate these effects. Vimentin, a further key player in reactive astrogliosis, showed strong immunoreactivity in GO and rGO challenged slices with a higher number as well as increased cell size of vimentin positive cells, compared to unstimulated or curcumin pre-incubated brain slices after 6 dos. By pre-incubating brain slices with curcumin prior to the incubation with GO and rGO, the higher numbers of vimentin positive cells could almost be alleviated to control level, but enlargement of cell bodies persisted.

In summary, GO and rGO did only slightly increase cytotoxicity in murine organotypic brain slices for a period of 3 - 6 dos. GO and rGO treatment provoked only slight or distinct induction of inflammation and reactive gliosis related genes on mRNA levels, and similar effects could be visualized on protein level. The pre-incubation with curcumin could restore GO/rGO-induced effects on cytotoxicity, mRNA expression and protein expression of cellular markers to (almost) control levels for all stimulations.

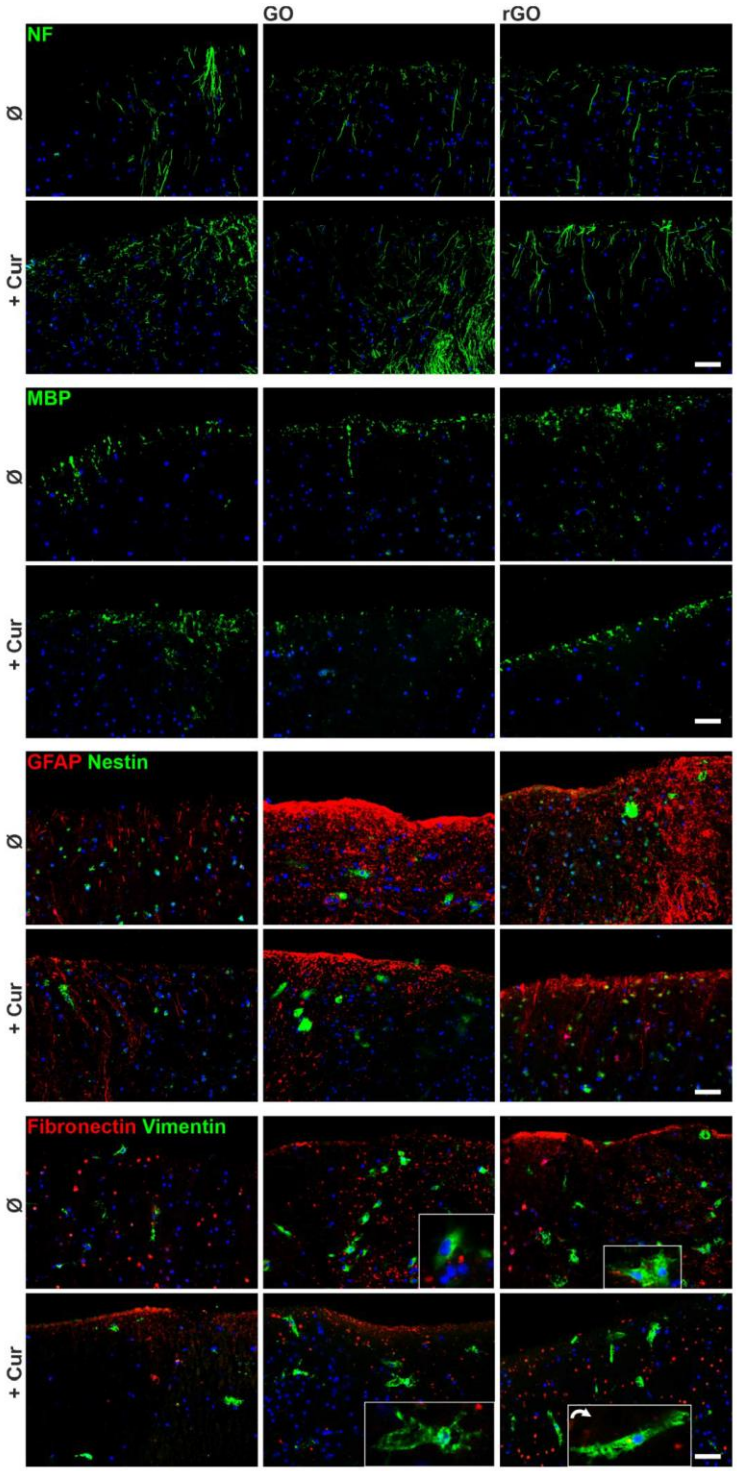
GO
rGO
NF
Ø
+ Cur
MBP
Ø
+ Cur
GFAP Nestin
Ø
+ Cur
Fibronectin Vimentin
Ø
+ Cur

Figure 5: Responses of murine organotypic brain slice cultures towards graphene oxide (GO) and reduced graphene oxide (rGO) with or without curcumin pre-incubation regarding immunoreactivity. Murine acute brain slices were pre-incubated with 1 µM Curcumin (Cur) until 2 div and challenged with GO and rGO for 6 dos, slices were cut in 10 µm cryosections and immunostained with antibodies against neurofilament-M (NF, neurons), MBP (oligodendrocytes), GFAP and nestin (astrocytes, glial precursors, reactive astrocytes) as well as fibronectin and vimentin (reactive astrocytes, glial scaring). Representative images from n = 2 independent experiments. Scale Bars indicate 50µm, inserts have different magnifications. Please refer to the supplement to Figure 5 for secondary antibody controls.

Discussion

During the last decades, great efforts have been made to develop novel treatment strategies to overcome the various difficulties in the treatment of brain disorders. Besides improvements in drug delivery, including specific drug design (pro-drugs, chimeric peptides), the use of vector vehicles (viral and nanoparticles, exosomes) and the manipulation of the BBB [49, 50], approaches for local manipulations have been pursued and in case of stimulation electrodes successfully made the step to clinical application [2]. In this study, we present two putative nanostructured GO and rGO based implant materials and investigated their influence on healthy brain cells and tissue with a special focus on the glial scarring reaction.

Recently, a high multiplicity of graphene based nanomaterials have been developed for brain applications such as biosensors, interfaces, drug delivery systems [17, 20, 51, 52] or the differentiation of neurons by electrical stimulation [53] due to their outstanding properties. Besides the extremely high specific surface area and low weight of the 2D materials, the high conductivity of graphene (and also reduced graphene oxide rGO) is one of the major advantages over other materials as it can significantly improve electrode performances [54]. Graphene oxide (GO) on the other hand, lacks this conductive behavior, but can be easily bio-functionalized via its hydrophilic functional groups and therefore can be used for other approaches such as the surface functionalization for increased biocompatibility or improved drug loading capacities for the use as a (pH-sensitive) drug delivery system [21, 55, 56]. To use the carbon 2D materials as macroscopic implant materials in the described applications, they have to be assembled into 3D structures, which retain the unique properties of the 2D building blocks. Several approaches have already been developed for the wet-chemical assembly of individual GO flakes into macroscopic GO and rGO (by subsequent chemical reduction of GO) networks, which are mostly based on template-free gelation of GO dispersions followed by freeze drying or critical point drying [57]. The here presented scaffolds, however, were fabricated using a highly versatile template with an open-porous framework-like structure, resulting in lightweight scaffolds (~ 2 mg/cm^3) with both tailorable macrostructure (shape, size) and microstructure (porosity, pore size) [57]. This is crucial in order to adjust the properties for to the

intended application. For instance, the high and tunable free volume of the scaffolds combined with large (several µm) and interconnected pores favor applications in 3D tissue engineering. In fact, similar scaffolds based on carbon nanotubes (CNTs) have already been successfully used for 3D cellular growth of fibroblast or osteoblast cells [58, 59]. Additionally, the good electrical conductivity of the rGO scaffolds (~ 1 S/m[1]) [38] makes them attractive for applications as neural implants as this is favorable for more efficient cellular signaling and function [60].

Concerning biocompatibility and/or toxicology of GO and rGO, several studies are available in general [19, 24, 25, 61-65], however, little is known about their effects in the CNS, especially regarding inflammation and reactive gliosis processes as a major force of glial foreign-body responses impairing the major functions of brain implants. Systemically applied rGO, although passing the blood-brain barrier, neither caused any cytotoxic effects in mouse and rats, nor did it cause any effects on inflammation in serum or hippocampus in rats [66, 67]. However, GO and rGO nanoparticles have been used to study their effects on ocular toxicity *in vitro* and *in vivo*. In the eye, GO caused intraocular inflammation and cell apoptosis in the cornea and in corneal epithelial cells in a duration-dependent manner, whilst rGO remained without any toxic effects [68]. In the brain, nanosheets of GO were observed to reduce the activity of synapses, whilst not affecting cultured hippocampal neurons survival [69, 70]. GO nanoribbons induced reactive oxygen species (ROS) production and autophagy in neuroblastoma cells, but did also not increase cell death [71]. Giving these heterogeneous observations from different neuronal and neuronal-related cell entities, more research is necessary to produce safe graphene based implants for brain applications that gives not only information about their toxic effects on neurons, but also of the glial cells as main promotors of the brain-foreign body response. First attempts to study the glial and neuro-glial response upon GO nanosheets or flakes have been made on primary astrocytes and primary astrocyte-neuron-co-cultures [72] as well as on primary rat glial cell cultures and 3D murine organotypic spinal cultures, that keep the normal presence and distribution of neurons and glial cells alive [54]. In the latter study, a GO nanosheet long-term stimulation for two weeks slightly (but not significantly) increased the microglia related cytokine and chemokine production by organotypic spinal cultures. The shorter GO nanosheet

stimulation of rat primary glial cells for 5 days, yielded a clear phenotypical switch of microglial cells to their amoeboid shaped, activated, pro-inflammatory state. This study also showed the cellular uptake of the soluble sheets. Likewise, cellular uptake of soluble GO flakes was also observed for astrocytes and identified as a major cause for alterations in membrane permeability, cytoskeleton rearrangement and differentiation status of astrocytes, and in neuron-astrocyte co-cultures also affecting excitability and synapse density [72]. Since we were interested in the use of 3D tetrapod-shaped scaffolds of GO and rGO for the use as brain implant materials, which had not yet been tested for their biocompatibility in the brain or with brain cells, we also used different *in vitro* models that give information about viability, and especially inflammation and reactive gliosis processes in the CNS. Therefore, either mono-cultures of human astrocytes and microglia or 3D tissue cultures of organotypic brain slices of mouse neuro cortices were challenged with GO and rGO templates, to analyze the single cell response as well as of complex tissue, preserving all different cell types. Comparing our results to the observations with GO nanosheet effects on microglial cells [54], we did hardly see any effects on microglia proliferation or survival in human microglial monocultures, but we detected more pronounced and robust induction of pro-inflammatory cytokines, while cytokine expression was hardly affected in murine organotypic brain slices (except for IL6 upon rGO challenge). Focusing on the GO/rGO template effects on astrocytes, we observed again hardly any effects on viability or proliferation, and only slight effects on the expression of intracellular (nestin) and extracellular markers (fibronectin, tenascin C) for reactive gliosis in cultured human astrocytes. These effects were even less when astrocytes were incubated with a conditioned medium from material challenged microglia. In organotypic brain slices, material challenge yielded more robust induction of intracellular cytoskeleton molecules GFAP, vimentin and nestin as well as the extracellular matrix component tenascin C, well-known markers for glial scaring [73-76]. Interestingly, in mRNA expression analyses, rGO provoked clearly higher effects than GO, but these findings were not corroborated on the morphology/protein expression level, where GO and rGO yielded almost the same impressions. These might be due to the fact that activation of glial cells is time dependent and

reversible, and different read outs may be differentially sensitive at different time points. While starting from a completely different question and using different methods, these results are at least in part in line with those of Chiacchiaretta and colleagues [72] when focusing on the GO induced remodeling processes within astrocytes, but also contradictive as some of our results (induction of nestin, vimentin positive cells) emphasize a switch of some astrocytes to a less differentiated, reactive state. For a short notice, not concerning the inflammatory and gliosis responses, neurons and oligodendrocyte were not impaired by GO/rGO challenge in our experimental model of organotypic brain slices, supporting the overall acceptable tolerance of GO and rGO by brain tissue observed by other studies [54, 68, 70].

Facing distinct effects of only a part of pro-inflammatory or reactive gliosis associated genes/proteins by the challenge of glial cell cultures or organotypic brain slices with GO or rGO scaffolds, we investigated, if an anti-inflammatory compound – we used the food additive curcumin as a model drug - can alleviate effects eventually caused by both materials. Curcumin is known to reduce successfully inflammation and glial scarring processes after spinal cord injury [31, 34, 77] and, in a first approach, curcumin loaded intracortical implants could improve neuronal survival and positively influence the stability of the blood-brain barrier for a period of 4 weeks [78]. Accordingly, in our study, the addition of curcumin alleviated the cytotoxic, inflammatory or glial scarring effects of both GO and rGO after 24 h in mono-cultures as well as after 6dos in murine organotypic brain slices effectively. Single stimulations with curcumin (without GO/rGO scaffolds) did not yield any effects, so that curcumin could alleviate potential glial cell responses towards brain implants.

Amongst many other approaches to improve brain implant biocompatibility, coatings for example with the interleukin 1 receptor antagonist (IL1Ra) have been implemented on chronically implanted neural electrodes, which could successfully reduce glial scarring already 1 week post implantation [79]. The application of IL1Ra was further improved by embedding the antagonist in protease-degradable poly(ethylenglycol) hydrogel coatings [80]. However, although microgel coatings on neural implants reduced astrocytic recruitment around the implant, microglial response and neuronal cell loss were not significantly improved [81]. In perspective,

curcumin as a promising anti-inflammatory and anti-glial scarring compound could be used in such coatings, to minimize the implant-induced foreign body response of the brain.

Conclusion

In summary, the GO and rGO scaffolds did not show pronounced effects on viability (cytotoxicity and proliferation) of human microglia and astrocyte cell lines as well as on murine organotypic brain slices. Moreover, both materials did not affect neurons as well as oligodendrocytes in organotypic brain slices. Although GO and rGO scaffolds both showed comparably mild responses, rGO caused stronger effects than GO on the expression of inflammation and glial scarring related genes in cell lines and slice cultures. However, most effects could be reduced to almost control level by curcumin pre- or co-incubation. Thus, highly porous, tetrapod-shaped GO and rGO scaffolds proved to be promising candidates as brain implants, e.g. conductive electrodes or drug delivery systems due to their high surface area for loading or coating with foreign body response attenuating drugs like curcumin.

Conflicts of Interest

There are no conflicts to declare.

Acknowledgements

We thank Judith Becker, Martina Burmester, Nicolas daSilva and Sonja Dahle for expert technical assistance. This work was supported by the Deutsche Forschungsgemeinschaft) under the contracts Ad183-27/1 and RTG 2154 (projects 3, 7 and 8), and the European Commission under the Graphene Flagship Core 2 grant No. 785219. The funding body did not have any influence on the design of the study.

Authors contributions

CS: Conceptualization, Investigation, Formal analysis, Methodology (Neuroscience), Visualization, writing original draft; FR: Conceptualization, Investigation, Methodology (Material Science), Visualization, writing original draft; FC: Methodology (Neuroscience, Mice), Investigation, review and editing; JHF: Methodology (Neuroscience), review and editing; RL: Methodology (Neuroscience), Resources, review and editing; ASN: Methodology (Material Science), Resources, review and editing; MRL: Methodology (Material Science), Resources, review and editing; XF: Methodology (Material Science), Resources, review and editing; YKM: Methodology (Material Science), review and editing; RA: Methodology (Material Science), Supervision, Resources, review and editing; FS: Methodology (Material Science), Supervision, Resources, review and editing; KH: Conceptualization, Investigation, Methodology (Neuroscience), Visualization, Supervision, writing original draft

References

1. R. Pandit, L. Chen and J. Gotz, *Adv Drug Deliv Rev*, 2019, DOI: 10.1016/j.addr.2019.11.009.
2. D. De Ridder, S. Perera and S. Vanneste, *Neuromodulation*, 2017, **20**, 206-214.
3. C. C. McIntyre and R. W. Anderson, *J Neurochem*, 2016, **139 Suppl 1**, 338-345.
4. P. P. Wang, J. Frazier and H. Brem, *Adv Drug Deliv Rev*, 2002, **54**, 987-1013.
5. H. Brem, M. G. Ewend, S. Piantadosi, J. Greenhoot, P. C. Burger and M. Sisti, *J Neurooncol*, 1995, **26**, 111-123.
6. H. Brem, M. S. Mahaley, Jr., N. A. Vick, K. L. Black, S. C. Schold, Jr., P. C. Burger, A. H. Friedman, I. S. Ciric, T. W. Eller, J. W. Cozzens and et al., *J Neurosurg*, 1991, **74**, 441-446.
7. H. Brem, S. Piantadosi, P. C. Burger, M. Walker, R. Selker, N. A. Vick, K. Black, M. Sisti, S. Brem, G. Mohr and et al., *Lancet*, 1995, **345**, 1008-1012.
8. A. Bregy, A. H. Shah, M. V. Diaz, H. E. Pierce, P. L. Ames, D. Diaz and R. J. Komotar, *Expert Rev Anticancer Ther*, 2013, **13**, 1453-1461.
9. F. Salle, W. Lahiani, E. Spagnuolo and S. Palfi, *Asian J Neurosurg*, 2018, **13**, 1171-1174.
10. R. Kumar, A. M. Lozano, Y. J. Kim, W. D. Hutchison, E. Sime, E. Halket and A. E. Lang, *Neurology*, 1998, **51**, 850-855.
11. A. L. Benabid, P. Pollak, C. Gervason, D. Hoffmann, D. M. Gao, M. Hommel, J. E. Perret and J. de Rougemont, *Lancet*, 1991, **337**, 403-406.
12. M. Hodaie, R. A. Wennberg, J. O. Dostrovsky and A. M. Lozano, *Epilepsia*, 2002, **43**, 603-608.
13. D. J. DiLorenzo, J. Jankovic, R. K. Simpson, H. Takei and S. Z. Powell, *Neuromodulation*, 2014, **17**, 405-418; discussion 418.
14. V. Vedam-Mai, C. Rodgers, A. Gureck, M. Vincent, G. Ippolito, A. Elkouzi, A. T. Yachnis, K. D. Foote and M. S. Okun, *Parkinsonism Relat Disord*, 2018, **54**, 51-55.
15. C. Marin and E. Fernandez, *Front Neuroeng*, 2010, **3**, 8.
16. V. S. Polikov, P. A. Tresco and W. M. Reichert, *J Neurosci Methods*, 2005, **148**, 1-18.
17. J. Liu, L. Cui and D. Losic, *Acta Biomater*, 2013, **9**, 9243-9257.
18. O. Akhavan, *J. Mater. Chem. B* 2016, **4**, 3169-3190.
19. M. C. Serrano, J. Patiño, C. García-Rama, M. L. Ferrer, J. L. G. Fierro, A. Tamayo, J. E. Collazos-Castro, F. d. Monte and M. C. Gutiérrez, *J. Mater. Chem. B* 2014, **2**, 5698-5706.
20. D. Kuzum, H. Takano, E. Shim, J. C. Reed, H. Juul, A. G. Richardson, J. de Vries, H. Bink, M. A. Dichter, T. H. Lucas, D. A. Coulter, E. Cubukcu and B. Litt, *Nature communications*, 2014, **5**, 5259.
21. G. Liu, H. Shen, J. Mao, L. Zhang, Z. Jiang, T. Sun, Q. Lan and Z. Zhang, *ACS Appl Mater Interfaces*, 2013, **5**, 6909-6914.
22. D. Depan, J. Shah and R. D. K. Misra, *Materials Science and Engineering: C* 2011, **31**, 1305-1312.
23. X. T. Zheng and C. M. Li, *Molecular pharmaceutics*, 2012, **9**, 615-621.
24. M. Tang, Q. Song, N. Li, Z. Jiang, R. Huang and G. Cheng, *Biomaterials*, 2013, **34**, 6402-6411.
25. A. Fabbro, D. Scaini, V. Leon, E. Vazquez, G. Cellot, G. Privitera, L. Lombardi, F. Torrisi, F. Tomarchio, F. Bonaccorso, S. Bosi, A. C. Ferrari, L. Ballerini and M. Prato, *ACS nano*, 2016, **10**, 615-623.
26. A. H. Palejwala, J. S. Fridley, J. A. Mata, E. L. Samuel, T. G. Luerssen, L. Perlaky, T. A. Kent, J. M. Tour and A. Jea, *Surg Neurol Int*, 2016, **7**, 75.
27. K. Zhou, S. Motamed, G. A. Thouas, C. C. Bernard, D. Li, H. C. Parkington, H. A. Coleman, D. I. Finkelstein and J. S. Forsythe, *PLoS One*, 2016, **11**, e0151589.
28. J. Lee, H. R. Cho, G. D. Cha, H. Seo, S. Lee, C. K. Park, J. W. Kim, S. Qiao, L. Wang, D. Kang, T. Kang, T. Ichikawa, J. Kim, H. Lee, W. Lee, S. Kim, S. T. Lee, N. Lu, T. Hyeon, S. H. Choi and D. H. Kim, *Nature communications*, 2019, **10**, 5205.

29. C. Boehler, C. Kleber, N. Martini, Y. Xie, I. Dryg, T. Stieglitz, U. G. Hofmann and M. Asplund, *Biomaterials*, 2017, **129**, 176-187.
30. E. Bondan, C. Cardoso and M. F. Martins, *Arq Neuropsiquiatr*, 2017, **75**, 546-552.
31. Y. F. Wang, J. N. Zu, J. Li, C. Chen, C. Y. Xi and J. L. Yan, *Neurosci Lett*, 2014, **560**, 51-56.
32. J. Yuan, W. Liu, H. Zhu, Y. Chen, X. Zhang, L. Li, W. Chu, Z. Wen, H. Feng and J. Lin, *Brain Res*, 2017, **1655**, 90-103.
33. J. Yuan, M. Zou, X. Xiang, H. Zhu, W. Chu, W. Liu, F. Chen and J. Lin, *J Surg Res*, 2015, **195**, 235-245.
34. L. Machova Urdzikova, K. Karova, J. Ruzicka, A. Kloudova, C. Shannon, J. Dubisova, R. Murali, S. Kubinova, E. Sykova, M. Jhanwar-Uniyal and P. Jendelova, *Int J Mol Sci*, 2015, **17**.
35. J. Adiwidjaja, A. J. McLachlan and A. V. Boddy, *Expert Opin Drug Metab Toxicol*, 2017, **13**, 953-972.
36. M. L. Lestari and G. Indrayanto, *Profiles Drug Subst Excip Relat Methodol*, 2014, **39**, 113-204.
37. K. Y. Yang, L. C. Lin, T. Y. Tseng, S. C. Wang and T. H. Tsai, *J Chromatogr B Analyt Technol Biomed Life Sci*, 2007, **853**, 183-189.
38. F. Rasch, F. Schutt, L. M. Saure, S. Kaps, J. Strobel, O. Polonskyi, A. S. Nia, M. R. Lohe, Y. K. Mishra, F. Faupel, L. Kienle, X. Feng and R. Adelung, *ACS Appl Mater Interfaces*, 2019, **11**, 44652-44663.
39. A. Shaygan Nia, S. Rana, D. Dohler, F. Jirsa, A. Meister, L. Guadagno, E. Koslowski, M. Bron and W. H. Binder, *Chemistry (Weinheim an der Bergstrasse, Germany)*, 2015, **21**, 10763-10770.
40. A. Shaygan Nia, S. Rana, D. Dohler, X. Noirfalise, A. Belfiore and W. H. Binder, *Chemical communications (Cambridge, England)*, 2014, **50**, 15374-15377.
41. Y. K. Mishra, S. Kaps, A. Schuchardt, I. Paulowicz, X. Jin, D. Gedamu, S. Freitag, M. Claus, S. Wille, A. Kovalev, S. N. Gorb and R. Adelung, *Particle & Particle Systems Characterization*, 2013, **30**, 775-783.
42. Y. K. Mishra, G. Modi, V. Cretu, V. Postica, O. Lupan, T. Reimer, I. Paulowicz, V. Hrkac, W. Benecke, L. Kienle and R. Adelung, *ACS Appl Mater Interfaces*, 2015, **7**, 14303-14316.
43. S. Henriksen, G. D. Tylden, A. Dumoulin, B. N. Sharma, H. H. Hirsch and C. H. Rinaldo, *J Virol*, 2014, **88**, 7556-7568.
44. B. Schweighardt, J. T. Shieh and W. J. Atwood, *J Neurovirol*, 2001, **7**, 155-162.
45. J. Schommer, M. Schrag, A. Nackenoff, G. Marwarha and O. Ghribi, *MethodsX*, 2017, **4**, 166-171.
46. L. Stoppini, P. A. Buchs and D. Muller, *Journal of neuroscience methods*, 1991, **37**, 173-182.
47. A. Mewes, H. Franke and D. Singer, *PloS one*, 2012, **7**, e45017.
48. V. Adamski, C. Schmitt, F. Ceynowa, R. Adelung, R. Lucius, M. Synowitz, K. Hattermann and J. Held-Feindt, *J Cancer Res Clin Oncol*, 2018, **144**, 1475-1485.
49. X. Dong, *Theranostics*, 2018, **8**, 1481-1493.
50. C. Saraiva, C. Praca, R. Ferreira, T. Santos, L. Ferreira and L. Bernardino, *J Control Release*, 2016, **235**, 34-47.
51. F. M. Tonelli, V. A. Goulart, K. N. Gomes, M. S. Ladeira, A. K. Santos, E. Lorencon, L. O. Ladeira and R. R. Resende, *Nanomedicine (London, England)*, 2015, **10**, 2423-2450.
52. T. Kuila, S. Bose, P. Khanra, A. K. Mishra, N. H. Kim and J. H. Lee, *Biosensors & bioelectronics*, 2011, **26**, 4637-4648.
53. H. G. Oh, D. H. Kim, W. H. Park, K. M. Lim, J. M. Lim and K. S. Song, *Journal of nanoscience and nanotechnology*, 2019, **19**, 7911-7915.
54. M. Musto, R. Rauti, A. F. Rodrigues, E. Bonechi, C. Ballerini, K. Kostarelos and L. Ballerini, *Frontiers in systems neuroscience*, 2019, **13**, 1.
55. N. Ma, B. Zhang, J. Liu, P. Zhang, Z. Li and Y. Luan, *International journal of pharmaceutics*, 2015, **496**, 984-992.

56. S. Su, J. Wang, J. Wei, R. Martinez-Zaguilan, J. Qiu and S. Wang, *New J. Chem.*, 2015, **39**, 5743-5749.
57. K. Shehzad, Y. Xu, C. Gao and X. Duan, *Chemical Society reviews*, 2016, **45**, 5541-5588.
58. M. Taale, F. Schutt, T. Carey, J. Marx, Y. K. Mishra, N. Stock, B. Fiedler, F. Torrisi, R. Adelung and C. Selhuber-Unkel, *ACS Appl Mater Interfaces*, 2019, **11**, 5325-5335.
59. M. Taale, F. Schutt, K. Zheng, Y. K. Mishra, A. R. Boccaccini, R. Adelung and C. Selhuber-Unkel, *ACS Appl Mater Interfaces*, 2018, **10**, 43874-43886.
60. Y. Ganji, Q. Li, E. S. Quabius, M. Bottner, C. Selhuber-Unkel and M. Kasra, *Materials science & engineering. C, Materials for biological applications*, 2016, **59**, 10-18.
61. S. Gurunathan, J. W. Han, V. Eppakayala and J. H. Kim, *Colloids and surfaces. B, Biointerfaces*, 2013, **105**, 58-66.
62. S. F. Kiew, L. V. Kiew, H. B. Lee, T. Imae and L. Y. Chung, *J Control Release*, 2016, **226**, 217-228.
63. C. Liao, Y. Li and S. C. Tjong, *Int J Mol Sci*, 2018, **19**.
64. K. Wang, J. Ruan, H. Song, J. Zhang, Y. Wo, S. Guo and D. Cui, *Nanoscale research letters*, 2011, **6**, 8.
65. X. Zhi, H. Fang, C. Bao, G. Shen, J. Zhang, K. Wang, S. Guo, T. Wan and D. Cui, *Biomaterials*, 2013, **34**, 5254-5261.
66. R. S. Cherian, S. Anju, W. Paul, A. Sabareeswaran and P. V. Mohanan, *Nanotechnology*, 2020, **31**, 075303.
67. M. C. Mendonca, E. S. Soares, M. B. de Jesus, H. J. Ceragioli, S. P. Irazusta, A. G. Batista, M. A. Vinolo, M. R. Marostica Junior and M. A. da Cruz-Hofling, *Journal of nanobiotechnology*, 2016, **14**, 53.
68. W. An, Y. Zhang, X. Zhang, K. Li, Y. Kang, S. Akhtar, X. Sha and L. Gao, *Exp Eye Res*, 2018, **174**, 59-69.
69. R. Rauti, N. Lozano, V. Leon, D. Scaini, M. Musto, I. Rago, F. P. Ulloa Severino, A. Fabbro, L. Casalis, E. Vazquez, K. Kostarelos, M. Prato and L. Ballerini, *ACS nano*, 2016, **10**, 4459-4471.
70. R. M. Rauti, M.; Bosi, S., Prato, M.; Ballerini, L., *Carbon*, 2019, **143**, 430-446.
71. E. Mari, S. Mardente, E. Morgante, M. Tafani, E. Lococo, F. Fico, F. Valentini and A. Zicari, *Int J Mol Sci*, 2016, **17**.
72. M. Chiacchiaretta, M. Bramini, A. Rocchi, A. Armirotti, E. Giordano, E. Vazquez, T. Bandiera, S. Ferroni, F. Cesca and F. Benfenati, *Nano letters*, 2018, **18**, 5827-5838.
73. J. Lin and W. Cai, *Journal of neurotrauma*, 2004, **21**, 1671-1682.
74. E. V. Jones and D. S. Bouvier, *Neural plasticity*, 2014, **2014**, 321209.
75. E. Moeendarbary, I. P. Weber, G. K. Sheridan, D. E. Koser, S. Soleman, B. Haenzi, E. J. Bradbury, J. Fawcett and K. Franze, *Nature communications*, 2017, **8**, 14787.
76. J. Frisen, C. B. Johansson, C. Torok, M. Risling and U. Lendahl, *The Journal of cell biology*, 1995, **131**, 453-464.
77. M. S. Lin, Y. H. Lee, W. T. Chiu and K. S. Hung, *J Surg Res*, 2011, **166**, 280-289.
78. K. A. Potter, M. Jorfi, K. T. Householder, E. J. Foster, C. Weder and J. R. Capadona, *Acta Biomater*, 2014, **10**, 2209-2222.
79. A. H. Taub, R. Hogri, A. Magal, M. Mintz and Y. Shacham-Diamand, *J Biomed Mater Res A*, 2012, **100**, 1854-1858.
80. S. M. Gutowski, J. T. Shoemaker, K. L. Templeman, Y. Wei, R. A. Latour, Jr., R. V. Bellamkonda, M. C. LaPlaca and A. J. Garcia, *Biomaterials*, 2015, **44**, 55-70.
81. S. M. Gutowski, K. L. Templeman, A. B. South, J. C. Gaulding, J. T. Shoemaker, M. C. LaPlaca, R. V. Bellamkonda, L. A. Lyon and A. J. Garcia, *J Biomed Mater Res A*, 2014, **102**, 1486-1499.

Supporting Information

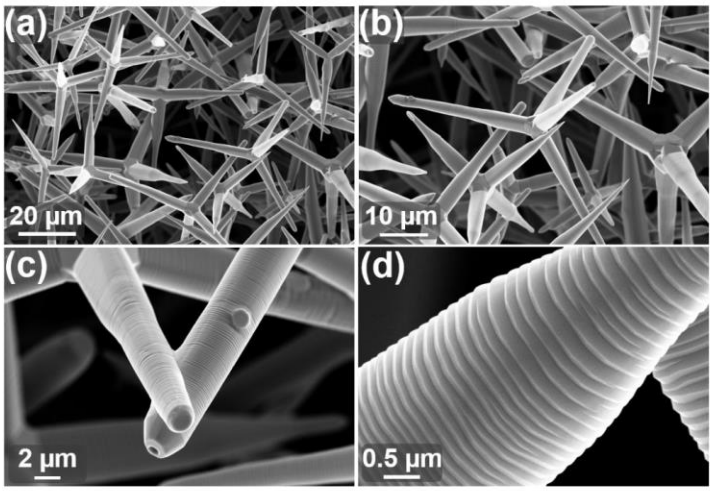

Figure S1, Supporting Information: SEM images of sacrifial t-ZnO template which is composed of interconnected, tetrapod-shaped microparticles (length of one tetrapod leg ~ 25 µm, diameter ~ 2 µm).

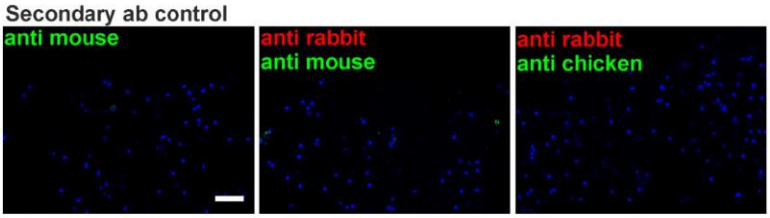

Figure S2, Supporting Information: Secondary antibody controls for immunohistochemical stainings shown in Figure 5. The primary antibodies were omitted during the staining procedure. Representative images from n = 2 independent experiments.

Liposomal encapsulated curcumin effectively attenuates neuroinflammatory and reactive astrogliosis reactions in glia cells and organotypic brain slices

In this manuscript, the antifibrotic and anti-inflammatory compound curcumin, which has been shown to effectively reduce glial scarring in spinal cord and brain injury in recent investigations (Bondan et al. 2017; Yuan et al. 2019) as well as to reduce GO and rGO material-induced neuroinflammation and glial scarring in different *in vitro* models (see our previous study in chapter 2.4), was encapsulated into a liposomal formulation of 80.6 % cholesterol, 15.6 % 1,2-dipalmitoyl-sn-glycero-3-phosphocholine (DPPC) as well as 3.8 % curcumin (cur), to increase long-term stability as well as bioavailability of the drug. In a first experiment, we could show that liposomes were adequately uptaken by both human immortalized astrocytes and microglial cells within 24 hours and did not cause any cytotoxic effects up to concentrations of 1 µM. To further prove the efficacy of our cur nanoformulation we developed two *in vitro* models to analyze neuro-inflammatory and glial scarring responses which may become alleviated under liposomal curcumin (LipoCur) pre-stimulation. In brief, monocultures of human microglia respective astrocyte cell lines were pre-stimulated with LipoCur, free cur as well as empty liposomes in the same corresponding concentrations prior to the addition of lipopolysaccharide (LPS) respective a cytokine cocktail of TNF-α, TGF-β and IL-1β for 24 hours. Whereas LPS is known to induce inflammation in microglial cells (Rosé et al. 1996; Heese et al. 1998), the cytokine cocktail used for the activation of astrocytes corresponds to the cytokines which were released by microglial cells upon inflammation. Upon LPS/cytokine stimulation, LipoCur and free cur in concentrations 100-times smaller (0.01 µM) then in our previous study could effectively reduce the expression of inflammatory and glial scarring markers on mRNA level within 24 hours. However, since the brain microenvironment strongly influences inflammatory and reactive gliosis reactions *in vivo*, we performed respective efficacy studies of LipoCur in a long-term stimulation model of murine organotypic cortex slices *in vitro*, which preserves the natural cell complexity in the brain. Brain slices were stimulated with LPS after pre-incubation with LipoCur, free cur or empty liposomes for eight days and cytotoxicity assays were performed on days two and eight, as well as gene expression levels of inflammatory related genes (representing microglial cell responses) were evaluated after eight days *in vitro*. Moreover, the effects of LPS and its pre-/co-stimulations with cur and liposomes have been evaluated on protein level by immunohistochemical (IHC) fluorescence staining of neurons, oligodendrocytes, astrocytes or extracellular matrix molecules for instance. We could show that LPS-induced cytotoxicity was significantly reduced by cur and LipoCur, whereas solely incubation with LipoCur, free drug or empty liposomes did not affect the brain slices' survival. Moreover, pro-inflammatory cytokines such as IL-1β or TNF-α, as well as glial scarring related molecules such as GFAP or tenascin-C were overexpressed upon LPS stimulation and could be alleviated significantly by LipoCur pre-incubation. Overall, the liposomal formulation of cur did reduce cytotoxic, inflammation- or glial scarring reactions in human cell lines and murine organotypic brain slices *in vitro*, and in most cases performed with higher efficacy and significance then the corresponding concentration of free drug.

Own contribution, presented in this article:

- Design of the study
- Performance of experiments
- Data analysis and visualization
- Discussion and interpretation of results
- Writing of original draft

ORIGINAL RESEARCH

Liposomal encapsulated curcumin effectively attenuates neuroinflammatory and reactive astrogliosis reactions in glia cells and organotypic brain slices

Christina Schmitt[1]

Anna Lechanteur[2]

François Cossais[1]

Coralie Bellefroid[2]

Philipp Arnold[1]

Ralph Lucius[1]

Janka Held-Feindt[3]

Geraldine Piel[2]

Kirsten Hattermann[1]

[1] Institute of Anatomy, University Kiel, Olshausenstr. 40, D-24098 Kiel, Germany; [2] Laboratory of Pharmaceutical Technology and Biopharmacy (LTPB), CIRM, University of Liège, Belgium; [3] Department of Neurosurgery, University Medical Center Schleswig-Holstein UKSH, Campus Kiel, Arnold-Heller-Str.3, House D, D-24105 Kiel, Germany

Key words: glial scar, neuroinflammation, nanoparticles, brain implants

Corresponding author

Kirsten Hattermann, PhD

Institute of Anatomy, University Kiel

Olshausenstr. 40

D-24098 Kiel

Phone: +49 431 880 2460 , Fax: +49 431 880 1557, Email: k.hattermann@anat.uni-kiel.de

Abstract

The polyphenolic spice and food coloring ingredient curcumin has beneficial effects in a broad variety of inflammatory diseases. Amongst them, curcumin has been shown to attenuate microglia reaction and prevent from glial scar formation in spinal cord and brain injuries. However, like a variety of other drugs, curcumin is quite instable and hardly bioavailable upon oral administration. Here, we describe a protocol for the efficient encapsulation of curcumin as a model for anti-inflammatory drugs yielding long-term stable, nontoxic liposomes with favorable physicochemical properties. In experimental models for neuroinflammation and reactive astrogliosis, we could show that liposomal curcumin can efficiently reduce reactivity of human microglia and astrocytes and preserve tissue integrity of murine organotypic cortex slices. In perspective, we want to administer this curcumin formulation in brain implant coatings to prevent from neuroinflammation and glial scar formation as foreign body responses of the brain towards implanted materials.

Introduction

Curcumin is a natural polyphenolic compound that can be obtained from the rhizome of turmeric, *Curcuma longa* [1], and is widely used as a spice and food coloring ingredient, but also in Ayurvedic medicine. Apart from its use as a food additive, beneficial effects of curcumin, its derivatives and analogues have been investigated *in vitro* and *in vivo* up to clinical trials in a broad variety of diseases, for example in cancer (e.g. breast, colorectal, pancreatic cancer) and inflammatory diseases [e.g. inflammatory bowel disease, osteoarthritis and rheumatoid arthritis [2-7]. In addition, the effects of curcumin and its derivatives have been studied in the context of neurodegenerative diseases, e.g. Alzheimer's and Parkinson's disease [8-11], pathological pain [12,13], epilepsy [14] and cerebral ischemia [15,16]. These and other studies revealed, that curcumin may influence on several intracellular signaling cascades, including the mitogen-activated protein kinase (MAPK), phosphoinositide 3-kinase (PI3K), nuclear factor 'kappa-light-chain-enhancer' of activated B-cells (NFκB), janus kinase/signal transducers and activators of transcription 3 (JAK/STAT3) and nuclear factor E2-related factor 2 (Nrf2) pathways [17-21], yielding neuroprotective and anti-inflammatory microglia-attenuating effects [20,22-25]. In recent studies, curcumin has also been described to prevent from glial scar formation in spinal cord and brain injuries [26-29]. In experimental studies on spinal cord injuries, curcumin could reduce *in vitro* and *in vivo* the

production of pro-inflammatory mediators (e.g. nitric oxide, NO; tumor necrosis factor α, TNFα; interleukins IL1β and IL2; chemokines CCL3, CCL5 and CXCL10), the reactive expression of gliosis/fibrosis markers (e.g. glial fibrillary acidic protein, GFAP, or α smooth muscle actin, α-SMA) and the deposition of chondroitin sulfate proteoglycans, presumably by modulating STAT3-, NFκB-, TGFβ1/2- and SOX9-signaling pathways [27-30]. Studies on locomotor and sensory recovery after spinal cord injury also showed beneficial effects mediated by curcumin alone [30] or in combined therapeutic approaches with mesenchymal stem cells [31]. However, curcumin is hydrophobic, quite instable in aqueous solutions, sensitive to light and hardly bioavailable in experimental studies [32-34]. These facts, and the failure of some recent clinical trials evoke a controversial debate on the usefulness of further experimental and clinical studies on the one hand side [35], but also paved the way for the development of better bioavailable and more stable curcumin formulations, for example by the use of micro-emulsions, nanofibers or nanoparticles [5,8,36-38]. In particular, drug-loaded nanoparticles offer several advantages over the bulk materials such as a high surface to volume ratio, a tailorable particle size or the ability to change chemical properties by surface functionalization. Moreover, they are known since years to be good carriers for the encapsulation, transportation and release of drugs with tailorable release kinetics of the pharmaceutical compound to the target side as well as enhanced solubility and stability of most drugs, resulting in improved pharmacokinetic profiles [39-41]. Especially liposomal formulations have successfully climbed the step from experimental concept to clinical application as an FDA approved nano-carrier for a variety of drugs [42], and liposomes have also been shown to be a promising formulation strategy for curcumin, due to their biocompatibility and biodegradable properties [43]. Liposomes are artificial membrane-like bilayer structures, consisting of cholesterol and other non-toxic phospholipids [44], that are formed by exposing the lipid headgroups to a highly hydrophilic aqueous surrounding [45]. The amphiphilic character of the liposomal structure therefore not only allows the encapsulation of hydrophilic but also hydrophobic drugs, such as curcumin [46], or even a combination of different drugs. Several reports show beneficial effects of liposomal curcumin formulations, for example improved effects on growth-inhibition and pro-apoptotic effects on cancer cells, higher anti-inflammative and -oxidative effects in vaginal inflammation models, increased bioavailability upon oral administration and improved skin-penetration in melanoma treatment [47-51]. However, only little has been shown yet for liposomal curcumin applications in the brain. In this context, nano-formulated curcumin has been shown to attenuate microglia activation and to protect the blood-brain barrier integrity [52,53].

The idea behind this study was to develop a liposomal nano-carrier formulation that may be suitable for local brain administration, for example in coatings of brain recording or stimulation electrodes or brain implants for drug delivery in order to alleviate foreign body reactions. The glial scarring process, evoked by foreign materials in the brain very frequently, leads to the formation of a fibrous sheath and immune cell infiltration, therefore impairing the function (or drug delivery) of brain implants [54,55]. The (co-)administration of an anti-inflammatory drug such as curcumin in a stable formulation could help to reduce the glial foreign body response. Thus, we developed a protocol for the encapsulation of curcumin in liposomal nano-carriers (we termed them LipoCur) and evaluated their physiochemical properties, long-term stability and *in vitro* drug release kinetic. As microglia promoted neuroinflammation and astrocyte mediated reactive gliosis mainly contribute to the brain foreign body response (compare Figure 1A) we focused in our first experimental approaches on these cell types. Using human microglia and astrocytes, we compared the effects of liposomal and free curcumin on cell viability. To experimentally mimic the foreign body response *in vitro,* we challenged human microglia with lipopolysaccharide (LPS) to induce neuroinflammation (Figure 1B) and stimulated human astrocytes with a cytokine cocktail to induce reactive gliosis (Figure 1C). In these experimental settings, we analyzed the effects of both liposomal and free curcumin on the expression of pro-inflammatory markers in microglial cells, and on the expression of glial scarring associated genes in cytokine-activated astrocytes. Additionally, we tested the effects of liposomal and free curcumin on LPS challenged acute brain slices obtained from mouse cortex to verify our observations in the complex tissue composition of the murine brain (Figure 1D).

Material and Methods

Preparation of liposomal nano-carriers

Briefly, lipids and curcumin were dissolved in 3mL absolute ethanol at a total concentration of 1.34mg/mL dipalmitoylphosphatidylcholine (DPPC, 16:0 PC, Avanti Polar Lipids, Alabaster, AL), 0.26mg/mL cholesterol (Sigma-Aldrich / Merck, Darmstadt, Germany) and 0.063mg/mL curcumin (Sigma-Aldrich) respectively and mixed by slightly shaking of a 100mL round bottom flask. The organic solvent was then removed using a rotary evaporator (Buchi R200, Flawil, Switzerland) for 1h at 37°C. The lipid film was rehydrated with 2mL ultrapure water, vortexed and directly extruded through a polycarbonate membrane (200 nm and 100 nm, Whatman®, Fisher Scientific, Merelbeke, Belgium) at 51°C. Thereafter, liposomes were purified by centrifugation to separate free curcumin from the nano-formulation. In brief, a first centrifugation step for 15min at 9,000 xg at room temperature (Centrifuge 5418, Eppendorf AG, Hamburg, Germany) separated free curcumin agglomerates (pellet) from the liposomal formulation (supernatant), whereas two ultracentrifugation steps for 1h at 100,000 xg at 4°C (OptimaTM L-90K, Beckman-Coulter, Brea, CA) separated the liposomal formulation (pellet) from the remaining free drug (supernatant). The final pellet was resuspended in 1.2mL ultrapure water. The pellet from the first centrifugation as well as the supernatants from the ultracentrifugation steps were kept for indirect quantification of the encapsulated curcumin concentration by high-performance liquid chromatography (HPLC, see below).

For freeze-drying of the liposomes (see paragraph *Freeze-drying of liposomal formulations*), the ultrapure water for the rehydration of the lipid film as well as the resuspension of the liposomal pellet after centrifugation were supplemented by 10% trehalose in the final protocol. To evaluate the most suitable condition for freeze-drying, at first different concentrations of trehalose were tested against each other and evaluated by their physico-chemical properties.

Freeze-drying of liposomal formulations

Freshly produced liposomes were freeze-dried using a vacuum freeze-dryer (Drywinner 8, Heto-Holten A/S, Allerod, Denmark). In brief, the samples were frozen from room temperature to -45° (cycle 1) under 1bar over a period of 3h and 30min. After that, primary drying was performed at -45°C for 15min (under 0.8bar pressure), at -15°C for 3h (under 0.1bar pressure) and then at -10°C for 12h (under 0.1bar

pressure). Finally, the secondary drying was carried out at 10°C for 5h (under 0.1bar pressure). The entire freeze-drying cycle took 23h and 45min. Freeze-dried samples were kept at 4°C under vacuum until further usage.

The mass yield of curcumin loaded liposomes was determined by gravimetric analysis of the dried liposomes dispersions. Briefly, liposome formulation without the addition of trehalose were freeze-dried as described before. The weight of the dried liposomes was measured and the mass yield (%) was calculated using equation 1.

[1] $$mass\ yield\ (\%) = \frac{weight\ of\ 200\mu L\ liposomes\ x\ 100}{theoretical\ weight\ of\ 200\mu L\ liposomes}$$

Physico-chemical properties of liposomes

Dynamic light scattering (DLS) and laser-Doppler electrophoresis

All samples of liposomes (empty or curcumin loaded) were analyzed three times for the size (nm), polydispersity index and zeta potential (mV) by Dynamic Light Scattering (DLS) (BIC 90 plus, Brookhaven Instruments Corp., Holtsville, NY) followed by Laser Doppler Anemometry, based on the electrophoretic mobility (Zetasizer Nano ZS, Malvern, UK), right after production. The measurements were performed following a 1:100 dilution of all the samples with ultrapure water, at 25°C. For long-term stability tests, aliquots of freeze-dried samples, stored at 4°C under vacuum, were rehydrated and analyzed over the time for up to 9 months in storage with three technical replicates, n=3.

High-performance liquid chromatography (HPLC)

The percentage of encapsulation efficiency (%EE) was determined indirectly (see equation 2) of the curcumin content lost during the centrifugation respective ultracentrifugation steps by a previously validated HPLC method (Agilent LC1100 Series, Agilent Technologies Santa Clara, CA, with OpenLab CDS LC ChemStation version C.01.05 as the software). Moreover, the drug loading capacity was determined by direct quantification of encapsulated curcumin in the final liposomal formulations, as described in equation 3. The elution was carried out in an isocratic mode with sample volumes of 10µL and a flow rate of 0.8 mL/min at ambient temperature and a wavelength of 427 nm. The separation was performed on a Xterra RP8 column (5µm, 4.6x250 mm, endcapped Waters®, Zellik, Belgium) and a

mobile phase consisting of 10% ultrapure water and 90% phase E1 (41% acetonitrile, 23% methanol and 36% acidified ultrapure water). Curcumin concentrations were calculated on the basis of linear calibration functions and with regard to the dilution factor. Standards as well as the curcumin pellet (centrifugation) were prepared in absolute ethanol and the supernatants (ultracentrifugation) and the liposomal formulation were diluted 1:3 with ethanol respective 1:10 with ethanol supplemented with 0.5% Triton-X. All samples were run as duplicates.

[2] $$\%EE = \frac{(total\ amount\ of\ curcumin) - (free\ curcumin)}{\text{total amount of curcumin}} * 100\%$$

[3] $$drug\ loading\ capacity\ \left(\frac{\mu g\ curcumin}{mg\ liposomes}\right) = \frac{amount\ of\ curcumin\ in\ 200\mu L\ liposomes * [\mu g]}{weight\ of\ 200\mu L\ liposomes\ [mg]}$$

Transmission Electron Microscopy

The morphology of the freeze-dried liposomes, empty as well as curcumin loaded, was analyzed by Transmission Electron Microscopy (TEM) after 9 months of storage as described before [56]. In brief, 3µL of diluted sample were added on a freshly glow discharged continuous carbon coated copper grid (Electron Microscopy Sciences, Hatfield, PA) and liposomes were allowed to adhere to the surface for 10 sec. The excess sample was blotted off from the side with filter paper, 5µL of half saturated uranyl acetate solution were added twice and removed two sec after each incubation. After drying at room temperature, grids were transferred to a JEOL JEM 1400Plus TEM operating at 100kV (Tokyo, Japan). Images were digitally recorded on a 4kx4k digital camera (F416, TVIPS, Germany).

In vitro curcumin release from liposomes

The *in vitro* drug release profiles of liposomes were studied with the dialysis method. In brief, freeze-dried curcumin loading liposomes were rehydrated in a final volume of 400µL ultrapure water and vigorously vortexed. To determine the total amount of curcumin available at time t=0 (X1), 10µL sample volume was kept for HPLC quantification. In parallel, 50µL of the sample were taken to quantify free curcumin outside the liposomes. For this, the 50µL were diluted in 950µL ultrapure water and centrifuged 15min at 9,000xg at room temperature. The remaining pellet, considered to be free curcumin, was diluted in 1mL ethanol and the free curcumin content (X2) was quantified via HPLC. Therefore the difference of concentration between X1 and X2 represents the actual amount of curcumin present inside the liposomes at t=0.

Then, the remaining 340µL of rehydrated samples were taken in dialysis bags (Biotech CE Tubing, MWCO 20kDA, Fisher Scientific) and dialyzed against 5mL ultrapure water containing 20% ethanol and 0.5% Tween-80 (1:50 acceptor/donator volume ratio to obtain sink condition) at 37°C, stirred at 25rpm for 7 days. At certain time points (0h, 1h, 3h, 6h, 8h, 10h, 24, 48h, 72h, 96h and 120h, respectively) 250µL sample volume was taken from the receptor compartment and replaced by the same volume of fresh receptor compartment media. The concentration of curcumin was then determined via HPLC and the accumulated drug release over the time was calculated taking X2 into account (as it will be directly released from the dialysis bag).

Cell lines and cell culture

The human fetal astrocyte cell line SVGA was kindly provided by the group of Christine Hanssen Rinaldo, University Hospital of North Norway [57] with the permission of W.J. Altwood [58]. The human microglia cell line HMC3 was purchased from the American Type Culture Collection (ATCC, Manassas, Virginia, USA). Cells were cultured in Dulbecco's modified Eagle's medium (DMEM; Life Technologies, Carlsbad, CA, USA) supplemented with 10% fetal bovine serum (FBS; PAN-Biotech GmbH, Aidenbach, Germany), 1% Penicillin-Streptomycin (10,000 U/ml; Thermo Fisher Scientific, Waltham, MA, USA) and 2mM additional L-Glutamine (Thermo Fisher Scientific). Cells were routinely checked for *Mycoplasma* contamination by nuclei staining and mycoplasma-specific PCR.

Cell stimulations

Cells were seeded in 6 well plates (Sarstedt, Nürnbrecht, Germany) one day prior to stimulation. For all stimulations, 0.01µM curcumin or the corresponding amount of liposomal encapsulated curcumin (or empty liposomes) were added to the cells 30min prior to further stimulation and maintained for the whole stimulation period. This procedure is termed "pre-incubation" in the following. Inflammatory reaction of microglia was induced by stimulation with 100ng/mL lipopolysaccharide (LPS) of *Salmonella typhimurium* (Sigma-Aldrich) for 24h. Astrocytes were stimulated for 24h with each 10ng/mL recombinant human tumor necrosis factor α (TNFα), transforming growth factor β1 (TGFβ1) and interleukin 1β (IL1β) (all Immunotools, Friesoythe, Germany) to induce gliosis reaction. Supernatants were collected for viability assays, cells were counted to determine effects on proliferation, and cells were lysed to isolate RNA (for quantitative reverse transcription PCR, qPCR).

Brain slices were pre-incubated with 0.01µM curcumin or the corresponding amount of liposomal encapsulated curcumin (or empty liposomes) 30min prior to further stimulation with 100 ng/mL LPS to induce inflammatory conditions for 8 days, while media and stimuli were changed on days 1, 2 and 5, and supernatants collected for subsequent cytotoxicity analysis on days 2 and 8 *in vitro* (div). After 8 days of stimulation, slices were either lysed for RNA isolation or fixed and embedded for immunohistochemistry.

Liposome cell uptake assay

Liposomes were stained with 0.25% nile red (Sigma-Aldrich) for 24h at room temperature. Free nile red was removed from liposomes by centrifugation at 3,000xg for 30min in filter membranes (Amicon, Sigma-Aldrich, molecular cutoff: 10,000 MWCO). 10^6 HMC3 or SVGA cells were seeded on glass cover slips and grown for 24h. Stained liposomes (or the nile red staining solution for control) were applied to the cells for 24h in concentrations corresponding to 0.01µM free curcumin. Cells were fixed with 4% paraformaldehyde (PFA, in phosphate buffered saline, PBS), rinsed with PBS (3x), incubated with Alexa Fluor 647 labelled wheat germ agglutinin (Thermo Fisher scientific, 1:200) for 1h, rinsed with PBS (3x). Then, nuclei were counterstained with 4′,6-diamidino-2-phenylindole (DAPI, Sigma-Aldrich, 30min) and cover slips were embedded after rinsing with PBS and distilled water using Shandon Immumount (Thermo Fisher scientific). Cover slips were inspected and documented using an Axiovert 200M microscope with Apotome (Zeiss, Oberkochem, Germany).

Cell viability

To measure viability, 7,000 HMC3 or SVGA cells/well were seeded on 96 well plates and grown for 24h. Then media were changed to DMEM containing 10% FBS plus respective stimuli or alone as positive control. After 72h incubation, proliferation was determined by the measurement of tetrazolium salt WST-1 cleavage (Roche, Mannheim, Germany) regarding ISO 10993-5 and normalized to unstimulated control (2 individual wells for each stimulus, as technical replicates, biological replicates as indicated in the respective figure legends).

Organotypic brain slices

For the generation of organotypic brain slices, female Sox10flox hGFAP:creeRT2 mice (16-24 weeks old, local Ethics Committee, agreement: V 242-70056/2015(91-7/15); the genetic modification was not relevant for the experimental procedure), were sacrificed by cervical dislocation and brains were carefully removed from the scull and rinsed in artificial cerebrospinal fluid (aCSF, 2mM CaCl2, 10mM D-Glucose, 1.3mM $MgCl_2$, 5mM KCl, 124mM NaCl, 26mM NaHCO3). Tissue slices of 400µm were obtained using a digital tissue slicer (Stölting, Wood Dale, IL). In brief, brains were dissected to obtain the cerebral cortex regions from both hemispheres, placed on wet filter papers, which were fixed below the blade of the slicer using adhesive film. To ensure minimal surface tension, the blade was wetted with aCSF before every cut [59]. Slices were prepared, separated and controlled under a binocular microscope and placed on membrane inserts (PICM03050, Millicell®-CM 0.4µm, Merck Millipore, Burlington, MA, USA) in 6-well plates. Wells contained 1.2mL of MEM/HEPES (Thermo Fisher Scientific), supplemented with 24% horse serum (Sigma Aldrich), 1% glutamine, 1% penicillin and streptomycin, 6mg/mL glucose and 168µg/mL sodium hydrogen phosphate , allowing brain slices to be provided by nutrients from the bottom and CO_2 from the top [protocol based and adjusted on [59-61]].

Cytotoxicity assay

To analyze the protective effects of liposomal and free curcumin on murine brain slices, slices were challenged with 100µg/mL LPS, in combination or not with 0.01µM free or liposomal curcumin respective empty liposomes. As positive control, brain slices were treated with 83.2ng/mL Digitonin solution instead of stimulation. Supernatants were collected and cytotoxicity was analyzed using the the CytoTox-Fluor™ Cytotoxicity Assay (Promega, Madison, WI) as described previously [62] on day 2 and 8 *in vitro*.

Immunohistochemistry

After stimulation (8 days), brain slices were briefly washed in PBS, fixed in 4% paraformaldehyde (in Tris-buffered saline, TBS) over night, equilibrated in 30% sucrose (in TBS, until slices sink down), embedded and frozen in Shandon Cryomatrix (Thermo Fisher Scientific) and cut in 10µm cryosections. Sections were washed with 0.1% Tween in TBS (TBS-T), blocked for autofluorescence with 1% sudan black (Merck, in 70% ethanol) and for unspecific binding with 0.5% glycine/0.5% bovine serum albumin (in TBS-T), incubated with primary antibodies over night at 4°C, washed 3x, incubated with Alexa Fluor 488 or 555 labelled secondary antibodies against respective host species (donkey IgG, 1:800, Thermo

Fisher scientific) at 37°C for 1h, washed (2x, TBS-T, 1x TBS), nuclei were counterstained with DAPI (Sigma-Aldrich) and slides embedded after washing in TBS-T and water with Shandon Immumount (Thermo Fisher Scientific). For secondary antibody controls, primary antibodies were omitted (compare Supplement to Figure 6). Commercially available primary antibodies were anti-GFAP (glial fibrillary acidic protein; rabbit, 1:100; DAKO, Glostrup, Denmark, Z0334), anti-fibronectin (rabbit, 1:400; Novus biologicals, Wiesbaden, Germany; NBP1-91258), anti-MBP (myelin basic protein; mouse, 1:400; Novus, NBP2-22121), anti-nestin (mouse, 4D11, 1:200; Novus, NBP1-92717) and anti-vimentin (chicken, 1:200; Novus, NB300-223),. The monoclonal antibody against neurofilament-M (clone 2H3) developed by T.M Jessell and J. Dodd, HHMI/Columbia University was obtained from the Developmental Studies Hybridoma Bank, created by the NICHD of the NIH and maintained at The University of Iowa, Department of Biology, Iowa City, IA 52242. Sections were inspected and documented using an Axiovert 200M Fluorescence Microscope.

Quantitative Reverse Transcription-PCR

HMC3 or SVGA cells were harvested and tissues homogenized using the QIAzol lysis reagent (Qiagen, Hilden, Germany) and total RNA was isolated following the manufacturer's protocol. Genomic DNA was digested by RNase-free Dnase (1U/µL, Promega, Madison, W, USA), and cDNA synthesis was performed using RevertAid™ H Minus M-MuLV Reverse Transcriptase (200U/µL, Thermo Fisher Scientific, Waltham, MA, USA). TaqMan primer probes and TaqMan™ Gene expression Master Mix (Thermo Fisher Scientific) were used to analyze samples with the ABI PRISM 7500 Sequence detection system. Analyzed genes were *gapdh* (human: Hs99999905_m1, mouse: Mm99999915_g1), *il6* (human: Hs00985639_m1, mouse: Mm00446190_m1), *il1β* (human: Hs01555410_m1, mouse: Mm00434228_m1), *tnfα* (human: Hs00174128_m1, mouse: Mm00443258_m1), *tgfβ* (human: Hs00171257_m1, mouse: Mm01178820_m1), *tenascin* (human: Hs01115665_m1), *nestin* (human: Hs0070120_s1), and *fibronectin* (human: Hs00277509_m1). Cycle of Threshold values (CT) were measured, and ΔCT values = CT [gene of interest] – CT[GAPDH] were calculated. Due to logarithmic reaction mode, a ΔC_T value of 3.33 corresponds to one magnitude lower gene expression compared to GAPDH. For stimuli-induced mRNA regulation ΔΔCT values were calculated: $\Delta\Delta CT = 2^{-(\Delta CT[stimulus] - \Delta CT[control])}$.

Statistical analysis

All values are shown as mean values ± standard deviation (SD). Statistical analysis was performed using GraphPad Prism® 5, (GraphPad Software, Inc.Version, CA). Asterisks or rhombs indicate statistical significance, whereas p values < 0.05 were considered as significant. Different statistical analyses were applied in function of experiments as reported in each figure legend.

Results

Preparation and characterization of liposomes

For the development of an effective curcumin delivery system for the alleviation of brain implant-induced foreign body reactions in the brain, a liposomal formulation using 80.6% (w/v) DPPC, 15.6% (w/v) cholesterol and 3.8% (w/v) curcumin was employed. Empty and curcumin loaded liposomes were produced by hydration of the lipid-thin film technique, followed by multiple times extrusion. Particle size analysis of liposomes encapsulating curcumin showed a size, PdI and Zeta Potential (ZP) of 180 ± 34nm, 0.170 ± 0.040 respective -26.1 ± 14.0mV (Table 1) on the day of preparation.

For long-term storage of liposomal formulations, trehalose was added to the final formulation as a cryo-protectant. To evaluate the most suitable trehalose concentration that does not alter the size, ZP or PdI after freeze-drying, different trehalose concentrations have been added to the liposomal formulations and physico-chemical properties have been evaluated before (Figure 2A) and after freeze-drying (Figure 2B). With the final concentration of 10% trehalose, sizes of 153 ± 48nm and 164 ± 22nm, PdI of 0.11 ± 0.05 and 0.25 ± 0.10, as well as ZP of -22.6 ± 6.2mV and -29.3 ± 3.8mV have been measured of curcumin loaded liposomes before respective after the freeze-drying process. Empty liposomes show a slightly bigger size and PdI as well as less negative ZP than curcumin loaded liposomes with 219 ± 82nm, 0.30 ± 0.10 and -17.2 ± 3.8mV respectively (Table 1).

With this final formulation, the curcumin encapsulation efficiency (EE) and drug loading capacity (DL) were evaluated by HPLC quantification on the day of preparation. As seen in table 1, EE values and DL of 68 ± 6 % respective 21.4 ± 1.8 % were obtained for liposomes without trehalose, and an EE 46 ± 9

% for liposomes containing trehalose. The total mass yield that was determined by HPLC and lyophilization was 78 ± 18 % (Table 1).

Regarding the long-term stability of fabricated liposomes, freeze-dried samples were stored in a vacuum at 4°C for up to 180 days and analyzed for their size, PdI and ZP and compared to the values directly after freeze-drying process (Figure 2C - E). Sizes slightly increased over the time from 180nm to 240nm (directly vs 180 days after freeze-drying), whereas only after 120 days significant changes to the fresh freeze-dried formulation could be noted. However, the ZP (Figure 2D) and the size distribution (Figure 2E) of the liposomal formulations did not vary over the time. In summary, 180 days old liposomes did not significant differ from freshly produced formulations in their size, PdI and ZP. Thereafter using the dialysis method, the *in vitro* drug release of curcumin was performed and evaluated by HPLC. The individual drug release profile of n=3 technical replicates is depicted in Figure 2F. After 10 hours, liposomes released 26.9% ± 4.5 of their curcumin cargo and a maximum with 34.8% ± 5.9 was released after 24 hours, which was followed by a sustained release drug profile over the time.

Concomitant with the above described physico-chemical characterization, we analyzed the morphology of the freeze-dried liposomes (LipoCur as well as empty LP) by Transmission Electron Microscopy (TEM) after 180 days of storage, and similar sizes could be evaluated visually (Figure 3A and B) as previously measured by DLS (Figure 2C). All vesicle types tended do have a spherical shape, with similar size distributions. Some of them seemed to be dented or hollow, putatively due to the preparation process with uranyl acetate for TEM.

Taken together, we could successfully establish a protocol for the encapsulation of curcumin into liposomes, yielding favorable physico-chemical properties, efficient encapsulation efficiencies and long-term stability of the liposomal formulation.

Cellular uptake and effects of liposomal curcumin on viability of human astrocytes and microglia cells

To study the uptake of liposomes by cells, empty liposomes (LP) and curcumin loaded liposomes (LipoCur) were fluorescently labeled with nile red and incubated with human microglia cells (HMC3) and

astrocytes (SVGA) for 24h. The final liposome concentration of 0.18µg/mL corresponded to a final concentration of 0.01µM curcumin. We observed that both cell types efficiently incorporated labeled liposomes (Figure 3C). Using infrared labelled wheat germ agglutinin which binds to and marks cell membranes, we could clearly demonstrate that red labelled liposomes were located within the cell boundaries in the cytoplasm.

Next, we investigated to what extend empty and curcumin loaded liposomes influenced on the viability of cultivated brain cells. Therefore, we stimulated microglia and astrocytes with empty LP, LipoCur and for comparison free curcumin (free Cur) for 3 days with concentrations ranging from 0.0001µM to 20µM curcumin (and corresponding amounts of loaded or empty liposomes). As shown in Figure 3D, concentrations up to 1µM did not significantly impair cell viability in both cell types. Empty and curcumin loaded liposomes showed widely comparable effects in this well tolerated concentration range, but liposomal curcumin was slightly less toxic in higher concentrations. Free curcumin was even well tolerated at higher concentrations (5 – 10µM), but was also toxic at 20µM for both cell lines.

Taken together, empty and curcumin loaded liposomes were efficiently taken up by microglia and astrocytes and did not impair cell viability at concentrations up to 1µM.

Effects of liposomal and free curcumin on neuroinflammation and reactive astrogliosis in vitro

Our concept of liposomal encapsulation of curcumin aimed to provide a drug formulation for local brain administration to attenuate foreign body reactions towards brain implants. Therefore, we tested in a next step if liposomal curcumin can alleviate neuroinflammatory and reactive astrogliosis processes *in vitro*. As an experimental model for neuroinflammation (Figure 1B) we stimulated microglia cells with lipopolysaccharide from *S. typhimurium* (100ng/mL), with or without pre-incubation with LipoCur and, for comparison, free curcumin or empty LP for 24h. LPS stimulation yielded a typical change to amoeboid morphology (Figure 4A) and induced expression of the cytokines IL6, IL1β, TGFβ and TNFα (Figure 4B, black bars). These effects could be clearly reduced by pre-incubation with free curcumin or LipoCur. However, due to high variations in the extent of microglia activation (compare error bar of LPS stimulation and LPS + empty LP), effects were not always significant, but stimulations with LPS and LipoCur frequently yielded less induction of inflammatory cytokines than LPS stimulations alone or LPS

together with empty LP. In comparison, mRNA expression of these cytokines was much more robust in controls that were not challenged with LPS, and neither free nor liposomal curcumin nor empty liposomes had any effect on expression levels.

As an experimental model for astrocyte reactivity, we used a cytokine cocktail (IL1β, TGFβ and TNFα, 10ng/mL each, 24h) to stimulate human astrocytes (Figure 1C). This cocktail affected astrocyte morphology, yielding for example nuclear deformation and alteration in cell size and shape. Again, this effect was almost completely abolished by pre-incubation with LipoCur (Figure 4C). As a choice of gliosis associated genes we analyzed mRNA expression of tenascin C, fibronectin and nestin, and observed that cytokine-mediated induction of these genes could be significantly reduced by pre-incubation with LipoCur or free curcumin, reaching or reaching almost levels of controls without cytokine cocktail (Figure 4D).

Taken together, our liposomal curcumin formulation was as effective as or even more potent than free curcumin in reducing microglia and astrocyte reactivity.

Effects of liposomal and free curcumin on viability and LPS response of organotypic murine brain slices

As cellular reactions are strongly influenced by their local tissue environment and cell neighbors, we decided to investigate in a next step the beneficial effects of LipoCur in comparison to free curcumin and empty LP in LPS-challenged organotypic brain slices (Figure 1D). Using 400 µm slices from one murine brain cortex region, the reactions of a whole brain tissue with all its cells types towards various stimuli could be analyzed.

First, we could show that LipoCur and free Cur could restore LPS-reduced viability of organotypic brain slices to control levels at early (2 div) and late (8 div) time points of incubations (Figure 5A). In a next step, we analyzed expression of inflammatory markers IL1β, IL6, TNFα and TGFβ on mRNA levels at 8 div. IL1β, IL6 and TNFα were induced upon LPS stimulation, and these effects were in trend or even significantly mildened by pre-incubation with LipoCur, and to lesser extend free Cur (Figure 5B). When interpreting these results, one has to keep in mind, that the microglial cells represent only one small portion of cells within the slices, so that smaller effects and higher variations should be expected. The

cytokine TGFβ was not induced by LPS stimulation at 8 div, so that pre-incubation with LipoCur or free Cur did not yield any effects.

Finally, we used fluorescence immunohistochemistry to visualize LPS-mediated cellular changes and restoration by pre-incubation with LipoCur or free curcumin (Figure 6). Stainings of neurofilament (NF) revealed that the neuronal network was clearly affected by LPS stimulation at 8 div, and these effects could be almost completely diminished by pre-incubation with LipoCur or free curcumin, but not by empty LP. Furthermore, markers for reactive astrogliosis (GFAP, nestin, fibronectin, vimentin) showed strong immunoreactivity in LPS-stimulated slices, and again these effects were alleviated by LipoCur and free curcumin, but not empty LP. However, stainings for oligodendrocytes (MBP, myelin basic protein), showed hardly any differences between LPS stimulations and controls, and within there were no effects observed upon stimulation with LipoCur or free curcumin.

Taken together, we could establish a protocol for the liposomal encapsulation of curcumin, yielding liposomes with favorable physiochemical properties, efficient drug encapsulation, *in vitro* drug release and long term stability. These liposomes (we termed them LipoCur) were taken up into the cytoplasmic cell compartment, and were well tolerated by human microglia and astrocytes as well as murine organotypic brain slices. In experimental models for neuroinflammation and reactive astrogliosis, LipoCur could efficiently reduce microglia and astrocyte reactivity, in some settings even more effective than free curcumin.

Discussion

The natural compound curcumin is a traditional coloring and flavoring food ingredient, and has attracted broad scientific interest due to its possible anti-oxidative and anti-inflammatory properties. In search of a drug, that may alleviate foreign body reactions provoked by brain implant materials, we gave a chance to curcumin as several previous reports had shown that curcumin treatment reduces the extent of experimental brain and spinal cord injuries. In animal models of spinal cord injuries, curcumin provided neuroprotection and attenuated microglial and astrocyte reactivity as shown by reduced GFAP-expression levels [29,63] and Nestin+/GFAP+ glial scar regions [27] as well as reduced expression of pro-inflammatory cytokines like IL1β, IL6, TNFα, TGFβ1 and 2 [27-29,64], involving different intracellular

signaling pathways, including STAT3, NFκB and TAK1/p38-MAPK activation. Additionally, curcumin reduced reactive gliosis in the rat brain stem after ethidium bromide injection yielding smaller GFAP+ glial scar regions [26].

However, like a multitude of other drugs, curcumin is quite instable and poorly bioavailable so that systemic application of the native drug will hardly achieve therapeutically relevant local concentrations [35]. In first attempts to apply curcumin locally to the brain, poly (vinyl alcohol) (PVA) based implants were loaded with curcumin and implanted into the rodent brain [65]. In comparison to neat implants, curcumin improved neuronal survival and blood brain integrity 4 weeks after implantation, but after 12 weeks curcumin benefits were lost [65]. Due to its known beneficial effects in CNS injuries, we chose curcumin as a model drug to develop a formulation that may attenuate glial scarring processes. To improve drug stability and compatibility with long-term administration implants (e.g. entrapping in slowly biodegradable coatings) we chose to encapsulate curcumin into liposomes, as these nano-carriers are widely used [44,47,66] and can be easily adapted to specific requirements. As an example, the physico-chemical properties of liposomes can be tailored by changing the phospholipids themselves or the ratio between them. As so, increasing the cholesterol concentration of liposomes can lead to a decrease of Zeta Potential (ZP) due to a reduction in sodium ion binding for example [67]. The ZP in general gives insight about the stability of the dispersion, as it influences the electric repulsion between particles. Furthermore, the stability and half-life of a liposome formulation can be strongly affected by pH as well as temperature [68]. In fact, increasing the pH and temperature can lead to higher membrane-fluidity and therefore to a decrease of drug-liposome aggregate stability [69,70]. Consequently, the physico-chemical properties, such as size, surface charge, membrane fluidity or lipid-transition temperature are important parameters to build a stable liposomal nano-carrier for curcumin. In previous work, Roy et al. have analyzed the impact of temperature, pH and composition of different biomimetic lipids and lipid-combinations such as eggphosphatidylcholine (EPC), dipalmitoylphosphatidylcholine (DPPC) or dipalmitoylphosphatidylglycerol (DPPG) on the stability of curcumin encapsulated into liposomes [71]. Amongst them, DPPC was the most pH-stable one with a sustained drug release at physiological pH. Pre-experiments in our laboratory comparing DPPC with EPC (data not shown) revealed, that higher encapsulation efficiencies of curcumin, as well as smaller PdIs could be obtained using DPPC as main phospholipid. Consequently, we chose DPPC as the backbone of our liposomal formulation.

Nonetheless, the right cryo-protectant must be chosen for the individual phospholipid combination upon freeze-drying. Amongst the huge variety of protectants reviewed in 2018 [72], there is no precise recommendation for our exact lipid combination available, yet. Based on the work of van Winden and Crommelin as well as Mohammed et al. [73,74] we chose to work with trehalose as cryo-protectant, to ensure stable curcumin nanoformulations with a sufficient EE% as well as drug release kinetic. With the final supplementation of 10% trehalose we could produce a stable liposomal formulation that can be stored up to 6 months at least. Moreover, the sustained release profile of our liposomal formulation at physiological temperatures and pH with a maximum of only 35% released curcumin cargo after 24h is well aligned with the findings of Roy et al, who highlighted the connection between the lipid transition temperature of DPPC and the slower release kinetics of curcumin liposomes [71]. Using other lipids than DPPC, such as EPC or SPC for example, Chen et al reported releases of 45-50% of their total curcumin cargo already after 24h [48]. Also Zhao et al. claim that their liposomal formulation of curcumin using soy lecithin released ≈50% after 24h and already 80% of their cargo after 78h [75]. Consequently, the surface charges as well as phase-transition temperatures of the bilayer lipid membranes clearly influences its liquidity and consequently its curcumin release, indicating that we produced a sufficient nano-carrier with favorable release kinetics for a long and sustained drug release of curcumin, using 80.6% (w/w) DPPC and 15.6% (w/w) cholesterol.

Concluding these aspects, we could successfully establish a protocol for liposomal curcumin formulation, yielding beneficial physico-chemical properties, efficient drug loading and long-term stability of the liposomes.

To investigate effects of liposomal encapsulated curcumin, we chose human cell lines of the two major cell types that contribute to glial scar formation, microglia and astrocytes. Therefore we experimentally split the reactive processes in two steps by activating microglial cells with LPS to analyze pro-inflammatory cytokine expression, and activating astrocytes with a pro-inflammatory cytokine mixture typically expressed in glial scarring [76] to analyze glial scarring associated genes. *In vitro*, curcumin has previously been shown to reduce the expression of pro-inflammatory mediators and cytokines in activated microglial cells [23,25,77-79], and these effects depended on the PI3K/Akt and HSP60/TLR4/MyD88/NFκB pathways [80,81]. Curcumin stimulation could also reduce reactivity/activation in astrocytes or astrocytic cell culture models upon different challenges [82,83]. For example, H_2O_2 mediated oxidative stress induced astrogliosis associated markers like GFAP and vimentin, which could

be attenuated by curcumin [84]. In accordance with these findings, we could show that our liposomal curcumin formulation could inhibit LPS-induced cytokine expression by human microglial cells at least as efficient as free curcumin. Furthermore, we simulated reactive astrogliosis by stimulating human astrocytes with a cytokine cocktail, and liposomal curcumin could efficiently reduce the cytokine-mediated upregulation of gliosis associated genes, exemplarily ECM components tenascin C and fibronectin, and the intracellular structure protein nestin.

Very recently, different other approaches have also shown that nanoformulations may improve curcumin stability and applicability, for example in cancer therapy [50,85] and brain disease models [36,86]. In a spinal cord injury model, Lipodisq-formulated curcumin was shown to be effective in reducing the glial scar formation [87], and in a demyelination model, curcumin nanoparticles reduced GFAP expression, signs of inflammation and demyelination even a bit more effective than free curcumin [88]. We could also show that our liposomal formulation of curcumin was more effective in inhibiting most of the analyzed pro-inflammatory and astrogliosis reactions, although differences between free and liposomal curcumin where quite faint in some aspects. This might be further improved by advanced design of the liposome composition. However, the efficacy of curcumin nanoformulations needs to be carefully evaluated as sometimes simple monolayer (2D) cell culture models are more susceptible than more complex 3D *in vitro* models [85]. Therefore, we used murine brain acute slices from the cerebral cortex as a second test system. We induced reactivity by application of LPS and observed induction of pro-inflammatory cytokines and reactive gliosis associated genes. In comparable brain slice models, curcumin has previously been shown to protect from Aβ1–42-induced toxicity [89] employing ß-catenin and PI3K signaling [90], to prevent cell death [91] as well as bilirubin-induced cell damage [92], and to reduce seizure-like events [93]. In our brain slice model, we could show that our liposomal curcumin formulation could alleviate cytotoxic effects of LPS stimulations, induction of pro-inflammatory cytokines and restore cellular loss and with reactive astrogliosis, being at least as effective as free curcumin. Thus, we could show in two different test systems (even from different species) that liposomal encapsulated curcumin (LipoCur) can effectively prevent reactive processes that occur in glial scar formation.

Conclusion

Curcumin can effectively reduce glial scarring associated microglia and astrocyte reactions in human cell culture models as well as murine acute brain slices. We developed a liposomal encapsulation protocol that may favor long-term stability of the drugs – here curcumin as an example- and compatibility to brain implant materials (e.g. biodegradable coatings or hydrogels). Liposomal curcumin is suitable for long-term storage (≤ 6 month), well tolerated by healthy cells in relevant concentrations and at least as effective in alleviating glial scarring reactions in human astrocytes and microglia as well as in murine acute brain slices.

Abbreviations

BBB, blood brain barrier; CT, cycle of threshold; DBS, deep brain stimulation; div, days in vitro; DL, Drug Loading; DLS, Dynamic Light Scattering; DMSO, dimethylsulfoxide; DPPC, dipalmitoylphosphatidylcholine; EE, Encapsulation Efficiency; ELISA, enzyme linked immunosorbent assay; GAPDH, glyceraldehyde 3-phosphate dehydrogenase; GFAP, glial fibrillary acidic protein; HIV, human immunodeficiency virus; HPLC, High Performance Liquid Chromatography; IHC, immunohistochemistry; IL1β, interleukin 1β; IL6, interleukin 6; LipoCur, liposomal encapsulated curcumin; LP, liposomes; LPS, lipopolysaccharide; qPCR, quantitative reverse transcription polymerase chain reaction; MAPK, mitogen-activated protein kinase; MBP, myelin basic protein; MY, mass yield; NF, neurofilament; NFκB, nuclear factor 'kappa-light-chain-enhancer' of activated B-cells; NO, nitric oxide; PdI, Polydispersity Index; PI3K, phosphoinositide 3-kinase; SD, standard deviation; STAT3, Signal Transducers and Activators of Transcription 3; TEM, Transmission Electron Microscopy; TGFβ1, transforming growth factor β1; TNFα, tumor necrosis factor α; ZP, zeta potential

Ethics approval and informed consent

Mouse brains were obtained and used in agreement with the local Ethics Committee [V 242-70056/2015(91-7/15)].

Author contributions

CS: Conceptualization, Investigation, Formal analysis, Methodology, Visualization, writing original draft; AL: Methodology, Investigation, Supervision, review and editing; FC: Methodology, Investigation, review and editing; CB: Methodology, Supervision, Resources, review and editing; PA: Methodology, Investigation, review and editing; RL: Methodology, Resources, review and editing; JHF: Conceptualization, review and editing; GP: Methodology, Resources, Supervision, review and editing; KH: Conceptualization, Investigation, Methodology, Visualization, Supervision, writing original draft

Acknowledgements

We thank Judith Becker, Martina Burmester, Sonja Dahle, Bettina Facompré, Frank Lichte, Gaby Steinkamp, Laurence Collard and Françoise Leonard for expert technical assistance.

This work was supported by the Deutsche Forschungsgemeinschaft (DFG, RTG2154, project 7 and 8). PA and the microscopy unit of the Institute of Anatomy, University Kiel, were supported by the DFG SFB877 (project number 125440785; A13 and Z3). The funding bodies did not have any influence on the design of the study.

Disclosure

The authors report no conflicts of interest in this work.

References

1. Linnaeus C. *Species Plantarum.* Stockholm: Lars Salvius; 1753.
2. Adiwidjaja J, McLachlan AJ, Boddy AV. Curcumin as a clinically-promising anti-cancer agent: pharmacokinetics and drug interactions. *Expert Opin Drug Metab Toxicol.* 2017;13(9):953-972.
3. Deguchi A. Curcumin targets in inflammation and cancer. *Endocr Metab Immune Disord Drug Targets.* 2015;15(2):88-96.
4. Naksuriya O, Okonogi S, Schiffelers RM, Hennink WE. Curcumin nanoformulations: a review of pharmaceutical properties and preclinical studies and clinical data related to cancer treatment. *Biomaterials.* 2014;35(10):3365-3383.
5. Wong KE, Ngai SC, Chan KG, Lee LH, Goh BH, Chuah LH. Curcumin Nanoformulations for Colorectal Cancer: A Review. *Front Pharmacol.* 2019;10:152.
6. Gupta SC, Patchva S, Aggarwal BB. Therapeutic roles of curcumin: lessons learned from clinical trials. *AAPS J.* 2013;15(1):195-218.
7. Yang M, Akbar U, Mohan C. Curcumin in Autoimmune and Rheumatic Diseases. *Nutrients.* 2019;11(5):pii: E1004.
8. Farkhondeh T, Samarghandian S, Pourbagher-Shahri AM, Sedaghat M. The impact of curcumin and its modified formulations on Alzheimer's disease. *J Cell Physiol.* 2019:16953-16965.
9. Lim GP, Chu T, Yang F, Beech W, Frautschy SA, Cole GM. The curry spice curcumin reduces oxidative damage and amyloid pathology in an Alzheimer transgenic mouse. *J Neurosci.* 2001;21(21):8370-8377.
10. Ramkumar M, Rajasankar S, Gobi VV, et al. Demethoxycurcumin, a Natural Derivative of Curcumin Abrogates Rotenone-induced Dopamine Depletion and Motor Deficits by Its Antioxidative and Anti-inflammatory Properties in Parkinsonian Rats. *Pharmacogn Mag.* 2018;14(53):9-16.
11. Tripanichkul W, Jaroensuppaperch EO. Ameliorating effects of curcumin on 6-OHDA-induced dopaminergic denervation, glial response, and SOD1 reduction in the striatum of hemiparkinsonian mice. *Eur Rev Med Pharmacol Sci.* 2013;17(10):1360-1368.
12. Arora V, Kuhad A, Tiwari V, Chopra K. Curcumin ameliorates reserpine-induced pain-depression dyad: behavioural, biochemical, neurochemical and molecular evidences. *Psychoneuroendocrinology.* 2011;36(10):1570-1581.
13. Sun J, Chen F, Braun C, et al. Role of curcumin in the management of pathological pain. *Phytomedicine.* 2018;48:129-140.
14. Drion CM, Borm LE, Kooijman L, et al. Effects of rapamycin and curcumin treatment on the development of epilepsy after electrically induced status epilepticus in rats. *Epilepsia.* 2016;57(5):688-697.
15. Bavarsad K, Barreto GE, Hadjzadeh MA, Sahebkar A. Protective Effects of Curcumin Against Ischemia-Reperfusion Injury in the Nervous System. *Mol Neurobiol.* 2018.
16. Zhang Y, Fang M, Sun Y, et al. Curcumin attenuates cerebral ischemia injury in Sprague-Dawley rats and PC12 cells by suppressing overactivated autophagy. *J Photochem Photobiol B.* 2018;184:1-6.
17. Deng Y, Lu X, Wang L, et al. Curcumin inhibits the AKT/NF-kappaB signaling via CpG demethylation of the promoter and restoration of NEP in the N2a cell line. *AAPS J.* 2014;16(4):649-657.
18. Dong W, Yang B, Wang L, et al. Curcumin plays neuroprotective roles against traumatic brain injury partly via Nrf2 signaling. *Toxicol Appl Pharmacol.* 2018;346:28-36.
19. Kim HY, Park EJ, Joe EH, Jou I. Curcumin suppresses Janus kinase-STAT inflammatory signaling through activation of Src homology 2 domain-containing tyrosine phosphatase 2 in brain microglia. *J Immunol.* 2003;171(11):6072-6079.
20. Shi X, Zheng Z, Li J, et al. Curcumin inhibits Abeta-induced microglial inflammatory responses in vitro: Involvement of ERK1/2 and p38 signaling pathways. *Neurosci Lett.* 2015;594:105-110.

21. Tu XK, Yang WZ, Chen JP, et al. Curcumin inhibits TLR2/4-NF-kappaB signaling pathway and attenuates brain damage in permanent focal cerebral ischemia in rats. *Inflammation.* 2014;37(5):1544-1551.
22. Mhillaj E, Tarozzi A, Pruccoli L, Cuomo V, Trabace L, Mancuso C. Curcumin and Heme Oxygenase: Neuroprotection and Beyond. *Int J Mol Sci.* 2019;20(10).
23. Yang Z, Zhao T, Zou Y, Zhang JH, Feng H. Curcumin inhibits microglia inflammation and confers neuroprotection in intracerebral hemorrhage. *Immunol Lett.* 2014;160(1):89-95.
24. Ghasemi F, Bagheri H, Barreto GE, Read MI, Sahebkar A. Effects of Curcumin on Microglial Cells. *Neurotox Res.* 2019.
25. Parada E, Buendia I, Navarro E, Avendano C, Egea J, Lopez MG. Microglial HO-1 induction by curcumin provides antioxidant, antineuroinflammatory, and glioprotective effects. *Mol Nutr Food Res.* 2015;59(9):1690-1700.
26. Bondan E, Cardoso C, Martins MF. Curcumin decreases astrocytic reaction after gliotoxic injury in the rat brainstem. *Arq Neuropsiquiatr.* 2017;75(8):546-552.
27. Wang YF, Zu JN, Li J, Chen C, Xi CY, Yan JL. Curcumin promotes the spinal cord repair via inhibition of glial scar formation and inflammation. *Neurosci Lett.* 2014;560:51-56.
28. Yuan J, Liu W, Zhu H, et al. Curcumin inhibits glial scar formation by suppressing astrocyte-induced inflammation and fibrosis in vitro and in vivo. *Brain Res.* 2017;1655:90-103.
29. Yuan J, Zou M, Xiang X, et al. Curcumin improves neural function after spinal cord injury by the joint inhibition of the intracellular and extracellular components of glial scar. *J Surg Res.* 2015;195(1):235-245.
30. Machova Urdzikova L, Karova K, Ruzicka J, et al. The Anti-Inflammatory Compound Curcumin Enhances Locomotor and Sensory Recovery after Spinal Cord Injury in Rats by Immunomodulation. *Int J Mol Sci.* 2015;17(1).
31. Ruzicka J, Urdzikova LM, Kloudova A, et al. Anti-inflammatory compound curcumin and mesenchymal stem cells in the treatment of spinal cord injury in rats. *Acta Neurobiol Exp (Wars).* 2018;78(4):358-374.
32. Lestari ML, Indrayanto G. Curcumin. *Profiles Drug Subst Excip Relat Methodol.* 2014;39:113-204.
33. Yang KY, Lin LC, Tseng TY, Wang SC, Tsai TH. Oral bioavailability of curcumin in rat and the herbal analysis from Curcuma longa by LC-MS/MS. *J Chromatogr B Analyt Technol Biomed Life Sci.* 2007;853(1-2):183-189.
34. Liu W, Zhai Y, Heng X, et al. Oral bioavailability of curcumin: problems and advancements. *J Drug Target.* 2016;24(8):694-702.
35. Nelson KM, Dahlin JL, Bisson J, Graham J, Pauli GF, Walters MA. The Essential Medicinal Chemistry of Curcumin. *J Med Chem.* 2017;60(5):1620-1637.
36. Del Prado-Audelo ML, Caballero-Floran IH, Meza-Toledo JA, et al. Formulations of Curcumin Nanoparticles for Brain Diseases. *Biomolecules.* 2019;9(2).
37. Fereydouni N, Darroudi M, Movaffagh J, et al. Curcumin nanofibers for the purpose of wound healing. *J Cell Physiol.* 2019;234(5):5537-5554.
38. Jamwal R. Bioavailable curcumin formulations: A review of pharmacokinetic studies in healthy volunteers. *J Integr Med.* 2018;16(6):367-374.
39. Khan I, Saeed K, Khan I. Nanoparticles: Properties, applications and toxicities. *Arabian Journal of Chemistry.* 2019;12(7):908-931.
40. Hoshyar N, Gray S, Han H, Bao G. The effect of nanoparticle size on in vivo pharmacokinetics and cellular interaction. *Nanomedicine.* 2016;11(6):673-692.
41. Choi YH, Han HK. Correction to: Nanomedicines: current status and future perspectives in aspect of drug delivery and pharmacokinetics. *Journal of pharmaceutical investigation.* 2019;49(1):201.
42. Bulbake U, Doppalapudi S, Kommineni N, Khan W. Liposomal Formulations in Clinical Use: An Updated Review. *Pharmaceutics.* 2017;9(2).
43. Johnston MJ, Semple SC, Klimuk SK, Ansell S, Maurer N, Cullis PR. Characterization of the drug retention and pharmacokinetic properties of liposomal nanoparticles

containing dihydrosphingomyelin. *Biochimica et biophysica acta.* 2007;1768(5):1121-1127.
44. Akbarzadeh A, Rezaei-Sadabady R, Davaran S, et al. Liposome: classification, preparation, and applications. *Nanoscale Res Lett.* 2013;8(1):102.
45. Sabin J, Prieto G, Ruso JM, Hidalgo-Alvarez R, Sarmiento F. Size and stability of liposomes: a possible role of hydration and osmotic forces. *The European physical journal E, Soft matter.* 2006;20(4):401-408.
46. Al-Jamal WT, Kostarelos K. Liposome-nanoparticle hybrids for multimodal diagnostic and therapeutic applications. *Nanomedicine.* 2007;2(1):85-98.
47. Basnet P, Hussain H, Tho I, Skalko-Basnet N. Liposomal delivery system enhances anti-inflammatory properties of curcumin. *Journal of pharmaceutical sciences.* 2012;101(2):598-609.
48. Chen Y, Wu Q, Zhang Z, Yuan L, Liu X, Zhou L. Preparation of curcumin-loaded liposomes and evaluation of their skin permeation and pharmacodynamics. *Molecules.* 2012;17(5):5972-5987.
49. Cheng C, Peng S, Li Z, Zou L, Liu W, Liu C. Improved bioavailability of curcumin in liposomes prepared using a pH-driven, organic solvent-free, easily scalable process. *RSC Adv.* 2017;7:25978-25986.
50. Feng T, Wei Y, Lee RJ, Zhao L. Liposomal curcumin and its application in cancer. *Int J Nanomedicine.* 2017;12:6027-6044.
51. Roy A, Saha S, Choudhury A, Bahadur S. Bioenhancement of Curcumin by Combined Approaches of Adjuvants and Liposomal Fabrication. *Asian Journal of Pharmaceutics* 2016;10 (4).
52. Mercanti G, Ragazzi E, Toffano G, Giusti P, Zusso M. Phosphatidylserine and curcumin act synergistically to down-regulate release of interleukin-1beta from lipopolysaccharide-stimulated cortical primary microglial cells. *CNS & neurological disorders drug targets.* 2014;13(5):792-800.
53. Wang Y, Luo J, Li SY. Nano-Curcumin Simultaneously Protects the Blood-Brain Barrier and Reduces M1 Microglial Activation During Cerebral Ischemia-Reperfusion Injury. *ACS Appl Mater Interfaces.* 2019;11(4):3763-3770.
54. Marin C, Fernandez E. Biocompatibility of intracortical microelectrodes: current status and future prospects. *Front Neuroeng.* 2010;3:8.
55. Polikov VS, Tresco PA, Reichert WM. Response of brain tissue to chronically implanted neural electrodes. *J Neurosci Methods.* 2005;148(1):1-18.
56. Arnold P, Himmels P, Weiss S, et al. Antigenic and 3D structural characterization of soluble X4 and hybrid X4-R5 HIV-1 Env trimers. *Retrovirology.* 2014;11:42.
57. Henriksen S, Tylden GD, Dumoulin A, Sharma BN, Hirsch HH, Rinaldo CH. The human fetal glial cell line SVG p12 contains infectious BK polyomavirus. *J Virol.* 2014;88(13):7556-7568.
58. Schweighardt B, Shieh JT, Atwood WJ. CD4/CXCR4-independent infection of human astrocytes by a T-tropic strain of HIV-1. *J Neurovirol.* 2001;7(2):155-162.
59. Schommer J, Schrag M, Nackenoff A, Marwarha G, Ghribi O. Method for organotypic tissue culture in the aged animal. *MethodsX.* 2017;4:166-171.
60. Stoppini L, Buchs PA, Muller D. A simple method for organotypic cultures of nervous tissue. *Journal of neuroscience methods.* 1991;37(2):173-182.
61. Mewes A, Franke H, Singer D. Organotypic brain slice cultures of adult transgenic P301S mice--a model for tauopathy studies. *PloS one.* 2012;7(9):e45017.
62. Adamski V, Schmitt C, Ceynowa F, et al. Effects of sequentially applied single and combined temozolomide, hydroxychloroquine and AT101 treatment in a long-term stimulation glioblastoma in vitro model. *J Cancer Res Clin Oncol.* 2018;144(8):1475-1485.
63. Lin MS, Lee YH, Chiu WT, Hung KS. Curcumin provides neuroprotection after spinal cord injury. *J Surg Res.* 2011;166(2):280-289.
64. Zhang N, Wei G, Ye J, et al. Effect of curcumin on acute spinal cord injury in mice via inhibition of inflammation and TAK1 pathway. *Pharmacol Rep.* 2017;69(5):1001-1006.

65. Potter KA, Jorfi M, Householder KT, Foster EJ, Weder C, Capadona JR. Curcumin-releasing mechanically adaptive intracortical implants improve the proximal neuronal density and blood-brain barrier stability. *Acta Biomater.* 2014;10(5):2209-2222.
66. Raza F, Zafar H, You X, Khan A, Wu J, Ge L. Cancer nanomedicine: focus on recent developments and self-assembled peptide nanocarriers. *Journal of materials chemistry B.* 2019.
67. Lakowicz JR. Principles of frequency-domain fluorescence spectroscopy and applications to cell membranes. *Sub-cellular biochemistry.* 1988;13:89-126.
68. Zhang JA, Pawelchak J. Effect of pH, ionic strength and oxygen burden on the chemical stability of EPC/cholesterol liposomes under accelerated conditions. Part 1: Lipid hydrolysis. *European journal of pharmaceutics and biopharmaceutics : official journal of Arbeitsgemeinschaft fur Pharmazeutische Verfahrenstechnik eV.* 2000;50(3):357-364.
69. Began G, Sudharshan E, Sankar KU, Rao AG. Interaction of curcumin with phosphatidylcholine: A spectrofluorometric study. *Journal of agricultural and food chemistry.* 2000;48(2):576.
70. Niu Y, Wang X, Chai S, Chen Z, An X, Shen W. Effects of curcumin concentration and temperature on the spectroscopic properties of liposomal curcumin. *Journal of agricultural and food chemistry.* 2012;60(7):1865-1870.
71. Roy B, Guha P, Bhattarai R, et al. Influence of Lipid Composition, pH, and Temperature on Physicochemical Properties of Liposomes with Curcumin as Model Drug. *Journal of oleo science.* 2016;65(5):399-411.
72. Franze S, Selmin F, Samaritani E, Minghetti P, Cilurzo F. Lyophilization of Liposomal Formulations: Still Necessary, Still Challenging. *Pharmaceutics.* 2018;10(3).
73. van Winden ECA, Crommelin DJ. Long term stability of freeze-dried, lyoprotected doxorubicin liposomes. *European Journal of Pharmaceutics and Biopharmaceutics.* 1997;43(3):295-307.
74. Mohammed AR, Coombes AG, Perrie Y. Amino acids as cryoprotectants for liposomal delivery systems. *European Journal of Pharmaceutical Sciences.* 2007;30(5):406-413.
75. Zhao M, Zhao M, Fu C, Yu Y, Fu A. Targeted therapy of intracranial glioma model mice with curcumin nanoliposomes. *International journal of nanomedicine.* 2018;13:1601-1610.
76. Sofroniew MV. Molecular dissection of reactive astrogliosis and glial scar formation. *Trends Neurosci.* 2009;32(12):638-647.
77. Jin CY, Lee JD, Park C, Choi YH, Kim GY. Curcumin attenuates the release of pro-inflammatory cytokines in lipopolysaccharide-stimulated BV2 microglia. *Acta Pharmacol Sin.* 2007;28(10):1645-1651.
78. Karlstetter M, Lippe E, Walczak Y, et al. Curcumin is a potent modulator of microglial gene expression and migration. *J Neuroinflammation.* 2011;8:125.
79. Guo L, Xing Y, Pan R, et al. Curcumin protects microglia and primary rat cortical neurons against HIV-1 gp120-mediated inflammation and apoptosis. *PLoS One.* 2013;8(8):e70565.
80. Cianciulli A, Calvello R, Porro C, Trotta T, Salvatore R, Panaro MA. PI3k/Akt signalling pathway plays a crucial role in the anti-inflammatory effects of curcumin in LPS-activated microglia. *Int Immunopharmacol.* 2016;36:282-290.
81. Ding F, Li F, Li Y, et al. HSP60 mediates the neuroprotective effects of curcumin by suppressing microglial activation. *Exp Ther Med.* 2016;12(2):823-828.
82. Qin X, Qiao H, Wu S, Cheng J, Wan Q, Liu R. Curcumin Inhibits Monocyte Chemoattractant Protein-1 Expression in TNF-alpha induced Astrocytes Through AMPK Pathway. *Neurochem Res.* 2018;43(4):775-784.
83. Seyedzadeh MH, Safari Z, Zare A, et al. Study of curcumin immunomodulatory effects on reactive astrocyte cell function. *Int Immunopharmacol.* 2014;22(1):230-235.
84. Daverey A, Agrawal SK. Curcumin alleviates oxidative stress and mitochondrial dysfunction in astrocytes. *Neuroscience.* 2016;333:92-103.

85. Kolter M, Wittmann M, Koll-Weber M, Suss R. The suitability of liposomes for the delivery of hydrophobic drugs - A case study with curcumin. *Eur J Pharm Biopharm.* 2019;140:20-28.
86. Bollimpelli VS, Kumar P, Kumari S, Kondapi AK. Neuroprotective effect of curcumin-loaded lactoferrin nano particles against rotenone induced neurotoxicity. *Neurochem Int.* 2016;95:37-45.
87. Krupa P, Svobodova B, Dubisova J, Kubinova S, Jendelova P, Machova Urdzikova L. Nano-formulated curcumin (Lipodisq) modulates the local inflammatory response, reduces glial scar and preserves the white matter after spinal cord injury in rats. *Neuropharmacology.* 2019;155:54-64.
88. Naeimi R, Safarpour F, Hashemian M, et al. Curcumin-loaded nanoparticles ameliorate glial activation and improve myelin repair in lyolecithin-induced focal demyelination model of rat corpus callosum. *Neurosci Lett.* 2018;674:1-10.
89. Hoppe JB, Haag M, Whalley BJ, Salbego CG, Cimarosti H. Curcumin protects organotypic hippocampal slice cultures from Abeta1-42-induced synaptic toxicity. *Toxicol In Vitro.* 2013;27(8):2325-2330.
90. Hoppe JB, Frozza RL, Pires EN, Meneghetti AB, Salbego C. The curry spice curcumin attenuates beta-amyloid-induced toxicity through beta-catenin and PI3K signaling in rat organotypic hippocampal slice culture. *Neurol Res.* 2013;35(8):857-866.
91. Choi GY, Kim HB, Hwang ES, et al. Curcumin Alters Neural Plasticity and Viability of Intact Hippocampal Circuits and Attenuates Behavioral Despair and COX-2 Expression in Chronically Stressed Rats. *Mediators Inflamm.* 2017;2017:6280925.
92. Dal Ben M, Bottin C, Zanconati F, Tiribelli C, Gazzin S. Evaluation of region selective bilirubin-induced brain damage as a basis for a pharmacological treatment. *Sci Rep.* 2017;7:41032.
93. Drion CM, Kooijman L, Aronica E, et al. Curcumin reduces development of seizurelike events in the hippocampal-entorhinal cortex slice culture model for epileptogenesis. *Epilepsia.* 2019;60(4):605-614.

Tables

Table 1 Characterization of empty and curcumin loaded liposomes (LipoCur), before and after freeze-drying

	Size [nm]	**PdI**	**ZP** [mV]	**DL** [%]	**MY** [%]	**EE** [%]
LipoCur (wo Tre, *before* FD)	180 ± 34	0.17 ± 0.04	-26.1 ± 14.0	21.4 ± 1.8	78 ± 18	68 ± 6
LipoCur (w Tre, *before* FD)	153 ± 48	0.11 ± 0.05	-22.6 ± 6.2	*	*	46 ± 9
LipoCur (w Tre, *after* FD)	164 ± 22	0.25 ± 0.10	-29.3 ± 3.8	*	*	*
Empty liposomes (w Tre, *after* FD)	219 ± 82	0.30 ± 0.10	-17.2 ± 3.8	-	-	-

Table and Figure legends

Table 1 Curcumin loaded liposomes (LipoCur) were analyzed prior to freeze drying (FD) with or without substitution of 10% trehalose (Tre), and with trehalose substitution after freeze drying regarding size (hydrodynamic diameter), polydispersity index (PdI), zeta potential (ZP), for comparison, data of empty liposomes are shown below. Drug loading (DL), mass yield (MY) and encapsulation efficacy (EE) were measured in freshly prepared liposomes, DL and MY only in freshly prepared liposomes without trehalose (* not determined). Mean values of n = 3 measurements from one batch ± SD are shown.

Figure 1 Graphical depiction of brain cell activation and the experimental cell culture based models. (A) Activated by tissue damage, microglial cells enter their activated state characterized by an amoeboid shape and the production of pro-inflammatory cytokines such as IL1β, IL6, TNFα and TGFβ. These cytokines exert neuroinflammatory reaction and turn astrocytes to a reactive state in which they upregulate the expression of gliosis specific genes. (B) Human microglial cells HMC3 were stimulated with LPS to induce an inflammatory reaction, which is amongst others represented by the production of inflammatory cytokines like IL1β, IL6, TNFα and TGFβ1. Expression of these mediators was analyzed on mRNA level by qPCR to investigate modulating effects of liposomal encapsulated curcumin (LipoCur) in comparison to free curcumin and empty liposomes on the inflammatory response of microglial cells. (C) In order to transfer the inflammatory response to astrocytes, human SVGA astrocytes were stimulated with a combination of the microglia produced cytokines IL1β, TNFα and TGFβ1 (with or without co-stimulation with LipoCur or free curcumin), and analyzed genes that are known to contribute to reactive gliosis and glial scar formation (Nestin, Vimentin, Tenascin-C, Fibronectin) by qPCR. (D) To study the cellular reactions in their tissue environment, we stimulated murine organotypic brain slices with LPS and analyzed by cytotoxicity assay, qPCR and immunohistochemistry whether LPS effects could be ameliorated by co-incubation with LipoCur or free curcumin.

Figure 2 Physicochemical properties of curcumin loaded liposomes. Hydrodynamic diameter, polydispersity index (PdI) and zeta potential were determined of curcumin loaded liposomes substituted

with different concentrations of trehalose before (A) and after (B) freeze drying (n=3 batches). Long-term analysis of hydrodynamic diameter (C), zeta potential (D) and PdI (E) of the freeze-dried liposomes using 10% trehalose revealed stability for at least 180 days. (n = 3 batches) (F) Curcumin loaded liposomes showed efficient sustained drug release over 96h. The instability of curcumin is mirrored by decreasing cumulative curcumin concentrations after prolonged time periods. (n=3). The statistical significance of the long-term stability was determined by One-Way-ANOVA followed by Bonferroni's multiple comparison test, comparing all days after freeze-drying with each other. A two-tailed paired t-test was employed to test for significance between liposomes before and directly after freeze-drying. *p<0.05, **p<0.005, *p<0.001.

Figure 3 Ultrastructure of curcumin loaded and empty liposomes, cellular uptake and cell viability of HMC3 microglia cells and SVGA astrocytes upon incubation with liposomal and free curcumin. (A) Curcumin loaded liposomes and (B) empty liposomes were visualized by transmission electron microscopy (TEM) at different magnifications. Similar average sizes and size distributions could be obtained as with DLS measurements after 180 days. (C) Liposomes were labelled red using nile red, and cellular uptake was monitored after 24h incubation with human microglia cells HMC3 or human astrocytes SVGA. Nuclei were counterstained with DAPI (shown in cyan) and membrane structures with Alexa Fluor-647 labelled wheat germ agglutinin (shown in blue) to visualize the localization of the red labelled liposomes within the cell boundaries. Representative images from n = 2 independent experiments, scale bars indicate 20µm. (D) To test the influence of liposomal curcumin on cell viability, human microglia cells (HMC3, left) or astrocytes (SVGA, right) were incubated with different concentrations of free curcumin (free Cur), curcumin loaded liposomes (LipoCur) containing the same amounts of curcumin (a final concentration of 1µM curcumin corresponds to 18µg/mL loaded liposomes) or the corresponding amounts of empty liposomes (empty LP) for 3 days. Viability was determined in duplicates using a WST-assay for n= 4-10 independent experiments, graphs show mean values ± SD. For HMC3 microglia, there was no significant reduction in viability to be observed up to 10µM for free curcumin (IC50 19.6µM), and up to 1µM for liposomal curcumin (IC50 5.3µM). Empty liposomes only reduced microglia viability starting from 90µg/ml (IC50 86.4µg/mL). SVGA cells showed quite similar results while being a bit more sensitive, with IC50 values of 11.6µM for free curcumin, 2.1µM for liposomal curcumin and 36.4µg/mL for empty liposomes. Statistical significant differences to

unstimulated controls (corresponding to 100%) were analyzed by One-Way-ANOVA followed by Dunnett's multiple comparison test and are indicated by rhombs (# p<0.05, ## p< 0.01, ### p<0.001), while differences between free and liposomal curcumin are analyzed by Two-Way-ANOVA followed by Bonferroni's multiple comparison test and marked by asterisks (**p<0.01).

Figure 4 Effects of liposomal and free curcumin on an experimental models of neuroinflammation (A,B) and reactive gliosis (C,D). (A) Upon stimulation with 100ng/mL LPS for 24h, HMC3 cells showed the typical amoeboid morphology of reactive microglia, which could be alleviated by pre-incubation with 0.01µM liposomal curcumin (LipoCur). Representative images of n = 2 independent stimulations, scale bar indicates 20µm. (B) Stimulation with 100ng/mL LPS for 24h also induced expression of pro-inflammatory cytokines IL6, IL1β, TNFα and TGFβ, as monitored by qPCR. These effects could be reduced by pre-incubation with 0.01µM curcumin and, in trend even more effective, by corresponding amounts of LipoCur. Please note that due to high variations of LPS-induced cytokine expression curcumin and LipoCur mediated reduction is not always significant, but trends can be seen for all investigated cytokines. Graphs show ΔΔCT values representing the n-fold expression in comparison to unstimulated controls. In non-inflammatory conditions (without LPS stimulation), neither curcumin, nor LipoCur, nor empty liposomes induced any changes in expression of these genes. (C) Stimulation with a combination of IL1β, TNFα and TGFβ (10ng/ml each) for 24h served to induce activation of human astrocyte cell line SVGA. Cells show nuclear deformations as a sign of cellular stress. Effects were almost completely abolished upon pre-incubation with 0.01µM LipoCur. Representative images from n = 2 experiments, scale bar indicates 20µm. (D) As representatives for reactive astrogliosis associated genes, expression of nestin, tenascin C and fibronectin was analyzed by qPCR and found to be induced upon stimulation with IL1β, TNFα and TGFβ (10ng/ml each) for 24h. These effects were significantly alleviated by pre-incubation with 0.01µM curcumin or LipoCur. LipoCur showed higher significance levels compared to soluble curcumin, and was in case of tenascin C even significantly more effective. In "normal" conditions (without cytokine stimulation), neither curcumin, nor LipoCur, nor empty liposomes induced any changes in expression of these genes. Shown are mean values ± SD from n= 5-15 independent experiments, asterisks indicate significant changes of stimulations compared to LPS control (B) and cytokines (D) or between the groups under the brackets. Data has been analyzed by Two-Way-ANOVA followed by Bonferroni's multiple comparison test (*p<0.05, **p<0.001, ***p<0.001).

Figure 5 Effects of liposomal and free curcumin on LPS-challenged organotypic brain slices, regarding cytotoxicity (A) and alteration of mRNA expression of pro-inflammatory cytokines (B). (A) Murine acute brain slices were treated with 100 µg/ml LPS with or without pre-incubation with 0.01µM free curcumin or LipoCur for 8 days, and cytotoxicity was measured from supernatants after 2 and 8 div by Cytotoxicity assay. LPS stimulation induced cytotoxicity (black bar) was completely abolished (compare unstimulated control: white bar) by simultaneous stimulation with LipoCur or free Cur, but not by empty liposomes (empty LP, grey bars). Neither curcumin nor LipoCur nor empty LP had significant effects on cytotoxicity in single stimulations (without LPS, grey bars). Measured extinctions were normalized to unstimulated control (=1), and mean values of 3 respective 5 independent experiments (± SD) are shown for cytotoxic effects after 2 respective 8 div. Asterisks indicate significant changes to LPS-stimulated slices (*p<0.05, **p<0.001, ***p<0.001), analyzed by Two-Way-ANOVA followed by Bonferroni's multiple comparison test. (B) Analyses of effects of LipoCur and free Cur on expression of cytokines revealed that both could at least in trend reduce LPS induced upregulation of inflammatory genes IL1β, IL6, and TNFα. TGFβ was not induced by LPS at 8 div, and consequently not affected by LipoCur or free Cur. Graphs show mean ΔΔCT values ± SD representing the n-fold expression in comparison to unstimulated controls. Data has been analyzed for statistically significance by Two-Way-ANOVA followed by Bonferroni's multiple comparison test. Asterisks indicate significant changes to LPS-stimulated slices or between stimulations (*p<0.05, **p<0.001, ***p<0.001).

Figure 6 Effects of liposomal (LipoCur) and free Curcumin on LPS-challenged organotypic brain slice morphology. Murine acute brain slices were treated with 100µg/ml LPS with or without 0.01µM free curcumin or LipoCur for 8 days, slices were cut in 10µm cryosections and immunostained with antibodies against neurofilament-M (NF, neurons), GFAP and nestin (astrocytes, glial precursors, reactive astrocytes), fibronectin and vimentin (reactive astrocytes, glial scaring) as well as MBP (oligodendrocytes). These exemplary pictures of n = 4 individual experiments show that LipoCur and free curcumin (but not empty liposomes) can effectively restore LPS-mediated loss of neurofilament and attenuate induction of reactive gliosis associated markers like GFAP, nestin, fibronectin and vimentin. Oligodendrocytes marked by MBP staining, however, were hardly affected by LPS stimulation and co-

stimulation with LipoCur or free curcumin. Scale Bars indicate 50µm, please refer to the supplement to Figure 6 for secondary antibody controls.

Supplement to Figure 6 Secondary antibody controls to fluorescence immunostainings in Figure 6. For secondary antibody controls, primary antibodies were omitted in the staining procedure, and sections were inspected with fluorescence exposure times identical to photographs in Figure 6. Representative examples of the unstimulated controls from n = 4 independent experiments.

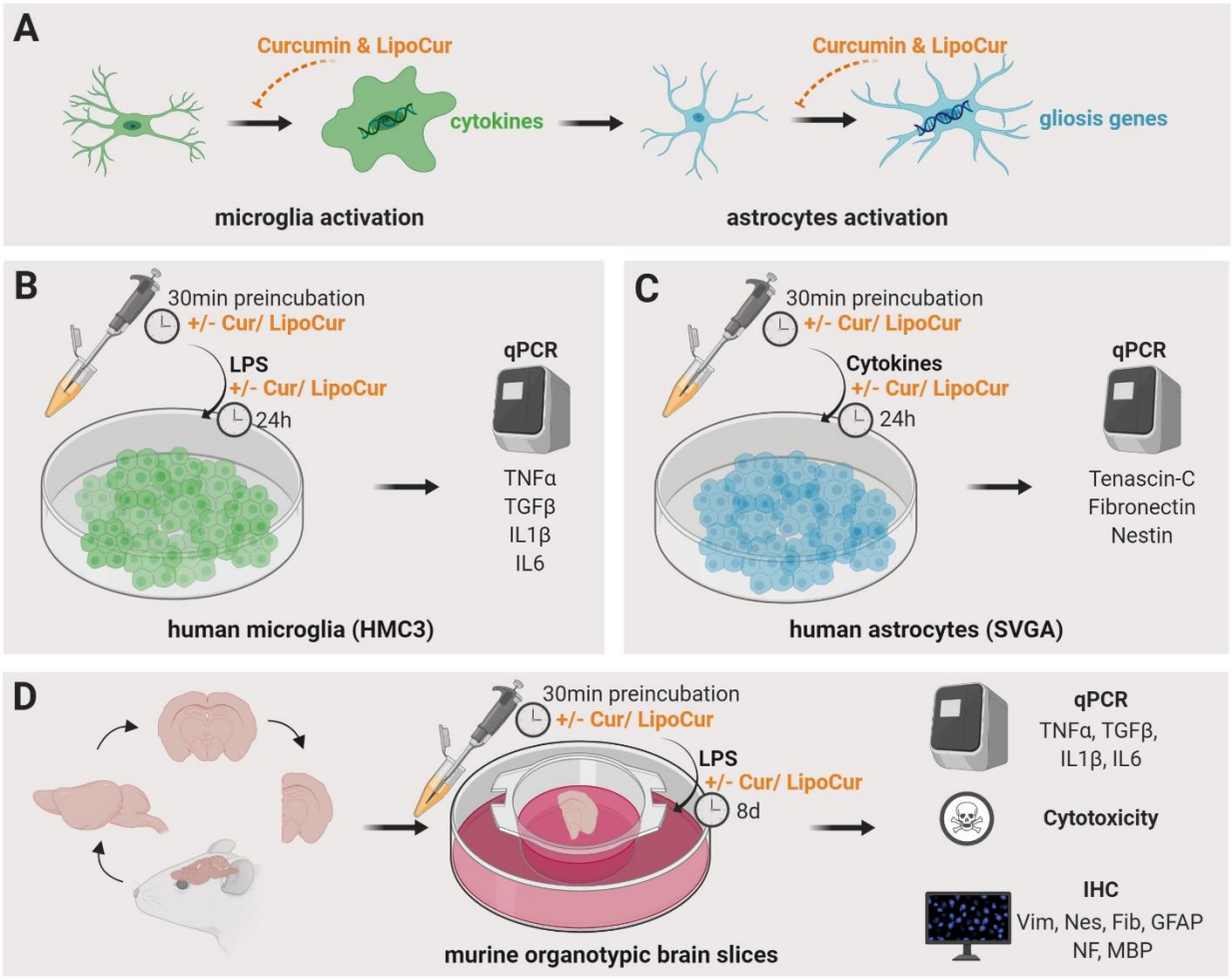
A
Curcumin & LipoCur
cytokines
Curcumin & LipoCur
gliosis genes
microglia activation
astrocytes activation
B
30min preincubation
+/- Cur/ LipoCur
LPS
+/- Cur/ LipoCur
24h
qPCR
TNFα
TGFβ
IL1β
IL6
human microglia (HMC3)
C
30min preincubation
+/- Cur/ LipoCur
Cytokines
+/- Cur/ LipoCur
24h
qPCR
Tenascin-C
Fibronectin
Nestin
human astrocytes (SVGA)
D
30min preincubation
+/- Cur/ LipoCur
LPS
+/- Cur/ LipoCur
8d
murine organotypic brain slices
qPCR
TNFα, TGFβ,
IL1β, IL6
Cytotoxicity
IHC
Vim, Nes, Fib, GFAP
NF, MBP

Figure 1

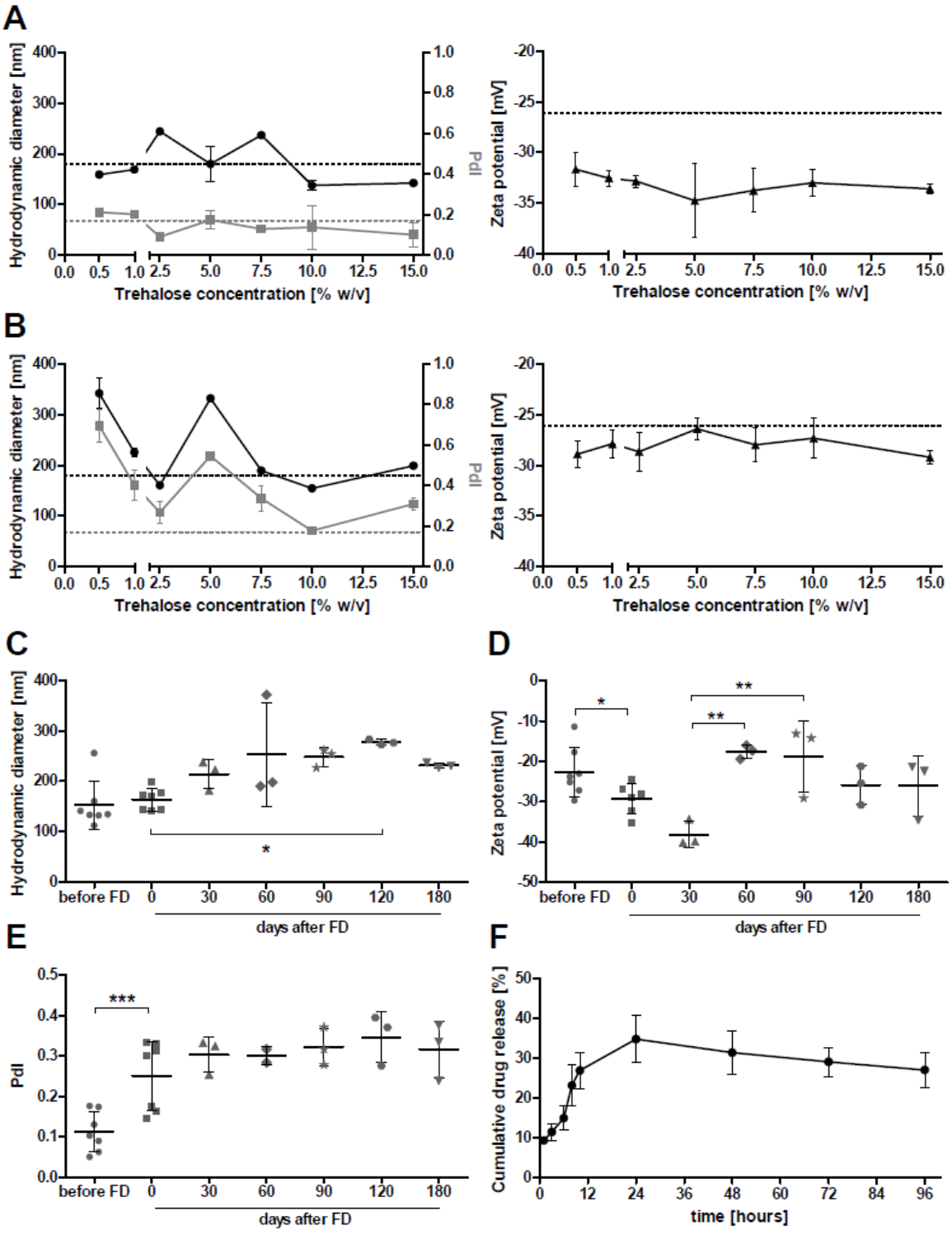
A
Hydrodynamic diameter [nm]
PdI
Trehalose concentration [% w/v]
Zeta potential [mV]
Trehalose concentration [% w/v]
B
Hydrodynamic diameter [nm]
PdI
Trehalose concentration [% w/v]
Zeta potential [mV]
Trehalose concentration [% w/v]
C
Hydrodynamic diameter [nm]
before FD
days after FD
D
Zeta potential [mV]
before FD
days after FD
E
PdI
before FD
days after FD
F
Cumulative drug release [%]
time [hours]

Figure 2

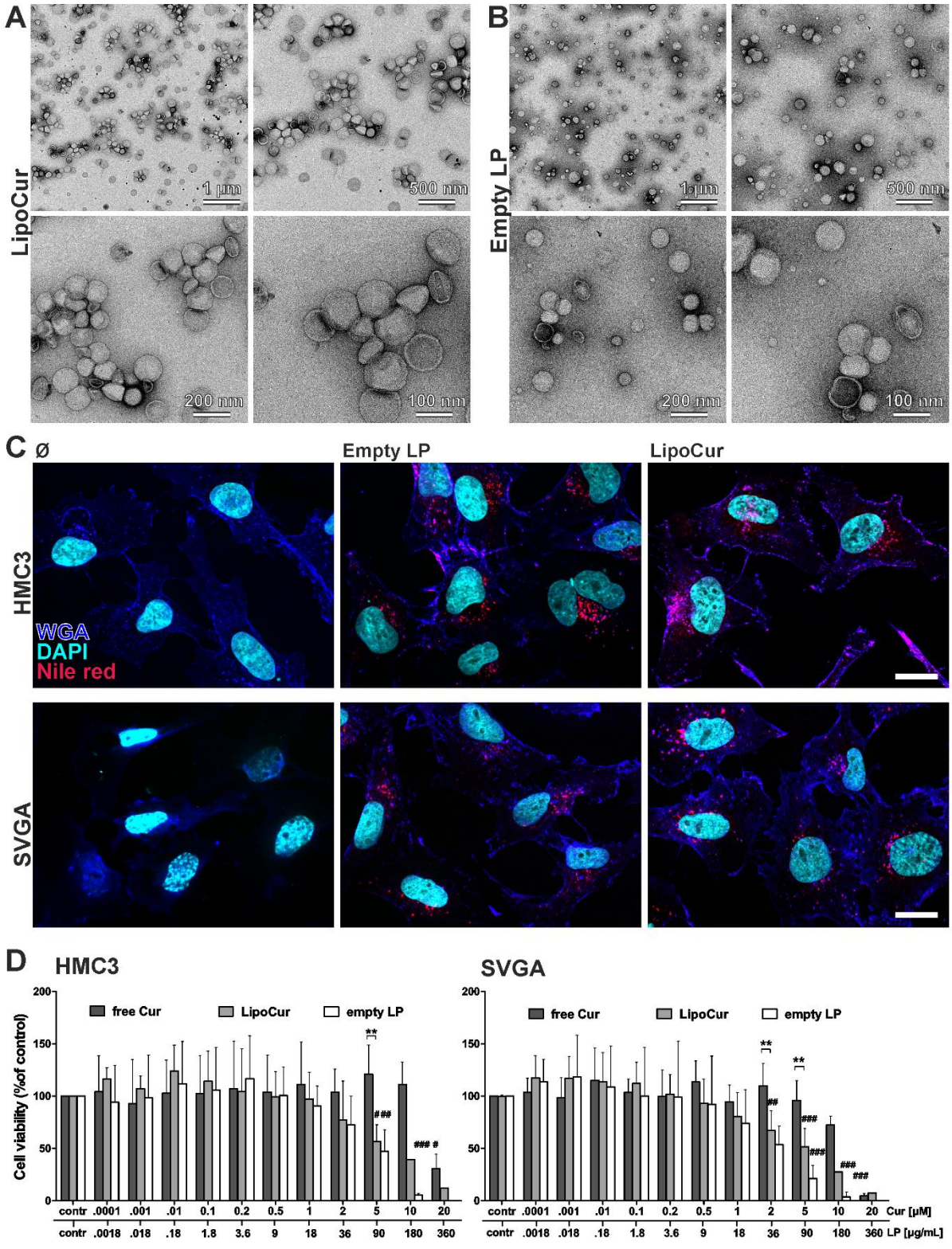
A
LipoCur
1 µm
500 nm
200 nm
100 nm
B
Empty LP
1 µm
500 nm
200 nm
100 nm
C
ø
Empty LP
LipoCur
HMC3
SVGA
WGA
DAPI
Nile red
D
HMC3
SVGA
free Cur
LipoCur
empty LP
Cell viability (%of control)
contr .0001 .001 .01 0.1 0.2 0.5 1 2 5 10 20 Cur [µM]
contr .0018 .018 .18 1.8 3.6 9 18 36 90 180 360 LP [µg/mL]

Figure 3

Figure

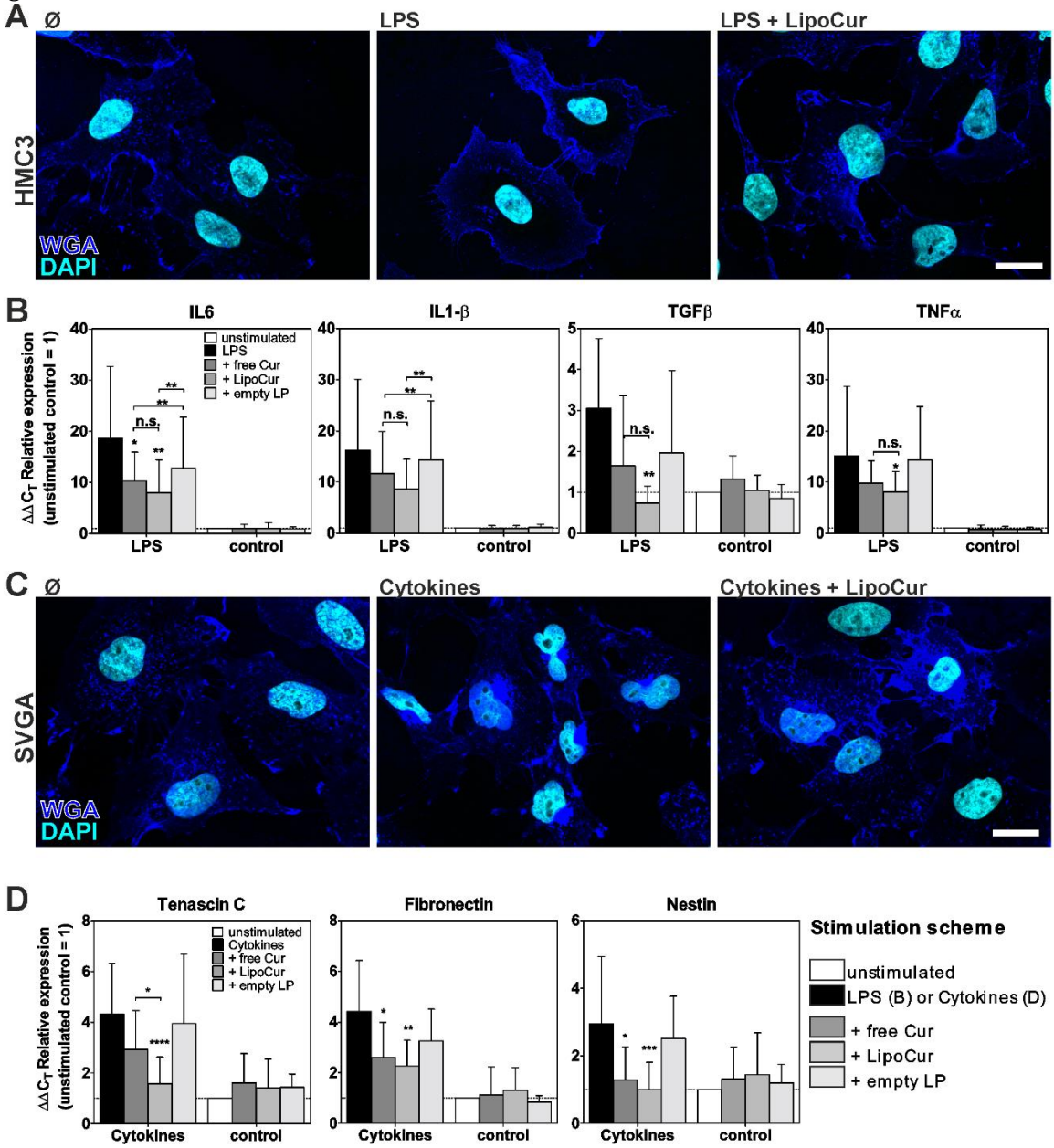

Figure 4

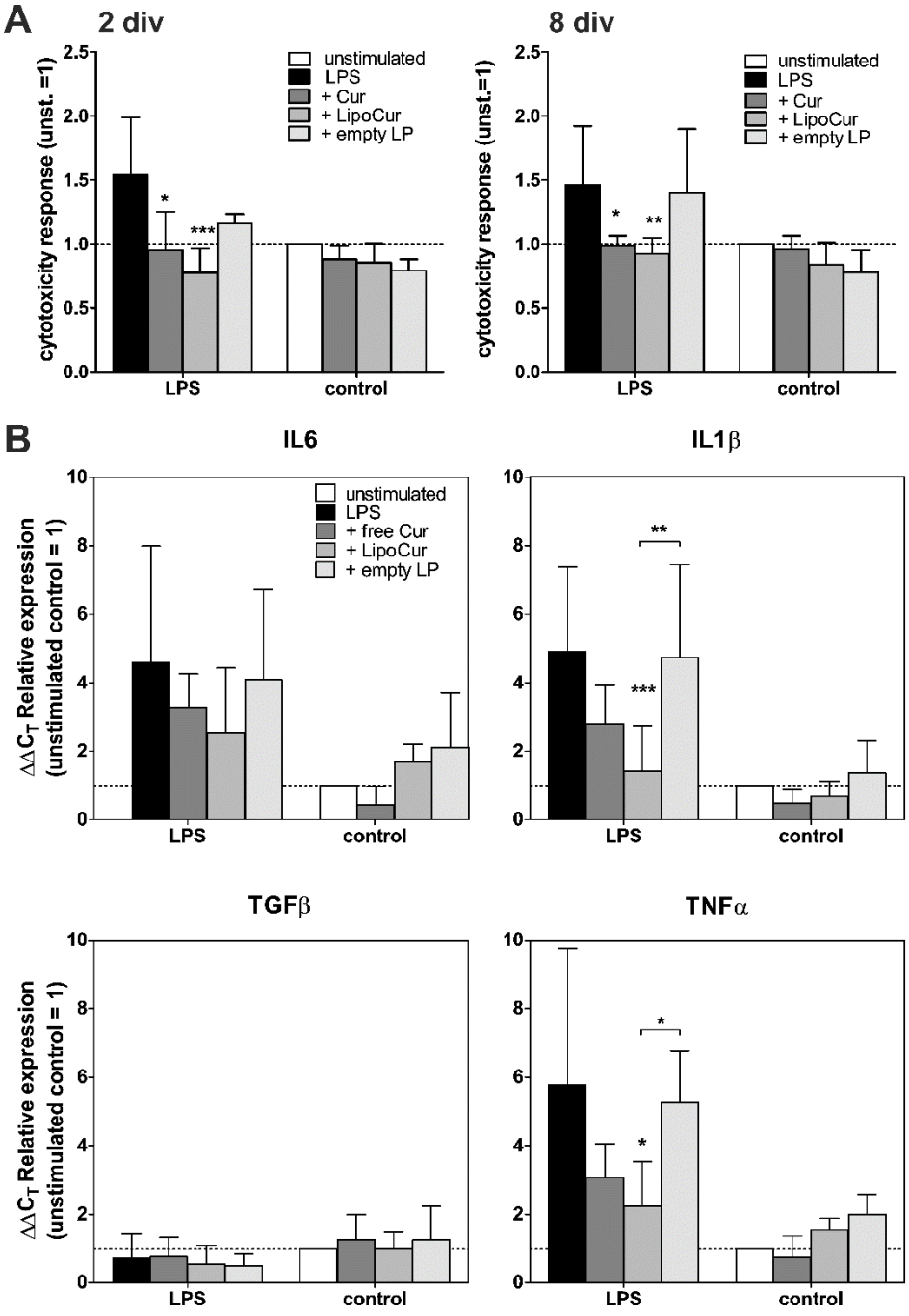
A
2 div
8 div
cytotoxicity response (unst. =1)
unstimulated
LPS
+ Cur
+ LipoCur
+ empty LP
LPS
control
B
IL6
IL1β
TGFβ
TNFα
ΔΔCT Relative expression
(unstimulated control = 1)
+ free Cur

Figure 5

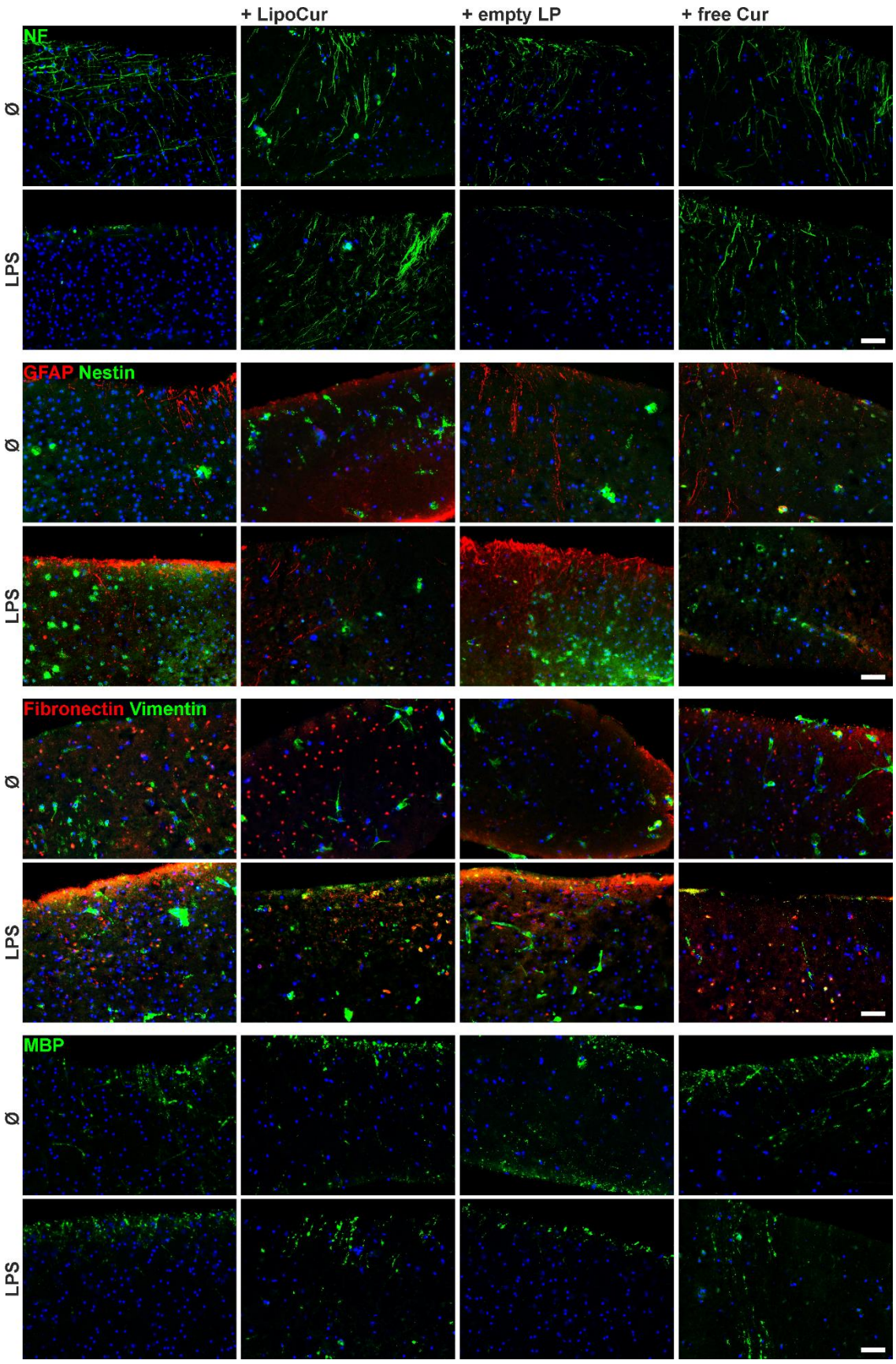
+ LipoCur
+ empty LP
+ free Cur
NF
Ø
LPS
GFAP Nestin
Ø
LPS
Fibronectin Vimentin
Ø
LPS
MBP
Ø
LPS

Figure 6

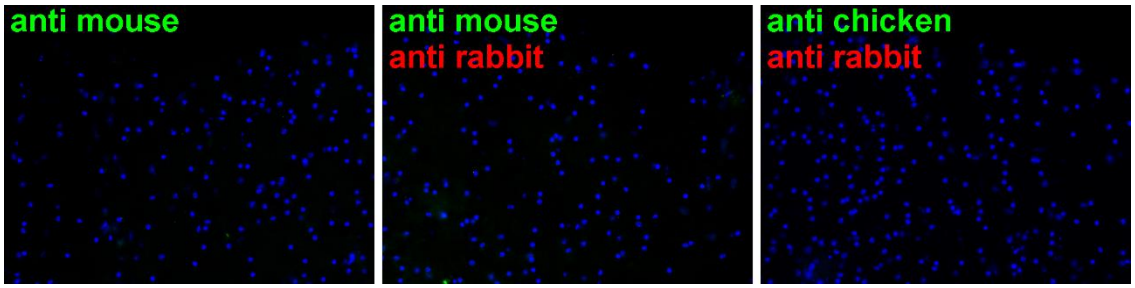

Supplement to Figure 6

3rd CHAPTER

Discussion

"Nothing in life is to be feared, it is only to be understood. Now is the time to understand more, so that we may fear less."

(Marie Curie)

The treatment of brain disorders, such as the highly malignant brain tumor *glioblastoma multiforme* remains to date challenging due to the low five years survival rate with only five out of 100 patients surviving in ages above 45 years (American Cancer Society 2019). Following the classical systemic drug administration as in most cases of the chemotherapeutic agent temozolomide in combination with radiotherapy (Stupp et al. 2005), patients continue to undergo multiple surgeries and poor prognosis, due to the heterogeneity of the tumor. Besides new therapeutically approaches such as alternative therapeutics, also the devotion of local drug administration systems such as brain implants raise hope. Thus, as part of the GRK "Materials4Brain" and in collaboration with Vivian Adamski (UKSH, Kiel) and Florian Rasch (technical faculty, Kiel), new treatment strategies were developed and tested in a new *in vitro* model to mimic distinct tumor resection statuses, as well as a polymeric drug delivery device for the local drug administration in the brain has been developed for the treatment of GBM. In this concern, it is noteworthy to mention, that my focus in this collaborative work was the investigation of effects of drugs and material-drug combinations on healthy cells of the brain, whilst Florian Rasch produced the material templates and Vivian Adamski investigated effects on GBM cells. Likewise, since surgeries and the implantation of drug-loaded materials can elicit brain foreign body responses of the healthy brain microenvironment, investigations on material-induced neuroinflammation and reactive astrogliosis have been studied in detail and been tried to alleviate by the application of anti-inflammatory drugs such as curcumin.

"The development of novel therapeutics, which inhibit more than one 'hallmark of cancer' (e.g., angiogenesis, GBM cell invasion, proliferation and/or apoptosis) and which act synergistically with standard treatment regimens, remains a critical objective" (Jarzabek et al. 2014)

As stated above, GBM patients' overall prognostic remains poor, due to the miscellaneous heterogeneity of the tumor mass which consists of cell subpopulations with different abilities to respond or escape to/from treatment (Yeh and Ramaswamy 2015). In fact, some of these subpopulations are able to enter a resting state called cellular dormancy, in which they do not respond to treatment and therefore may be the cause for recurrences of the tumor after resection. One approach to circumvent chemoresistance in tumors can be the use of drug combinations that act through different mechanisms of action or by sequentially applying them (Keith et al. 2005). If patients are not part of clinical trials in which alternative treatment approaches are being evaluated, the standard therapy persists the treatment with radiotherapy concomitant with adjuvant temozolomide oral systemic application (Zhang et al. 2012). Temozolomide is a prodrug which at physiological pH is converted to its active compound MTIC, that as an alkylating agent induces cell cycle arrest at G2/M phase and therefore apoptosis (Alonso et al. 2007). Besides apoptosis, also autophagy as another mechanism of action can be a promising target in tumor therapy (Paglin et al. 2001).

Respecting this it has been shown recently, that GBM cells not only uphold proliferation by oxidative phosphorylation and aerobic glycolysis but also by autophagy (Rabinowitz and White 2010; Kriel et al. 2018). Hence, regarding the molecular crosstalk between regulators of apoptosis and autophagy, recent investigations focus on the combination of chemotherapeutics with either autophagy inhibitors such as quinoline-based therapeutics or autophagy inducers such as AT101 (Rangwala et al. 2014; Arcella et al. 2013). Indeed quinoline-based drugs such as CQ and HCQ as well as the naturally occurring BH3 mimetic AT101 have gained interest in various cancer therapy approaches to date (Maclean et al. 2008; Dutta et al. 1994; Rosenfeldt et al. 2013; Qiu et al. 2002; Mohammad et al. 2005; Wolter et al. 2006; Meng et al. 2008). As such, Hu et al. have combined bevacizumab with CQ in mice GBM models (Hu et al. 2012), or Shen and others used vandetanib-CQ combinations (Shen et al. 2013) in similar *in vivo* approaches and could significantly suppress tumor growth [for review see (Verbaanderd et al. 2017)]. Conversely, AT101 could decrease proliferation in *in vitro* and *in vivo* studies in the treatment of GBM (Voss et al. 2010; Coyle et al. 1994) since it binds to the BH3 groove of Bcl-2, Bcl-X_L respective Mcl-1 (Qiu et al. 2002) and therefore decreases proliferation of cancer cells. However, Jarzabek and others stated in 2013, that there is the need for novel therapeutics that in fact inhibit more than one "hallmark of cancer", by addressing different mechanism of action such as angiogenesis, proliferation and/or apoptosis or GBM cell invasion for instance (Jarzabek et al. 2013).

Hence, many studies on drug combinations for GBM treatment are available. As such, Golden and others were the first to demonstrate that the simultaneous treatment of TMZ with CQ can cause protein/growth arrest and DNA damage in U87MG mice models (Golden et al. 2014). Likewise, the efficacy of TMZ and concomitant HCQ therapy was studied in combination with radiotherapy in 92 GBM patients, whereas high maximum tolerated doses pf 600 mg/day were indicated, however without consistent response on autophagy inhibition (Rosenfeld et al. 2014). However, previous studies are deficient in sequentially application of drugs in combination with standard radio-chemotherapy. Therefore, our study (chapter 2.1) focusses on the comparison between simultaneous and sequentially applied treatment regimen of the standard therapeutic agent temozolomide, concomitant with the autophagy inhibitor HCQ respective the autophagy-induced apoptosis inductor AT101. In addition, to provide efficient tumor growth control however keeping negative side effects as low as possible, the drug combinations were not only tested on GBM cells (as performed by Vivian Adamski) but also on healthy astrocytes. Hence, multiple GBM cell lines are available, amongst which it is known that they differently respond or even are naturally resistant to TMZ treatment. Therefore, adapted GBM cell lines with resistances to TMZ have been developed to study more deeply the mechanism of TMZ resistance (Lee 2016). To address this issue, in our studies the two GBM cell lines LN229 and A172 have been employed as they in principal respond to TMZ however with different extend (Adamski et al. 2017; Lee 2016) and have shown to be able to escape treatment by switching into a dormant state (Adamski et al. 2017). Therefore, cells were stimulated with drug concentrations of 50 µM TMZ, 6 µM HCQ and 2.5 µM AT101 similar to liquor/plasma concentrations *in vivo* (Rosenfeld et al. 2014) for a period of six days and cytotoxic effects as well as on proliferation were determined after days three and six.

In a first attempt, cells were stimulated with the single drugs TMZ, HCQ respective AT101 or simultaneously with combinations of TMZ+HCQ or TMZ+AT101 for six days, to evaluate the single effects as well as combined effects over three and six days (see figure 6, A). Whereas the therapeutically standard TMZ caused 9.95-fold ± 4.29 dead cells in A172, respective 12.54-fold ± 3.12 in LN229 and up to 8.12-fold ± 4.29 in SVGA, the single administration of either HCQ or AT101 were less effective on both GBM cell lines and therefore also less harmful for healthy astrocytes. These results are in line with the investigations of Wolpin and others, who demonstrated in phase II study of pancreatic cancer a negative efficacy of single applied HCQ [(Wolpin et al. 2014) for review see (Chude and Amaravadi 2017)]. Moreover similar investigations on the response of astrocytes have been made with an alternative Bcl-2

inhibitor, ABT-737, which has also shown to be less harmful in low concentrations than on GBM cell lines (Vidomanova et al. 2016). Further, Jarzabek et al. have reported, that AT101 solely did not beneficially improve tumor growth control in an *in vitro* long-term stimulation model as well as in a mouse *in vivo* model (Jarzabek et al. 2014). However, Voss and others as well as Coyle et al. demonstrated that AT101 could decrease proliferation in GBM cells *in vitro* (Voss et al. 2010; Coyle et al. 1994).

Interestingly, the combined therapy of TMZ+HCQ caused with significance an up to two times higher number of dead cells in A172 and around three times higher amount in LN229 after six days compared to TMZ solely, however also with significant increasing cytotoxic effects on SVGA. In contrast to that, Rosenfeld et al. demonstrated in a clinical trial that a concomitant therapy of TMZ with high doses of HCQ, however below the maximum tolerated dose with 600 mg/day, in combination with radiotherapy did not consistently inhibit autophagy and therefore not cause significant improvement in GBM therapy (Rosenfeld et al. 2014). Moreover, in maximum tolerated doses of 800 mg/day, HCQ in co-stimulation with TMZ did cause many negative side effects in patients, such as grade three and four neutropenia and thrombocytopenia (Rosenfeld et al. 2014). In contrast to that, CQ combined with classical GBM therapy was reported to have positive effects on GBM growth control in humans (Briceño et al. 2003; Briceño et al. 2007), however it is known that HCQ causes less negative side effects and therefore allows higher doses of HCQ compared to CQ *in vivo* (Schroeder and Gerber 2014; Sundelin and Terman 2002).

Contrary to that we could demonstrate, that the co-stimulation with AT101 does positively influence the survival of healthy astrocytes, as stimulations of TMZ+AT101 over six days increased cytotoxic effects of TMZ around four times in A172 and three times in LN229 whilst being less toxic to SVGA astrocytes. This effect of AT101 to sensitize TMZ-induced cell death in GBM cells has been confirmed already some years ago (Voss et al. 2010; Jarzabek et al. 2014). Concomitant with these findings, the synergy quantification after Chou-Talalay (Chou 2010; Chou and Talalay 1984) proofed that the combined treatment of TMZ+HCQ as well as TMZ+AT101 had additive or even synergistic effects in human glioma cell lines, however on human astrocytes being either less effective or as theoretically expected. Moreover Golden and others could demonstrate that combined therapy of gossypol and TMZ inhibits tumor-associated angiogenesis, proliferation as well as invasion (Golden et al. 2015).

In a second step, single drugs or drug combinations were given sequentially, so that the treatment scheme was switched on day three, as described in figure 6, A. Overall, we could show that sequentially applied treatment-schedules are more efficient than simultaneously applied, however with some extinctions. For instance, stimulations starting with TMZ for three days and switching to HCQ, AT101 or the combination of TMZ+HCQ respective TMZ+AT101, stimulations did not cause stronger cytotoxic effects on healthy astrocytes than the standard TMZ therapy, nor did it affect the relative growth rate of astrocytes negatively. Conversely, effects on the growth rates as well as cytotoxicity of both A172 and LN229 GBM cell lines were moderate. Interestingly, the exact same combinations, however in a different order starting with HCQ or AT101 and switching to TMZ or the TMZ-drug combination did not cause any effects on cytotoxicity as well as on proliferation on astrocytes as well as GBM cell lines, showing that in some cases sequential stimulations being significantly less effective on GBM cells, however less harmful on healthy cells. In comparison to our findings, in a phase I clinical trial starting with an initial HCQ administration followed by a dose-intense combination of TMZ+HCQ a good tolerance in patients with advanced solid tumors has been shown, however with only moderate improvement on the progression-free survival of the patients (Rangwala et al. 2014). In addition, treatment schedules starting with the combined treatment of TMZ+HCQ for three days and switching to HCQ did significantly increase the n-fold amount of dead cells in A172 and LN229 to similar levels as the simultaneous combined treatment of TMZ+HCQ over six days as well as decrease the relative growth rate tremendously, however being also very toxic for healthy astrocytes. Contradictory to these findings, combinations starting with TMZ+AT101 and switching to AT101 significantly increased the n-fold number of dead cells in both GBM cell lines whilst being as/ or

less effective on healthy human astrocytes. More interestingly, while this sequentially applied drug combination did decrease proliferation in both GBM cell lines, we could demonstrate even an induction on proliferation on SVGA astrocytes.

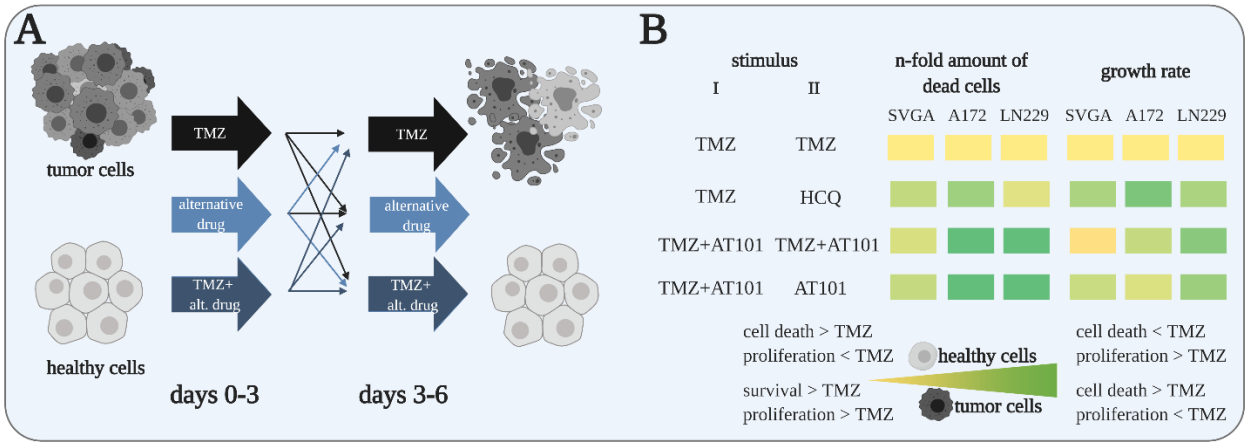

Figure 6: Treatment schedule of simultaneous or sequentially applied drugs or drug combinations over three respective six days (A), as well as a simplified overview of the most promising treatment regimens as a heatmap (B). *Healthy human astrocytes as well as two GBM cell lines (A172 and LN229) were stimulated with the standard therapeutic agent temozolomide (TMZ) or an alternative drug such as hydroxychloroquine (HCQ) or AT101, respective the combination of TMZ with HCQ/AT101 for three days. On day three, stimulation regimen either stayed the same (continuous stimulation) or switched to either the single drug TMZ, HCQ or AT101 or the combination of TMZ with alternative drug (sequential stimulation). Cytotoxicity and proliferative effects of drugs/drug combinations on cells was determined after days three and six (A). The most promising drug combinations after six days stimulation are highlighted in a heatmap, compared to the response to TMZ (yellow). The greener the heatmap, the more advantageous was the treatment over TMZ standard therapy, with a better tumor growth control whilst keeping healthy human astrocytes as unaffected as possible (B). This figure was generated using the Biorender software.*

A summary of the most efficient drug treatment schedules for the improved growth control and cytotoxicity on GBM cells, combined with the smallest negative side effects on healthy astrocytes is depicted in the heatmap of figure 6, B. Respecting this, the most promising drug combinations were sequences of TMZ/HCQ, TMZ+AT101/AT101 as well as the simultaneous treatment TMZ+AT101/TMZ+AT101 over six days. Moreover, we could demonstrate the necessity to not only readout a drugs' cytotoxic effects upon stimulation, but also to investigate the proliferation of cells, as their response can be quite distinct to the same stimulus. Proliferation data especially implicates the amount of remaining tumor cells after treatment, that in perspective could be the tumor fraction responsible for recurrences. Therefore, it is necessary to develop treatment strategies that do include both factors in GBM treatment and recurrence. Our investigations show, that our long-term *in vitro* model comparing drug-effects on different drug-responding GBM cells in comparison to healthy human astrocytes is a suitable model to investigate drug-combinations for the treatment of GBM. The fact, that some stimulations seemed to be very promising in the treatment of GBM cells, but indeed also more drastically affected healthy SVGA astrocytes, emphasizes the need to investigate drug-effects not only on target cells but also on the target-cell microenvironment.

"Novel *in vitro* models can help to predict the *in vivo* efficacy of new therapeutics in brain tumors"

The previous discussed results emphasize the need for better test methods of suitable drug candidates and drug concentrations in GBM therapy, as the tumor is characterized by a highly heterogeneous tumor cell population and since its therapeutic success is highly influenced by the tumor microenvironment. Moreover, some interesting drug candidates might fail in *in vivo* studies or in clinical trials due to too strong side effects on healthy brain tissue. Indeed, several GBM *in vitro* models have been developed such as GBM

neurospheres, the cultivation of GBM monocultures in a 3D system or patient derived 3D microtumors which can be used for prediction of the clinical outcome of patients (Laks et al. 2009) respective as recently shown the high-throughput screening of drugs (Gilbert et al. 2018). However, these systems lack the influence of the tumor microenvironment as well as the cytotoxic effects of drug candidates on healthy brain cells. Moreover, the patient's prognosis highly depends on the success rate of the tumor removal: Whilst the total resection of the tumor is the preferred scenario, the reality in most cases stays the subtotal resection of the tumor mass in consequence to an impracticable location of the tumor.

Therefore, to take the different scenarios of tumor resection, the heterogeneity of the tumor as well as the tumor environment into account, we developed a dual co-culture model mimicking the total and subtotal resection of an average GBM tumor which is suitable for local applied drug or drug/implant combination testing (see figure 7, A). In brief, the average size of a resection cavity of 3 cm diameter was consulted to calculate the overall surface fraction of around 28.3 cm^2 which can get into direct contact with locally applied drugs or brain drug delivery systems (Murray 2012; Bette et al. 2018). Moreover, the relative ratio between tumor cells and healthy brain cells was determined based on published data. In the healthy brain, the knowledge about cell ratios is quite diverse, however Bartheld et al. describe numbers of around 40 % oligodendrocytes, 40 % astrocytes respective 20 % microglia (Bartheld et al. 2016). Likewise, there are no case reports about the cell ratios in GBM patients after a total resection of the tumor, whereas it is known that GBM cells strongly interact with their microenvironment leading to an increase of astrocyte migration towards the tumor tissue as well as tumor infiltrating microglia/macrophages and therefore change the ratios of cells in the direct tumor surrounding (Matias et al. 2018; Oliveira et al. 2017; Quail and Joyce 2017). Thus, regarding the increase of astrocytes in the direct tumor microenvironment as well as a decrease of tumor-infiltrating microglial cells due to the tumor resection, we calculated the ratio of cells for the complete resection model with 80 % astrocytes, 10 % microglia and 10 % remaining tumor cells (see figure 7, C). Conversely, for the incomplete resection – as this represents the majority of cases – more data is available on the remaining cell populations after resection. It has been described by Roggendorf and others that the tumor microenvironment consists of 30 % glial cells which can be divided up into 1 % reactive astrocytes as well as 29 % tumor associated microglia respective macrophages (see figure 7, B), therefore we chose these cell ratios for the incomplete resection model. Final cell numbers were determined dividing the surface area of the resection cavity by the respective cell ratio and each cell types' average size. Moreover, to also include the aspect of tumor heterogeneity, we employed two different primary cultures (PC) of human GBM cells for both *in vitro* models that respond differently to TMZ treatment.

To evaluate the applicability of the *in vitro* dual co-culture, we compared data on proliferation and cytotoxicity of monocultures versus dual co-culture upon stimulation with the most promising drug combination of TMZ+AT101 over three days followed with three days single AT101 stimulation which was evaluated previously. Interestingly in the incomplete resection model, we could demonstrate that effects (growth rate as well as cytotoxicity) on HMC3 microglial cells upon drug stimulation are comparable between mono cultivation as well as in co-cultivation, whereas both primary GBM cell cultures responded slightly less to the treatment with higher proliferation rates and smaller amounts of dead cells compared to mono cultivation. Likewise, SVGA astrocytes, when cultivated in the incomplete dual co-culture were affected more in respect of cytotoxic effects upon drug-stimulation but also in controls compared to monocultures. This effect was significantly higher after three days of cultivation with an almost two times higher death rate compared to mono cultivation. Contrary to that in the complete resection model, no effects of co-cultivation were detectable for SVGA astrocytes as well as HMC3 microglial cells when cultivated with both primary GBM cell types, however both glioblastoma primary cultures responded less on the drug treatment schedule when cultivated in co-culture.

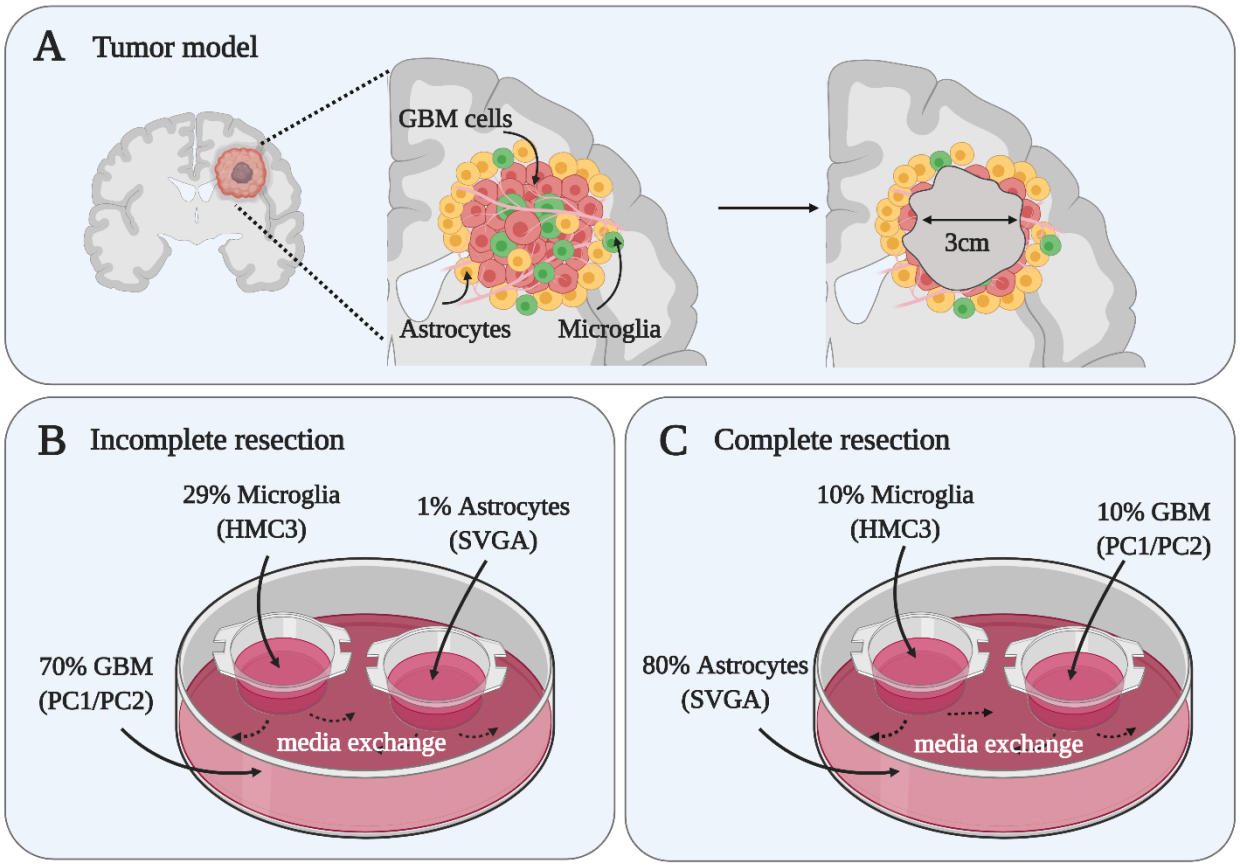

Figure 7: Illustration of the implemented in vitro dual co-culture model for the incomplete and complete resection of an average size GBM tumor. *The direct tumor microenvironment consists besides blood vessels of around 30 % glial cells, such as microglia and astrocytes which are also partially infiltrating the bulk tumor mass (A). Based on literature the ratios of glial cell types and GBM cells in respect of the resection state (incomplete resection, B and complete resection, C) were determined. This figure was generated with Biorender.com*

Concomitant with these findings, we demonstrated on the one hand the influence of the GBM-microenvironment on the survival of GBM cells upon treatment, and vice versa the influence of GBM cells on the overall survival of the healthy tumor surrounding. To analyze in more detail the factors influencing the undergoing of astrocytes especially in dual co-cultures of the incomplete resection (as they were more prominent), we evaluated on the one hand the effects of GBM population-size on the survival and growth rate of astrocytes and on the other hand the mRNA expression of different chemokines and cytokines in PC1 glioblastoma cells after co-cultivation with SVGA astrocytes and HMC3 microglia cells. In brief, we could determine a significant positive correlation between increasing amounts of seeded PC1 GBM cells and the percentage of dead SVGA astrocytes cells. Conversely, we observed a negative correlation between the amount of GBM cells and the growth rate of astrocytes. The more GBM cells are present in the incomplete dual co-culture, the higher the percentage of dead cells as well as the lower the growth rates of SVGA astrocytes. Indeed, distinct reactions of tumor cells upon drug-stimulation have been described comparing monocultures or two-dimensional (2D) culture systems with 3D networks of heterogeneous cell populations (Imamura et al. 2015). As such, Imamura et al. observed drug resistances and protective effects from paclitaxel-induced apoptosis in 3D breast cancer models compared to 2D models (Imamura et al. 2015). Similar, other studies have demonstrated distinct effects of tumor cells on drug treatment when cultivated in monocultures or in 3D networks such as in organotypic brain slice models (Chadwick et al. 2015; Kenny et al. 2015). Moreover, the protective effect of microglia and astrocytes on the survival of

GBM cells has been already described by others [(Hattermann et al. 2014; Matias et al. 2018), an overview of the influence of the microenvironment in GBM is given in figure 8].

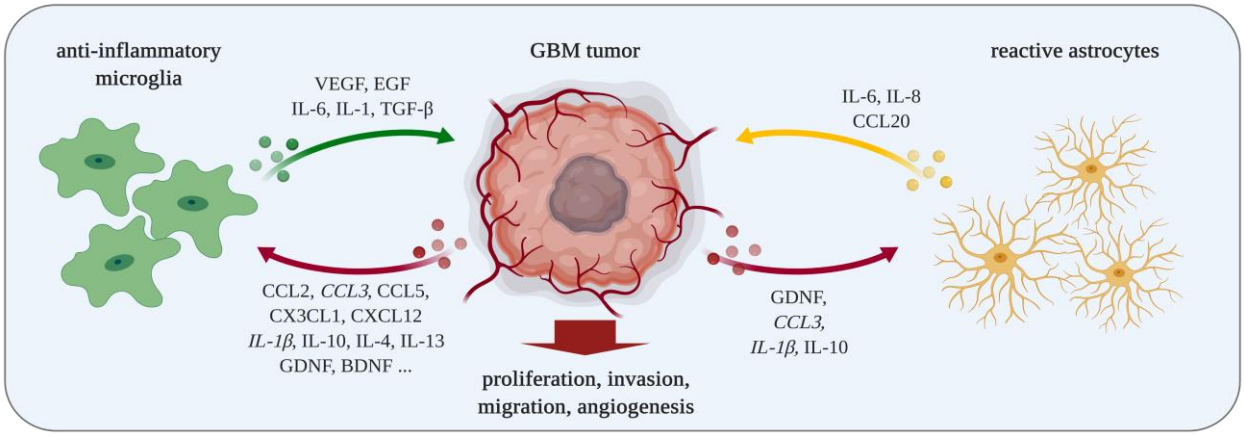

Figure 8: Simplified illustration of the rescuing effects of microglia and astrocytes in the GBM-microenvironment on the survival of GBM cells*. The figure was designed using the Biorender software and is adjusted to (Matias et al. 2018) and our own results (shown in italic).*

In fact, tumor associated macrophages and microglia are represented in higher numbers with increasing tumor grade and have tended to act pro-tumorigenic (Hattermann et al. 2014). Therefore, we analyzed possible soluble factors in GBM cells (PC1) after three days, which when released may be responsible for the effects on healthy brain cells in the incomplete resection model. Therefore, the gene expression of several cytokines and chemokines in GBM cells was determined and likewise the expression of possible receptors on astrocytes and microglia. Interestingly we could show, that cytokines such as IL-1β, TNF-α and IL-6 are upregulated in monocultures upon stimulation, however either less regulated or even down regulated upon co-cultivation in the incomplete dual co-culture. This effect was more prominent for the chemokine CCL3 which was even significantly upregulated for both, the mono as well as co-cultivation, however significantly less upregulated in co-culture. In line with our findings, it has been described in literature that glioma cells can induce the anti-inflammatory phenotype in microglial cells by the release of several cytokines and chemokines and therefore in turn cause microglia to release factors which have shown to stimulate tumor growth (Hambardzumyan et al. 2016; Lisi et al. 2017). In this context, the influence of the anti-inflammatory microglia phenotype on the aggressiveness and prognosis of GBM patients has been mentioned (Mieczkowski et al. 2015; Iglesia et al. 2016; Gieryng et al. 2017b). Likewise, other studies revealed the ability of tumor cells, by releasing factors such as IL10, to stimulate the anti-inflammatory phenotype of astrocytes [(Guan et al. 2018), for more information revise (Matias et al. 2018)].

In summary, we were able to establish an *in vitro* model for the complete and incomplete GBM resection that allows to study responses of each single cell population towards drug stimulation as for cytotoxicity, proliferation but also on mRNA level. Moreover, comparing our dual co-cultures to current mono-culture systems, our model reflects closer the *in vivo* conditions and responses towards treatment since it allows paracrine communication between different cell types. In addition, we focused on the development of a surgical-relevant *in vitro* test system, as to date no *in vitro* models are available which mimic the different resection scenarios and also give the opportunity to analyze single cell responses in detail. However, we are aware that our dual co-culture systems only allow paracrine crosstalk and exchange of molecules due to the separate growing in cell culture inserts. Moreover it has been described, that monolayer-cultivation of cells such as colorectal cancer or cardiac cells, does not mirror responses towards cytotoxic treatments as observed in patients, due to a profound phenotypical change upon cultivation (Caragher et al. 2019; Zschenker et al. 2012; Luca et al. 2013; Pontes Soares et al. 2012). Therefore, to study the cell-cell interconnectivity more detailed, other already implemented models can be employed that may

reflect better the endocrine crosstalk (Caragher et al. 2019; Lenting et al. 2017). As such, biopsy-derived organotypic spheroids or organotypic brain slice models that comprise the interconnectivity between different cell types might be of interest (Kenny et al. 2015; Chadwick et al. 2015; Caragher et al. 2019), which might be also more stable to culture conditions without serum addition. In particular, it is well described that serum addition does not represent physiological *in vivo* conditions (William et al. 2017), nevertheless in preliminary experiments on cultivation conditions, HMC3 microglia were clearly affected in low/no serum conditions (data not shown), therefore clearly limiting our *in vitro* co-culture models. However, other culture systems do on the one hand not allow to mimic the resection state of the tumor as precise cell numbers and ratios between different cell types cannot be obtained, and on the other hand limit the possibility to investigate single cell responses on proliferation, cytotoxicity as well as on gene expression level upon the influence of cell-cell interaction. As such in a very recent approach, patient derived tumor cells were co-cultivated in 3D scaffold matrices containing brain-ECM components with healthy astrocytes, whereas GBM cells as well as astrocytes were incubated with different stains individually to allow real-time imaging of the differentiated cells (Sood et al. 2019). However, although this approach delivers great improvements in the co-cultivation of healthy brain tissue with GBM cells in vitro, cell dependent responses are still hard to quantify in these systems as well as patients' tumor resection-scenarios are challenging to reflect.

In perspective, there is the need to develop and employ better *in vitro* test systems that allow biologically relevant investigations of drug-cell interactions which mimic more closely the *in vivo* situation. With the development of our GBM (in)complete dual co-culture model we believe that our *in vitro* platform can help to analyze drug-efficacies more detailed especially for the application in local drug delivery systems.

"Local drug administration into the brain can improve patients' outcome due to site-specific therapy and non-systemic *in vivo* toxicity"

The previous described investigations imply the necessity to develop on the one hand new treatment strategies that can significantly influence the tumor growth control as well as prevent tumor recurrences and on the other hand reduce negative side effects in patients as well as increase patients' compliance towards treatment. However, many chemotherapeutics are administered systemically with concomitant negative side effects, as such also the standard chemotherapeutic compound temozolomide. Whilst TMZ is able to pass the blood-brain barrier, other molecules or possible drug candidates for GBM therapy struggle due to their size, structure or chemical properties and therefore are limited in their *in vivo* efficacy. Therefore, approaches to successfully transport drugs through the BBB include the surface functionalization of NPs with proteins to target specifically glucose-transporters for instance respective the targeting of surface receptors such as the neonatal Fc receptor or insulin receptor. Other strategies are based on the use of suitable sizes and surface charges of drug-carriers, as the uptake of molecules through the BBB is highly size-dependent (Bozzuto and Molinari 2015). However, although small molecules are supposed to be freely transported through the BBB, only 2 % of them really manage the transport across the BBB (Pardridge 2005). In fact, the permeation of molecules decreases 100-fold when the molecular weight increases from 300 Da to only 450 Da (Fischer et al. 1998).

One promising approach to circumvent the challenging drug delivery through the BBB is by local administration of the drug to the target site using brain implants. Major advantages besides the direct application towards the target site is the tailorable release kinetic, such as an immediately release, the option to lengthen the release or even to establish a pulsatile drug release in function of the disease condition and the mechanism of action of the drugs (Sanjay et al. 2018). In fact, many strategies to develop drug delivery devices have been introduced, all based on several different release-mechanisms such as chemically controlled biodegradable materials (Makadia and Siegel 2011; Kumari et al. 2010; Zeng et al. 2003),

diffusion-based drug release (Langer and Folkman 1976; Stevenson et al. 2012) or by drug loaded hydrogels or osmotic pumps for instance (Bastiancich et al. 2016; Verma et al. 2004). As such, the FDA approved Gliadel® wafer, consisting of biodegradable polyanhydride loaded with carmustine is one of the most well studied local drug delivery devices for GBM treatment to date, however still not sufficiently improving GBM patients' outcome. Moreover, Brem and others have demonstrated that TMZ-loaded polymer wafers could decrease the TMZ-associated negative side effects in local applications, as lower plasma concentrations where also measured due to a degradation-dependent drug release (Brem et al. 2007).

Besides this, micro- and nanochannel derived systems have gained interest in recent years, as they offer improved control mechanisms of the drug release kinetics, for example offering zero-order or pulsatile release kinetics (Celia et al. 2014; Duan et al. 2013; Yang et al. 2010; Yang et al. 2018). Yang and others for instance developed a reservoir-based microchannel system of PDMS which by tailoring microchannel length, width, number and straightness is able to release drugs with a zero-order release kinetic (Yang et al. 2018). However, most approaches are time- and cost-intensive and limited in their size due to the fabrication process (Stevenson et al. 2012; Sanjay et al. 2016; Martin et al. 2005). Therefore, in collaboration with the technical faculty Kiel as well as the UKSH Kiel, macroscopic 3D microchannel matrixes of PDMS have been produced for the local delivery of alternative therapeutically compounds to treat GBM. Whereas the production and physicochemical analysis of the templates were performed at the technical faculty, release-studies of AT101 were determined at the UKSH and efficacy studies of drug-loaded templates were performed *in vitro* on glioblastoma cells (UKSH) and on healthy cells by me (institute of anatomy). In brief, highly sacrificial Zinc Oxide (ZnO) tetrapodal templates have been produced in a bottom-up approach as described before (Mishra et al. 2013; Mishra et al. 2015; Gedamu et al. 2014), followed by an infiltration with PDMS. After curing of PDMS and removal of ZnO by wet-chemical etching, a 3D hollow microchannel network of PDMS with inverse structures of the former ZnO tetrapodal network remains, which was used for vacuum-infiltration of AT101 (see figure 9 B).

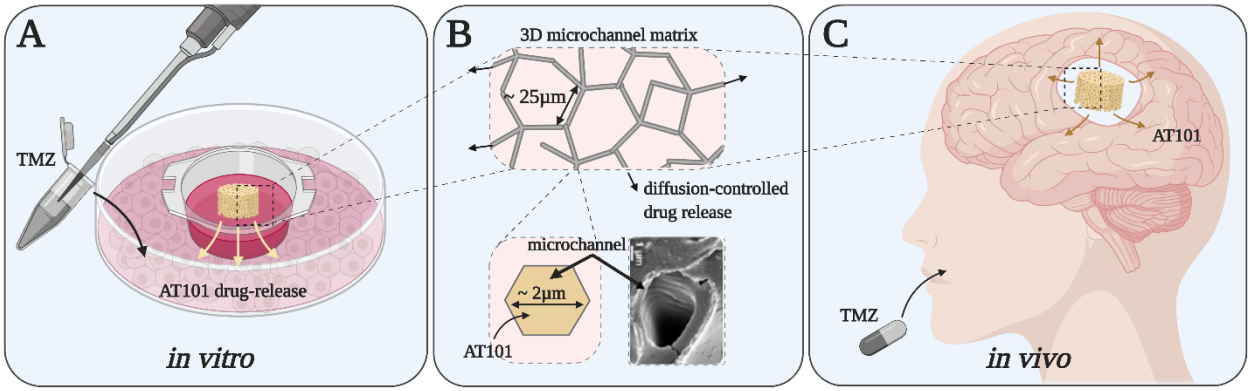

Figure 9: Illustration of the in vitro and in vivo applicability of AT101-releasing highly sacrificial PDMS templates in co-stimulation with temozolomide. *Human SVGA astrocytes as well as LN299 and A172 glioblastoma cell lines were stimulated by template releasing AT101 as well as free temozolomide (TMZ) application in therapeutic concentrations in vitro (A). The PDMS template consists of a 3D hollow microchannel matrix with a diameter of around 2 µm which can be infiltrated with hydrophilic as well as hydrophobic drugs and shows a classical diffusion-controlled drug release (B). In perspective in vivo applications, AT101 can be locally administered by brain-implants in concomitant systemic application of TMZ via oral drug administration (C). Figure was created using the Biorender software and adapted to our submitted work.*

By adjusting the size of the DDS, the number of microchannels, variation of the open microchannels employing laser surface structuring or the drug-concentration used for infiltration, the release kinetics of AT101 could be easily adapted and tailored. Characteristically, the AT101 release could be tailored in function of infiltrated AT101 concentration as well as porosity of the implant and did match with typical diffusion-driven release profiles starting with a fast increasing concentration followed by a slower release until finally saturation of the drug (Pedraza et al. 2013). In line with this, other drug delivery based systems such as 3D printed PDMS layers cross-linked by UV light as well as solvent casting and leaching methods to release anti-inflammatory drugs such as prednisolone or dexamethasone were able to achieve a long-term

drug release over four weeks (Holländer et al. 2018; Jiang et al. 2017). In 2010, Ranganath et al. have described a diffusion-controlled release of paclitaxel from PLGA nanofiber discs as well as PLGA-microspheres entrapped in hydrogel matrixes for over 42 days, and could demonstrate significant tumor inhibition in glioblastoma xenograft mouse models *in vivo* (Ranganath et al. 2010).

Consequently, as the drug-loaded DDS should be tested for its efficacy in the treatment of GBM cells whilst not affecting the healthy brain microenvironment, a relatively fast increasing drug concentration of ≈ 4.5 µM AT101 within the first 24 hours was necessary to be able to reach therapeutically concentrations for *in vitro* applications. Therefore, using a final infiltrated concentration of 6.5 mM AT101 and a porosity of 48 %, a concentration of ≈ 4 µM AT101 was released after 24 hours and a calculated maximum release of 6.1 µM was determined after six days *in vitro,* which in fact represents more than 90 % of the total infiltrated drug-concentration. These results are in line with recent approaches, were AT101-releasing chitosan coated nanofibrous implants have been produced and tested for their efficacy on HeLa cells *in vitro* as well as on Graffi myeloid tumor model *in vivo (Ignatova et al. 2012; Ignatova et al. 2014),* whereas after two and four hours 15 % respective 55 % of the total infiltrated drug was released. Moreover, as the release-control of drugs remains a major obstacle due to possible cytotoxic burst release, Wrzeszcz et al. have coated their PDMS filament-based dexamethasone-loaded chochlear implant with a biodegradable hydrogel to reduce the initial burst (Wrzeszcz et al. 2014). Furthermore, hydrogel implant-encapsulation can prevent cell and protein adhesion and therefore minimize inflammatory reactions due to brain foreign body responses (Wrzeszcz et al. 2014; Dalu et al. 2000; Xue et al. 2017).

Further, for efficacy studies, monocultures of two different TMZ-responding GBM cell lines have been chosen as well as healthy astrocytes to study the influence of our drug delivery system on cytotoxic effects as well as on growth rates over six days *in vitro*. Hence, as we already demonstrated the advantage of sequentially applied simultaneous treatment of TMZ and AT101 for three days followed with three days of single AT101 treatment (see previous two chapters), cells were stimulated locally by the AT101-releasing PDMS template and systemically by free TMZ co-stimulation for three days followed by the solely stimulation with an AT101-releasing PDMS template for another three days. In brief, the drug-loaded implants were placed into cell culture inserts with a pore diameter of 0.4 µm, allowing a diffusion dependent release through the pores towards the underneath cultured cells (figure 9 A). Thereafter, treatment success as well as the influence of the templates themselves were determined on days three and six via cytotoxicity assay as well as proliferation by comparing percentage of dead cells and growth rates of template-treated cells with free drug stimulation-controls. Interestingly, controls of respective DMSO concentrations either freely added or by release from the PDMS template did not affect GBM cell lines as well as SVGA astrocytes differently after three and six days, indicating no negative side effects due to the material itself. These results are in line with previous publicized works highlighting the biocompatibility of PDMS (Chou et al. 2013; Guo and Deweerth 2009; Lacour et al. 2010). In fact, Ereifej et al. demonstrated that nanopatterning of PDMS increases inflammatory and glial scarring reactions of glial cells in brain *in vitro* (Ereifej et al. 2013). Moreover, when infiltrated with AT101 and co-stimulated with TMZ, only moderate effects on cytotoxicity and growth rates could be detected for SVGA astrocytes. Contrary to that, GBM cells responded similarly as in our previous studies towards the treatment schedule with around 50-60 % dead cells and clearly reduced growth rates after six days of treatment. Hence, the percentage of dead cells was in trend even higher for GBM cells when treated with AT101-DDS combined with free TMZ therapy and therefore more efficient than the free drug administration. In other studies, the encapsulation of AT101 into polymeric nanoparticles did not increase the *in vitro* efficacy of AT101, as the growth inhibition of human prostate cancer PC-3 cells *in vitro* was similar as the free drug (Jin et al. 2015; Liu et al. 2014). However, Liu and others could demonstrate the improved efficacy of the nano formulated drug in *in vivo* studies with a more enhanced tumor-suppression effect and reduced systemic toxicity compared with free AT101 (Liu et al. 2014). Similar effects were determined earlier by Li and others who encapsulated AT101-enriched cottonseed oil in liposomes and were not able to improve AT101 efficacy in *in vitro* models of breast cancer, however clearly stated an improved efficacy of the formulation in an *in vivo* xenograft mouse tumor model (Li et al. 2011). In addition, similar studies to increase treatment efficiencies by synergistically stimulating GBM cells with hydrogel-releasing combinations of TMZ and paclitaxel have revealed promising results

with a sustained drug release over one month in mice *in vivo* (Zhao et al. 2019). In particular, the co-delivery efficiently suppressed tumor growth in a U87MG orthotopic tumor model. In other studies, using 3D bioprinted hydrogels loaded with ATRA-polymeric particles, a sustained drug release with tunable release kinetics was ensured as well as the potential to induce apoptosis in U87 GBM cells (Mirani et al. 2019). However, as our recent studies only represent first *in vitro* data on GBM tumor growth control as well as on effects on healthy astrocytes upon AT101-releasing PDMS templates, there is the need to study the potentially advantageous effects of the AT101 template over free AT101 stimulation in *in vivo* systems. Especially since we are aiming to locally apply the drug by non-toxic sustained releasing PDMS-templates directly towards tumor cells, the systemic negative side effects of the drug can be reduced. In particular, for the *in vivo* applicability of this system, one could think about a systemically oral administration of TMZ concomitant with a local drug administration of AT101 by drug loaded brain implants (figure 9 C).

Nonetheless, whilst for *in vitro* assays a comparably fast increase of concentration is necessary, the requirements for DDS for *in vivo* application is different. Here, the favorable release profile can be described by a prolonged respective sustained- or zero-order-release profile. In fact, in a very recent study of gossypol as a male contraceptive, the drug was released successfully over 20 days in rats *in vivo* from gossypol/PEG layer-by-layer films (Wen et al. 2018). However, this approach is very time consuming and is limited when thinking about upscaling. Our bottom-up approach however is easily to fabricate with no spatial limitations. Here, homogeneous PDMS scaffolds with high drug-loading capacities and sufficient short-term release of AT101 were produced which can be easily adapted by tailoring to the macroscopic size, the microchannel density (porosity) or the fraction of open microchannels. In perspective, to achieve sustained or zero-order release profiles in our highly porous microchannel PDMS-scaffolds, the number of open microchannels could be reduced via laser structuring approach and consequently allowing in next steps to include the testing in our dual co-culture *in vitro* system as well as *in vivo* (performed by the group of Prof. Dr. Dr. Held-Feindt) in GBM-xenograft animal models.

“The choice of implant materials and their design is critical for the brain foreign body response and can be alleviated by anti-inflammatory/fibrotic compounds”

Besides the necessity to study the *in vitro* and *in vivo* efficacy of drug delivery devices for the local drug administration in the brain, it is also important to investigate the single material-induced responses, in particular under consideration of the healthy brain tissue. In fact, besides the application as drug delivery systems, especially brain foreign body reactions towards long-term electrodes and micro-sensing devices have been extensively studied to date (Gulino et al. 2019; Ludwig et al. 2006; Polikov et al. 2005). In this regard, graphene-based materials have gained interest in the past years for applications in drug delivery, brain electrodes as well as the differentiation of neurons under electrical stimulation for example (Huang et al. 2012; Li et al. 2008b). Amongst them, GO can be easily surface-functionalized due to its hydrophilic functional groups, whereas rGO offers an extraordinary conductivity. Hence, nanoparticles of GO and rGO as well as nanosheets of GO have been studied for their toxicity *in vitro* and partly *in vivo*, indicating diverse reactions of biological systems towards these materials (Bramini et al. 2018; Cheon et al. 2016; Dasari Shareena et al. 2018). However, since the biocompatibility of a material is highly influenced also by the materials’ shape, porosity, size etc. (Mendes et al. 2015), it is noteworthy to notice that GO and rGO scaffold materials of a highly porous microstructured tetrapodal networks have not been tested yet for their biocompatibility and probability of causing brain foreign body reactions *in vitro*. Therefore, our study focused on the evaluation of two putative nanostructured GO and rGO based scaffold materials on glial cell reactions as well as on organotypic brain slices with the special focus on the inflammatory and glial scarring reaction.

In brief, GO and rGO highly porous and easily size-tunable scaffolds were produced in a collaborative work with Florian Rasch (technical faculty Kiel), in a similar approach as the previous described PDMS-microchannel templates (see figure 10 A for the microstructure of rGO and GO, exemplary shown for rGO).

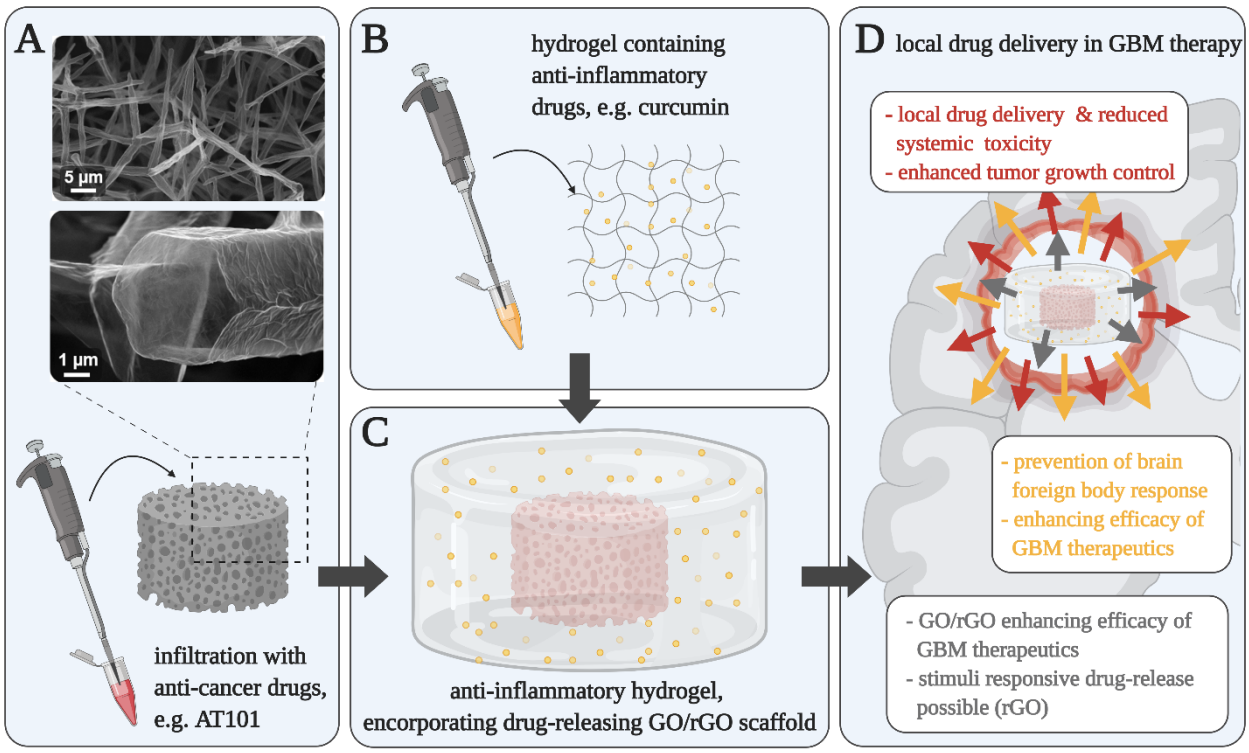

Figure 10: Schematic overview of a possible in vivo application of tetrapodal-structured highly porous GO and rGO scaffolds (A) for their local administration in brain disorders (here exemplary shown for GBM therapy) under prevention of material-induced inflammatory and glial scarring responses (D). *Materials are loaded with anti-cancer drugs (A) and incorporated into curcumin-loaded hydrogels (B,C) to dually targeting cancer cells with material-specific as well as drug-releasing properties and specifically reducing material-induced brain foreign body response by additional curcumin release (C,D). This figure was generated using the Biorender software.*

To study the effects of both materials on the healthy brain microenvironment, we investigated effects on cell proliferation, cytotoxicity and mRNA level for the expression of inflammatory- or glial scarring related genes in human astrocytes and microglial cells as well as in murine organotypic brain slices where protein level and morphology were also assessed by immunohistochemistry. In short time incubation models using SVGA astrocytes as well as HMC3 microglia, cells were indirectly incubated with the respective materials for 24 hours. In brief, with ethanol sterilized materials were placed in cell culture inserts above the cell carpet, allowing only an indirect contact with cells. Interestingly we could observe only slight effects on the percentage of dead cells after 24 hours incubation with materials in HMC3 microglia as well as SVGA astrocytes, however a bit more prominent for SVGA. Concomitant with these findings only slight reductions in growth rates were detectable, however significantly reduced for astrocytes and stronger for GO materials. Contrary to that, when analyzing the gene expression of inflammatory and glial scarring related genes, effects were overall stronger for rGO incubations in microglial cells as well as in astrocytes than for GO. These results are in line with studies of Li et al. who have exposed GO and rGO particles to different mammalian cells *in vitro* as well as the respiratory tract *in vivo* (Li et al. 2018b). In fact, they could show that rGO did not affect cell viability in both models, however GO in function of the surface oxidation state and carbon radical content did (Li et al. 2018b). Moreover, it is well known that cell interactions between microglia and astrocytes strongly influence inflammation and glial scarring reactions. Therefore, in a next step GO/rGO-incubated HMC3 microglia conditioned media was used to stimulate SVGA astrocytes for 24 hours. Surprisingly we could determine that material-induced reactions towards percentages of dead cells, influences on the growth rate of astrocytes as well as their gene expression of glial scarring-related genes such as tenascin-C, nestin and fibronectin were completely reversed to baseline levels, indicating a protective effect of microglial cells on material-induced effects in astrocytes. Indeed, it

is well known that activated microglia provoke astrocytes reactivity (Liddelow et al. 2017), however the potentially protective effect of the crosstalk between microglia and astrocytes in gliosis processes is less well described. In fact, Armbrust and Röhl have demonstrated that the co-incubation of astrocytes with conditioned media from LPS-activated microglia reduces oxidative stress in astrocytes when challenged with hydrogen peroxide (Armbrust and Röhl 2008). Moreover, they were also able to show that astrocytes co-stimulated with conditioned microglia media without LPS stimulation was also able to weaken oxidative stress in astrocytes, however in lesser extent. Therefore, these results indicate together with our own findings, that activated microglia play also a key role in the prevention of astrogliosis processes.

These findings pronounce the need for *in vitro* test systems that more closely mimic the *in vivo* condition, as cell-cell communication plays as crucial role in neuroinflammation and gliosis as well as brain foreign body reactions. Indeed, Polikov et al. have developed an *in vitro* model of glial scarring around neuroelectrodes in the CNS (Polikov et al. 2006). Cultivated astrocytes, neurons and microglial cells, derived from mechanically dissociated embryonic midbrains, were either injured (control) or co-cultivated with an electric microwire and showed similar responses as to be expected in *in vivo* applications (Polikov et al. 2006). Amongst others, technologies such as electrospun microfiber scaffolds or hydrogels are used to better reflect the 3D microenvironments of cells *in vitro* [for review see (Watson et al. 2017)]. Hence, several groups have reported the more "*in-vivo*-like" morphology and properties of astrocytes cultivated in a 3D hydrogel compared to the rather flat and polygonal growth in 2D cultures (East et al. 2013; Balasubramanian et al. 2016), however lacking the co-cultivation with different cell types. Therefore, since we wanted to investigate material-induced reactions in the complex brain tissue, we employed murine organotypic brain slice cultures that preserve the cell-cell interconnectivity over a long period of time *in vitro*.

In our experimental setting, similar to the *in vitro* data on monocultures of SVGA astrocytes and HMC3 microglia, the cytotoxic effects of GO and rGO challenged murine organotypic brain slices were moderate after three and six days of stimulation (dos) and only significantly increased for stimulations with GO after three dos. These results are in line with other investigations. Whilst rGO nanoparticles systemically applied and also locally on cornea cells did not cause any toxic effects, GO induced inflammation and time-dependent apoptosis (An et al. 2018). In other approaches using nanosheets of GO, no significant effects on the inflammatory response of murine organotypic spinal cord slices occurred after long-term stimulation (Musto et al. 2019), however in cultures of rat primary glial cells inflammatory reactions occurred after short-term application (Musto et al. 2019). Nonetheless, when investigating material-mediated effects on inflammation and glial scarring related genes, effects were more pronounced after rGO incubation. Whilst GO did not cause any effects on inflammation and glial scarring, rGO clearly induced IL-6 expression as well as tenascin-C and nestin expression after six dos. In 2015, 3D porous scaffolds of GO have been implanted in spinal cord injured rats, without showing any negative effects on local or systemic cytotoxicity nor biocompatibility after chronic implantation (López-Dolado et al. 2015). In fact, rolled GO fibers have been used as biocompatible materials for the drive of neuronal growth and differentiation in neuronal stem cells *in vitro* [(Akhavan et al. 2016), for review see (Bramini et al. 2018)]. Whereas these findings are similar with our *in vitro* data on HMC3 microglia and SVGA astrocytes when cultivated as monocultures, rGO-induced inflammatory processes in the brain have, to my best knowledge, not been described yet in literature. However, Bengtson and others have demonstrated that pulmonary exposure to GO and rGO particles causes acute inflammation reactions towards GO, whereas causing a chronic and more prolonged reaction towards rGO exposure in mice (Bengtson et al. 2017). Despite, surface functionalized nanosheets of rGO with albumin have been produced and loaded with doxorubicin for cancer treatment (Cheon et al. 2016). Indeed, they demonstrated an efficient near-infrared induced photothermal therapy in brain tumor cells, however without cytotoxic effects upon dose-dependent uptake without infrared stimulus. Hence, we

were able to demonstrate in immunohistochemical stainings of organotypic brain slices after six days of stimulation with GO and rGO highly porous scaffold materials, that neurons as well as oligodendrocytes were not affected negatively. However, protein expressions of GFAP or vimentin for example clearly indicated an induction of reactive astrogliosis upon both materials.

Since inflammatory and glial scarring reactions towards GO and rGO are not beneficial in terms of implant function, we wanted to investigate in a next step if material-induced effects can be alleviated by co-stimulation with an anti-inflammatory therapeutic compound. Besides others, there are a broad variety of targeting mechanisms/signaling pathways to reduce neuro-inflammatory and astrogliosis processes. During glial reactions, certain receptors, transcription factors or signaling molecules become activated such as toll-like-receptor (TLR), NF-κB, nuclear factor E2-related factor (Nrf2), activator protein 1 (AP-1) or P38 mitogen-activated protein kinases (p38MAPK), c-Jun N-terminal kinases (JNK), Janus kinase/signal transducers and activators of transcription 3 (JAK/STAT3) pathway etc. which are common for inflammatory processes. Moreover, inflammatory processes also cause an alteration in protein expression such as GFAP, vimentin in astrocytes or enzymes like nitric oxide synthase (NOS) in microglial cells [for review see (Glass et al. 2010; Colangelo et al. 2014)]. In particular, NF-κB translocation in reactive astrocytes causes inflammatory responses and glial proliferation (Colangelo et al. 2014), or the JAK/Stat pathway for instance is actively transducing inflammatory signals which are mediated by gf or cytokines such as IL-6, E ciliary neurotrophic factor (CNTF), epidermal growth factor (EGF) or tumor growth factor alpha (TGF-α). Therefore antioxidant molecules such as curcumin can inhibit NF-κB or STAT3 (Okada et al. 2006; Karlstetter et al. 2011) and therefore reduce aspects of astrogliosis (Colangelo et al. 2014). In fact, using curcumin in pre- or co-stimulation with the GO or rGO incubation in HMC3 microglia and SVGA astrocyte cell models as well as in murine organotypic brain slices, we were able to alleviate successfully material-induced reactions in respect of cytotoxic effects or on proliferation as well as on mRNA and protein level (almost) to control levels. Further, we could show that curcumin after eight days of stimulation did not negatively influence neurons, oligodendrocytes or active proteins in the glial scarring response in organotypic brain slices. These glia-protective effects are in line with recent studies, as such curcumin caused reduced neurotoxicity and the upregulation of proinflammatory genes upon LPS stimulation in BV2 microglia, as well as influenced the migration behavior of activated microglia (Karlstetter et al. 2011). Further, Lee and others claim that the neuroprotective effect of curcumin is mainly mediated by inhibition of microglial cell activation (Lee et al. 2007).Very recently Yuan and others demonstrated that curcumin inhibits glial scar formation by dual-targeting of inflammation and fibrosis (Yuan et al. 2017). As such curcumin regulated NF-κb and SOX-9 signaling pathways and therefore reduced SOX-9-induced CSPG deposition, alpha smooth muscle actin (α-SMA) expression in astrocytes and glial scar formation of both intracellular and extracellular glial scar components in spinal cord injured rats (Yuan et al. 2017; Yuan et al. 2019). Indeed, we could also demonstrate in our *in vitro* models, that not only material-induced inflammation can be regulated by curcumin but also fibrosis processes. Apart from that, most studies are focusing on the anti-glial scarring effects of curcumin on spinal cord injury (Yuan et al. 2019; Machova Urdzikova et al. 2015; Ruzicka et al. 2018). Despite, Bondan et al. have shown that curcumin can reduce astrocytic reactions upon gliotoxic injuries in the rat brainstem (Bondan et al. 2017) or in other studies its therapeutic effects in the treatment of Parkinson's or Alzheimer's disease (Motawi et al. 2020; Liu et al. 2020; Voulgaropoulou et al. 2019), making aware of the multitude of applications possible with curcumin.

Hence, we were able to produce highly porous tetrapodal-structured GO and rGO scaffolds with unique physical and mechanical properties, such as the conductivity for rGO materials, the high surface to volume ratio, a good capacity for drug loading as well as surface functionalization. In fact, both material scaffolds provoked either only moderate inflammatory or glial scarring reactions, or reactions which were reversible by pre-/co-stimulation with curcumin *in vitro*. Moreover, in contrast to studies on GO/rGO nanoparticles or -sheets in which cytotoxic effects have been explained due to particle-uptake by cells, our tetrapodal

microstructured GO/rGO materials represent stable scaffold materials which show a clear advantage in biocompatibility over these systems. At this point one has to mention that this work is indeed dealing with very heterogeneous topics such as the material-choice as well as its shape and microstructure, the *in vitro* biocompatibility in different *in vitro* models, analyzing the effects of the brain foreign body reaction with regard on anti-inflammatory and -glial scarring therapies but also mentioning possible biological applications as in cancer therapy. This is also reflected by the interdisciplinary collaboration with Florian Rasch (technical faculty), so that I decided to highlight several possible aspects of application in this discussion, without allowing me to mirror/discuss all different topics and approaches in detail.

In perspective, by adjusting the stiffness of a brain implant material, for example by surrounding it with a hydrogel of the same mechanical properties as of the healthy brain, may help to elicit brain foreign body reactions towards the implant material [see figure 10, B-D, (Moeendarbary et al. 2017)]. Likewise, Nguyen and others have produced mechanical-adaptive implants of PVA which when inserted become compliant and were able to reduce neuroinflammatory responses *in vivo* compared to stiff systems (Nguyen et al. 2014). Moreover, to increase biocompatibility of rGO materials, the reduction of GO to rGO is a crucial step, as it is usually maintained by micromechanical methods, epitaxial growth method, thermal reduction or chemically (Muthoosamy et al. 2015). However, most commonly used chemicals such as hydrazine highly toxic and have been shown to tend to agglomerate irreversibly and convert into graphite (Perera et al. 2012). To address this, Muthoosamy et al. have produced thin-layered reduced graphene oxide, reduced by an ecofriendly mushroom extract strategy, has been shown to be biocompatible and non-toxic in colon and brain cancer cell lines *in vitro* (Muthoosamy et al. 2015). Moreover, to respond directly after implantation *in vivo* on possible occurring surgery- or material-induced inflammatory or glial scarring responses, one could think about an encapsulation of curcumin into the implant-surrounding hydrogel with a prolonged curcumin release. Interestingly, Potter et al. combined the strategy of mechanical-adaptive brain implants with the anti-inflammatory properties of curcumin (Potter et al. 2014). They were able to produce curcumin-releasing softening polymer implants, which caused over four weeks minimal brain foreign body reactions concomitant with lower neuron-toxicity and higher BBB stability than neat polymers.

Moreover, curcumin-releasing graphene-based implants could not only be interesting for the regulation of implant-induced neuroinflammatory and glial scarring responses, but also in the treatment of *glioblastoma multiforme* for example (see figure 10). Yet the therapeutic potential of curcumin in the treatment of brain tumors is a steadily increasing field of research (Shabaninejad et al. 2020). Is has been shown that curcumin has radio sensitizing properties in different cancers (Sak 2019), affects migration and invasion (Park et al. 2019), induces autophagy (Maiti et al. 2019), promotes TMZ-induced apoptosis (Huang et al. 2019) as well as increases tumor growth control in combinations with AT101 (Mehner et al. 2019) in GBM cells *in vitro* (see figure 11, left). Interestingly, graphene-based materials have gained interest in GBM therapy as well. Likewise it has been shown, that nano-GO downregulates genes of oxidative phosphorylation in U87 GBM cells and may be the reason for GO's anti-proliferative and -migrative effects in GBM cells (Szmidt et al. 2019). Further the pro-apoptotic properties of rGO plates upon U87 and U118 GBM cells has been evaluated (Jaworski et al. 2013). Recently, the same group also demonstrated that apoptosis in U87 upon rGO-flake incubation is related to the presence of oxygen-containing functional groups and electron clouds, therefore indicating that the cytotoxicity of graphene-based materials decreases with the amount of oxygen-containing functional groups and therefore is smaller for rGO than for GO or graphene (Szczepaniak et al. 2018). Thus, investigating the effects of curcumin-releasing GO and rGO tetrapodal shaped scaffolds might be on the one hand site an interesting approach for the local treatment of GBM and on the other hand for the alleviation of implant-induced inflammatory and glial scarring reactions in the healthy brain (see figure 10 D).

"The bioavailability and efficient delivery of curcumin can be made possible in the form of nano-curcumin which preserves the properties of curcumin and ascertains that it reaches the affected tissue" (Gera et al. 2017)

We could successfully demonstrate that curcumin can attenuate implant-induced inflammatory and glial scarring reactions in human astrocyte and microglia cell lines as well as organotypic brain slices towards highly porous GO and rGO microchannel templates after short (24 hours in cell lines) and long-term administration (six days in organotypic brain slices). However targeting neuro-inflammation as well as glial scarring by curcumin remains a challenge due to its low bioavailability as well as instability (Kharat et al. 2017; Ma et al. 2019). A simple way to solve limiting factors of curcumin can be the use of novel curcumin derivates or new formulations, such as by encapsulation into polymeric nanoparticles or liposomes [(Hussain et al. 2017; Liao et al. 2019), for review see (Yallapu et al. 2012) and figure 11].

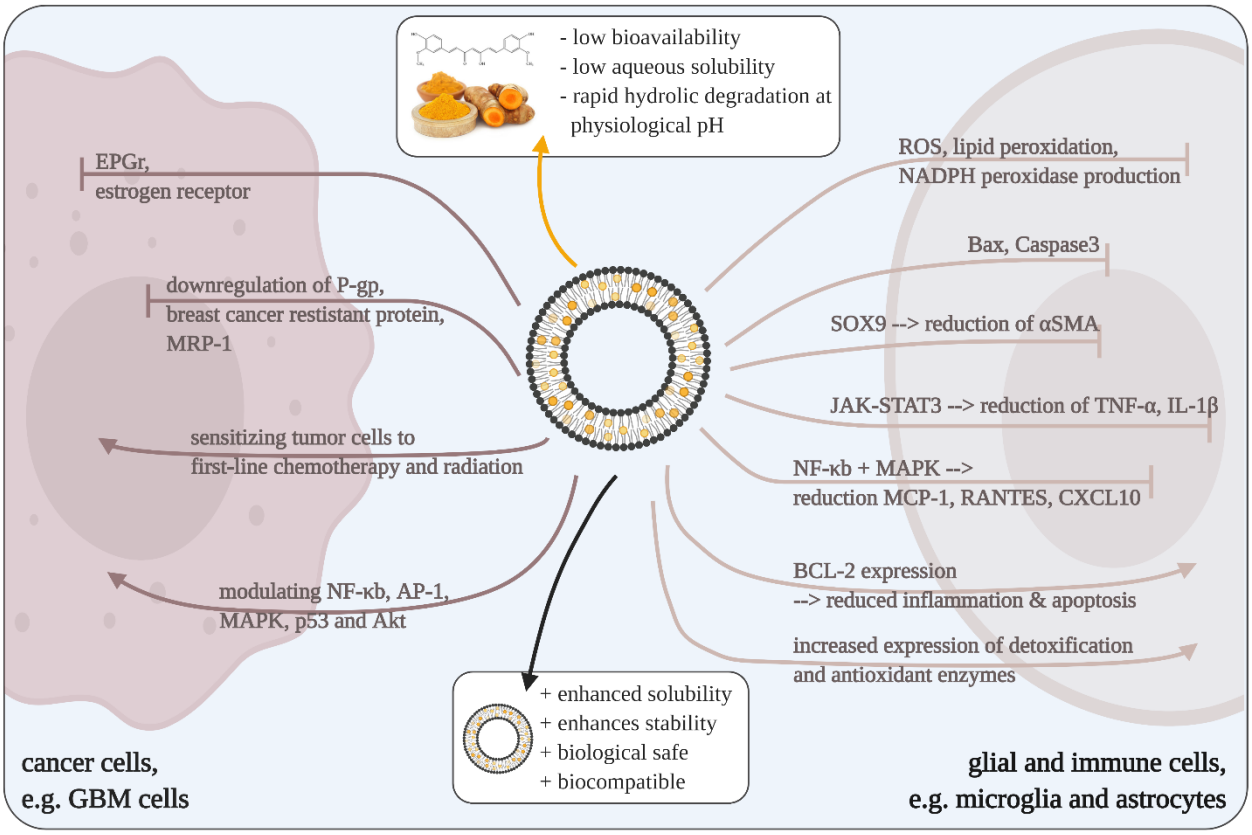

Figure 11: Schematic overview of the investigated influence of curcumin on cellular pathways and mechanisms important for the treatment of cancer cells (left) as well as for its anti-inflammatory and -oxidative effects preserving the healthy cell-microenvironment (right). *Besides the tremendous advantages of curcumin, it has a very low bioavailability and stability which when encapsulated into nanoformulations such as liposomes can be significantly improved. The represented effects (inhibitory or inductive) were collected from several different references (Yallapu et al. 2012; Krupa et al. 2019; Hao et al. 2017; Liu et al. 2016; Yu et al. 2018; Caillaud et al. 2018; Sharma et al. 2019; Hatcher et al. 2008; Kunnumakkara et al. 2008; Landis-Piwowar et al. 2006; Yallapu et al. 2010). The figure was generated using the Biorender software.*

Therefore, we decided to encapsulate curcumin into biocompatible liposomes which allow long-term storage and increased *in vitro* efficacy. This work was partly performed in the laboratory of pharmaceutical technology and biopharmacy in Liège, Belgium during my stay abroad, however *in vitro* efficacy studies were performed in the institute of anatomy in Kiel, Germany. In brief, liposomes with a final formulation of DPPC/Chol/Cur in a molar ratio of 80.6/15.6/3.8, have been produced by the classical lipid-thin film hydration method followed by extrusion at 51 °C (10 °C higher the lipid transition temperature of DPPC) and analyzed physico-chemically for their size, polydispersity and zeta potential as well as curcumin encapsulation efficiency. In first attempts, different lipids such as egg phosphatidylcholine (EPC) and DPPC

as well as variations of lipid-ratios have been evaluated for the successful encapsulation of curcumin. However, using formulations of DPPC increased the encapsulation efficiency of curcumin from around 45 % (data not shown) to 68 %, as well as allowed a robust reproducibility of sizes, PdI and zeta potential of ca. 250 nm, 0.3 respective -25 mV (average over six month). These results were in line with previous published data from Roy et al., who have evaluated the influence of different lipids on the physico-chemical properties of curcumin-encapsulating liposomes as well as their release-kinetics and pH and temperature-dependent stability (Roy et al. 2016). In fact, DPPC amongst other lipids or lipid combinations was able to reach the highest curcumin entrapment efficiencies concomitant with a sustained release profile releasing less than 10 % of the total incorporated drug over 80 hours at 25 °C. Contrary to that, we have performed our drug-release studies under physiological conditions at 37 °C, whereas around 35 % of the total incorporated curcumin was released from our nanoformulations after 24 hours. Other studies employing liposomal formulations show similar sustained release profiles of curcumin, however releasing over 70 % of the total encapsulated drug after 24 hours (Jin et al. 2016). Conversely Thakur Choudhury et al. as well as Tefas et al. obtained a release-kinetic similar to our formulation by releasing around 30 % of curcumin after 24 hours *in vitro* (Choudhury et al. 2016; Tefas et al. 2017). Moreover, since the planned efficacy studies on the produced liposomes needed to be performed in Kiel, liposomes' long-term stability was a crucial factor. Therefore, different cryoprotectants have been evaluated for their capability to lyophilize the final liposomal formulation without changing its physico-chemical properties. By supplementing the final liposomal formulation with 10 % trehalose in its aqueous solution, we were able to produce liposomal formulations with stable physical properties over up to six months, with a sustained drug release profile. Contrary to our observations, Hinrichs and others claim that oligosaccharides as cryoprotectants are more promising than disaccharides such as sucrose or trehalose, due to their higher glass transition temperature (T_g) and therefore storing capability at higher temperatures (Hinrichs et al. 2005). However, they have only used lipid combinations of DOTAP:DOPE:DSPE-PEG which due to their lipid-specific properties cannot be directly compared with our formulation. In another approach, doxorubicin encapsulating liposomes of DPPC:DPPG:Chol (10:4:1) were lyoprotected with either lactose, maltose or trehalose and represented easily reconstitutable formulations with up to six months stable physical and chemical parameters in storage up to 30 °C (van Winden and Crommelin 1997). Concomitant with these findings Kim and Jeong could preserve properties of freeze-dried liposomes with trehalose over 12 months storage at 4 °C (Kim and Jeong 1995). However, one has to clearly state that the lipids used as well as the lipid-ratio and hydrophobicity/hydrophilic character of a drug influences the success of lyoprotectants for the freeze-drying process. Hence, liposomal formulations using DPPC:Chol:Cur with exact the same molar ratios of 80.6:15.6:3.8 used in our study are not yet described in literature, therefore limiting the comparability of our results.

However, since the encapsulation efficiency of lyophilized liposomes has not been evaluated over the time, this shows a clear limitation of our study. Nonetheless, our *in vitro* efficacy data which was collected over a period of up to six months clearly indicates the efficiency of the liposomal formulation even after six months in storage at 4 °C. In brief, rising concentrations of empty and cur loaded liposomes in comparison to free cur were evaluated for their biocompatibility in HMC3 microglia and SVGA astrocytes after three days by WST-1 assay. We could demonstrate that liposomal formulations do not cause any negative effects on cell viability up to concentrations of 2 µM or the respective amount of empty liposomes. Moreover, fluorescent-labeled liposomal formulations were effectively uptaken by cells during 24 hours of incubation. Hence, in our studies on GO and rGO materials concentrations of 1 µM free cur were used to alleviate material-induced inflammation and glial scarring reactions. However, pre-experiments of cur loaded liposomal formulations revealed that LPS-induced inflammatory reactions in microglial cells could be significantly reduced by 100-fold smaller concentrations of curcumin (data not shown). Similarly, Hoppe et al. produced curcumin loaded lipid-core nanoparticles which in animal models of Alzheimer's disease allowed the reduction of the administered dose from 50 mg/kg (i.p.) to its 20-times lower concentration of 2.5 mg/kg, to reach therapeutically neuroprotective effects (Hoppe et al. 2013). Therefore, concentrations of 0.01 µM cur were used in this study, to evaluate the efficiency of liposomal encapsulation of cur vs. the free drug.

In a well-described model of microglia-inflammation, HMC3 microglia cells were challenged with LPS for 24 hours to induce inflammatory reactions, which may be reversed by pre- and co-stimulations (further named as co-stimulations) of free cur or LipoCur. We could show, that LPS induced the expression of typical inflammatory related genes such as IL-6, TNF-α, TGF-β or IL-1β and that the expression was reduced by co-stimulation with cur as well as LipoCur, whereas with increasing significance using LipoCur. Concomitant with these findings, morphological changes of microglia upon LPS stimulations to their activated state were reversed by LipoCur formulations. In fact Karlstetter et al. have demonstrated that NO-levels were reduced as well as anti-inflammatory genes were upregulated in LPS-challenged BV2 microglia upon curcumin co-stimulation, however using in our point of view quite high curcumin concentrations of 20 µM (Karlstetter et al. 2011). We further developed an *in vitro* glial scarring model by challenging SVGA astrocytes with inflammatory cytokines such as TNF-α, TGF-β and IL-1β overexpressed by activated microglia (further named cytokine stimulation) to induce reactive astrogliosis in astrocytes. In fact, typical glial scarring related genes were upregulated upon cytokine stimulation as well as morphological changes were visible, however could be significantly alleviated by cur and LipoCur, whilst in a greater extend for liposomal formulations to almost control levels. These results are in line with the findings of Yuan and others who observed reduced signs of reactive astrogliosis, like CSPG deposition and α-SMA and GFAP expression in astrocytes as well as altered astrocyte phenotype upon pre-stimulation of TNF-α, TGF-β_1 and $_2$ as well as IL-1β-challenged astrocytes with 1 µM free curcumin after 48 hours (Yuan et al. 2017). For a summary of anti-inflammatory and neuroprotective effects of curcumin, please revise figure 11. Apart from that, Yoo and others implemented an *in vitro* glial scarring model to mimic the chemical spinal cord injury (Yoo et al. 2016). By challenging rat spinal cord astrocytes with rising concentrations of kainite, instead of – as in our case – proinflammatory cytokines, they could show the induction of astrogliosis markers such as GFAP, vimentin or CSPG upon 50 µM kainate incubation, which was reversible by co-stimulation of a kainate-inhibitor.

Besides the evaluation of LipoCur efficacy in easily performable and reproducible *in vitro* models of human microglia and astrocyte monocultures we wanted to investigate anti-inflammatory and -glial scarring properties of LipoCur also in a 3D *in vitro* model of murine organotypic brain slices which preserves the cell-interconnectivity in their *in vivo*-like microenvironment. Therefore, brain slices were challenged with LPS, assuming an activation of microglial cells and as a domino effect by the microglia-specific release of inflammatory molecules also the induction of reactive gliosis. By pre-stimulation of LPS challenged slices with 0.01 µM LipoCur, free cur or the respective amount of empty liposomes, not only the LPS-induced cytotoxic effects on brain slices but also LPS-induced inflammatory-related gene expression could be inhibited after two and eight days *in vitro*. In fact, we were able to demonstrate that cur or liposomal formulations solely do not affect negatively brain slices survival as well as inflammatory responses over eight days. Similarly, in *in vivo* studies of spinal cord injury, nanoformulated curcumin could reduce glial scarring as well as inflammatory-related genes after local administration in the first two weeks (Krupa et al. 2019). In a rat epilepsy model curcumin supplementation could significantly reduce pro-inflammatory cytokine and chemokine expression as well as GFAP-expression in rat hippocampus and cortex (Kaur et al. 2015) as well as reduce IL-1β gene expression in a rat epilepsy hippocampal cortex slice culture model (Drion et al. 2019). Interestingly, other than in our HMC3 microglia cell model, TGF-β was not upregulated upon LPS stimulation in organotypic brain slices and therefore no effects of cur and its nanoformulations were detectable. Similar, Drion and others observed no induced TGF-β expression in their epilepsy model and therefore cur did not affect its expression (Drion et al. 2019). At this point one has to mention that our organotypic brain slice model cannot mirror single cell responses on gene expression level, as it preserves the whole latter of cells present in the mouse cortex. Therefore, cell-specific effects might be less pronounced regarding the ratio between the respective cell type and the total amount of cells present, or also mechanistically mildened by the influence of other cells. However, it has been shown that *in vitro* brain slice models express selected genes and proteins in similar extend as *in vivo* and therefore deliver results that are more comparable to the *in vivo* situation (Bahr 1995; Mielke et al. 2005).

At last, effects of cur and LipoCur on LPS-challenged murine organotypic brain slices after eight days were also determined on protein level by immunohistochemical stainings of neurons, oligodendrocytes as

well as for extra- and intracellular proteins that play a role in glial scarring process. We could successfully prove that the LPS-dependent undergo of neurons and oligodendrocytes can be completely prevented by co-stimulation with LipoCur as well as free drug. In line with our findings, a study in 2014 demonstrated the specifically axon protective effect of curcumin on primary neurons via the inhibition of MyD88/p38 MAPK [see figure 11 and (Ghasemi et al. 2019; Tegenge et al. 2014)]. Moreover, it has been shown that curcumin protects pre-oligodendrocytes from cytotoxic effects of LPS-activated microglia in rats *in vitro* and *in vivo* (He et al. 2010), however in relatively high concentrations of 10 µM compared to our used concentration of only 0.01 µM. In addition, LPS-induced protein expression of GFAP, nestin, fibronectin as well as vimentin was reduced to baseline upon co-stimulation with LipoCur as well as free drug in a similar extend as on gene-expression level in our SVGA astrocyte monoculture model.

In summary, we were able to produce a long-term stable liposomal formulation of curcumin with appropriate encapsulation efficiency and drug-release profile. In particular, in different *in vitro* models of neuro inflammation and glial scarring the liposomal formulation improved the *in vitro* efficacy of the drug to reduce inflammation- respective glial scarring-related gene expression levels to their baseline as well as in murine organotypic brain slices also on protein-level. In fact, LipoCur prevented organotypic brain slices from LPS-induced cell death as well as LPS-induced undergo of neurons in a greater extent than free cur. Further, since some effects such as on gene expression level were less pronounced in organotypic brain slices as well as vice-versa more profound such as in immunohistochemically stainings than in monocultures of human microglia and astrocytes, the limitation of 2D monolayer cultures over 3D models is clearly visible. Similar findings were reported by Kolter et al. in 2019, who have stated the limitations of monolayer cultures in the prediction of drug and nanocarrier interactions, as curcumin had a clearly reduced *in vitro* efficacy in their 3D culture models than in 2D (Kolter et al. 2019). Therefore, 3D cultures such as our murine organotypic brain slice model, which preserves the whole variety of brain cells *in vitro* for a prolonged period of time in their natural microenvironment are necessary and suitable tools to study drug-, nanocarrier- as well as brain foreign body reactions *in vitro*. Our study confirms the neuroprotective and anti-inflammatory and -glial scarring effects of curcumin (Yuan et al. 2017; Bondan et al. 2017) as well as its increased efficiency upon encapsulation into nanoformulations (Djiokeng Paka et al. 2016; Gera et al. 2017; Dende et al. 2017), however in much smaller effective concentrations than in other studies. Further, our work shows, that liposomal formulations are suitable carriers for (chemically instable) drugs, and that our formulation efficiently helped to prevent glial scarring reactions in different brain *in vitro* and *ex vivo* models, without any formulation-related negative side effects. Therefore, also other possible drug candidates with a poor bioavailability could be tested, employing our nanoformulation, to efficiently prevent brain foreign body reactions with an improved drug efficacy.

Literature

Abnet, K.; Fawcett, J. W.; Dunnett, S. B. (1991): Interactions between meningeal cells and astrocytes in vivo and in vitro. In *Brain research. Developmental brain research* 59 (2), pp. 187–196. DOI: 10.1016/0165-3806(91)90099-5.

Adamski, Vivian; Hempelmann, Annika; Flüh, Charlotte; Lucius, Ralph; Synowitz, Michael; Hattermann, Kirsten; Held-Feindt, Janka (2017): Dormant glioblastoma cells acquire stem cell characteristics and are differentially affected by Temozolomide and AT101 treatment. In *Oncotarget* 8 (64), pp. 108064–108078. DOI: 10.18632/oncotarget.22514.

Adamski, Vivian; Schmitt, Christina; Ceynowa, Florian; Adelung, Rainer; Lucius, Ralph; Synowitz, Michael et al. (2018): Effects of sequentially applied single and combined temozolomide, hydroxychloroquine and AT101 treatment in a long-term stimulation glioblastoma in vitro model. In *J Cancer Res Clin Oncol* 144 (8), pp. 1475–1485. DOI: 10.1007/s00432-018-2680-y.

Agrawal, Mukta; Ajazuddin; Tripathi, Dulal K.; Saraf, Swarnlata; Saraf, Shailendra; Antimisiaris, Sophia G. et al. (2017): Recent advancements in liposomes targeting strategies to cross blood-brain barrier (BBB) for the treatment of Alzheimer's disease. In *Journal of controlled release : official journal of the Controlled Release Society* 260, pp. 61–77. DOI: 10.1016/j.jconrel.2017.05.019.

Akbarzadeh, A.; Rezaei-Sadabady, R.; Davaran, S.; Joo, S. W.; Zarghami, N.; Hanifehpour, Y. et al. (2013): Liposome. classification, preparation, and applications. In *Nanoscale research letters* 8 (1), p. 102. DOI: 10.1186/1556-276X-8-102.

Akhavan, Omid; Ghaderi, Elham; Shirazian, Soheil A.; Rahighi, Reza (2016): Rolled graphene oxide foams as three-dimensional scaffolds for growth of neural fibers using electrical stimulation of stem cells. In *Carbon* 97, pp. 71–77. DOI: 10.1016/j.carbon.2015.06.079.

Al-Jamal, Wafa' T.; Kostarelos, Kostas (2007): Liposome-nanoparticle hybrids for multimodal diagnostic and therapeutic applications. In *Nanomedicine (London, England)* 2 (1), pp. 85–98. DOI: 10.2217/17435889.2.1.85.

Alonso, Marta M.; Gomez-Manzano, Candelaria; Bekele, B. Nebiyou; Yung, W. K. Alfred; Fueyo, Juan (2007): Adenovirus-based strategies overcome temozolomide resistance by silencing the O6-methylguanine-DNA methyltransferase promoter. In *Cancer research* 67 (24), pp. 11499–11504. DOI: 10.1158/0008-5472.CAN-07-5312.

American Cancer Society (2019): Cancer Facts & Figures. In *Atlanta: American Cancer Society*.

An, Wenzhen; Zhang, Ying; Zhang, Xuan; Li, Kang; Kang, Yujun; Akhtar, Shahnaz et al. (2018): Ocular toxicity of reduced graphene oxide or graphene oxide exposure in mouse eyes. In *Exp Eye Res* 174, pp. 59–69. DOI: 10.1016/j.exer.2018.05.024.

Arai, Takao; Benny, Ofra; Joki, Tatsuhiro; Menon, Lata G.; Machluf, Marcelle; Abe, Toshiaki et al. (2010): Novel local drug delivery system using thermoreversible gel in combination with polymeric microspheres or liposomes. In *Anticancer research* 30 (4), pp. 1057–1064.

Arcella, Antonietta; Biagioni, Francesca; Antonietta Oliva, Maria; Bucci, Domenico; Frati, Alessandro; Esposito, Vincenzo et al. (2013): Rapamycin inhibits the growth of glioblastoma. In *Brain research* 1495, pp. 37–51. DOI: 10.1016/j.brainres.2012.11.044.

Arévalo, Ángelo S. T.; Erices, José I.; Uribe, Daniel A.; Howden, Jake; Niechi, Ignacio; Muñoz, Sebastián et al. (2017): Current Therapeutic Alternatives and New Perspectives in Glioblastoma Multiforme. In *Current medicinal chemistry* 24 (25), pp. 2781–2795. DOI: 10.2174/0929867324666170303122241.

Armbrust, E.; Röhl, C. (2008): Time- and activation-dependency of the protective effect of microglia on astrocytes exposed to peroxide-induced oxidative stress. In *Toxicology in vitro : an international journal published in association with BIBRA* 22 (5), pp. 1399–1404. DOI: 10.1016/j.tiv.2008.02.008.

Ashby, Lynn S.; Smith, Kris A.; Stea, Baldassarre (2016): Gliadel wafer implantation combined with standard radiotherapy and concurrent followed by adjuvant temozolomide for treatment of newly diagnosed high-grade glioma. A systematic literature review. In *World journal of surgical oncology* 14 (1), p. 225. DOI: 10.1186/s12957-016-0975-5.

Ashton, Randolph S.; Banerjee, Akhilesh; Punyani, Supriya; Schaffer, David V.; Kane, Ravi S. (2007): Scaffolds based on degradable alginate hydrogels and poly(lactide-co-glycolide) microspheres for stem cell culture. In *Biomaterials* 28 (36), pp. 5518–5525. DOI: 10.1016/j.biomaterials.2007.08.038.

Attwell, David; Buchan, Alastair M.; Charpak, Serge; Lauritzen, Martin; Macvicar, Brian A.; Newman, Eric A. (2010): Glial and neuronal control of brain blood flow. In *Nature* 468 (7321), pp. 232–243. DOI: 10.1038/nature09613.

Aum, David J.; Tierney, Travis S. (2018): Deep brain stimulation. Foundations and future trends. In *Frontiers in bioscience (Landmark edition)* 23, pp. 162–182. DOI: 10.2741/4586.

Babcock, Alicia A.; Kuziel, William A.; Rivest, Serge; Owens, Trevor (2003): Chemokine Expression by Glial Cells Directs Leukocytes to Sites of Axonal Injury in the CNS. In *J. Neurosci.* 23 (21), pp. 7922–7930. DOI: 10.1523/JNEUROSCI.23-21-07922.2003.

Babu, Anu; Mohammed, Sabira; Harikumar, K. B. (2019): Antioxidant Properties of Curcumin. Impact on Neurological Disorders. In Tahira Farooqui, Akhlaq A. Farooqui (Eds.): Curcumin for neurological and psychiatric disorders. Neurochemical and pharmacological properties. London, United Kingdom, San Diego, CA, United States: Academic Press, an imprint of Elsevier, pp. 155–167.

Bagó, Juli R.; Pegna, Guillaume J.; Okolie, Onyi; Mohiti-Asli, Mahsa; Loboa, Elizabeth G.; Hingtgen, Shawn D. (2016): Electrospun nanofibrous scaffolds increase the efficacy of stem cell-mediated therapy of surgically resected glioblastoma. In *Biomaterials* 90, pp. 116–125. DOI: 10.1016/j.biomaterials.2016.03.008.

Bahr, B. A. (1995): Long-term hippocampal slices. A model system for investigating synaptic mechanisms and pathologic processes. In *Journal of neuroscience research* 42 (3), pp. 294–305. DOI: 10.1002/jnr.490420303.

Bailey, P. and Cushing, H. (1926): A classification of the tumours of the glioma group on a histogenetic basis: With a correlated study of prognosis. Pp. 175, with 108 illustrations. In *Philadelphia, London, and Montreal: J. B. Lippincott Company. 21s. net* 8.

Balandin, Alexander A.; Ghosh, Suchismita; Bao, Wenzhong; Calizo, Irene; Teweldebrhan, Desalegne; Miao, Feng; Lau, Chun Ning (2008): Superior thermal conductivity of single-layer graphene. In *Nano letters* 8 (3), pp. 902–907. DOI: 10.1021/nl0731872.

Balasubramanian, Swarnalatha; Packard, John A.; Leach, Jennie B.; Powell, Elizabeth M. (2016): Three-Dimensional Environment Sustains Morphological Heterogeneity and Promotes Phenotypic Progression During Astrocyte Development. In *Tissue engineering. Part A* 22 (11-12), pp. 885–898. DOI: 10.1089/ten.TEA.2016.0103.

Balvers, Rutger K.; Dirven, Clemens M. F.; Leenstra, Sieger; Lamfers, Martine L. M. (2017): Malignant Glioma In Vitro Models. On the Utilization of Stem-like Cells. In *Current cancer drug targets* 17 (3), pp. 255–266. DOI: 10.2174/1568009616666160813191809.

Balvers, Rutger K.; Kleijn, Anne; Kloezeman, Jenneke J.; French, Pim J.; Kremer, Andreas; van den Bent, Martin J. et al. (2013): Serum-free culture success of glial tumors is related to specific molecular profiles and expression of extracellular matrix-associated gene modules. In *Neuro-oncology* 15 (12), pp. 1684–1695. DOI: 10.1093/neuonc/not116.

Bartheld, C. S. von; Bahney, J.; Herculano-Houzel, S. (2016): The search for true numbers of neurons and glial cells in the human brain. A review of 150 years of cell counting. In *The Journal of comparative neurology* 524 (18), pp. 3865–3895. DOI: 10.1002/cne.24040.

Basnet, P.; Hussain, H.; Tho, I.; Skalko-Basnet, N. (2012): Liposomal delivery system enhances anti-inflammatory properties of curcumin. In *Journal of pharmaceutical sciences* 101 (2), pp. 598–609. DOI: 10.1002/jps.22785.

Basso, João; Miranda, Ana; Nunes, Sandra; Cova, Tânia; Sousa, João; Vitorino, Carla; Pais, Alberto (2018): Hydrogel-Based Drug Delivery Nanosystems for the Treatment of Brain Tumors. In *Gels (Basel, Switzerland)* 4 (3). DOI: 10.3390/gels4030062.

Bastiancich, C.; Bianco, J.; Vanvarenberg, K.; Ucakar, B.; Joudiou, N.; Gallez, B. et al. (2017): Injectable nanomedicine hydrogel for local chemotherapy of glioblastoma after surgical resection. In *Journal of controlled release : official journal of the Controlled Release Society* 264, pp. 45–54. DOI: 10.1016/j.jconrel.2017.08.019.

Bastiancich, C.; Danhier, P.; Préat, V.; Danhier, F. (2016): Anticancer drug-loaded hydrogels as drug delivery systems for the local treatment of glioblastoma. In *Journal of controlled release : official journal of the Controlled Release Society* 243, pp. 29–42. DOI: 10.1016/j.jconrel.2016.09.034.

Bastiat, Guillaume; Plourde, François; Motulsky, Aude; Furtos, Alexandra; Dumont, Yvan; Quirion, Rémi et al. (2010): Tyrosine-based rivastigmine-loaded organogels in the treatment of Alzheimer's disease. In *Biomaterials* 31 (23), pp. 6031–6038. DOI: 10.1016/j.biomaterials.2010.04.009.

Belousov, Andrei; Titov, Sergei; Shved, Nikita; Garbuz, Mikhail; Malykin, Grigorii; Gulaia, Valeriia et al. (2019): The Extracellular Matrix and Biocompatible Materials in Glioblastoma Treatment. In *Front Bioeng Biotechnol* 7, p. 341. DOI: 10.3389/fbioe.2019.00341.

Benabid, A. L.; Koudsié, A.; Benazzouz, A.; Fraix, V.; Ashraf, A.; Le Bas, J. F. et al. (2000): Subthalamic stimulation for Parkinson's disease. In *Archives of medical research* 31 (3), pp. 282–289. DOI: 10.1016/s0188-4409(00)00077-1.

Bengtson, Stefan; Knudsen, Kristina B.; Kyjovska, Zdenka O.; Berthing, Trine; Skaug, Vidar; Levin, Marcus et al. (2017): Differences in inflammation and acute phase response but similar genotoxicity in mice following pulmonary exposure to graphene oxide and reduced graphene oxide. In *PloS one* 12 (6), e0178355. DOI: 10.1371/journal.pone.0178355.

Benny, Ofra; Duvshani-Eshet, Maayan; Cargioli, Theresa; Bello, Lorenzo; Bikfalvi, Andreas; Carroll, Rona S.; Machluf, Marcelle (2005): Continuous delivery of endogenous inhibitors from poly(lactic-co-glycolic acid) polymeric microspheres inhibits glioma tumor growth. In *Clinical cancer research : an official journal of the American Association for Cancer Research* 11 (2 Pt 1), pp. 768–776.

Bette, Stefanie; Barz, Melanie; Wiestler, Benedikt; Huber, Thomas; Gerhardt, Julia; Buchmann, Niels et al. (2018): Prognostic Value of Tumor Volume in Glioblastoma Patients. Size Also Matters for Patients

with Incomplete Resection. In *Annals of surgical oncology* 25 (2), pp. 558–564. DOI: 10.1245/s10434-017-6253-0.

Bikhezar, Fatima; Kruijff, Robin M. de; van der Meer, Astrid J. G. M.; Torrelo Villa, Guzman; van der Pol, Susanne M. A.; Becerril Aragon, Gabriel et al. (2019): Preclinical evaluation of binimetinib (MEK162) delivered via polymeric nanocarriers in combination with radiation and temozolomide in glioma. In *Journal of neuro-oncology. DOI:* 10.1007/s11060-019-03365-y.

Biran, Roy; Martin, David C.; Tresco, Patrick A. (2005): Neuronal cell loss accompanies the brain tissue response to chronically implanted silicon microelectrode arrays. In *Experimental neurology* 195 (1), pp. 115–126. DOI: 10.1016/j.expneurol.2005.04.020.

Blasi, Paolo; Giovagnoli, Stefano; Schoubben, Aurélie; Ricci, Maurizio; Rossi, Carlo (2007): Solid lipid nanoparticles for targeted brain drug delivery. In *Advanced drug delivery reviews* 59 (6), pp. 454–477. DOI: 10.1016/j.addr.2007.04.011.

Bobo, R. H.; Laske, D. W.; Akbasak, A.; Morrison, P. F.; Dedrick, R. L.; Oldfield, E. H. (1994): Convection-enhanced delivery of macromolecules in the brain. In *Proceedings of the National Academy of Sciences of the United States of America* 91 (6), pp. 2076–2080. DOI: 10.1073/pnas.91.6.2076.

Bondan, Eduardo; Cardoso, Carolina; Martins, Maria de Fátima (2017): Curcumin decreases astrocytic reaction after gliotoxic injury in the rat brainstem. In *Arq Neuropsiquiatr* 75 (8), pp. 546–552. DOI: 10.1590/0004-282x20170092.

Bota, Daniela A.; Desjardins, Annick; Quinn, Jennifer A.; Affronti, Mary L.; Friedman, Henry S. (2007): Interstitial chemotherapy with biodegradable BCNU (Gliadel) wafers in the treatment of malignant gliomas. In *Therapeutics and clinical risk management* 3 (5), pp. 707–715.

Bozzuto, Giuseppina; Molinari, Agnese (2015): Liposomes as nanomedical devices. In *International journal of nanomedicine* 10, pp. 975–999. DOI: 10.2147/IJN.S68861.

Bramini, Mattia; Alberini, Giulio; Colombo, Elisabetta; Chiacchiaretta, Martina; DiFrancesco, Mattia L.; Maya-Vetencourt, José F. et al. (2018): Interfacing Graphene-Based Materials With Neural Cells. In *Front Syst Neurosci* 12, p. 12. DOI: 10.3389/fnsys.2018.00012.

Brem, H.; Langer, R. (1996): Polymer-based drug delivery to the brain. In *Sci. Med.*, pp. 52–61.

Brem, Sarah; Tyler, Betty; Li, Khan; Pradilla, Gustavo; Legnani, Federico; Caplan, Justin; Brem, Henry (2007): Local delivery of temozolomide by biodegradable polymers is superior to oral administration in a rodent glioma model. In *Cancer chemotherapy and pharmacology* 60 (5), pp. 643–650. DOI: 10.1007/s00280-006-0407-2.

Brewer, G. J.; Torricelli, J. R.; Evege, E. K.; Price, P. J. (1993): Optimized survival of hippocampal neurons in B27-supplemented Neurobasal, a new serum-free medium combination. In *Journal of neuroscience research* 35 (5), pp. 567–576. DOI: 10.1002/jnr.490350513.

Briceño, Eduardo; Calderon, Alejandra; Sotelo, Julio (2007): Institutional experience with chloroquine as an adjuvant to the therapy for glioblastoma multiforme. In *Surgical neurology* 67 (4), pp. 388–391. DOI: 10.1016/j.surneu.2006.08.080.

Briceño, Eduardo; Reyes, Sandra; Sotelo, Julio (2003): Therapy of glioblastoma multiforme improved by the antimutagenic chloroquine. In *Neurosurgical focus* 14 (2), e3. DOI: 10.3171/foc.2003.14.2.4.

Brightman, M. W.; Reese, T. S. (1969): Junctions between intimately apposed cell membranes in the vertebrate brain. In *The Journal of cell biology* 40 (3), pp. 648–677. DOI: 10.1083/jcb.40.3.648.

Brown, Guy C.; Neher, Jonas J. (2014): Microglial phagocytosis of live neurons. In *Nature reviews. Neuroscience* 15 (4), pp. 209–216. DOI: 10.1038/nrn3710.

Burda, J. E.; Sofroniew, M. V. (2014): Reactive gliosis and the multicellular response to CNS damage and disease. In *Neuron* 81 (2), pp. 229–248. DOI: 10.1016/j.neuron.2013.12.034.

Bushunow, P.; Reidenberg, M. M.; Wasenko, J.; Winfield, J.; Lorenzo, B.; Lemke, S. et al. (1999): Gossypol treatment of recurrent adult malignant gliomas. In *Journal of neuro-oncology* 43 (1), pp. 79–86. DOI: 10.1023/a:1006267902186.

Caillaud, Martial; Chantemargue, Benjamin; Richard, Laurence; Vignaud, Laetitia; Favreau, Frédéric; Faye, Pierre-Antoine et al. (2018): Local low dose curcumin treatment improves functional recovery and remyelination in a rat model of sciatic nerve crush through inhibition of oxidative stress. In *Neuropharmacology* 139, pp. 98–116. DOI: 10.1016/j.neuropharm.2018.07.001.

Camp, E. R.; Wang, C.; Little, E. C.; Watson, P. M.; Pirollo, K. F.; Rait, A. et al. (2013): Transferrin receptor targeting nanomedicine delivering wild-type p53 gene sensitizes pancreatic cancer to gemcitabine therapy. In *Cancer gene therapy* 20 (4), pp. 222–228. DOI: 10.1038/cgt.2013.9.

Caragher, Seamus; Chalmers, Anthony J.; Gomez-Roman, Natividad (2019): Glioblastoma's Next Top Model. Novel Culture Systems for Brain Cancer Radiotherapy Research. In *Cancers* 11 (1). DOI: 10.3390/cancers11010044.

Carroll, Robert E.; Benya, Richard V.; Turgeon, Danielle Kim; Vareed, Shaiju; Neuman, Malloree; Rodriguez, Luz et al. (2011): Phase IIa clinical trial of curcumin for the prevention of colorectal neoplasia. In *Cancer prevention research (Philadelphia, Pa.)* 4 (3), pp. 354–364. DOI: 10.1158/1940-6207.CAPR-10-0098.

Celia, Christian; Ferrati, Silvia; Bansal, Shyam; van de Ven, Anne L.; Ruozi, Barbara; Zabre, Erika et al. (2014): Sustained zero-order release of intact ultra-stable drug-loaded liposomes from an implantable nanochannel delivery system. In *Advanced healthcare materials* 3 (2), pp. 230–238. DOI: 10.1002/adhm.201300188.

Chabot, S.; Williams, G.; Yong, V. W. (1997): Microglial production of TNF-alpha is induced by activated T lymphocytes. Involvement of VLA-4 and inhibition by interferonbeta-1b. In *The Journal of clinical investigation* 100 (3), pp. 604–612. DOI: 10.1172/JCI119571.

Chaboub, Lesley S.; Deneen, Benjamin (2012): Developmental origins of astrocyte heterogeneity. The final frontier of CNS development. In *Developmental neuroscience* 34 (5), pp. 379–388. DOI: 10.1159/000343723.

Chadwick, Emily J.; Yang, David P.; Filbin, Mariella G.; Mazzola, Emanuele; Sun, Yu; Behar, Oded et al. (2015): A Brain Tumor/Organotypic Slice Co-culture System for Studying Tumor Microenvironment and Targeted Drug Therapies. In *Journal of visualized experiments : JoVE* (105), e53304. DOI: 10.3791/53304.

Chaichana, Kaisorn L.; Jusue-Torres, Ignacio; Lemos, Ana Maria; Gokaslan, Aaron; Cabrera-Aldana, Eibar Ernesto; Ashary, Ahmed et al. (2014): The butterfly effect on glioblastoma. Is volumetric extent of resection more effective than biopsy for these tumors? In *Journal of neuro-oncology* 120 (3), pp. 625–634. DOI: 10.1007/s11060-014-1597-9.

Chen, W.; He, J.; Olson, J. J.; Lu, D. R. (1997): Carboplatin-Loaded PLGA Microspheres for Intracerebral Implantation. In Vivo Characterization. In *Drug delivery* 4 (4), pp. 301–311. DOI: 10.3109/10717549709052017.

Chen, Y.; Wu, Q.; Zhang, Z.; Yuan, L.; Liu, X.; Zhou, L. (2012): Preparation of curcumin-loaded liposomes and evaluation of their skin permeation and pharmacodynamics. In *Molecules* 17 (5), pp. 5972–5987. DOI: 10.3390/molecules17055972.

Chen, Yung-Chu; Chiang, Chi-Feng; Chen, Li-Fang; Liang, Po-Chin; Hsieh, Wen-Yuan; Lin, Win-Li (2014): Polymersomes conjugated with des-octanoyl ghrelin and folate as a BBB-penetrating cancer cell-targeting delivery system. In *Biomaterials* 35 (13), pp. 4066–4081. DOI: 10.1016/j.biomaterials.2014.01.042.

Chen, Zeming; Liu, Fuyao; Chen, Yanke; Liu, Jun; Wang, Xiaoying; Chen, Ann T. et al. (2017): Targeted Delivery of CRISPR/Cas9-Mediated Cancer Gene Therapy via Liposome-Templated Hydrogel Nanoparticles. In *Advanced functional materials* 27 (46). DOI: 10.1002/adfm.201703036.

Cheon, Yeong Ah; Bae, Jun Hyuk; Chung, Bong Geun (2016): Reduced Graphene Oxide Nanosheet for Chemo-photothermal Therapy. In *Langmuir : the ACS journal of surfaces and colloids* 32 (11), pp. 2731–2736. DOI: 10.1021/acs.langmuir.6b00315.

Cherian, R. S.; Anju, S.; Paul, Willi; Sabareeswaran, A.; Mohanan, P. V. (2020): Organ distribution and biological compatibility of surface-functionalized reduced graphene oxide. In *Nanotechnology* 31 (7), p. 75303. DOI: 10.1088/1361-6528/ab4bff.

Chou, Namsun; Yoo, Soonki; Kim, Sohee (2013): A largely deformable surface type neural electrode array based on PDMS. In *IEEE transactions on neural systems and rehabilitation engineering : a publication of the IEEE Engineering in Medicine and Biology Society* 21 (4), pp. 544–553. DOI: 10.1109/TNSRE.2012.2210560.

Chou, Ting-Chao (2010): Drug combination studies and their synergy quantification using the Chou-Talalay method. In *Cancer research* 70 (2), pp. 440–446. DOI: 10.1158/0008-5472.CAN-09-1947.

Chou, Ting-Chao; Talalay, Paul (1984): Quantitative analysis of dose-effect relationships. The combined effects of multiple drugs or enzyme inhibitors. In *Advances in Enzyme Regulation* 22, pp. 27–55. DOI: 10.1016/0065-2571(84)90007-4.

Choudhury, Somsubhra Thakur; Das, Nirmalendu; Ghosh, Swarupa; Ghosh, Debasree; Chakraborty, Somsuta; Ali, Nahid (2016): Vesicular (liposomal and nanoparticulated) delivery of curcumin. A comparative study on carbon tetrachloride-mediated oxidative hepatocellular damage in rat model. In *International journal of nanomedicine* 11, pp. 2179–2193. DOI: 10.2147/IJN.S101886.

Chude, Cynthia I.; Amaravadi, Ravi K. (2017): Targeting Autophagy in Cancer. Update on Clinical Trials and Novel Inhibitors. In *International journal of molecular sciences* 18 (6). DOI: 10.3390/ijms18061279.

Clarke, Jennifer L.; Molinaro, Annette M.; Cabrera, Juan R.; DeSilva, Ashley A.; Rabbitt, Jane E.; Prey, Joshua et al. (2017): A phase 1 trial of intravenous liposomal irinotecan in patients with recurrent high-grade glioma. In *Cancer chemotherapy and pharmacology* 79 (3), pp. 603–610. DOI: 10.1007/s00280-017-3247-3.

Colangelo, A. M.; Alberghina, L.; Papa, M. (2014): Astrogliosis as a therapeutic target for neurodegenerative diseases. In *Neuroscience letters* 565, pp. 59–64. DOI: 10.1016/j.neulet.2014.01.014.

Colletti, V.; Fiorino, F.; Sacchetto, L.; Miorelli, V.; Carner, M. (2001): Hearing habilitation with auditory brainstem implantation in two children with cochlear nerve aplasia. In *International journal of pediatric otorhinolaryngology* 60 (2), pp. 99–111. DOI: 10.1016/s0165-5876(01)00465-7.

Conti, Luciano; Pollard, Steven M.; Gorba, Thorsten; Reitano, Erika; Toselli, Mauro; Biella, Gerardo et al. (2005): Niche-independent symmetrical self-renewal of a mammalian tissue stem cell. In *PLoS biology* 3 (9), e283. DOI: 10.1371/journal.pbio.0030283.

Cordon-Cardo, C.; O'Brien, J. P.; Casals, D.; Rittman-Grauer, L.; Biedler, J. L.; Melamed, M. R.; Bertino, J. R. (1989): Multidrug-resistance gene (P-glycoprotein) is expressed by endothelial cells at blood-brain barrier sites. In *Proceedings of the National Academy of Sciences of the United States of America* 86 (2), pp. 695–698. DOI: 10.1073/pnas.86.2.695.

Cornelison, R. Chase; Munson, Jennifer M. (2018): Perspective on Translating Biomaterials Into Glioma Therapy. Lessons From in vitro Models. In *Frontiers in materials* 5. DOI: 10.3389/fmats.2018.00027.

Coyle, T.; Levante, S.; Shetler, M.; Winfield, J. (1994): In vitro and in vivo cytotoxicity of gossypol against central nervous system tumor cell lines. In *Journal of neuro-oncology* 19 (1), pp. 25–35. DOI: 10.1007/bf01051046.

Cregg, J. M.; DePaul, M. A.; Filous, A. R.; Lang, B. T.; Tran, A.; Silver, J. (2014): Functional regeneration beyond the glial scar. In *Experimental neurology* 253, pp. 197–207. DOI: 10.1016/j.expneurol.2013.12.024.

Cui, Xinyan; Wiler, James; Dzaman, Marta; Altschuler, Richard A.; Martin, David C. (2003): In vivo studies of polypyrrole/peptide coated neural probes. In *Biomaterials* 24 (5), pp. 777–787. DOI: 10.1016/s0142-9612(02)00415-5.

Cui, Yanna; Zhang, Meng; Zeng, Feng; Jin, Hongyue; Xu, Qin; Huang, Yongzhuo (2016): Dual-Targeting Magnetic PLGA Nanoparticles for Codelivery of Paclitaxel and Curcumin for Brain Tumor Therapy. In *ACS applied materials & interfaces* 8 (47), pp. 32159–32169. DOI: 10.1021/acsami.6b10175.

Dalu, Abraham; Blaydes, Betty S.; Lomax, Larry G.; Delclos, K.Barry (2000): A comparison of the inflammatory response to a polydimethylsiloxane implant in male and female Balb/c mice. In *Biomaterials* 21 (19), pp. 1947–1957. DOI: 10.1016/S0142-9612(00)00078-8.

Daneman, Richard (2012): The blood-brain barrier in health and disease. In *Annals of neurology* 72 (5), pp. 648–672. DOI: 10.1002/ana.23648.

Daneman, Richard; Prat, Alexandre (2015): The Blood–Brain Barrier. In *Cold Spring Harbor Perspectives in Biology* 7 (1). DOI: 10.1101/cshperspect.a020412.

Daneman, Richard; Zhou, Lu; Kebede, Amanuel A.; Barres, Ben A. (2010): Pericytes are required for blood-brain barrier integrity during embryogenesis. In *Nature* 468 (7323), pp. 562–566. DOI: 10.1038/nature09513.

Dang, W.; Saltzman, W. M. (1994): Controlled release of macromolecules from a degradable polyanhydride matrix. In *Journal of biomaterials science. Polymer edition* 6 (3), pp. 297–311. DOI: 10.1163/156856294x00374.

Dasari Shareena, Thabitha P.; McShan, Danielle; Dasmahapatra, Asok K.; Tchounwou, Paul B. (2018): A Review on Graphene-Based Nanomaterials in Biomedical Applications and Risks in Environment and Health. In *Nano-micro letters* 10 (3). DOI: 10.1007/s40820-018-0206-4.

Davalos, Dimitrios; Grutzendler, Jaime; Yang, Guang; Kim, Jiyun V.; Zuo, Yi; Jung, Steffen et al. (2005): ATP mediates rapid microglial response to local brain injury in vivo. In *Nature neuroscience* 8 (6), pp. 752–758. DOI: 10.1038/nn1472.

Daverey, Amita; Agrawal, Sandeep K. (2016): Curcumin alleviates oxidative stress and mitochondrial dysfunction in astrocytes. In *Neuroscience* 333, pp. 92–103. DOI: 10.1016/j.neuroscience.2016.07.012.

DeAngelis, L. M. (2001): Brain tumors. In *The New England journal of medicine* 344 (2), pp. 114–123. DOI: 10.1056/NEJM200101113440207.

Del Zoppo, G. J.; Milner, R.; Mabuchi, T.; Hung, S.; Wang, X.; Koziol, J. A. (2006): Vascular matrix adhesion and the blood-brain barrier. In *Biochemical Society transactions* 34 (Pt 6), pp. 1261–1266. DOI: 10.1042/BST0341261.

Dende, Chaitanya; Meena, Jairam; Nagarajan, Perumal; Nagaraj, Viswanathan Arun; Panda, Amulya Kumar; Padmanaban, Govindarajan (2017): Nanocurcumin is superior to native curcumin in preventing degenerative changes in Experimental Cerebral Malaria. In *Scientific reports* 7 (1), p. 10062. DOI: 10.1038/s41598-017-10672-9.

Di Bei; Marszalek, Jacob; Youan, Bi-Botti C. (2009): Formulation of dacarbazine-loaded cubosomes-part I. Influence of formulation variables. In *AAPS PharmSciTech* 10 (3), pp. 1032–1039. DOI: 10.1208/s12249-009-9293-3.

Di Meo, Francesco; Margarucci, Sabrina; Galderisi, Umberto; Crispi, Stefania; Peluso, Gianfranco (2019): Curcumin, Gut Microbiota, and Neuroprotection. In *Nutrients* 11 (10). DOI: 10.3390/nu11102426.

Djiokeng Paka, Ghislain; Doggui, Sihem; Zaghmi, Ahlem; Safar, Ramia; Dao, Lé; Reisch, Andreas et al. (2016): Neuronal Uptake and Neuroprotective Properties of Curcumin-Loaded Nanoparticles on SK-N-SH Cell Line. Role of Poly(lactide-co-glycolide) Polymeric Matrix Composition. In *Molecular pharmaceutics* 13 (2), pp. 391–403. DOI: 10.1021/acs.molpharmaceut.5b00611.

Domb, A. J. (1995): Polymeric carriers for regional drug therapy. In *Molecular medicine today* 1 (3), pp. 134–139. DOI: 10.1016/s1357-4310(95)80091-3.

Donaruma, L. Guy (1988): Definitions in biomaterials, D. F. Williams, Ed., Elsevier, Amsterdam, 1987, 72 pp. In *J. Polym. Sci. B Polym. Lett. Ed.* 26 (9), p. 414. DOI: 10.1002/pol.1988.140260910.

Dong, Xiaowei (2018): Current Strategies for Brain Drug Delivery. In *Theranostics* 8 (6), pp. 1481–1493. DOI: 10.7150/thno.21254.

Donoghue, John P. (2002): Connecting cortex to machines. Recent advances in brain interfaces. In *Nature neuroscience* 5 Suppl, pp. 1085–1088. DOI: 10.1038/nn947.

Drion, Cato M.; Kooijman, Lieneke; Aronica, Eleonora; van Vliet, Erwin A.; Wadman, Wytse J.; Chameau, Pascal; Gorter, Jan A. (2019): Curcumin reduces development of seizurelike events in the hippocampal-entorhinal cortex slice culture model for epileptogenesis. In *Epilepsia* 60 (4), pp. 605–614. DOI: 10.1111/epi.14667.

Duan, Ruixue; Xia, Fan; Jiang, Lei (2013): Constructing tunable nanopores and their application in drug delivery. In *ACS nano* 7 (10), pp. 8344–8349. DOI: 10.1021/nn405092w.

Dutta, Purabi; Karmali, Rashida; Pinto, John T.; Rivlin, Richard S. (1994): Enhanced growth of mammary adenocarcinoma in rats by chloroquine and quinacrine. In *Cancer letters* 76 (2-3), pp. 113–119. DOI: 10.1016/0304-3835(94)90386-7.

East, Emma; Johns, Noémie; Georgiou, Melanie; Golding, Jon P.; Loughlin, A. Jane; Kingham, Paul J.; Phillips, James B. (2013): A 3D in vitro model reveals differences in the astrocyte response elicited by potential stem cell therapies for CNS injury. In *Regenerative medicine* 8 (6), pp. 739–746. DOI: 10.2217/rme.13.61.

Eccleston, D. S.; Horrigan, M. C.; Ellis, S. G. (1996): Rationale for local drug delivery. In *Seminars in interventional cardiology : SIIC* 1 (1), pp. 8–16.

Eisemann, Tanja; Costa, Barbara; Strelau, Jens; Mittelbronn, Michel; Angel, Peter; Peterziel, Heike (2018): An advanced glioma cell invasion assay based on organotypic brain slice cultures. In *BMC cancer* 18 (1), p. 103. DOI: 10.1186/s12885-018-4007-4.

Eles, J. R.; Vazquez, A. L.; Snyder, N. R.; Lagenaur, C.; Murphy, M. C.; Kozai, T. D.; Cui, X. T. (2017): Neuroadhesive L1 coating attenuates acute microglial attachment to neural electrodes as revealed by live two-photon microscopy. In *Biomaterials* 113, pp. 279–292. DOI: 10.1016/j.biomaterials.2016.10.054.

Elkharraz, K.; Faisant, N.; Guse, C.; Siepmann, F.; Arica-Yegin, B.; Oger, J. M. et al. (2006): Paclitaxel-loaded microparticles and implants for the treatment of brain cancer. Preparation and physicochemical characterization. In *International journal of pharmaceutics* 314 (2), pp. 127–136. DOI: 10.1016/j.ijpharm.2005.07.028.

Emerich, D. F.; Tracy, M. A.; Ward, K. L.; Figueiredo, M.; Qian, R.; Henschel, C.; Bartus, R. T. (1999): Biocompatibility of poly (DL-lactide-co-glycolide) microspheres implanted into the brain. In *Cell transplantation* 8 (1), pp. 47–58. DOI: 10.1177/096368979900800114.

Eng, L. F.; Reier, P. J.; Houle, J. D. (1987): Astrocyte activation and fibrous gliosis. Glial fibrillary acidic protein immunostaining of astrocytes following intraspinal cord grafting of fetal CNS tissue. In *Progress in brain research* 71, pp. 439–455. DOI: 10.1016/s0079-6123(08)61845-2.

Ereifej, Evon S.; Cheng, Mark Ming-Cheng; Mao, Guangzhao; VandeVord, Pamela J. (2013): Examining the inflammatory response to nanopatterned polydimethylsiloxane using organotypic brain slice methods. In *Journal of neuroscience methods* 217 (1-2), pp. 17–25. DOI: 10.1016/j.jneumeth.2013.04.023.

Fang, Chen; Wang, Kui; Stephen, Zachary R.; Mu, Qingxin; Kievit, Forrest M.; Chiu, Daniel T. et al. (2015): Temozolomide nanoparticles for targeted glioblastoma therapy. In *ACS applied materials & interfaces* 7 (12), pp. 6674–6682. DOI: 10.1021/am5092165.

Fantin, Alessandro; Vieira, Joaquim M.; Gestri, Gaia; Denti, Laura; Schwarz, Quenten; Prykhozhij, Sergey et al. (2010): Tissue macrophages act as cellular chaperones for vascular anastomosis downstream of VEGF-mediated endothelial tip cell induction. In *Blood* 116 (5), pp. 829–840. DOI: 10.1182/blood-2009-12-257832.

Fawcett, J. W.; Asher, R. A. (1999): The glial scar and central nervous system repair. In *Brain research bulletin* 49 (6), pp. 377–391. DOI: 10.1016/s0361-9230(99)00072-6.

Fazeny-Dörner, B.; Veitl, M.; Wenzel, C.; Rössler, K.; Ungersböck, K.; Dieckmann, K. et al. (2003): Survival with dacarbazine and fotemustine in newly diagnosed glioblastoma multiforme. In *British journal of cancer* 88 (4), pp. 496–501. DOI: 10.1038/sj.bjc.6600769.

Feng, T.; Wei, Y.; Lee, R. J.; Zhao, L. (2017): Liposomal curcumin and its application in cancer. In *International journal of nanomedicine* 12, pp. 6027–6044. DOI: 10.2147/IJN.S132434.

Filosa, Jessica A.; Bonev, Adrian D.; Straub, Stephen V.; Meredith, Andrea L.; Wilkerson, M. Keith; Aldrich, Richard W.; Nelson, Mark T. (2006): Local potassium signaling couples neuronal activity to vasodilation in the brain. In *Nature neuroscience* 9 (11), pp. 1397–1403. DOI: 10.1038/nn1779.

Fischer, H.; Gottschlich, R.; Seelig, A. (1998): Blood-brain barrier permeation. Molecular parameters governing passive diffusion. In *The Journal of membrane biology* 165 (3), pp. 201–211. DOI: 10.1007/s002329900434.

Fitch, M. T.; Silver, J. (2008): CNS injury, glial scars, and inflammation. Inhibitory extracellular matrices and regeneration failure. In *Experimental neurology* 209 (2), pp. 294–301. DOI: 10.1016/j.expneurol.2007.05.014.

Fournier, E.; Passirani, C.; Montero-Menei, C. N.; Benoit, J. P. (2003): Biocompatibility of implantable synthetic polymeric drug carriers. Focus on brain biocompatibility. In *Biomaterials* 24 (19), pp. 3311–3331. DOI: 10.1016/s0142-9612(03)00161-3.

Fu, Chuan; Pan, Su; Ma, Yue; Kong, Weijian; Qi, Zhiping; Yang, Xiaoyu (2019): Effect of electrical stimulation combined with graphene-oxide-based membranes on neural stem cell proliferation and differentiation. In *Artif Cells Nanomed Biotechnol* 47 (1), pp. 1867–1876. DOI: 10.1080/21691401.2019.1613422.

Garcia-Garcia, E.; Andrieux, K.; Gil, S.; Couvreur, P. (2005): Colloidal carriers and blood-brain barrier (BBB) translocation. A way to deliver drugs to the brain? In *International journal of pharmaceutics* 298 (2), pp. 274–292. DOI: 10.1016/j.ijpharm.2005.03.031.

Gaudet, A. D.; Fonken, L. K. (2018): Glial Cells Shape Pathology and Repair After Spinal Cord Injury. In *Neurotherapeutics : the journal of the American Society for Experimental NeuroTherapeutics* 15 (3), pp. 554–577. DOI: 10.1007/s13311-018-0630-7.

Gedamu, Dawit; Paulowicz, Ingo; Kaps, Sören; Lupan, Oleg; Wille, Sebastian; Haidarschin, Galina et al. (2014): Rapid fabrication technique for interpenetrated ZnO nanotetrapod networks for fast UV sensors. In *Advanced materials (Deerfield Beach, Fla.)* 26 (10), pp. 1541–1550. DOI: 10.1002/adma.201304363.

Georgieva, Julia V.; Hoekstra, Dick; Zuhorn, Inge S. (2014): Smuggling Drugs into the Brain. An Overview of Ligands Targeting Transcytosis for Drug Delivery across the Blood-Brain Barrier. In *Pharmaceutics* 6 (4), pp. 557–583. DOI: 10.3390/pharmaceutics6040557.

Gera, Meeta; Sharma, Neelesh; Ghosh, Mrinmoy; Huynh, Do Luong; Lee, Sung Jin; Min, Taesun et al. (2017): Nanoformulations of curcumin. An emerging paradigm for improved remedial application. In *Oncotarget* 8 (39), pp. 66680–66698. DOI: 10.18632/oncotarget.19164.

Ghasemi, Faezeh; Bagheri, Hossein; Barreto, George E.; Read, Morgayn I.; Sahebkar, Amirhossein (2019): Effects of Curcumin on Microglial Cells. In *Neurotoxicity research* 36 (1), pp. 12–26. DOI: 10.1007/s12640-019-00030-0.

Gieryng, A.; Pszczolkowska, D.; Walentynowicz, K. A.; Rajan, W. D.; Kaminska, B. (2017a): Immune microenvironment of gliomas. In *Laboratory investigation; a journal of technical methods and pathology* 97 (5), pp. 498–518. DOI: 10.1038/labinvest.2017.19.

Gieryng, Anna; Pszczolkowska, Dominika; Bocian, Katarzyna; Dabrowski, Michal; Rajan, Wenson David; Kloss, Michal et al. (2017b): Immune microenvironment of experimental rat C6 gliomas resembles human glioblastomas. In *Scientific reports* 7 (1), p. 17556. DOI: 10.1038/s41598-017-17752-w.

Gilbert, Ashley N.; Anderson, Joshua C.; Duarte, Christine W.; Shevin, Rachael S.; Langford, Catherine P.; Singh, Raj et al. (2018): Combinatorial Drug Testing in 3D Microtumors Derived from GBM Patient-Derived Xenografts Reveals Cytotoxic Synergy in Pharmacokinomics-informed Pathway Interactions. In *Scientific reports* 8 (1), p. 8412. DOI: 10.1038/s41598-018-26840-4.

Ginestra, Paola (2019): Manufacturing of polycaprolactone - Graphene fibers for nerve tissue engineering. In *J Mech Behav Biomed Mater* 100, p. 103387. DOI: 10.1016/j.jmbbm.2019.103387.

Giulian, D.; Li, J.; Leara, B.; Keenen, C. (1994a): Phagocytic microglia release cytokines and cytotoxins that regulate the survival of astrocytes and neurons in culture. In *Neurochemistry international* 25 (3), pp. 227–233. DOI: 10.1016/0197-0186(94)90066-3.

Giulian, D.; Li, J.; Li, X.; George, J.; Rutecki, P. A. (1994b): The impact of microglia-derived cytokines upon gliosis in the CNS. In *Developmental neuroscience* 16 (3-4), pp. 128–136. DOI: 10.1159/000112099.

Glass, Christopher K.; Saijo, Kaoru; Winner, Beate; Marchetto, Maria Carolina; Gage, Fred H. (2010): Mechanisms underlying inflammation in neurodegeneration. In *Cell* 140 (6), pp. 918–934. DOI: 10.1016/j.cell.2010.02.016.

Golden, Encouse B.; Cho, Hee-Yeon; Hofman, Florence M.; Louie, Stan G.; Schönthal, Axel H.; Chen, Thomas C. (2015): Quinoline-based antimalarial drugs. A novel class of autophagy inhibitors. In *Neurosurgical focus* 38 (3), E12. DOI: 10.3171/2014.12.FOCUS14748.

Golden, Encouse B.; Cho, Hee-Yeon; Jahanian, Ardeshir; Hofman, Florence M.; Louie, Stan G.; Schönthal, Axel H.; Chen, Thomas C. (2014): Chloroquine enhances temozolomide cytotoxicity in malignant gliomas by blocking autophagy. In *Neurosurgical focus* 37 (6), E12. DOI: 10.3171/2014.9.FOCUS14504.

Gomez-Zepeda, David; Taghi, Méryam; Scherrmann, Jean-Michel; Decleves, Xavier; Menet, Marie-Claude (2019): ABC Transporters at the Blood-Brain Interfaces, Their Study Models, and Drug Delivery Implications in Gliomas. In *Pharmaceutics* 12 (1). DOI: 10.3390/pharmaceutics12010020.

Gordon, Grant R. J.; Howarth, Clare; Macvicar, Brian A. (2011): Bidirectional control of arteriole diameter by astrocytes. In *Experimental physiology* 96 (4), pp. 393–399. DOI: 10.1113/expphysiol.2010.053132.

Groothuis, Jitte; Ramsey, Nick F.; Ramakers, Geert M. J.; van der Plasse, Geoffrey (2014): Physiological challenges for intracortical electrodes. In *Brain Stimul* 7 (1), pp. 1–6. DOI: 10.1016/j.brs.2013.07.001.

Guan, Xiudong; Hasan, Md Nabiul; Maniar, Shelly; Jia, Wang; Sun, Dandan (2018): Reactive Astrocytes in Glioblastoma Multiforme. In *Molecular neurobiology* 55 (8), pp. 6927–6938. DOI: 10.1007/s12035-018-0880-8.

Gulino, Maurizio; Kim, Donghoon; Pané, Salvador; Santos, Sofia Duque; Pêgo, Ana Paula (2019): Tissue Response to Neural Implants. The Use of Model Systems Toward New Design Solutions of Implantable Microelectrodes. In *Frontiers in neuroscience* 13, p. 689. DOI: 10.3389/fnins.2019.00689.

Guo, Liang; Deweerth, Stephen P. (2009): PDMS-based conformable microelectrode arrays with selectable novel 3-D microelectrode geometries for surface stimulation and recording. In *Conference proceedings : ... Annual International Conference of the IEEE Engineering in Medicine and Biology Society. IEEE Engineering in Medicine and Biology Society. Annual Conference* 2009, pp. 1623–1626. DOI: 10.1109/IEMBS.2009.5333446.

Ha, Sookhee N.; Hochman, Jerome; Sheridan, Robert P. (2007): Mini review on molecular modeling of P-glycoprotein (Pgp). In *Current topics in medicinal chemistry* 7 (15), pp. 1525–1529. DOI: 10.2174/156802607782194806.

Hambardzumyan, Dolores; Gutmann, David H.; Kettenmann, Helmut (2016): The role of microglia and macrophages in glioma maintenance and progression. In *Nature neuroscience* 19 (1), pp. 20–27. DOI: 10.1038/nn.4185.

Hao, Qin; Wang, Hui-Wei; Yu, Qian; Shen, Juan; Zhao, Lin; Shi, Fang-Fang et al. (2017): Effects of curcumin on the recovery of hind limb function after spinal cord injury in rats and its mechamism. In *Zhongguo ying yong sheng li xue za zhi = Zhongguo yingyong shenglixue zazhi = Chinese journal of applied physiology* 33 (5), pp. 441–444. DOI: 10.12047/j.cjap.5548.2017.106.

Hatcher, H.; Planalp, R.; Cho, J.; Torti, F. M.; Torti, S. V. (2008): Curcumin. From ancient medicine to current clinical trials. In *Cellular and molecular life sciences : CMLS* 65 (11), pp. 1631–1652. DOI: 10.1007/s00018-008-7452-4.

Hattermann, Kirsten; Sebens, Susanne; Helm, Ole; Schmitt, Anne Dorothée; Mentlein, Rolf; Mehdorn, H. Maximilian; Held-Feindt, Janka (2014): Chemokine expression profile of freshly isolated human glioblastoma-associated macrophages/microglia. In *Oncology reports* 32 (1), pp. 270–276. DOI: 10.3892/or.2014.3214.

He, Liu-fang; Chen, Hui-Jin; Qian, Long-hua; Chen, Guan-yi; Buzby, Jeffrey S. (2010): Curcumin protects pre-oligodendrocytes from activated microglia in vitro and in vivo. In *Brain research* 1339, pp. 60–69. DOI: 10.1016/j.brainres.2010.04.014.

Heese, K.; Fiebich, B. L.; Bauer, J.; Otten, U. (1998): NF-kappaB modulates lipopolysaccharide-induced microglial nerve growth factor expression. In *Glia* 22 (4), pp. 401–407. DOI: 10.1002/(sici)1098-1136(199804)22:4<401::aid-glia9>3.0.co;2-5.

Hicks, Jill; Platt, Simon; Stewart, Georgina; Senneca, Christine; Holmes, Shannon; Kent, Marc et al. (2019): Intratumoral temozolomide in spontaneous canine gliomas. Feasibility of a novel therapy using implanted microcylinders. In *Veterinary medicine and science* 5 (1), pp. 5–18. DOI: 10.1002/vms3.124.

Hinrichs, W. L. J.; Sanders, N. N.; Smedt, S. C. de; Demeester, J.; Frijlink, H. W. (2005): Inulin is a promising cryo- and lyoprotectant for PEGylated lipoplexes. In *Journal of controlled release : official journal of the Controlled Release Society* 103 (2), pp. 465–479. DOI: 10.1016/j.jconrel.2004.12.011.

Holländer, Jenny; Hakala, Risto; Suominen, Jaakko; Moritz, Niko; Yliruusi, Jouko; Sandler, Niklas (2018): 3D printed UV light cured polydimethylsiloxane devices for drug delivery. In *International journal of pharmaceutics* 544 (2), pp. 433–442. DOI: 10.1016/j.ijpharm.2017.11.016.

Hoppe, Juliana B.; Coradini, Karine; Frozza, Rudimar L.; Oliveira, Claudia M.; Meneghetti, André B.; Bernardi, Andressa et al. (2013): Free and nanoencapsulated curcumin suppress β-amyloid-induced cognitive impairments in rats. Involvement of BDNF and Akt/GSK-3β signaling pathway. In *Neurobiology of learning and memory* 106, pp. 134–144. DOI: 10.1016/j.nlm.2013.08.001.

Hu, Yu-Long; DeLay, Michael; Jahangiri, Arman; Molinaro, Annette M.; Rose, Samuel D.; Carbonell, W. Shawn; Aghi, Manish K. (2012): Hypoxia-induced autophagy promotes tumor cell survival and adaptation to antiangiogenic treatment in glioblastoma. In *Cancer research* 72 (7), pp. 1773–1783. DOI: 10.1158/0008-5472.CAN-11-3831.

Huang, Bor-Ren; Tsai, Chon-Haw; Chen, Chun-Chuan; Way, Tzong-Der; Kao, Jung-Yie; Liu, Yu-Shu et al. (2019): Curcumin Promotes Connexin 43 Degradation and Temozolomide-Induced Apoptosis in Glioblastoma Cells. In *The American journal of Chinese medicine* 47 (3), pp. 657–674. DOI: 10.1142/S0192415X19500344.

Huang, Xiao; Zeng, Zhiyuan; Fan, Zhanxi; Liu, Juqing; Zhang, Hua (2012): Graphene-based electrodes. In *Advanced materials (Deerfield Beach, Fla.)* 24 (45), pp. 5979–6004. DOI: 10.1002/adma.201201587.

Hussain, Zahid; Thu, Hnin Ei; Amjad, Muhammad Wahab; Hussain, Fahad; Ahmed, Tarek A.; Khan, Shahzeb (2017): Exploring recent developments to improve antioxidant, anti-inflammatory and antimicrobial efficacy of curcumin. A review of new trends and future perspectives. In *Materials science & engineering. C, Materials for biological applications* 77, pp. 1316–1326. DOI: 10.1016/j.msec.2017.03.226.

Iglesia, Michael D.; Parker, Joel S.; Hoadley, Katherine A.; Serody, Jonathan S.; Perou, Charles M.; Vincent, Benjamin G. (2016): Genomic Analysis of Immune Cell Infiltrates Across 11 Tumor Types. In *Journal of the National Cancer Institute* 108 (11). DOI: 10.1093/jnci/djw144.

Ignatova, Milena; Kalinov, Kalin; Manolova, Nevena; Toshkova, Reneta; Rashkov, Iliya; Alexandrov, Marin (2014): Quaternized chitosan-coated nanofibrous implants loaded with gossypol prepared by electrospinning and their efficacy against Graffi myeloid tumor. In *Journal of biomaterials science. Polymer edition* 25 (3), pp. 287–306. DOI: 10.1080/09205063.2013.857543.

Ignatova, Milena; Manolova, Nevena; Toshkova, Reneta; Rashkov, Iliya; Gardeva, Elena; Yossifova, Liliya; Alexandrov, Marin (2012): Quaternized chitosan-coated nanofibrous materials containing

gossypol. Preparation by electrospinning, characterization and antiproliferative activity towards HeLa cells. In *International journal of pharmaceutics* 436 (1-2), pp. 10–24. DOI: 10.1016/j.ijpharm.2012.06.035.

Iliff, Jeffrey J.; Wang, Minghuan; Liao, Yonghong; Plogg, Benjamin A.; Peng, Weiguo; Gundersen, Georg A. et al. (2012): A paravascular pathway facilitates CSF flow through the brain parenchyma and the clearance of interstitial solutes, including amyloid β. In *Science translational medicine* 4 (147), 147ra111. DOI: 10.1126/scitranslmed.3003748.

Imamura, Yoshinori; Mukohara, Toru; Shimono, Yohei; Funakoshi, Yohei; Chayahara, Naoko; Toyoda, Masanori et al. (2015): Comparison of 2D- and 3D-culture models as drug-testing platforms in breast cancer. In *Oncology reports* 33 (4), pp. 1837–1843. DOI: 10.3892/or.2015.3767.

Immordino, Maria Laura; Dosio, Franco; Cattel, Luigi (2006): Stealth liposomes. Review of the basic science, rationale, and clinical applications, existing and potential. In *International journal of nanomedicine* 1 (3), pp. 297–315.

Jain, Anjana; Kim, Young-Tae; McKeon, Robert J.; Bellamkonda, Ravi V. (2006): In situ gelling hydrogels for conformal repair of spinal cord defects, and local delivery of BDNF after spinal cord injury. In *Biomaterials* 27 (3), pp. 497–504. DOI: 10.1016/j.biomaterials.2005.07.008.

Janzer, R. C.; Raff, M. C. (1987): Astrocytes induce blood-brain barrier properties in endothelial cells. In *Nature* 325 (6101), pp. 253–257. DOI: 10.1038/325253a0.

Jarzabek, M. A.; Amberger-Murphy, V.; Callanan, J. J.; Gao, C.; Zagozdzon, A. M.; Shiels, L. et al. (2014): Interrogation of gossypol therapy in glioblastoma implementing cell line and patient-derived tumour models. In *British journal of cancer* 111 (12), pp. 2275–2286. DOI: 10.1038/bjc.2014.529.

Jarzabek, Monika A.; Sweeney, Kieron J.; Evans, Rhys L.; Jacobs, Andreas H.; Stupp, Roger; O'Brien, Donncha et al. (2013): Molecular imaging in the development of a novel treatment paradigm for glioblastoma (GBM). An integrated multidisciplinary commentary. In *Drug discovery today* 18 (21-22), pp. 1052–1066. DOI: 10.1016/j.drudis.2013.06.004.

Jaworski, Sławomir; Sawosz, Ewa; Grodzik, Marta; Winnicka, Anna; Prasek, Marta; Wierzbicki, Mateusz; Chwalibog, André (2013): In vitro evaluation of the effects of graphene platelets on glioblastoma multiforme cells. In *International journal of nanomedicine* 8, pp. 413–420. DOI: 10.2147/IJN.S39456.

Jeevanandam, Jaison; Barhoum, Ahmed; Chan, Yen S.; Dufresne, Alain; Danquah, Michael K. (2018): Review on nanoparticles and nanostructured materials. History, sources, toxicity and regulations. In *Beilstein journal of nanotechnology* 9, pp. 1050–1074. DOI: 10.3762/bjnano.9.98.

Jeong, Hey-Kyeong; Ji, Kyungmin; Min, Kyungjin; Joe, Eun-Hye (2013): Brain Inflammation and Microglia. Facts and Misconceptions. In *Exp Neurobiol* 22 (2), p. 59. DOI: 10.5607/en.2013.22.2.59.

Jhaveri, Aditi; Deshpande, Pranali; Pattni, Bhushan; Torchilin, Vladimir (2018): Transferrin-targeted, resveratrol-loaded liposomes for the treatment of glioblastoma. In *Journal of controlled release : official journal of the Controlled Release Society* 277, pp. 89–101. DOI: 10.1016/j.jconrel.2018.03.006.

Jiang, Kaiyuan; Weaver, Jessica D.; Li, Yangjunyi; Chen, Xiongjian; Liang, Jiapu; Stabler, Cherie L. (2017): Local release of dexamethasone from macroporous scaffolds accelerates islet transplant engraftment by promotion of anti-inflammatory M2 macrophages. In *Biomaterials* 114, pp. 71–81. DOI: 10.1016/j.biomaterials.2016.11.004.

Jin, Cai-Ling; Chen, Mei-Ling; Wang, Ying; Kang, Xiao-Chun; Han, Guang-Ye; Xu, Su-Ling (2015): Preparation of novel (-)-gossypol nanoparticles and the effect on growth inhibition in human prostate

cancer PC-3 cells in vitro. In *Experimental and therapeutic medicine* 9 (3), pp. 675–678. DOI: 10.3892/etm.2015.2172.

Jin, Hong-Hao; Lu, Qun; Jiang, Jian-Guo (2016): Curcumin liposomes prepared with milk fat globule membrane phospholipids and soybean lecithin. In *Journal of dairy science* 99 (3), pp. 1780–1790. DOI: 10.3168/jds.2015-10391.

Kam, L.; Shain, W.; Turner, J. N.; Bizios, R. (2002): Selective adhesion of astrocytes to surfaces modified with immobilized peptides. In *Biomaterials* 23 (2), pp. 511–515. DOI: 10.1016/s0142-9612(01)00133-8.

Karimi-Abdolrezaee, Soheila; Billakanti, Rohini (2012): Reactive astrogliosis after spinal cord injury-beneficial and detrimental effects. In *Molecular neurobiology* 46 (2), pp. 251–264. DOI: 10.1007/s12035-012-8287-4.

Karlstetter, Marcus; Lippe, Elena; Walczak, Yana; Moehle, Christoph; Aslanidis, Alexander; Mirza, Myriam; Langmann, Thomas (2011): Curcumin is a potent modulator of microglial gene expression and migration. In *Journal of neuroinflammation* 8, p. 125. DOI: 10.1186/1742-2094-8-125.

Kaur, Harpreet; Patro, Ishan; Tikoo, Kulbhushan; Sandhir, Rajat (2015): Curcumin attenuates inflammatory response and cognitive deficits in experimental model of chronic epilepsy. In *Neurochemistry international* 89, pp. 40–50. DOI: 10.1016/j.neuint.2015.07.009.

Kaurav, Hemlata; Kapoor, Deepak N. (2017): Implantable systems for drug delivery to the brain. In *Therapeutic delivery* 8 (12), pp. 1097–1107. DOI: 10.4155/tde-2017-0082.

Keith, Curtis T.; Borisy, Alexis A.; Stockwell, Brent R. (2005): Multicomponent therapeutics for networked systems. In *Nature reviews. Drug discovery* 4 (1), pp. 71–78. DOI: 10.1038/nrd1609.

Kenny, Hilary A.; Lal-Nag, Madhu; White, Erin A.; Shen, Min; Chiang, Chun-Yi; Mitra, Anirban K. et al. (2015): Quantitative high throughput screening using a primary human three-dimensional organotypic culture predicts in vivo efficacy. In *Nature communications* 6, p. 6220. DOI: 10.1038/ncomms7220.

Khan, Abdur Rauf; Yang, Xiaoye; Fu, Manfei; Zhai, Guangxi (2018): Recent progress of drug nanoformulations targeting to brain. In *Journal of controlled release : official journal of the Controlled Release Society* 291, pp. 37–64. DOI: 10.1016/j.jconrel.2018.10.004.

Khan, Muhammad Sohail; Muhammad, Tahir; Ikram, Muhammad; Kim, Myeong Ok (2019): Dietary Supplementation of the Antioxidant Curcumin Halts Systemic LPS-Induced Neuroinflammation-Associated Neurodegeneration and Memory/Synaptic Impairment via the JNK/NF-κB/Akt Signaling Pathway in Adult Rats. In *Oxidative medicine and cellular longevity* 2019, p. 7860650. DOI: 10.1155/2019/7860650.

Kharat, Mahesh; Du, Zheyuan; Zhang, Guodong; McClements, David Julian (2017): Physical and Chemical Stability of Curcumin in Aqueous Solutions and Emulsions. Impact of pH, Temperature, and Molecular Environment. In *Journal of agricultural and food chemistry* 65 (8), pp. 1525–1532. DOI: 10.1021/acs.jafc.6b04815.

Kim, Carla F. Bender; Jackson, Erica L.; Woolfenden, Amber E.; Lawrence, Sharon; Babar, Imran; Vogel, Sinae et al. (2005): Identification of bronchioalveolar stem cells in normal lung and lung cancer. In *Cell* 121 (6), pp. 823–835. DOI: 10.1016/j.cell.2005.03.032.

Kim, Chong-Kook; Jeong, Eun Ju (1995): Development of dried liposome as effective immuno-adjuvant for hepatitis b surface antigen. In *International journal of pharmaceutics* 115 (2), pp. 193–199. DOI: 10.1016/0378-5173(94)00258-7.

Kim, Dong-Hwan; Martin, David C. (2006): Sustained release of dexamethasone from hydrophilic matrices using PLGA nanoparticles for neural drug delivery. In *Biomaterials* 27 (15), pp. 3031–3037. DOI: 10.1016/j.biomaterials.2005.12.021.

Klueglich, Matthias; Ring, Arne; Scheuerer, Stefan; Trommeshauser, Dirk; Schuijt, Chris; Liepold, Bernd; Berndl, Gunther (2005): Ibuprofen extrudate, a novel, rapidly dissolving ibuprofen formulation. Relative bioavailability compared to ibuprofen lysinate and regular ibuprofen, and food effect on all formulations. In *Journal of clinical pharmacology* 45 (9), pp. 1055–1061. DOI: 10.1177/0091270005279579.

Kolter, Melanie; Wittmann, Maximilian; Köll-Weber, Monika; Süss, Regine (2019): The suitability of liposomes for the delivery of hydrophobic drugs - A case study with curcumin. In *European journal of pharmaceutics and biopharmaceutics : official journal of Arbeitsgemeinschaft fur Pharmazeutische Verfahrenstechnik e.V* 140, pp. 20–28. DOI: 10.1016/j.ejpb.2019.04.013.

Kornev, Vladimir A.; Grebenik, Ekaterina A.; Solovieva, Anna B.; Dmitriev, Ruslan I.; Timashev, Peter S. (2018): Hydrogel-assisted neuroregeneration approaches towards brain injury therapy. A state-of-the-art review. In *Computational and structural biotechnology journal* 16, pp. 488–502. DOI: 10.1016/j.csbj.2018.10.011.

Kou, J. H.; Emmett, C.; Shen, P.; Aswani, S.; Iwamoto, T.; Vaghefi, F. et al. (1997): Bioerosion and biocompatibility of poly(D,L,-lactic-co-glycolic acid) implants in brain. // Bioerosion and biocompatibility of poly(d,l-lactic-co-glycolic acid) implants in brain. In *Journal of controlled release : official journal of the Controlled Release Society* 43 (2-3), pp. 123–130. DOI: 10.1016/S0168-3659(96)01477-0.

Kozai, Takashi D. Y.; Jaquins-Gerstl, Andrea S.; Vazquez, Alberto L.; Michael, Adrian C.; Cui, X. Tracy (2015): Brain tissue responses to neural implants impact signal sensitivity and intervention strategies. In *ACS chemical neuroscience* 6 (1), pp. 48–67. DOI: 10.1021/cn500256e.

Kozai, Takashi D. Y.; Jaquins-Gerstl, Andrea S.; Vazquez, Alberto L.; Michael, Adrian C.; Cui, X. Tracy (2016): Dexamethasone retrodialysis attenuates microglial response to implanted probes in vivo. In *Biomaterials* 87, pp. 157–169. DOI: 10.1016/j.biomaterials.2016.02.013.

Kriel, Jurgen; Müller-Nedebock, Kristian; Maarman, Gerald; Mbizana, Siyasanga; Ojuka, Edward; Klumperman, Bert; Loos, Ben (2018): Coordinated autophagy modulation overcomes glioblastoma chemoresistance through disruption of mitochondrial bioenergetics. In *Scientific reports* 8 (1), p. 10348. DOI: 10.1038/s41598-018-28590-9.

Krupa, Petr; Svobodova, Barbora; Dubisova, Jana; Kubinova, Sarka; Jendelova, Pavla; Machova Urdzikova, Lucia (2019): Nano-formulated curcumin (Lipodisq™) modulates the local inflammatory response, reduces glial scar and preserves the white matter after spinal cord injury in rats. In *Neuropharmacology* 155, pp. 54–64. DOI: 10.1016/j.neuropharm.2019.05.018.

Kumar Naraharisetti, Pavan; Yung Sheng Ong, Benjamin; Wei Xie, Jing; Kam Yiu Lee, Timothy; Wang, Chi-Hwa; Sahinidis, Nikolaos V. (2007): In vivo performance of implantable biodegradable preparations delivering Paclitaxel and Etanidazole for the treatment of glioma. In *Biomaterials* 28 (5), pp. 886–894. DOI: 10.1016/j.biomaterials.2006.09.044.

Kumari, Avnesh; Yadav, Sudesh Kumar; Yadav, Subhash C. (2010): Biodegradable polymeric nanoparticles based drug delivery systems. In *Colloids and surfaces. B, Biointerfaces* 75 (1), pp. 1–18. DOI: 10.1016/j.colsurfb.2009.09.001.

Kunnumakkara, Ajaikumar B.; Anand, Preetha; Aggarwal, Bharat B. (2008): Curcumin inhibits proliferation, invasion, angiogenesis and metastasis of different cancers through interaction with multiple cell signaling proteins. In *Cancer letters* 269 (2), pp. 199–225. DOI: 10.1016/j.canlet.2008.03.009.

Kuramitsu, Shunichiro; Motomura, Kazuya; Natsume, Atsushi; Wakabayashi, Toshihiko (2015): Double-edged Sword in the Placement of Carmustine (BCNU) Wafers along the Eloquent Area. A Case Report. In *NMC case report journal* 2 (1), pp. 40–45. DOI: 10.2176/nmccrj.2014-0025.

La Puente, Pilar de; Fettig, Nicole; Luderer, Micah J.; Jin, Abbey; Shah, Shruti; Muz, Barbara et al. (2018): Injectable Hydrogels for Localized Chemotherapy and Radiotherapy in Brain Tumors. In *Journal of pharmaceutical sciences* 107 (3), pp. 922–933. DOI: 10.1016/j.xphs.2017.10.042.

La Rocca, Renato V.; Mehdorn, H. Maximilian (2009): Localized BCNU chemotherapy and the multimodal management of malignant glioma. In *Current medical research and opinion* 25 (1), pp. 149–160. DOI: 10.1185/03007990802611935.

Lacour, Stéphanie P.; Benmerah, Samia; Tarte, Edward; FitzGerald, James; Serra, Jordi; McMahon, Stephen et al. (2010): Flexible and stretchable micro-electrodes for in vitro and in vivo neural interfaces. In *Medical & biological engineering & computing* 48 (10), pp. 945–954. DOI: 10.1007/s11517-010-0644-8.

Laks, Dan R.; Masterman-Smith, Michael; Visnyei, Koppany; Angenieux, Brigitte; Orozco, Nicholas M.; Foran, Ian et al. (2009): Neurosphere formation is an independent predictor of clinical outcome in malignant glioma. In *Stem cells (Dayton, Ohio)* 27 (4), pp. 980–987. DOI: 10.1002/stem.15.

Landis, D. M. (1994): The early reactions of non-neuronal cells to brain injury. In *Annual review of neuroscience* 17, pp. 133–151. DOI: 10.1146/annurev.ne.17.030194.001025.

Landis-Piwowar, Kristin R.; Milacic, Vesna; Di Chen; Yang, Huanjie; Zhao, Yunfeng; Chan, Tak Hang et al. (2006): The proteasome as a potential target for novel anticancer drugs and chemosensitizers. In *Drug resistance updates : reviews and commentaries in antimicrobial and anticancer chemotherapy* 9 (6), pp. 263–273. DOI: 10.1016/j.drup.2006.11.001.

Langer, R.; Folkman, J. (1976): Polymers for the sustained release of proteins and other macromolecules. In *Nature* 263 (5580), pp. 797–800. DOI: 10.1038/263797a0.

Lasic, D. D. (1998): Novel applications of liposomes. In *Trends in biotechnology* 16 (7), pp. 307–321. DOI: 10.1016/s0167-7799(98)01220-7.

Lee, Changgu; Wei, Xiaoding; Kysar, Jeffrey W.; Hone, James (2008): Measurement of the elastic properties and intrinsic strength of monolayer graphene. In *Science (New York, N.Y.)* 321 (5887), pp. 385–388. DOI: 10.1126/science.1157996.

Lee, Hae Sung; Jung, Ki Kyung; Cho, Jae Youl; Rhee, Man Hee; Hong, Sungyoul; Kwon, Moosik et al. (2007): Neuroprotective effect of curcumin is mainly mediated by blockade of microglial cell activation. In *Die Pharmazie* 62 (12), pp. 937–942.

Lee, Sang Y. (2016): Temozolomide resistance in glioblastoma multiforme. In *Genes & diseases* 3 (3), pp. 198–210. DOI: 10.1016/j.gendis.2016.04.007.

Leece, Rebecca; Xu, Jordan; Ostrom, Quinn T.; Chen, Yanwen; Kruchko, Carol; Barnholtz-Sloan, Jill S. (2017): Global incidence of malignant brain and other central nervous system tumors by histology, 2003-2007. In *Neuro-oncology* 19 (11), pp. 1553–1564. DOI: 10.1093/neuonc/nox091.

Lenting, Krissie; Verhaak, Roel; Ter Laan, Mark; Wesseling, Pieter; Leenders, William (2017): Glioma. Experimental models and reality. In *Acta neuropathologica* 133 (2), pp. 263–282. DOI: 10.1007/s00401-017-1671-4.

Lewis, D. H. (Ed.) (1990): Controlled release of bioactive agents from lactide/glycolide polymers. With assistance of M. Chasin and R. Langer, Eds. Biodegradable Polymers as Drug Delivery Systems. New

York: Marcel Dekker. Available online at https://www.scirp.org/(S(351jmbntvnsjt1aadkposzje))/reference/ReferencesPapers.aspx?ReferenceID=438888.

Li, Hong; Piao, Longzhu; Xu, Pingping; Ye, Weiping; Zhong, Saiyi; Lin, Shu-Hong et al. (2011): Liposomes containing (-)-gossypol-enriched cottonseed oil suppress Bcl-2 and Bcl-xL expression in breast cancer cells. In *Pharmaceutical research* 28 (12), pp. 3256–3264. DOI: 10.1007/s11095-011-0498-2.

Li, Qiang; Lin, Haishuang; Rauch, Jack; Deleyrolle, Loic P.; Reynolds, Brent A.; Viljoen, Hendrik J. et al. (2018a): Scalable Culturing of Primary Human Glioblastoma Tumor-Initiating Cells with a Cell-Friendly Culture System. In *Scientific reports* 8 (1), p. 3531. DOI: 10.1038/s41598-018-21927-4.

Li, Ruibin; Guiney, Linda M.; Chang, Chong Hyun; Mansukhani, Nikhita D.; Ji, Zhaoxia; Wang, Xiang et al. (2018b): Surface Oxidation of Graphene Oxide Determines Membrane Damage, Lipid Peroxidation, and Cytotoxicity in Macrophages in a Pulmonary Toxicity Model. In *ACS nano* 12 (2), pp. 1390–1402. DOI: 10.1021/acsnano.7b07737.

Li, Shouwei; Jiang, Tao; Li, Guilin; Wang, Zhongcheng (2008a): Impact of p53 status to response of temozolomide in low MGMT expression glioblastomas. Preliminary results. In *Neurological research* 30 (6), pp. 567–570. DOI: 10.1179/174313208X297913.

Li, Xiaolin; Wang, Xinran; Zhang, Li; Lee, Sangwon; Dai, Hongjie (2008b): Chemically derived, ultrasmooth graphene nanoribbon semiconductors. In *Science (New York, N.Y.)* 319 (5867), pp. 1229–1232. DOI: 10.1126/science.1150878.

Lian, T.; Ho, R. J. (2001): Trends and developments in liposome drug delivery systems. In *Journal of pharmaceutical sciences* 90 (6), pp. 667–680. DOI: 10.1002/jps.1023.

Liao, Chengzhu; Li, Yuchao; Tjong, Sie Chin (2018): Graphene Nanomaterials. Synthesis, Biocompatibility, and Cytotoxicity. In *International journal of molecular sciences* 19 (11). DOI: 10.3390/ijms19113564.

Liao, Se-Chun; Hsu, Wei-Hsiang; Huang, Zi-Yi; Chuang, Kun-Lin; Lin, Kuan-Ting; Tseng, Chia-Ling et al. (2019): Bioactivity Evaluation of a Novel Formulated Curcumin. In *Nutrients* 11 (12). DOI: 10.3390/nu11122982.

Liddelow, Shane A.; Guttenplan, Kevin A.; Clarke, Laura E.; Bennett, Frederick C.; Bohlen, Christopher J.; Schirmer, Lucas et al. (2017): Neurotoxic reactive astrocytes are induced by activated microglia. In *Nature* 541 (7638), pp. 481–487. DOI: 10.1038/nature21029.

Lillehei, K. O.; Kong, Q.; Withrow, S. J.; Kleinschmidt-DeMasters, B. (1996): Efficacy of intralesionally administered cisplatin-impregnated biodegradable polymer for the treatment of 9L gliosarcoma in the rat. In *Neurosurgery* 39 (6), 1191-7; discussion 1197-9. DOI: 10.1097/00006123-199612000-00023.

Ling, E. A.; Wong, W. C. (1993): The origin and nature of ramified and amoeboid microglia. A historical review and current concepts. In *Glia* 7 (1), pp. 9–18. DOI: 10.1002/glia.440070105.

Lingineni, Karthik; Belekar, Vilas; Tangadpalliwar, Sujit R.; Garg, Prabha (2017): The role of multidrug resistance protein (MRP-1) as an active efflux transporter on blood-brain barrier (BBB) permeability. In *Molecular diversity* 21 (2), pp. 355–365. DOI: 10.1007/s11030-016-9715-6.

Liong, Monty; Lu, Jie; Kovochich, Michael; Xia, Tian; Ruehm, Stefan G.; Nel, Andre E. et al. (2008): Multifunctional inorganic nanoparticles for imaging, targeting, and drug delivery. In *ACS nano* 2 (5), pp. 889–896. DOI: 10.1021/nn800072t.

Lisi, L.; Ciotti, G. M. P.; Braun, D.; Kalinin, S.; Currò, D.; Dello Russo, C. et al. (2017): Expression of iNOS, CD163 and ARG-1 taken as M1 and M2 markers of microglial polarization in human glioblastoma and the surrounding normal parenchyma. In *Neuroscience letters* 645, pp. 106–112. DOI: 10.1016/j.neulet.2017.02.076.

Liu, Hao; Li, Ke; Lan, Lan; Ma, Jingwen; Zeng, Yun; Xu, Liang; Wu, Daocheng (2014): Double-layered hyaluronic acid/stearic acid-modified polyethyleneimine nanoparticles encapsulating (-)-gossypol. A nanocarrier for chiral anticancer drugs. In *Journal of materials chemistry. B* 2 (32), pp. 5238–5248. DOI: 10.1039/C4TB00539B.

Liu, Jingyi; Liu, Chao; Zhang, Jinfeng; Zhang, Yunming; Liu, Keyin; Song, Ju-Xian et al. (2020): A Self-Assembled α-Synuclein Nanoscavenger for Parkinson's Disease. In *ACS nano*. *DOI:* 10.1021/acsnano.9b06453.

Liu, Shenbin; Li, Qian; Zhang, Meng-Ting; Mao-Ying, Qi-Liang; Hu, Lang-Yue; Wu, Gen-Cheng et al. (2016): Curcumin ameliorates neuropathic pain by down-regulating spinal IL-1β via suppressing astroglial NALP1 inflammasome and JAK2-STAT3 signalling. In *Scientific reports* 6, p. 28956. DOI: 10.1038/srep28956.

López-Dolado, Elisa; González-Mayorga, Ankor; Portolés, María Teresa; Feito, María José; Ferrer, María Luisa; Del Monte, Francisco et al. (2015): Subacute Tissue Response to 3D Graphene Oxide Scaffolds Implanted in the Injured Rat Spinal Cord. In *Advanced healthcare materials* 4 (12), pp. 1861–1868. DOI: 10.1002/adhm.201500333.

Lopresti, Adrian L. (2018): The Problem of Curcumin and Its Bioavailability. Could Its Gastrointestinal Influence Contribute to Its Overall Health-Enhancing Effects? In *Advances in nutrition (Bethesda, Md.)* 9 (1), pp. 41–50. DOI: 10.1093/advances/nmx011.

Löscher, Wolfgang; Potschka, Heidrun (2005): Blood-brain barrier active efflux transporters. ATP-binding cassette gene family. In *NeuroRx : the journal of the American Society for Experimental NeuroTherapeutics* 2 (1), pp. 86–98. DOI: 10.1602/neurorx.2.1.86.

Louis, David N.; Ellison, David W.; Brat, Daniel J.; Aldape, Kenneth; Capper, David; Hawkins, Cynthia et al. (2019): cIMPACT-NOW. A practical summary of diagnostic points from Round 1 updates. In *Brain pathology (Zurich, Switzerland)* 29 (4), pp. 469–472. DOI: 10.1111/bpa.12732.

Lu, Yaxin; Yu, Yeling; Tang, Xing (2007): Sucrose acetate isobutyrate as an in situ forming system for sustained risperidone release. In *Journal of pharmaceutical sciences* 96 (12), pp. 3252–3262. DOI: 10.1002/jps.21091.

Luca, Anna C.; Mersch, Sabrina; Deenen, René; Schmidt, Stephan; Messner, Isabelle; Schäfer, Karl-Ludwig et al. (2013): Impact of the 3D microenvironment on phenotype, gene expression, and EGFR inhibition of colorectal cancer cell lines. In *PloS one* 8 (3), e59689. DOI: 10.1371/journal.pone.0059689.

Ludwig, Kip A.; Uram, Jeffrey D.; Yang, Junyan; Martin, David C.; Kipke, Daryl R. (2006): Chronic neural recordings using silicon microelectrode arrays electrochemically deposited with a poly(3,4-ethylenedioxythiophene) (PEDOT) film. In *Journal of neural engineering* 3 (1), pp. 59–70. DOI: 10.1088/1741-2560/3/1/007.

Ma, Juan; Liu, Rui; Wang, Xiang; Liu, Qian; Chen, Yunan; Valle, Russell P. et al. (2015): Crucial Role of Lateral Size for Graphene Oxide in Activating Macrophages and Stimulating Pro-inflammatory Responses in Cells and Animals. In *ACS nano* 9 (10), pp. 10498–10515. DOI: 10.1021/acsnano.5b04751.

Ma, Ziwei; Wang, Na; He, Haibing; Tang, Xing (2019): Pharmaceutical strategies of improving oral systemic bioavailability of curcumin for clinical application. In *Journal of controlled release : official journal of the Controlled Release Society* 316, pp. 359–380. DOI: 10.1016/j.jconrel.2019.10.053.

Machova Urdzikova, Lucia; Karova, Kristyna; Ruzicka, Jiri; Kloudova, Anna; Shannon, Craig; Dubisova, Jana et al. (2015): The Anti-Inflammatory Compound Curcumin Enhances Locomotor and Sensory Recovery after Spinal Cord Injury in Rats by Immunomodulation. In *International journal of molecular sciences* 17 (1). DOI: 10.3390/ijms17010049.

Maclean, Francesca L.; Horne, Malcolm K.; Williams, Richard J.; Nisbet, David R. (2018): Review. Biomaterial systems to resolve brain inflammation after traumatic injury. In *APL bioengineering* 2 (2), p. 21502. DOI: 10.1063/1.5023709.

Maclean, Francesca L.; Wang, Yi; Walker, Rohan; Horne, Malcolm K.; Williams, Richard J.; Nisbet, David R. (2017): Reducing Astrocytic Scarring after Traumatic Brain Injury with a Multifaceted Anti-Inflammatory Hydrogel System. In *ACS Biomater. Sci. Eng.* 3 (10), pp. 2542–2549. DOI: 10.1021/acsbiomaterials.7b00524.

Maclean, Kirsteen H.; Dorsey, Frank C.; Cleveland, John L.; Kastan, Michael B. (2008): Targeting lysosomal degradation induces p53-dependent cell death and prevents cancer in mouse models of lymphomagenesis. In *The Journal of clinical investigation* 118 (1), pp. 79–88. DOI: 10.1172/JCI33700.

Maiti, Panchanan; Scott, Jason; Sengupta, Dipanwita; Al-Gharaibeh, Abeer; Dunbar, Gary L. (2019): Curcumin and Solid Lipid Curcumin Particles Induce Autophagy, but Inhibit Mitophagy and the PI3K-Akt/mTOR Pathway in Cultured Glioblastoma Cells. In *International journal of molecular sciences* 20 (2). DOI: 10.3390/ijms20020399.

Makadia, Hirenkumar K.; Siegel, Steven J. (2011): Poly Lactic-co-Glycolic Acid (PLGA) as Biodegradable Controlled Drug Delivery Carrier. In *Polymers* 3 (3), pp. 1377–1397. DOI: 10.3390/polym3031377.

Manini, Ivana; Caponnetto, Federica; Bartolini, Anna; Ius, Tamara; Mariuzzi, Laura; Di Loreto, Carla et al. (2018): Role of Microenvironment in Glioma Invasion. What We Learned from In Vitro Models. In *International journal of molecular sciences* 19 (1). DOI: 10.3390/ijms19010147.

Marin, Cristina; Fernández, Eduardo (2010): Biocompatibility of intracortical microelectrodes. Current status and future prospects. In *Frontiers in neuroengineering* 3, p. 8. DOI: 10.3389/fneng.2010.00008.

Marques-Torrejon, Maria Angeles; Gangoso, Ester; Pollard, Steven M. (2018): Modelling glioblastoma tumour-host cell interactions using adult brain organotypic slice co-culture. In *Disease models & mechanisms* 11 (2). DOI: 10.1242/dmm.031435.

Martin, Frank; Walczak, Robbie; Boiarski, Anthony; Cohen, Michael; West, Teri; Cosentino, Carlo et al. (2005): Tailoring width of microfabricated nanochannels to solute size can be used to control diffusion kinetics. In *Journal of controlled release : official journal of the Controlled Release Society* 102 (1), pp. 123–133. DOI: 10.1016/j.jconrel.2004.09.024.

Martinez, Marilyn N.; Amidon, Gordon L. (2002): A mechanistic approach to understanding the factors affecting drug absorption. A review of fundamentals. In *Journal of clinical pharmacology* 42 (6), pp. 620–643. DOI: 10.1177/00970002042006005.

Matias, D.; Balca-Silva, J.; da Graca, G. C.; Wanjiru, C. M.; Macharia, L. W.; Nascimento, C. P. et al. (2018): Microglia/Astrocytes-Glioblastoma Crosstalk. Crucial Molecular Mechanisms and Microenvironmental Factors. In *Frontiers in cellular neuroscience* 12, p. 235. DOI: 10.3389/fncel.2018.00235.

McConnell, George C.; Rees, Howard D.; Levey, Allan I.; Gutekunst, Claire-Anne; Gross, Robert E.; Bellamkonda, Ravi V. (2009): Implanted neural electrodes cause chronic, local inflammation that is correlated with local neurodegeneration. In *Journal of neural engineering* 6 (5), p. 56003. DOI: 10.1088/1741-2560/6/5/056003.

McGirt, Matthew J.; Chaichana, Kaisorn L.; Gathinji, Muraya; Attenello, Frank J.; Than, Khoi; Olivi, Alessandro et al. (2009): Independent association of extent of resection with survival in patients with malignant brain astrocytoma. In *Journal of neurosurgery* 110 (1), pp. 156–162. DOI: 10.3171/2008.4.17536.

McKeon, R. J.; Schreiber, R. C.; Rudge, J. S.; Silver, J. (1991): Reduction of neurite outgrowth in a model of glial scarring following CNS injury is correlated with the expression of inhibitory molecules on reactive astrocytes. In *J. Neurosci.* 11 (11), pp. 3398–3411. DOI: 10.1523/JNEUROSCI.11-11-03398.1991.

McRae, A.; Dahlström, A. (1994): Transmitter-loaded polymeric microspheres induce regrowth of dopaminergic nerve terminals in striata of rats with 6-OH-DA induced parkinsonism. In *Neurochemistry international* 25 (1), pp. 27–33. DOI: 10.1016/0197-0186(94)90049-3.

Mehner, Moiken; Kubelt, Carolin; Adamski, Vivian; Schmitt, Christina; Synowitz, Michael; Held-Feindt, Janka (2019): Combined treatment of AT101 and demethoxycurcumin yields an enhanced anti-proliferative effect in human primary glioblastoma cells. In *J Cancer Res Clin Oncol. DOI:* 10.1007/s00432-019-03107-7.

Meilander, Nancy J.; Pasumarthy, Murali K.; Kowalczyk, Tomasz H.; Cooper, Mark J.; Bellamkonda, Ravi V. (2003): Sustained release of plasmid DNA using lipid microtubules and agarose hydrogel. In *Journal of controlled release : official journal of the Controlled Release Society* 88 (2), pp. 321–331. DOI: 10.1016/s0168-3659(03)00007-5.

Meletis, Konstantinos; Barnabé-Heider, Fanie; Carlén, Marie; Evergren, Emma; Tomilin, Nikolay; Shupliakov, Oleg; Frisén, Jonas (2008): Spinal cord injury reveals multilineage differentiation of ependymal cells. In *PLoS biology* 6 (7), e182. DOI: 10.1371/journal.pbio.0060182.

Mendes, Rafael Gregorio; Koch, Britta; Bachmatiuk, Alicja; Ma, Xing; Sanchez, Samuel; Damm, Christine et al. (2015): A size dependent evaluation of the cytotoxicity and uptake of nanographene oxide. In *J. Mater. Chem. B* 3 (12), pp. 2522–2529. DOI: 10.1039/C5TB00180C.

Mendonça, Monique Culturato Padilha; Soares, Edilene Siqueira; Jesus, Marcelo Bispo de; Ceragioli, Helder José; Batista, Ângela Giovana; Nyúl-Tóth, Ádám et al. (2016a): PEGylation of Reduced Graphene Oxide Induces Toxicity in Cells of the Blood-Brain Barrier. An in Vitro and in Vivo Study. In *Mol Pharm* 13 (11), pp. 3913–3924. DOI: 10.1021/acs.molpharmaceut.6b00696.

Mendonça, Monique Culturato Padilha; Soares, Edilene Siqueira; Jesus, Marcelo Bispo de; Ceragioli, Helder José; Irazusta, Silvia Pierre; Batista, Ângela Giovana et al. (2016b): Reduced graphene oxide. nanotoxicological profile in rats. In *J Nanobiotechnology* 14 (1), p. 53. DOI: 10.1186/s12951-016-0206-9.

Menei, P.; Boisdron-Celle, M.; Croué, A.; Guy, G.; Benoit, J. P. (1996): Effect of stereotactic implantation of biodegradable 5-fluorouracil-loaded microspheres in healthy and C6 glioma-bearing rats. In *Neurosurgery* 39 (1), 117-23; discussion 123-4. DOI: 10.1097/00006123-199607000-00023.

Menei, P.; Daniel, V.; Montero-Menei, C.; Brouillard, M.; Pouplard-Barthelaix, A.; Benoit, J. P. (1993): Biodegradation and brain tissue reaction to poly(D,L-lactide-co-glycolide) microspheres. In *Biomaterials* 14 (6), pp. 470–478. DOI: 10.1016/0142-9612(93)90151-q.

Meng, Yang; Tang, Wenhua; Dai, Yao; Wu, Xiaoqing; Liu, Meilan; Ji, Qing et al. (2008): Natural BH3 mimetic (-)-gossypol chemosensitizes human prostate cancer via Bcl-xL inhibition accompanied by

increase of Puma and Noxa. In *Molecular cancer therapeutics* 7 (7), pp. 2192–2202. DOI: 10.1158/1535-7163.MCT-08-0333.

Mercanzini, André; Reddy, Sai T.; Velluto, Diana; Colin, Philippe; Maillard, Anne; Bensadoun, Jean-Charles et al. (2010): Controlled release nanoparticle-embedded coatings reduce the tissue reaction to neuroprostheses. In *Journal of controlled release : official journal of the Controlled Release Society* 145 (3), pp. 196–202. DOI: 10.1016/j.jconrel.2010.04.025.

Mieczkowski, Jakub; Kocyk, Marta; Nauman, Pawel; Gabrusiewicz, Konrad; Sielska, Małgorzata; Przanowski, Piotr et al. (2015): Down-regulation of IKKβ expression in glioma-infiltrating microglia/macrophages is associated with defective inflammatory/immune gene responses in glioblastoma. In *Oncotarget* 6 (32), pp. 33077–33090. DOI: 10.18632/oncotarget.5310.

Mielke, John G.; Comas, Tanya; Woulfe, John; Monette, Robert; Chakravarthy, Balu; Mealing, Geoffrey A. R. (2005): Cytoskeletal, synaptic, and nuclear protein changes associated with rat interface organotypic hippocampal slice culture development. In *Brain research. Developmental brain research* 160 (2), pp. 275–286. DOI: 10.1016/j.devbrainres.2005.09.009.

Mikhailova, Valeriia; Gulaia, Valeriia; Tiasto, Vladlena; Rybtsov, Stanislav; Yatsunskaya, Margarita; Kagansky, Alexander (2018): Towards an advanced cell-based in vitro glioma model system. In *AIMS genetics* 5 (2), pp. 91–112. DOI: 10.3934/genet.2018.2.91.

Mirani, Bahram; Pagan, Erik; Shojaei, Shahla; Duchscherer, Jade; Toyota, Brian D.; Ghavami, Saeid; Akbari, Mohsen (2019): A 3D bioprinted hydrogel mesh loaded with all-trans retinoic acid for treatment of glioblastoma. In *European journal of pharmacology* 854, pp. 201–212. DOI: 10.1016/j.ejphar.2019.04.007.

Mishra, Yogendra K.; Kaps, Sören; Schuchardt, Arnim; Paulowicz, Ingo; Jin, Xin; Gedamu, Dawit et al. (2013): Fabrication of Macroscopically Flexible and Highly Porous 3D Semiconductor Networks from Interpenetrating Nanostructures by a Simple Flame Transport Approach. In *Part. Part. Syst. Charact.* 30 (9), pp. 775–783. DOI: 10.1002/ppsc.201300197.

Mishra, Yogendra Kumar; Modi, Gaurav; Cretu, Vasilii; Postica, Vasile; Lupan, Oleg; Reimer, Tim et al. (2015): Direct Growth of Freestanding ZnO Tetrapod Networks for Multifunctional Applications in Photocatalysis, UV Photodetection, and Gas Sensing. In *ACS applied materials & interfaces* 7 (26), pp. 14303–14316. DOI: 10.1021/acsami.5b02816.

Mittapalli, Rajendar K.; Manda, Vamshi K.; Adkins, Chris E.; Geldenhuys, Werner J.; Lockman, Paul R. (2010): Exploiting nutrient transporters at the blood-brain barrier to improve brain distribution of small molecules. In *Therapeutic delivery* 1 (6), pp. 775–784. DOI: 10.4155/tde.10.76.

Mo, Jianbin; He, Lizhen; Ma, Bin; Chen, Tianfeng (2016): Tailoring Particle Size of Mesoporous Silica Nanosystem To Antagonize Glioblastoma and Overcome Blood-Brain Barrier. In *ACS applied materials & interfaces* 8 (11), pp. 6811–6825. DOI: 10.1021/acsami.5b11730.

Moeendarbary, E.; Weber, I. P.; Sheridan, G. K.; Koser, D. E.; Soleman, S.; Haenzi, B. et al. (2017): The soft mechanical signature of glial scars in the central nervous system. In *Nature communications* 8, p. 14787. DOI: 10.1038/ncomms14787.

Moen, Marit D.; Lyseng-Williamson, Katherine A.; Scott, Lesley J. (2009): Liposomal amphotericin B. A review of its use as empirical therapy in febrile neutropenia and in the treatment of invasive fungal infections. In *Drugs* 69 (3), pp. 361–392. DOI: 10.2165/00003495-200969030-00010.

Mohamed, Hanan R. H.; Welson, Mary; Yaseen, Ahmed Essa; El-Ghor, Akmal A. (2019): Estimation of genomic instability and mutation induction by graphene oxide nanoparticles in mice liver and brain tissues. In *Environ Sci Pollut Res Int. DOI:* 10.1007/s11356-019-06930-0.

Mohammad, Ramzi M.; Wang, Shaomeng; Aboukameel, Amro; Chen, Ben; Wu, Xihan; Chen, Jianyong; Al-Katib, Ayad (2005): Preclinical studies of a nonpeptidic small-molecule inhibitor of Bcl-2 and Bcl-X(L) (-)-gossypol against diffuse large cell lymphoma. In *Molecular cancer therapeutics* 4 (1), pp. 13–21.

Motawi, Tarek K.; Sadik, Nermin A. H.; Hamed, Manal A.; Ali, Sanaa A.; Khalil, Wagdy K. B.; Ahmed, Yomna R. (2020): Potential therapeutic effects of antagonizing adenosine A2A receptor, curcumin and niacin in rotenone-induced Parkinson's disease mice model. In *Molecular and cellular biochemistry* 465 (1-2), pp. 89–102. DOI: 10.1007/s11010-019-03670-0.

Murray, J. D. (2012): Glioblastoma brain tumours. Estimating the time from brain tumour initiation and resolution of a patient survival anomaly after similar treatment protocols. In *Journal of biological dynamics* 6 Suppl 2, pp. 118–127. DOI: 10.1080/17513758.2012.678392.

Musto, Mattia; Rauti, Rossana; Rodrigues, Artur Filipe; Bonechi, Elena; Ballerini, Clara; Kostarelos, Kostas; Ballerini, Laura (2019): 3D Organotypic Spinal Cultures. Exploring Neuron and Neuroglia Responses Upon Prolonged Exposure to Graphene Oxide. In *Front Syst Neurosci* 13, p. 1. DOI: 10.3389/fnsys.2019.00001.

Muthoosamy, Kasturi; Bai, Renu Geetha; Abubakar, Ibrahim Babangida; Sudheer, Surya Mudavasseril; Lim, Hong Ngee; Loh, Hwei-San et al. (2015): Exceedingly biocompatible and thin-layered reduced graphene oxide nanosheets using an eco-friendly mushroom extract strategy. In *International journal of nanomedicine* 10, pp. 1505–1519. DOI: 10.2147/IJN.S75213.

Nathaniel, E.J.H.; Nathaniel, D. R. (Eds.) (1981): The reactive astrocyte. pp. 249-301. With assistance of S. Federoff. Academic Press. Orlando: Advances in cellular neurobiology.

Nedzvetsky, V. S.; Agca, C. A.; Kyrychenko, S. V. (2017): Neuroprotective effect of curcumin on LPS-activated astrocytes is related to the prevention of GFAP and NF-kB upregulation 49 (4), pp. 305–307. DOI: 10.1007/s11062-017-9687-x.

Nguyen, Jessica K.; Park, Daniel J.; Skousen, John L.; Hess-Dunning, Allison E.; Tyler, Dustin J.; Rowan, Stuart J. et al. (2014): Mechanically-compliant intracortical implants reduce the neuroinflammatory response. In *Journal of neural engineering* 11 (5), p. 56014. DOI: 10.1088/1741-2560/11/5/056014.

Nimmerjahn, Axel; Kirchhoff, Frank; Helmchen, Fritjof (2005): Resting microglial cells are highly dynamic surveillants of brain parenchyma in vivo. In *Science (New York, N.Y.)* 308 (5726), pp. 1314–1318. DOI: 10.1126/science.1110647.

Nortley, Ross; Attwell, David (2017): Control of brain energy supply by astrocytes. In *Current opinion in neurobiology* 47, pp. 80–85. DOI: 10.1016/j.conb.2017.09.012.

Ogawa, Junko; Pao, Gerald M.; Shokhirev, Maxim N.; Verma, Inder M. (2018): Glioblastoma Model Using Human Cerebral Organoids. In *Cell reports* 23 (4), pp. 1220–1229. DOI: 10.1016/j.celrep.2018.03.105.

Ohgaki, Hiroko; Kleihues, Paul (2005): Population-based studies on incidence, survival rates, and genetic alterations in astrocytic and oligodendroglial gliomas. In *Journal of neuropathology and experimental neurology* 64 (6), pp. 479–489. DOI: 10.1093/jnen/64.6.479.

Okada, Seiji; Nakamura, Masaya; Katoh, Hiroyuki; Miyao, Tamaki; Shimazaki, Takuya; Ishii, Ken et al. (2006): Conditional ablation of Stat3 or Socs3 discloses a dual role for reactive astrocytes after spinal cord injury. In *Nature medicine* 12 (7), pp. 829–834. DOI: 10.1038/nm1425.

Oliveira, A. I.; Anjo, S. I.; Vieira de Castro, J.; Serra, S. C.; Salgado, A. J.; Manadas, B.; Costa, B. M. (2017): Crosstalk between glial and glioblastoma cells triggers the "go-or-grow" phenotype of tumor cells. In *Cell communication and signaling : CCS* 15 (1), p. 37. DOI: 10.1186/s12964-017-0194-x.

Opydo-Chanek, Małgorzata; Gonzalo, Oscar; Marzo, Isabel (2017): Multifaceted anticancer activity of BH3 mimetics. Current evidence and future prospects. In *Biochemical pharmacology* 136, pp. 12–23. DOI: 10.1016/j.bcp.2017.03.006.

Ostrom, Quinn T.; Kinnersley, Ben; Armstrong, Georgina; Rice, Terri; Chen, Yanwen; Wiencke, John K. et al. (2018): Age-specific genome-wide association study in glioblastoma identifies increased proportion of 'lower grade glioma'-like features associated with younger age. In *International journal of cancer* 143 (10), pp. 2359–2366. DOI: 10.1002/ijc.31759.

Ozeki, Tetsuya; Hashizawa, Kosuke; Kaneko, Daiki; Imai, Yoshihiro; Okada, Hiroaki (2010): Treatment of rat brain tumors using sustained-release of camptothecin from poly(lactic-co-glycolic acid) microspheres in a thermoreversible hydrogel. In *Chemical & pharmaceutical bulletin* 58 (9), pp. 1142–1147. DOI: 10.1248/cpb.58.1142.

Ozeki, Tetsuya; Kaneko, Daiki; Hashizawa, Kosuke; Imai, Yoshihiro; Tagami, Tatsuaki; Okada, Hiroaki (2012): Combination therapy of surgical tumor resection with implantation of a hydrogel containing camptothecin-loaded poly(lactic-co-glycolic acid) microspheres in a C6 rat glioma model. In *Biological & pharmaceutical bulletin* 35 (4), pp. 545–550. DOI: 10.1248/bpb.35.545.

Paglin, S.; Hollister, T.; Delohery, T.; Hackett, N.; McMahill, M.; Sphicas, E. et al. (2001): A novel response of cancer cells to radiation involves autophagy and formation of acidic vesicles. In *Cancer research* 61 (2), pp. 439–444.

Pandit, Rucha; Chen, Liyu; Götz, Jürgen (2019): The blood-brain barrier. Physiology and strategies for drug delivery. In *Advanced drug delivery reviews. DOI:* 10.1016/j.addr.2019.11.009.

Paolicelli, Rosa C.; Bolasco, Giulia; Pagani, Francesca; Maggi, Laura; Scianni, Maria; Panzanelli, Patrizia et al. (2011): Synaptic pruning by microglia is necessary for normal brain development. In *Science (New York, N.Y.)* 333 (6048), pp. 1456–1458. DOI: 10.1126/science.1202529.

Papadia, Konstantina; Giannou, Anastasios D.; Markoutsa, Eleni; Bigot, Christian; Vanhoute, Greejte; Mourtas, Spyridon et al. (2017): Multifunctional LUV liposomes decorated for BBB and amyloid targeting - B. In vivo brain targeting potential in wild-type and APP/PS1 mice. In *European journal of pharmaceutical sciences : official journal of the European Federation for Pharmaceutical Sciences* 102, pp. 180–187. DOI: 10.1016/j.ejps.2017.03.010.

Pardridge, W. M.; Boado, R. J.; Black, K. L.; Cancilla, P. A. (1992): Blood-brain barrier and new approaches to brain drug delivery. In *The Western journal of medicine* 156 (3), pp. 281–286.

Pardridge, William M. (2005): The blood-brain barrier. Bottleneck in brain drug development. In *NeuroRx : the journal of the American Society for Experimental NeuroTherapeutics* 2 (1), pp. 3–14. DOI: 10.1602/neurorx.2.1.3.

Pardridge, William M. (2012): Drug transport across the blood-brain barrier. In *Journal of cerebral blood flow and metabolism : official journal of the International Society of Cerebral Blood Flow and Metabolism* 32 (11), pp. 1959–1972. DOI: 10.1038/jcbfm.2012.126.

Park, Ki Su; Yoon, Sang Youl; Park, Seong Hyun; Hwang, Jeong Hyun (2019): Anti-Migration and Anti-Invasion Effects of Curcumin via Suppression of Fascin Expression in Glioblastoma Cells. In *Brain tumor research and treatment* 7 (1), pp. 16–24. DOI: 10.14791/btrt.2019.7.e28.

Patel, Sohil H.; Halpern, Casey H.; Shepherd, Timothy M.; Timpone, Vincent M. (2017): Electrical stimulation and monitoring devices of the CNS. An imaging review. In *Journal of neuroradiology = Journal de neuroradiologie* 44 (3), pp. 175–184. DOI: 10.1016/j.neurad.2016.12.005.

Patel, Toral; Zhou, Jiangbing; Piepmeier, Joseph M.; Saltzman, W. Mark (2012): Polymeric nanoparticles for drug delivery to the central nervous system. In *Advanced drug delivery reviews* 64 (7), pp. 701–705. DOI: 10.1016/j.addr.2011.12.006.

Pedraza, Eileen; Brady, Ann-Christina; Fraker, Christopher A.; Stabler, Cherie L. (2013): Synthesis of macroporous poly(dimethylsiloxane) scaffolds for tissue engineering applications. In *Journal of biomaterials science. Polymer edition* 24 (9), pp. 1041–1056. DOI: 10.1080/09205063.2012.735097.

Pelin, Marco; Fusco, Laura; Martín, Cristina; Sosa, Silvio; Frontiñán-Rubio, Javier; González-Domínguez, Jose Miguel et al. (2018): Graphene and graphene oxide induce ROS production in human HaCaT skin keratinocytes. The role of xanthine oxidase and NADH dehydrogenase. In *Nanoscale* 10 (25), pp. 11820–11830. DOI: 10.1039/c8nr02933d.

Perera, Sanjaya D.; Mariano, Ruperto G.; Nijem, Nour; Chabal, Yves; Ferraris, John P.; Balkus, Kenneth J. (2012): Alkaline deoxygenated graphene oxide for supercapacitor applications. An effective green alternative for chemically reduced graphene. In *Journal of Power Sources* 215, pp. 1–10. DOI: 10.1016/j.jpowsour.2012.04.059.

Pesaran, B.; Musallam, S.; Andersen, R. A. (2006): Cognitive neural prosthetics. In *Current biology : CB* 16 (3), R77-80. DOI: 10.1016/j.cub.2006.01.043.

Petr, Geraldine T.; Sun, Yan; Frederick, Natalie M.; Zhou, Yun; Dhamne, Sameer C.; Hameed, Mustafa Q. et al. (2015): Conditional deletion of the glutamate transporter GLT-1 reveals that astrocytic GLT-1 protects against fatal epilepsy while neuronal GLT-1 contributes significantly to glutamate uptake into synaptosomes. In *The Journal of neuroscience : the official journal of the Society for Neuroscience* 35 (13), pp. 5187–5201. DOI: 10.1523/JNEUROSCI.4255-14.2015.

Pisapia, David J.; Magge, Rajiv; Ramakrishna, Rohan (2017): Improved Pathologic Diagnosis-Forecasting the Future in Glioblastoma. In *Frontiers in neurology* 8, p. 707. DOI: 10.3389/fneur.2017.00707.

Polikov, Vadim S.; Block, Michelle L.; Fellous, Jean-Marc; Hong, Jau-Shyong; Reichert, W. Monty (2006): In vitro model of glial scarring around neuroelectrodes chronically implanted in the CNS. In *Biomaterials* 27 (31), pp. 5368–5376. DOI: 10.1016/j.biomaterials.2006.06.018.

Polikov, Vadim S.; Tresco, Patrick A.; Reichert, William M. (2005): Response of brain tissue to chronically implanted neural electrodes. In *Journal of neuroscience methods* 148 (1), pp. 1–18. DOI: 10.1016/j.jneumeth.2005.08.015.

Pontes Soares, Carolina; Midlej, Victor; Oliveira, Maria Eduarda Weschollek de; Benchimol, Marlene; Costa, Manoel Luis; Mermelstein, Cláudia (2012): 2D and 3D-organized cardiac cells shows differences in cellular morphology, adhesion junctions, presence of myofibrils and protein expression. In *PloS one* 7 (5), e38147. DOI: 10.1371/journal.pone.0038147.

Pont-Lezica, Lorena; Beumer, Wouter; Colasse, Sabrina; Drexhage, Hemmo; Versnel, Marjan; Bessis, Alain (2014): Microglia shape corpus callosum axon tract fasciculation. Functional impact of prenatal inflammation. In *The European journal of neuroscience* 39 (10), pp. 1551–1557. DOI: 10.1111/ejn.12508.

Potter, Kelsey A.; Buck, Amy C.; Self, Wade K.; Callanan, Megan E.; Sunil, Smrithi; Capadona, Jeffrey R. (2013): The effect of resveratrol on neurodegeneration and blood brain barrier stability surrounding intracortical microelectrodes. In *Biomaterials* 34 (29), pp. 7001–7015. DOI: 10.1016/j.biomaterials.2013.05.035.

Potter, Kelsey A.; Buck, Amy C.; Self, Wade K.; Capadona, Jeffrey R. (2012): Stab injury and device implantation within the brain results in inversely multiphasic neuroinflammatory and neurodegenerative responses. In *Journal of neural engineering* 9 (4), p. 46020. DOI: 10.1088/1741-2560/9/4/046020.

Potter, Kelsey A.; Jorfi, Mehdi; Householder, Kyle T.; Foster, E. Johan; Weder, Christoph; Capadona, Jeffrey R. (2014): Curcumin-releasing mechanically adaptive intracortical implants improve the proximal neuronal density and blood-brain barrier stability. In *Acta biomaterialia* 10 (5), pp. 2209–2222. DOI: 10.1016/j.actbio.2014.01.018.

Qingyun, L.; Barres, Ben A. (2018): Microglia and macrophages in brain homeostasis and disease. In *Nature reviews. Immunology* 18, pp. 225–242.

Qiu, Jianping; Levin, Lonny R.; Buck, Jochen; Reidenberg, Marcus M. (2002): Different pathways of cell killing by gossypol enantiomers. In *Experimental biology and medicine (Maywood, N.J.)* 227 (6), pp. 398–401. DOI: 10.1177/153537020222700605.

Qu, Mengke; Lin, Qing; He, Shanshan; Wang, Luyao; Fu, Yao; Zhang, Zhirong; Zhang, Ling (2018): A brain targeting functionalized liposomes of the dopamine derivative N-3,4-bis(pivaloyloxy)-dopamine for treatment of Parkinson's disease. In *Journal of controlled release : official journal of the Controlled Release Society* 277, pp. 173–182. DOI: 10.1016/j.jconrel.2018.03.019.

Quail, D. F.; Joyce, J. A. (2017): The Microenvironmental Landscape of Brain Tumors. In *Cancer cell* 31 (3), pp. 326–341. DOI: 10.1016/j.ccell.2017.02.009.

Rabinowitz, Joshua D.; White, Eileen (2010): Autophagy and metabolism. In *Science (New York, N.Y.)* 330 (6009), pp. 1344–1348. DOI: 10.1126/science.1193497.

Rahman, Ruman (2014): Biomaterial-based local drug delivery to brain tumors. In *Therapeutic delivery* 5 (12), pp. 1243–1245. DOI: 10.4155/tde.14.83.

Rainer, Michael K. (2008): Risperidone long-acting injection. A review of its long term safety and efficacy. In *Neuropsychiatric disease and treatment* 4 (5), pp. 919–927. DOI: 10.2147/ndt.s3311.

Ranganath, Sudhir H.; Fu, Yilong; Arifin, Davis Y.; Kee, Irene; Zheng, Lin; Lee, How-Sung et al. (2010): The use of submicron/nanoscale PLGA implants to deliver paclitaxel with enhanced pharmacokinetics and therapeutic efficacy in intracranial glioblastoma in mice. In *Biomaterials* 31 (19), pp. 5199–5207. DOI: 10.1016/j.biomaterials.2010.03.002.

Rangwala, Reshma; Leone, Robert; Chang, Yunyoung C.; Fecher, Leslie A.; Schuchter, Lynn M.; Kramer, Amy et al. (2014): Phase I trial of hydroxychloroquine with dose-intense temozolomide in patients with advanced solid tumors and melanoma. In *Autophagy* 10 (8), pp. 1369–1379. DOI: 10.4161/auto.29118.

Ransohoff, Richard M.; Perry, V. Hugh (2009): Microglial physiology. Unique stimuli, specialized responses. In *Annual review of immunology* 27, pp. 119–145. DOI: 10.1146/annurev.immunol.021908.132528.

Recinos, Violette Renard; Tyler, Betty M.; Bekelis, Kimon; Sunshine, Sarah Brem; Vellimana, Ananth; Li, Khan Wayne; Brem, Henry (2010): Combination of intracranial temozolomide with intracranial carmustine improves survival when compared with either treatment alone in a rodent glioma model. In *Neurosurgery* 66 (3), 530-7; discussion 537. DOI: 10.1227/01.NEU.0000365263.14725.39.

Rose, C. R.; Chatton, J-Y (2016): Astrocyte sodium signaling and neuro-metabolic coupling in the brain. In *Neuroscience* 323, pp. 121–134. DOI: 10.1016/j.neuroscience.2015.03.002.

Rosé, S. D.; Byers, D. M.; Morash, S. C.; Fedoroff, S.; Cook, H. W. (1996): Lipopolysaccharide stimulates differential expression of myristoylated protein kinase C substrates in murine microglia. In *Journal of neuroscience research* 44 (3), pp. 235–242. DOI: 10.1002/(SICI)1097-4547(19960501)44:3<235::AID-JNR4>3.0.CO;2-H.

Rosenfeld, Myrna R.; Ye, Xiaobu; Supko, Jeffrey G.; Desideri, Serena; Grossman, Stuart A.; Brem, Steven et al. (2014): A phase I/II trial of hydroxychloroquine in conjunction with radiation therapy and concurrent and adjuvant temozolomide in patients with newly diagnosed glioblastoma multiforme. In *Autophagy* 10 (8), pp. 1359–1368. DOI: 10.4161/auto.28984.

Rosenfeldt, Mathias T.; O'Prey, Jim; Morton, Jennifer P.; Nixon, Colin; MacKay, Gillian; Mrowinska, Agata et al. (2013): p53 status determines the role of autophagy in pancreatic tumour development. In *Nature* 504 (7479), pp. 296–300. DOI: 10.1038/nature12865.

Roy, B.; Guha, P.; Bhattarai, R.; Nahak, P.; Karmakar, G.; Chettri, P.; Panda, A. K. (2016): Influence of Lipid Composition, pH, and Temperature on Physicochemical Properties of Liposomes with Curcumin as Model Drug. In *Journal of oleo science* 65 (5), pp. 399–411. DOI: 10.5650/jos.ess15229.

Russier, Julie; Treossi, Emanuele; Scarsi, Alessia; Perrozzi, Francesco; Dumortier, Hélène; Ottaviano, Luca et al. (2013): Evidencing the mask effect of graphene oxide. A comparative study on primary human and murine phagocytic cells. In *Nanoscale* 5 (22), pp. 11234–11247. DOI: 10.1039/c3nr03543c.

Ruzicka, Jiri; Urdzikova, Lucia Machova; Svobodova, Barbora; Amin, Anubhav G.; Karova, Kristyna; Dubisova, Jana et al. (2018): Does combined therapy of curcumin and epigallocatechin gallate have a synergistic neuroprotective effect against spinal cord injury? In *Neural Regen Res* 13 (1), pp. 119–127. DOI: 10.4103/1673-5374.224379.

Saad, Hassan; Krisht, Khaled M.; Yang, Wei-Hsun; Lopez-Gonzalez, Miguel Angel; Aboud, Emad; Krisht, Ali F. (2017): Biocompatible Amniotic Sac Implant Maintains a Scar-Free Brain Surface During Recurrent Glioma Surgery. In *World neurosurgery* 107, pp. 308–313. DOI: 10.1016/j.wneu.2017.07.143.

Safaiyan, Shima; Kannaiyan, Nirmal; Snaidero, Nicolas; Brioschi, Simone; Biber, Knut; Yona, Simon et al. (2016): Age-related myelin degradation burdens the clearance function of microglia during aging. In *Nature neuroscience* 19 (8), pp. 995–998. DOI: 10.1038/nn.4325.

Sak, Katrin (2019): Radiosensitizing Potential of Curcumin in Different Cancer Models. In *Nutrition and cancer*, pp. 1–14. DOI: 10.1080/01635581.2019.1681480.

Sakai, Koji; Teshima, Tetsuhiko F.; Nakashima, Hiroshi; Ueno, Yuko (2019): Graphene-based neuron encapsulation with controlled axonal outgrowth. In *Nanoscale* 11 (28), pp. 13249–13259. DOI: 10.1039/c9nr04165f.

Salam, M. T.; Sawan, M.; Dang, Khoa Nguyen (2011): A novel low-power-implantable epileptic seizure-onset detector. In *IEEE transactions on biomedical circuits and systems* 5 (6), pp. 568–578. DOI: 10.1109/TBCAS.2011.2157153.

Sanjay, Sharma T.; Dou, Maowei; Fu, Guanglei; Xu, Feng; Li, XiuJun (2016): Controlled Drug Delivery Using Microdevices. In *Current pharmaceutical biotechnology* 17 (9), pp. 772–787. DOI: 10.2174/1389201017666160127110440.

Sanjay, Sharma T.; Zhou, Wan; Dou, Maowei; Tavakoli, Hamed; Ma, Lei; Xu, Feng; Li, XiuJun (2018): Recent advances of controlled drug delivery using microfluidic platforms. In *Advanced drug delivery reviews* 128, pp. 3–28. DOI: 10.1016/j.addr.2017.09.013.

Santhanam, Gopal; Ryu, Stephen I.; Yu, Byron M.; Afshar, Afsheen; Shenoy, Krishna V. (2006): A high-performance brain-computer interface. In *Nature* 442 (7099), pp. 195–198. DOI: 10.1038/nature04968.

Saucier-Sawyer, Jennifer K.; Deng, Yang; Seo, Young-Eun; Cheng, Christopher J.; Zhang, Junwei; Quijano, Elias; Saltzman, W. Mark (2015): Systemic delivery of blood-brain barrier-targeted polymeric nanoparticles enhances delivery to brain tissue. In *Journal of drug targeting* 23 (7-8), pp. 736–749. DOI: 10.3109/1061186X.2015.1065833.

Sawyer, Andrew J.; Piepmeier, Joseph M.; Saltzman, W. Mark (2006): New methods for direct delivery of chemotherapy for treating brain tumors. In *The Yale journal of biology and medicine* 79 (3-4), pp. 141–152.

Sawyer, Andrew J.; Saucier-Sawyer, Jennifer K.; Booth, Carmen J.; Liu, Jie; Patel, Toral; Piepmeier, Joseph M.; Saltzman, W. Mark (2011): Convection-enhanced delivery of camptothecin-loaded polymer nanoparticles for treatment of intracranial tumors. In *Drug delivery and translational research* 1 (1), pp. 34–42. DOI: 10.1007/s13346-010-0001-3.

Schafer, Dorothy P.; Lehrman, Emily K.; Kautzman, Amanda G.; Koyama, Ryuta; Mardinly, Alan R.; Yamasaki, Ryo et al. (2012): Microglia sculpt postnatal neural circuits in an activity and complement-dependent manner. In *Neuron* 74 (4), pp. 691–705. DOI: 10.1016/j.neuron.2012.03.026.

Schnyder, Anita; Huwyler, Jörg (2005): Drug transport to brain with targeted liposomes. In *NeuroRx : the journal of the American Society for Experimental NeuroTherapeutics* 2 (1), pp. 99–107. DOI: 10.1602/neurorx.2.1.99.

Schroeder, R. L.; Gerber, J. P. (2014): Chloroquine and hydroxychloroquine binding to melanin. Some possible consequences for pathologies. In *Toxicology reports* 1, pp. 963–968. DOI: 10.1016/j.toxrep.2014.10.019.

Shabaninejad, Zahra; Pourhanifeh, Mohammad Hossein; Movahedpour, Ahmad; Mottaghi, Reza; Nickdasti, Ali; Mortezapour, Erfan et al. (2020): Therapeutic potentials of curcumin in the treatment of glioblstoma. In *European journal of medicinal chemistry* 188, p. 112040. DOI: 10.1016/j.ejmech.2020.112040.

Sharma, Manu; Sharma, Shipra; Wadhwa, Jyoti (2019): Improved uptake and therapeutic intervention of curcumin via designing binary lipid nanoparticulate formulation for oral delivery in inflammatory bowel disorder. In *Artificial cells, nanomedicine, and biotechnology* 47 (1), pp. 45–55. DOI: 10.1080/21691401.2018.1543191.

Shen, J.; Zheng, H.; Ruan, J.; Fang, W.; Li, A.; Tian, G. et al. (2013): Autophagy inhibition induces enhanced proapoptotic effects of ZD6474 in glioblastoma. In *British journal of cancer* 109 (1), pp. 164–171. DOI: 10.1038/bjc.2013.306.

Shergalis, Andrea; Bankhead, Armand; Luesakul, Urarika; Muangsin, Nongnuj; Neamati, Nouri (2018): Current Challenges and Opportunities in Treating Glioblastoma. In *Pharmacological reviews* 70 (3), pp. 412–445. DOI: 10.1124/pr.117.014944.

Siefker-Radtke, Arlene; Zhang, Xin-Qiao; Guo, Charles C.; Shen, Yu; Pirollo, Kathleen F.; Sabir, Sharjeel et al. (2016): A Phase l Study of a Tumor-targeted Systemic Nanodelivery System, SGT-94, in Genitourinary Cancers. In *Molecular therapy : the journal of the American Society of Gene Therapy* 24 (8), pp. 1484–1491. DOI: 10.1038/mt.2016.118.

Sierra, Amanda; Encinas, Juan M.; Deudero, Juan J. P.; Chancey, Jessica H.; Enikolopov, Grigori; Overstreet-Wadiche, Linda S. et al. (2010): Microglia shape adult hippocampal neurogenesis through apoptosis-coupled phagocytosis. In *Cell stem cell* 7 (4), pp. 483–495. DOI: 10.1016/j.stem.2010.08.014.

Silverman, Jeffrey A.; Reynolds, Laurie; Deitcher, Steven R. (2013): Pharmacokinetics and pharmacodynamics of vincristine sulfate liposome injection (VSLI) in adults with acute lymphoblastic leukemia. In *Journal of clinical pharmacology* 53 (11), pp. 1139–1145. DOI: 10.1002/jcph.155.

Sliwa, Marcin; Markovic, Darko; Gabrusiewicz, Konrad; Synowitz, Michael; Glass, Rainer; Zawadzka, Malgorzata et al. (2007): The invasion promoting effect of microglia on glioblastoma cells is inhibited by cyclosporin A. In *Brain : a journal of neurology* 130 (Pt 2), pp. 476–489. DOI: 10.1093/brain/awl263.

Sood, Disha; Tang-Schomer, Min; Pouli, Dimitra; Mizzoni, Craig; Raia, Nicole; Tai, Albert et al. (2019): 3D extracellular matrix microenvironment in bioengineered tissue models of primary pediatric and adult brain tumors. In *Nature communications* 10 (1), p. 4529. DOI: 10.1038/s41467-019-12420-1.

Spataro, L.; Dilgen, J.; Retterer, S.; Spence, A. J.; Isaacson, M.; Turner, J. N.; Shain, W. (2005): Dexamethasone treatment reduces astroglia responses to inserted neuroprosthetic devices in rat neocortex. In *Experimental neurology* 194 (2), pp. 289–300. DOI: 10.1016/j.expneurol.2004.08.037.

Sridar, S.; Churchward, M. A.; Mushahwar, V. K.; Todd, K. G.; Elias, A. L. (2017): Peptide modification of polyimide-insulated microwires. Towards improved biocompatibility through reduced glial scarring. In *Acta biomaterialia* 60, pp. 154–166. DOI: 10.1016/j.actbio.2017.07.026.

Steffens, Luiza; Morás, Ana Moira; Arantes, Pablo Ricardo; Masterson, Kevin; Cao, Zhi; Nugent, Michael; Moura, Dinara Jaqueline (2019): Electrospun PVA-Dacarbazine nanofibers as a novel nano brain-implant for treatment of glioblastoma. In silico and in vitro characterization. In *European journal of pharmaceutical sciences : official journal of the European Federation for Pharmaceutical Sciences* 143, p. 105183. DOI: 10.1016/j.ejps.2019.105183.

Stevens, Beth; Allen, Nicola J.; Vazquez, Luis E.; Howell, Gareth R.; Christopherson, Karen S.; Nouri, Navid et al. (2007): The classical complement cascade mediates CNS synapse elimination. In *Cell* 131 (6), pp. 1164–1178. DOI: 10.1016/j.cell.2007.10.036.

Stevenson, Cynthia L.; Santini, John T.; Langer, Robert (2012): Reservoir-based drug delivery systems utilizing microtechnology. In *Advanced drug delivery reviews* 64 (14), pp. 1590–1602. DOI: 10.1016/j.addr.2012.02.005.

Stoller, Meryl D.; Park, Sungjin; Zhu, Yanwu; An, Jinho; Ruoff, Rodney S. (2008): Graphene-based ultracapacitors. In *Nano letters* 8 (10), pp. 3498–3502. DOI: 10.1021/nl802558y.

Stupp, Roger; Mason, Warren P.; van den Bent, Martin J.; Weller, Michael; Fisher, Barbara; Taphoorn, Martin J. B. et al. (2005): Radiotherapy plus concomitant and adjuvant temozolomide for glioblastoma. In *The New England journal of medicine* 352 (10), pp. 987–996. DOI: 10.1056/NEJMoa043330.

Sundelin, Staffan P.; Terman, Alexei (2002): Different effects of chloroquine and hydroxychloroquine on lysosomal function in cultured retinal pigment epithelial cells. In *APMIS : acta pathologica, microbiologica, et immunologica Scandinavica* 110 (6), pp. 481–489. DOI: 10.1034/j.1600-0463.2002.100606.x.

Szarowski, D. H.; Andersen, M. D.; Retterer, S.; Spence, A. J.; Isaacson, M.; Craighead, H. G. et al. (2003): Brain responses to micro-machined silicon devices. In *Brain research* 983 (1-2), pp. 23–35. DOI: 10.1016/s0006-8993(03)03023-3.

Szczepaniak, Jaroslaw; Strojny, Barbara; Chwalibog, Ewa Sawosz; Jaworski, Slawomir; Jagiello, Joanna; Winkowska, Magdalena et al. (2018): Effects of Reduced Graphene Oxides on Apoptosis and Cell Cycle of Glioblastoma Multiforme. In *International journal of molecular sciences* 19 (12). DOI: 10.3390/ijms19123939.

Szmidt, Maciej; Stankiewicz, Adrian; Urbańska, Kaja; Jaworski, Sławomir; Kutwin, Marta; Wierzbicki, Mateusz et al. (2019): Graphene oxide down-regulates genes of the oxidative phosphorylation complexes in a glioblastoma. In *BMC molecular biology* 20 (1), p. 2. DOI: 10.1186/s12867-018-0119-2.

Tao, Jie; Zhang, Jiumeng; Hu, Yu; Yang, Yuan; Gou, Zhiyuan; Du, Ting et al. (2017): A conformal hydrogel nanocomposite for local delivery of paclitaxel. In *Journal of biomaterials science. Polymer edition* 28 (1), pp. 107–118. DOI: 10.1080/09205063.2016.1250344.

Tefas, Lucia Ruxandra; Sylvester, Bianca; Tomuta, Ioan; Sesarman, Alina; Licarete, Emilia; Banciu, Manuela; Porfire, Alina (2017): Development of antiproliferative long-circulating liposomes co-encapsulating doxorubicin and curcumin, through the use of a quality-by-design approach. In *Drug design, development and therapy* 11, pp. 1605–1621. DOI: 10.2147/DDDT.S129008.

Tegenge, Million Adane; Rajbhandari, Labchan; Shrestha, Shiva; Mithal, Aditya; Hosmane, Suneil; Venkatesan, Arun (2014): Curcumin protects axons from degeneration in the setting of local neuroinflammation. In *Experimental neurology* 253, pp. 102–110. DOI: 10.1016/j.expneurol.2013.12.016.

Tejada, Silvia; Manayi, Azadeh; Daglia, Maria; Nabavi, Seyed F.; Sureda, Antoni; Hajheydari, Zohreh et al. (2016): Wound Healing Effects of Curcumin. A Short Review. In *Current pharmaceutical biotechnology* 17 (11), pp. 1002–1007. DOI: 10.2174/1389201017666160721123109.

Thelin, Jonas; Jörntell, Henrik; Psouni, Elia; Garwicz, Martin; Schouenborg, Jens; Danielsen, Nils; Linsmeier, Cecilia Eriksson (2011): Implant size and fixation mode strongly influence tissue reactions in the CNS. In *PloS one* 6 (1), e16267. DOI: 10.1371/journal.pone.0016267.

Thiebaut, F.; Tsuruo, T.; Hamada, H.; Gottesman, M. M.; Pastan, I.; Willingham, M. C. (1989): Immunohistochemical localization in normal tissues of different epitopes in the multidrug transport protein P170. Evidence for localization in brain capillaries and crossreactivity of one antibody with a muscle protein. In *The journal of histochemistry and cytochemistry : official journal of the Histochemistry Society* 37 (2), pp. 159–164. DOI: 10.1177/37.2.2463300.

Tyler, Betty; Fowers, Kirk D.; Li, Khan W.; Recinos, Violette Renard; Caplan, Justin M.; Hdeib, Alia et al. (2010): A thermal gel depot for local delivery of paclitaxel to treat experimental brain tumors in rats. In *Journal of neurosurgery* 113 (2), pp. 210–217. DOI: 10.3171/2009.11.JNS08162.

Ueno, Masaki; Fujita, Yuki; Tanaka, Tatsuhide; Nakamura, Yuka; Kikuta, Junichi; Ishii, Masaru; Yamashita, Toshihide (2013): Layer V cortical neurons require microglial support for survival during postnatal development. In *Nature neuroscience* 16 (5), pp. 543–551. DOI: 10.1038/nn.3358.

van Rooy, Inge; Cakir-Tascioglu, Serpil; Hennink, Wim E.; Storm, Gert; Schiffelers, Raymond M.; Mastrobattista, Enrico (2011): In vivo methods to study uptake of nanoparticles into the brain. In *Pharmaceutical research* 28 (3), pp. 456–471. DOI: 10.1007/s11095-010-0291-7.

van Winden, E.C.A; Crommelin, D.J.A (1997): Long term stability of freeze-dried, lyoprotected doxorubicin liposomes. In *European Journal of Pharmaceutics and Biopharmaceutics* 43 (3), pp. 295–307. DOI: 10.1016/S0939-6411(97)00058-1.

Verbaanderd, Ciska; Maes, Hannelore; Schaaf, Marco B.; Sukhatme, Vikas P.; Pantziarka, Pan; Sukhatme, Vidula et al. (2017): Repurposing Drugs in Oncology (ReDO)-chloroquine and hydroxychloroquine as anti-cancer agents. In *Ecancermedicalscience* 11, p. 781. DOI: 10.3332/ecancer.2017.781.

Verma, Rajan K.; Arora, Sachin; Garg, Sanjay (2004): Osmotic pumps in drug delivery. In *Critical reviews in therapeutic drug carrier systems* 21 (6), pp. 477–520. DOI: 10.1615/critrevtherdrugcarriersyst.v21.i6.20.

Vidomanova, Eva; Racay, Peter; Pilchova, Ivana; Halasova, Erika; Hatok, Jozef (2016): Microfluidic profiling of apoptosis-related genes after treatment with BH3-mimetic agents in astrocyte and glioblastoma cell lines. In *Oncology reports* 36 (6), pp. 3188–3196. DOI: 10.3892/or.2016.5191.

Voss, Valerie; Senft, Christian; Lang, Verena; Ronellenfitsch, Michael W.; Steinbach, Joachim P.; Seifert, Volker; Kögel, Donat (2010): The pan-Bcl-2 inhibitor (-)-gossypol triggers autophagic cell death in malignant glioma. In *Molecular cancer research : MCR* 8 (7), pp. 1002–1016. DOI: 10.1158/1541-7786.MCR-09-0562.

Voulgaropoulou, S. D.; van Amelsvoort, T. A. M. J.; Prickaerts, J.; Vingerhoets, C. (2019): The effect of curcumin on cognition in Alzheimer's disease and healthy aging. A systematic review of pre-clinical and clinical studies. In *Brain research* 1725, p. 146476. DOI: 10.1016/j.brainres.2019.146476.

Wang, K.; Walz, W. (2003): Unusual topographical pattern of proximal astrogliosis around a cortical devascularizing lesion. In *Journal of neuroscience research* 73 (4), pp. 497–506. DOI: 10.1002/jnr.10683.

Wang, Kan; Ruan, Jing; Song, Hua; Zhang, Jiali; Wo, Yan; Guo, Shouwu; Cui, Daxiang (2011): Biocompatibility of Graphene Oxide. In *Nanoscale Research Letters* 6 (1), p. 8. DOI: 10.1007/s11671-010-9751-6.

Wang, Paul P.; Frazier, James; Brem, Henry (2002): Local drug delivery to the brain. In *Advanced drug delivery reviews* 54 (7), pp. 987–1013. DOI: 10.1016/s0169-409x(02)00054-6.

Watson, P. Marc D.; Kavanagh, Edel; Allenby, Gary; Vassey, Matthew (2017): Bioengineered 3D Glial Cell Culture Systems and Applications for Neurodegeneration and Neuroinflammation. In *SLAS discovery : advancing life sciences R & D* 22 (5), pp. 583–601. DOI: 10.1177/2472555217691450.

Weldon, D. T.; Rogers, S. D.; Ghilardi, J. R.; Finke, M. P.; Cleary, J. P.; O'Hare, E. et al. (1998): Fibrillar beta-amyloid induces microglial phagocytosis, expression of inducible nitric oxide synthase, and loss of a select population of neurons in the rat CNS in vivo. In *J. Neurosci.* 18 (6), pp. 2161–2173.

Wellman, S. M.; Kozai, T. D. Y. (2017): Understanding the Inflammatory Tissue Reaction to Brain Implants To Improve Neurochemical Sensing Performance. In *ACS chemical neuroscience* 8 (12), pp. 2578–2582. DOI: 10.1021/acschemneuro.7b00403.

Wen, N.; Dong, Y.; Song, R.; Zhang, W.; Sun, C.; Zhuang, X. et al. (2018): Zero-Order Release of Gossypol Improves Its Antifertility Effect and Reduces Its Side Effects Simultaneously. In *Biomacromolecules* 19 (6), pp. 1918–1925. DOI: 10.1021/acs.biomac.7b01648.

Wicks, Robert T.; Azadi, Javad; Mangraviti, Antonella; Zhang, Irma; Hwang, Lee; Joshi, Avadhut et al. (2015): Local delivery of cancer-cell glycolytic inhibitors in high-grade glioma. In *Neuro-oncology* 17 (1), pp. 70–80. DOI: 10.1093/neuonc/nou143.

William, Doreen; Mokri, Poroshista; Lamp, Nora; Linnebacher, Michael; Classen, Carl Friedrich; Erbersdobler, Andreas; Schneider, Björn (2017): Amplification of the EGFR gene can be maintained and modulated by variation of EGF concentrations in in vitro models of glioblastoma multiforme. In *PloS one* 12 (9), e0185208. DOI: 10.1371/journal.pone.0185208.

Wolpin, Brian M.; Rubinson, Douglas A.; Wang, Xiaoxu; Chan, Jennifer A.; Cleary, James M.; Enzinger, Peter C. et al. (2014): Phase II and pharmacodynamic study of autophagy inhibition using hydroxychloroquine in patients with metastatic pancreatic adenocarcinoma. In *The oncologist* 19 (6), pp. 637–638. DOI: 10.1634/theoncologist.2014-0086.

Wolter, Keith G.; Wang, Steven J.; Henson, Bradley S.; Wang, Shaomeng; Griffith, Kent A.; Kumar, Bhavna et al. (2006): (-)-gossypol inhibits growth and promotes apoptosis of human head and neck

squamous cell carcinoma in vivo. In *Neoplasia (New York, N.Y.)* 8 (3), pp. 163–172. DOI: 10.1593/neo.05691.

Woodroofe, M. N.; Sarna, G. S.; Wadhwa, M.; Hayes, G. M.; Loughlin, A. J.; Tinker, A.; Cuzner, M. L. (1991): Detection of interleukin-1 and interleukin-6 in adult rat brain, following mechanical injury, by in vivo microdialysis. Evidence of a role for microglia in cytokine production. In *Journal of Neuroimmunology* 33 (3), pp. 227–236. DOI: 10.1016/0165-5728(91)90110-S.

Wrzeszcz, Antonina; Dittrich, Barbara; Haamann, Daniel; Aliuos, Pooyan; Klee, Doris; Nolte, Ingo et al. (2014): Dexamethasone released from cochlear implant coatings combined with a protein repellent hydrogel layer inhibits fibroblast proliferation. In *Journal of biomedical materials research. Part A* 102 (2), pp. 442–454. DOI: 10.1002/jbm.a.34719.

Wu, Yakun; Wang, Fanfan; Wang, Shunhao; Ma, Juan; Xu, Ming; Gao, Ming et al. (2018): Reduction of graphene oxide alters its cyto-compatibility towards primary and immortalized macrophages. In *Nanoscale* 10 (30), pp. 14637–14650. DOI: 10.1039/c8nr02798f.

Xue, Peng; Li, Qian; Li, Yuan; Sun, Lihong; Zhang, Lei; Xu, Zhigang; Kang, Yuejun (2017): Surface Modification of Poly(dimethylsiloxane) with Polydopamine and Hyaluronic Acid To Enhance Hemocompatibility for Potential Applications in Medical Implants or Devices. In *ACS applied materials & interfaces* 9 (39), pp. 33632–33644. DOI: 10.1021/acsami.7b10260.

Yallapu, Murali M.; Jaggi, Meena; Chauhan, Subhash C. (2012): Curcumin nanoformulations. A future nanomedicine for cancer. In *Drug discovery today* 17 (1-2), pp. 71–80. DOI: 10.1016/j.drudis.2011.09.009.

Yallapu, Murali M.; Maher, Diane M.; Sundram, Vasudha; Bell, Maria C.; Jaggi, Meena; Chauhan, Subhash C. (2010): Curcumin induces chemo/radio-sensitization in ovarian cancer cells and curcumin nanoparticles inhibit ovarian cancer cell growth. In *Journal of ovarian research* 3, p. 11. DOI: 10.1186/1757-2215-3-11.

Yan, Yuanliang; Xu, Zhijie; Dai, Shuang; Qian, Long; Sun, Lunquan; Gong, Zhicheng (2016): Targeting autophagy to sensitive glioma to temozolomide treatment. In *Journal of experimental & clinical cancer research : CR* 35, p. 23. DOI: 10.1186/s13046-016-0303-5.

Yang, Dasom; Lee, Jung Seung; Choi, Chang-Kuk; Lee, Hong-Pyo; Cho, Seung-Woo; Ryu, WonHyoung (2018): Microchannel system for rate-controlled, sequential, and pH-responsive drug delivery. In *Acta biomaterialia* 68, pp. 249–260. DOI: 10.1016/j.actbio.2017.12.013.

Yang, Hu (2010): Nanoparticle-mediated brain-specific drug delivery, imaging, and diagnosis. In *Pharmaceutical research* 27 (9), pp. 1759–1771. DOI: 10.1007/s11095-010-0141-7.

Yang, Seung Yun; Yang, Jeong-A; Kim, Eung-Sam; Jeon, Gumhye; Oh, Eun Ju; Choi, Kwan Yong et al. (2010): Single-file diffusion of protein drugs through cylindrical nanochannels. In *ACS nano* 4 (7), pp. 3817–3822. DOI: 10.1021/nn100464u.

Yeh, Albert C.; Ramaswamy, Sridhar (2015): Mechanisms of Cancer Cell Dormancy--Another Hallmark of Cancer? In *Cancer research* 75 (23), pp. 5014–5022. DOI: 10.1158/0008-5472.CAN-15-1370.

Yoo, Jong Yoon; Hwang, Chang Ho; Hong, Hea Nam (2016): A Model of Glial Scarring Analogous to the Environment of a Traumatically Injured Spinal Cord Using Kainate. In *Annals of rehabilitation medicine* 40 (5), pp. 757–768. DOI: 10.5535/arm.2016.40.5.757.

Yu, Song; Wang, Xu; He, Xingliang; Wang, Yue; Gao, Sujie; Ren, Lu; Shi, Yan (2016): Curcumin exerts anti-inflammatory and antioxidative properties in 1-methyl-4-phenylpyridinium ion (MPP(+))-stimulated

mesencephalic astrocytes by interference with TLR4 and downstream signaling pathway. In *Cell stress & chaperones* 21 (4), pp. 697–705. DOI: 10.1007/s12192-016-0695-3.

Yu, Yangyang; Shen, Qian; Lai, Yihong; Park, Sun Y.; Ou, Xingmei; Lin, Dongxu et al. (2018): Anti-inflammatory Effects of Curcumin in Microglial Cells. In *Frontiers in pharmacology* 9, p. 386. DOI: 10.3389/fphar.2018.00386.

Yuan, J.; Liu, W.; Zhu, H.; Chen, Y.; Zhang, X.; Li, L. et al. (2017): Curcumin inhibits glial scar formation by suppressing astrocyte-induced inflammation and fibrosis in vitro and in vivo. In *Brain research* 1655, pp. 90–103. DOI: 10.1016/j.brainres.2016.11.002.

Yuan, Jiaying; Botchway, Benson O. A.; Zhang, Yong; Tan, Xiaoning; Wang, Xizhi; Liu, Xuehong (2019): Curcumin Can Improve Spinal Cord Injury by Inhibiting TGF-β-SOX9 Signaling Pathway. In *Cellular and molecular neurobiology* 39 (5), pp. 569–575. DOI: 10.1007/s10571-019-00671-x.

Yung-Chih, Kuo; I-Hsuan, Lee (2016): Delivery of doxorubicin to glioblastoma multiforme in vitro using solid lipid nanoparticles with surface aprotinin and melanotransferrin antibody for enhanced chemotherapy. In *Journal of the Taiwan Institute of Chemical Engineers* 61, pp. 32–45. Available online at https://doi.org/10.1016/j.jtice.2015.12.012.

Zamboni, William C. (2008): Concept and clinical evaluation of carrier-mediated anticancer agents. In *The oncologist* 13 (3), pp. 248–260. DOI: 10.1634/theoncologist.2007-0180.

Zeng, Jing; Xu, Xiaoyi; Chen, Xuesi; Liang, Qizhi; Bian, Xinchao; Yang, Lixin; Jing, Xiabin (2003): Biodegradable electrospun fibers for drug delivery. In *Journal of Controlled Release* 92 (3), pp. 227–231. DOI: 10.1016/S0168-3659(03)00372-9.

Zhang, Bo; Wei, Peng; Zhou, Zhixiang; Wei, Taotao (2016): Interactions of graphene with mammalian cells. Molecular mechanisms and biomedical insights. In *Advanced drug delivery reviews* 105 (Pt B), pp. 145–162. DOI: 10.1016/j.addr.2016.08.009.

Zhang, Jihong; Stevens, Malcolm F. G.; Bradshaw, Tracey D. (2012): Temozolomide. Mechanisms of action, repair and resistance. In *Current molecular pharmacology* 5 (1), pp. 102–114. DOI: 10.2174/1874467211205010102.

Zhang, Jingfei; Malik, Aqsa; Choi, Hyun B.; Ko, Rebecca W. Y.; Dissing-Olesen, Lasse; Macvicar, Brian A. (2014): Microglial CR3 activation triggers long-term synaptic depression in the hippocampus via NADPH oxidase. In *Neuron* 82 (1), pp. 195–207. DOI: 10.1016/j.neuron.2014.01.043.

Zhao, Mengnan; Bozzato, Elia; Joudiou, Nicolas; Ghiassinejad, Sina; Danhier, Fabienne; Gallez, Bernard; Préat, Véronique (2019): Codelivery of paclitaxel and temozolomide through a photopolymerizable hydrogel prevents glioblastoma recurrence after surgical resection. In *Journal of controlled release : official journal of the Controlled Release Society* 309, pp. 72–81. DOI: 10.1016/j.jconrel.2019.07.015.

Zhao, Mengnan; Danhier, Fabienne; Bastiancich, Chiara; Joudiou, Nicolas; Ganipineni, Lakshmi Pallavi; Tsakiris, Nikolaos et al. (2018): Post-resection treatment of glioblastoma with an injectable nanomedicine-loaded photopolymerizable hydrogel induces long-term survival. In *International journal of pharmaceutics* 548 (1), pp. 522–529. DOI: 10.1016/j.ijpharm.2018.07.033.

Zhong, Yinghui; Bellamkonda, Ravi V. (2007): Dexamethasone-coated neural probes elicit attenuated inflammatory response and neuronal loss compared to uncoated neural probes. In *Brain research* 1148, pp. 15–27. DOI: 10.1016/j.brainres.2007.02.024.

Zhong, Yinghui; Bellamkonda, Ravi V. (2008): Biomaterials for the central nervous system. In *J R Soc Interface* 5 (26), pp. 957–975. DOI: 10.1098/rsif.2008.0071.

Zielasek, J.; Müller, B.; Hartung, H. P. (1996): Inhibition of cytokine-inducible nitric oxide synthase in rat microglia and murine macrophages by methyl-2,5-dihydroxycinnamate. In *Neurochemistry international* 29 (1), pp. 83–87. DOI: 10.1016/0197-0186(95)00136-0.

Zlokovic, Berislav V. (2008): The blood-brain barrier in health and chronic neurodegenerative disorders. In *Neuron* 57 (2), pp. 178–201. DOI: 10.1016/j.neuron.2008.01.003.

Zschenker, Oliver; Streichert, Thomas; Hehlgans, Stephanie; Cordes, Nils (2012): Genome-wide gene expression analysis in cancer cells reveals 3D growth to affect ECM and processes associated with cell adhesion but not DNA repair. In *PloS one* 7 (4), e34279. DOI: 10.1371/journal.pone.0034279.

Publication bibliography

Publicized articles:

Mehner M, Kubelt C, Adamski V, **Schmitt C**, Synowitz M, Held-Feindt J; Combined treatment of AT101 and demethoxycurcumin yields an enhanced anti-proliferative effect in human primary glioblastoma cells. J Cancer Res Clin Oncol 146, 117–126 (2020) doi:10.1007/s00432-019-03107-7

Schmitt C*, Adamski V*, Rasch F, Adelung R, Lucius R, Synowitz M, Hattermann K, Held-Feindt J; Establishment of an in vivo adapted in vitro glioblastoma(in)complete resection co-culture model suitable for drug testing. Ann Anat., 228:151440, 2019 Nov 11. doi: 10.1016/j.aanat.2019.151440

Schmitt C, Lucius R, Synowitz M, Held-Feindt J, Hattermann K; APOBEC3B is expressed in human glioma, and influences cell proliferation and temozolomide resistance. Oncology Reports, 40, 2742-2749, 2018. doi:10.3892/or.2018.6698

Adamski V*, **Schmitt C***, Ceynowa F, Adelung R, Lucius R, Synowitz M,Hattermann K, Held-Feindt J; Effects of sequentially applied single and combined temozolomide, hydroxychloroquine and AT101 treatment in a long-term stimulation glioblastoma in vitro model. J Cancer Res Clin Oncol,144:1475−1485, 2018. doi:10.1007/s00432-018-2680-y

Tu L, Lu Z, Dieser K, **Schmitt C**, Chan SW, Ngan MP, Andrews PLR, Nalivaiko E and Rudd JA; Brain Activation by H1 Antihistamines Challenges Conventional View of Their Mechanism of Action in Motion Sickness: A Behavioral, c-Fos and Physiological Study in Suncus murinus (House Musk Shrew). Front. Physiol. 8:412; 2017. doi: 10.3389/fphys.2017.00412

Submitted articles:

Schmitt C, Rasch F, Cossais F, Heldt-Feind J, Lucius R, Shaygan Nia A, Lohe MR, Feng X, Mishra YK, Adelung R, Schütt F, Hattermann K, Little, reversible glial scarring responses on tetrapod-shaped graphene oxide and reduced graphene oxide 3D scaffolds in brain *in vitro* and *ex vivo* models. 2020, submitted, Biomaterials Science

Schmitt C, Lechanteur A, Cossais F, Bellefroid C, Arnold P, Lucius R, Heldt-Feind J, Piel G, Hattermann K, Liposomal encapsulated curcumin effectively attenuates neuroinflammatory and reactive astrogliosis reactions in glia cells and organotypic brain slices. 2020, in revision, Int. J. Nanomed.

Rasch F*, **Schmitt C***, Saure LM*, Meyer R*, Adamski V, Dengiz D, Scherließ R, Lucius R, Synowitz M, Mishra YK, Hattermann K, Adelung R, Held-Feindt J, Schütt F. Development of a 3 D porous PDMS-network for glioblastoma therapy. 2020, submitted, ACS Biomaterials Science & Engineering

* Authors share first authorship

Authors share senior authorship

Danksagung

„It is easier to reach our potential when we learn the value of including others into our quest."

(John Wooden)

An dieser Stelle möchte ich mich von Herzen bei all meinen Wegbegleitern der letzten drei Jahre bedanken, ohne deren Mithilfe die Anfertigung dieser Promotionsschrift nicht möglich gewesen wäre:

Mein ganz besonderer Dank gilt meiner Doktormutter PD Dr. Kirsten Hattermann-Koch, für die Betreuung der Arbeit und die zahlreichen bereichernden und konstruktiven Gespräche auf privater und wissenschaftlicher Ebene. Du hast mir stets die Möglichkeit gegeben meinen eigenen Weg zu gehen, meine Ideen in das Projekt einzubringen und diesem damit meinen persönlichen Charakter zu verleihen.

Ich danke Prof. Dr. Regina Scherließ für die hilfsbereite und wissenschaftliche Betreuung meiner Dissertation als Zweitgutachterin.

Außerdem möchte ich mich bei Prof. Dr. Geraldine Piel und Dr. Anna Lechanteur für die Betreuung meines Auslandsaufenthaltes in ihrem Labor in Belgien bedanken. Ich bekam die Möglichkeit ein für mich wissenschaftliches „Herzens"-Projekt eigenständig zu planen und durchzuführen.

Ganz besonders möchte ich mich auch bei Prof. Dr. Dr. Janka Held-Feindt bedanken, die ohne zu zögern meine Betreuung während Kirstens Elternzeit übernommen hat. Auch danach warst du nicht nur eine wichtige Ansprechpartnerin und Kooperationspartnerin, sondern wurdest mir durch unsere vielzähligen wissenschaftlichen und privaten Gespräche auch zu einer wahren Freundin.

Ein weiterer Dank gilt Dr. François Cossais, der für wissenschaftliche Fragestellungen immer ein offenes Ohr hatte. Deine perfektionierte Ironie hat so manchen Arbeitstag erhellt und auch im Privaten bist du zu einem sehr guten Freund für mich geworden.

Ferner möchte ich mich bei Sonja Dahle, Martina Burmester und Nicolas Da Silva für ihre Unterstützung, immerzu gute Laune und Hilfsbereitschaft bedanken. Ganz besonders möchte ich mich an dieser Stelle auch bei Judith Becker bedanken, die mir in den letzten drei Jahren so manchen Tag gerettet hat. Ohne dich hätte ich das ein oder andere Kooperationsprojekt auf Grund des Arbeitsumfanges niemals bearbeiten können. Ohne euch alle wäre der Alltag nicht so schön gewesen und ich werde unsere Gespräche sehr vermissen.

Ein weiterer Dank gilt den Menschen, die ich durch meine Arbeit am Anatomischen Institut oder im Graduiertenkolleg Materials4Brain ins Herz geschlossen habe. Dazu zählt vor allem Madlen Kunke, die mich mit ihrer durchweg positiven und mitreißenden Art während der gesamten Zeit aufgeheitert und verstanden hat, für mich da war und zu einer sehr guten Freundin wurde. Außerdem möchte ich Vivian Adamski, Anna Buschoff, Florian Rasch und Igor Barg nicht unerwähnt lassen. Ihr wart tolle Kooperationspartner und wurdet gute Freunde.

Eine ganz besonders wichtige Energiequelle waren außerdem die Besuche aus der Heimat von Freunden und das gemeinsame Reisen mit meinem Bruder, Torsten Schmitt, meiner guten Freundin, Yvonne Graber und meinem Partner, Jónatas Cardoso. Besonders bei Jónatas möchte ich mich für seine Unterstützung, Liebe, Zuversicht und Geduld bei der Anfertigung dieser Doktorarbeit bedanken.

Mein ganz besonderer Dank aber gilt meinen Eltern, Peter und Ulla Schmitt, die mir meinen bisherigen Lebensweg ermöglichten und denen ich diese Arbeit widme. Ihr wart immer für mich da, habt an mich geglaubt und mich durchweg unterstützt. Danke.

Eidesstattliche Erklärung

Hiermit erkläre ich an Eides Statt, dass ich die vorliegende Dissertation nach Inhalt und Form selbstständig unter der Beratung durch meine Betreuerin und ohne fremde Hilfe oder nicht aufgeführte Quellen angefertigt habe. Wörtlich oder inhaltlich zitierte Stellen sind als solche kenntlich gemacht. Außerdem versichere ich, dass weder ich noch ein anderer diese Arbeit an einer anderen Stelle im Rahmen eines Promotionsprüfungsverfahrens vorgelegt haben. Teile dieser Arbeit wurden bereits in wissenschaftlichen Fachmagazinen publiziert oder sind zur Veröffentlichung eingereicht. Weiterhin wurde die Arbeit unter Einhaltung der Regeln über gute wissenschaftliche Praxis der Deutschen Forschungsgemeinschaft erstellt. Zusätzlich bekräftige ich, dass mir noch kein akademischer Grad entzogen wurde.

Kiel, den

Christina Schmitt